Kevin Hendrik Reindert Rouwenhorst was born on March 16th, 1995 in Haaksbergen, the Netherlands. After graduating with a VWO+ diploma from Het Assink Lyceum in Haaksbergen, he started studying Advanced Technology at the University of Twente in 2013. During his bachelor study, he was part of the 11th board of S.A. Astatine, the study association of Advanced Technology and Nanotechnology, which was given the award for 'Best part-time board of 2016-2017' by the Student Union. He executed his BSc thesis on 'Rheology controlled extrusion' at Apollo Tyres Ltd. in Vadodara, India. During the summer of 2016, he participated in the Future Chemist International Summer Camp at the University of Science and Technology of China (USTC) in Hefei, China.

In 2016, he started his MSc on Chemical & Process Engineering at the University of Twente. During his internship, he performed his first research on ammonia synthesis at Haldor Topsøe A/S in Kongens Lyngby, Denmark. In 2018, he graduated cum laude and with honours from his MSc Chemical & Process Engineering. He wrote his MSc thesis on 'Power-to-ammonia-to-power for local electricity storage in 2025' under the supervision of dr. ir. A.G.J. Van der Ham in the Sustainable Process Technology group at the University of Twente. His MSc thesis was awarded with the 1st prize in the category gas industry (sponsored by the KVGN) by the Koninklijke Hollandse Maatschappij der Wetenschappen (KHMW, English: Royal Dutch Society of Sciences).

He continued research at the University of Twente with a PhD project on 'Plasma-catalytic ammonia synthesis' under the supervision of prof. dr. ir. L. Lefferts in the Catalytic Processes & Materials group at the University of Twente. The results of this research is presented in this PhD thesis. During his PhD research, he presented his work on various ammonia energy conferences and plasma chemistry conferences. He has published various articles, various book chapters, an encyclopaedia article, and filed for two patents. Furthermore, he is the lead author of a recent report (Innovation Outlook: Renewable Ammonia) of the International Renewable Energy Agency (IRENA) and the Ammonia Energy Association (AEA). During the final year of his PhD research, he worked part-time as Innovation Engineer at Proton Ventures and as Technology Manager at the Ammonia Energy Association (AEA).

9 789036 554190

NITROGEN FIXATION WITH RENEWABLE ELECTRICITY Kevin H.R. Rouwenhorst

NITROGEN FIXATION WITH RENEWABLE ELECTRICITY

Plasma Catalysis As An Alternative For Small-Scale Ammonia Synthesis?

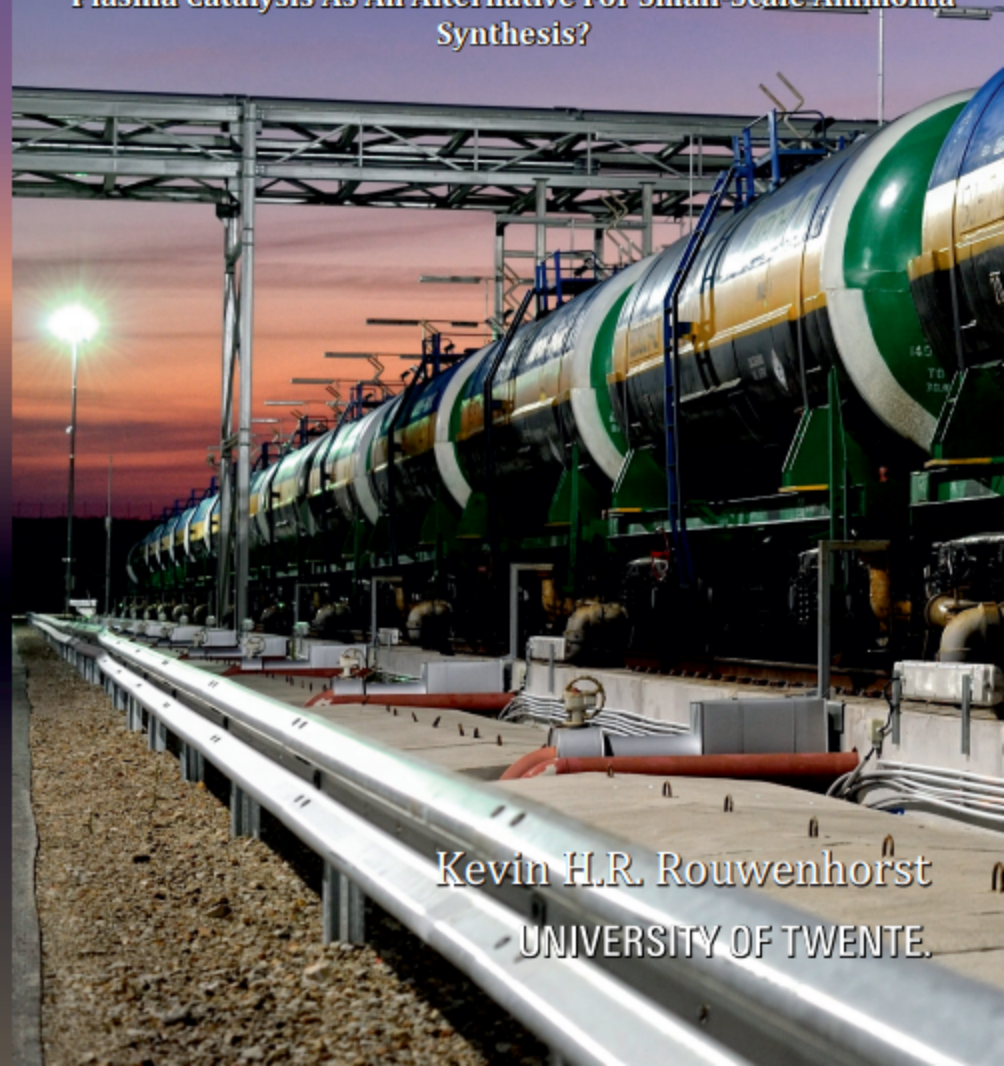

Kevin H.R. Rouwenhorst
UNIVERSITY OF TWENTE.

NITROGEN FIXATION WITH RENEWABLE ELECTRICITY

PLASMA CATALYSIS AS AN ALTERNATIVE FOR SMALL-SCALE AMMONIA SYNTHESIS?

Kevin Hendrik Reindert Rouwenhorst

NITROGEN FIXATION WITH RENEWABLE ELECTRICITY

PLASMA CATALYSIS AS AN ALTERNATIVE FOR SMALL-SCALE AMMONIA SYNTHESIS?

PROEFSCHRIFT

ter verkrijging van
de graad van doctor aan de Universiteit Twente,
op gezag van de rector magnificus,
prof. dr. ir. A. Veldkamp,
volgens besluit van het College voor Promoties
in het openbaar te verdedigen
op vrijdag 9 september 2022 om 16.45 uur

door

Kevin Hendrik Reindert Rouwenhorst
geboren op 16 maart 1995
te Haaksbergen, Nederland

Dit proefschrift is goedgekeurd door:

Promotor
prof. dr. ir. L. Lefferts

Cover design: B. Geerdink
Printed by: Gildeprint
Lay-out: K.H.R. Rouwenhorst
ISBN: 978-90-365-5419-0
DOI: 10.3990/1.9789036554190

The cover image depicts ammonia loading and unloading trains. Permission for its use has been granted by Proton Ventures B.V.

PROMOTIECOMMISSIE:

Voorzitter/secretaris:	prof.dr. J.L. Herek	University of Twente
Promotor:	prof.dr.ir. L. Lefferts	University of Twente
Leden:	prof.dr. J.G.E. Gardeniers	University of Twente
	prof.dr. G. Mul	University of Twente
	dr. B. Vigeland	Yara A/S
	prof.dr. A.M.B. Bogaerts	University of Antwerp
	prof.dr. F. Gallucci	Eindhoven University of Technology

Contents

Chapter 1

The Current and future role of ammonia: plasma catalysis as an option?

Summary

Ammonia is one of the most produced chemicals, mainly synthesized for fertilizer applications. Renewable ammonia is considered as a zero carbon fuel and hydrogen carriers of the future. However, renewable resources such as wind and solar are fluctuating. This has spurred research interest in alternative technologies for renewable ammonia production methods better suited to fluctuating electricity sources. Plasma catalysis is proposed as an option for electricity-driven ammonia synthesis. Lastly, the outline of the thesis is highlighted.

This chapter has partially based on:

Rouwenhorst, K. H. R., Krzywda, P. M., Benes, N. E., Mul, G., & Lefferts, L. (2020). Ammonia Production Technologies. In R. Bañares-Alcántara & A. Valera-Medina (Eds.), Techno-Economic Challenges of Green Ammonia as Energy Vector (pp. 41-84). Elsevier Science Publishing Co Inc. doi: 10.1016/B978-0-12-820560-0.00004-7

Rouwenhorst, K. H. R., Krzywda, P.M., Benes, N. E., Mul, G., & Lefferts, L. (2020). Ammonia, 4. Green Ammonia Production. In Ullmann's Encyclopedia of Industrial Chemistry. doi: 10.1002/14356007.w02_w02

IRENA, & Ammonia Energy Association (Lead author: **Rouwenhorst, K. H. R.**) (2022). Innovation Outlook: Renewable Ammonia. Abu Dhabi (United Arab Emirates). ISBN: 978-92-9260-423-3

1.1 The Malthusian disaster prevented

In 1798, Thomas R. Malthus published *An Essay on the Principle of Population*, in which he argued that an exponential increase in human population would lead to starvation due to the finite resources of the earth and the exponential potential for population increase [1]. A century later, in 1898, Sir William Crookes gave a historical speech at *the British Association for the Advancement of Science* in Bristol, in which he argued that the world population would starve by 1921 due to population growth combined with the depletion of natural nitrate fertilizer deposits located in Chile [2]. Only half of the required nitrogen fixation could be obtained from natural sources (guano and Chile saltpetre) and from ammonium sulphate (a byproduct in coke ovens) around the turn of the 20th century [3]. Crookes called onto the scientists around the world to develop a synthetic process for nitrogen fixation and many heeded the call.

Early industrialized synthetic nitrogen fixation technologies include a plasma-based nitrogen fixation process (the Birkeland-Eyde process), and a cyanamide process (the Frank-Caro process) [4,5]. However, the energy consumption per fixed nitrogen atom was high. Furthermore, these processes were expensive to operate [5]. The synthesis of ammonia (NH_3) from its elements was considered as a desirable alternative (**Equation 1**). Many researchers attempted to synthesize ammonia from its elements, but to little avail. By 1907, Walther Nernst among other prominent researchers concluded that synthetic nitrogen fixation in the form of ammonia was not feasible [6].

Equation 1: $3H_2 + N_2 \rightleftharpoons 2NH_3$ **with** $\Delta H_r = -92\ kJ\ mol^{-1}$

However, one year later, in 1908, Fritz Haber and Robert Le Rossignol showed the feasibility of synthetic nitrogen fixation in the form of ammonia at high temperature (500-550°C) and high pressure (100-200 atm) [7]. In the years to follow, Carl Bosch and co-workers solved engineering challenges of operating such processes at high temperatures and pressures [8], while Mittasch and co-workers developed a multicomponent iron-based catalyst for mass production of ammonia as an alternative to the scarce osmium catalyst used in the first laboratory experiments [9,10]. By 1913, the first synthetic ammonia synthesis plant was operational in Oppau, Ludwigshafen and it was coined the *Haber-Bosch process* in the years to follow.

The Malthusian disaster of the 20th century was prevented due to the invention of the Haber-Bosch process, resulting in various Nobel prizes being awarded for the discovery of ammonia synthesis (Fritz Haber for Chemistry in 1918), its commercialization and engineering solutions (Carl Bosch for Chemistry in 1931), its application to underfed populations (Norman Borlaug for Peace in 1970), the understanding of the reaction mechanism on the iron-based catalyst (Gerhard Ertl for Chemistry in 2007). Hunger is currently a political issue rather than an intrinsic necessity.

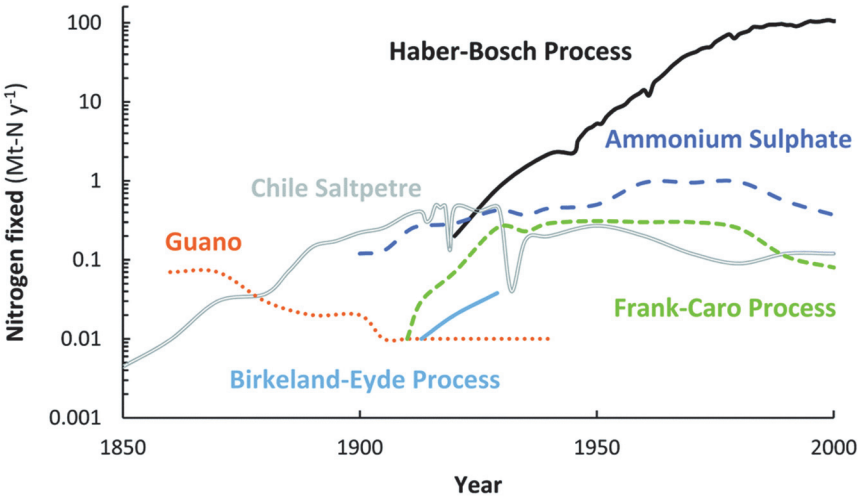

Figure 1: Annual consumption of fixed nitrogen from various natural sources and from industrial nitrogen fixation technologies. Adapted from Ref. [11]**.**

As shown in **Figure 1**, the Haber-Bosch remains the dominant nitrogen fixation technology. Since its introduction in 1913 up till now, the global population increased from about 1.8 billion people to 7.9 billion people today. Without the Haber-Bosch process, the world would be about 40-50% less populated [12], with a substantial portion of the population starving. About half of the nitrogen in the human body has been processed via the Haber-Bosch process [12]. Thus, the Haber-Bosch process is one of the most important inventions of the 20th century [3,12].

1.2 Ammonia synthesis technologies

Ammonia is among the most produced chemicals, with a demand of 183 Mt ammonia in 2020 [13]. The Haber-Bosch process consumes about 1-2% of the global primary energy. Currently, essentially all ammonia is produced from fossil-based hydrogen from natural gas and coal. Utilization of fossil feedstock is mainly due to economic reasons [14]. Ammonia synthesis consumes about 5% of the global natural gas production, at the cost of 1.0% of the global CO_2 equivalent emissions [12,15].

After solving the famine crisis of the 20th century, the global population and wealth increased. However, with increasing populations and increasing wealth, the carbon emissions and nitrogen oxide emissions have increased steadily over the past decades, due to the use of fossil fuels and intensive agriculture. This has been inducing climate change and nitrification ever since [16]. Thus, the challenge of the 21st century is mitigation of emissions towards a circular economy, while maintaining or improving the living standards of the global population. A key challenge herein is the efficient storage of electricity from renewable sources, for use in the desired location and at the desired moment in time [17]. Ammonia may play a key role in decarbonizing the energy landscape

within the *hydrogen economy*. Decarbonized ammonia synthesis is briefly discussed hereafter. An overview of terminology for ammonia synthesis based on hydrogen feedstock is shown in **Figure 2**.

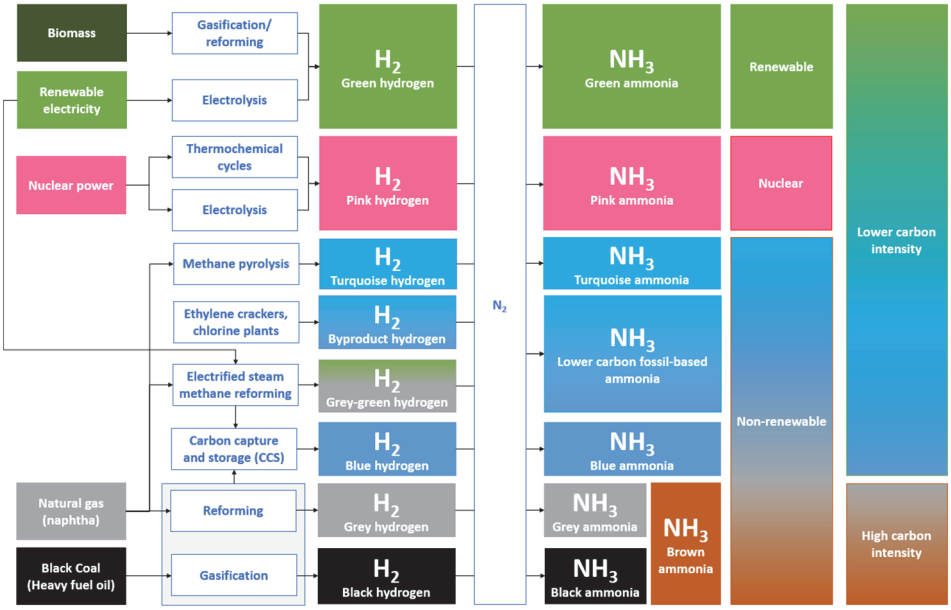

Figure 2: Overview of terminology for ammonia synthesis, based on hydrogen feedstock. Adapted and modified from Ref. [14]**.**

1.2.1 Fossil-based ammonia production

Fossil-based ammonia production utilizes fossil-based hydrogen derived from natural gas, oil, and coal. The hydrogen is produced via reforming or gasification processes, with subsequent gas clean-up steps [18–20]. Atmospheric nitrogen is typically introduced during hydrogen production. The last step of the feedstock processing is CO_2 removal, which occurs via absorption. The resulting stream of hydrogen and nitrogen (with residual methane and argon) is sometimes termed *forming gas*. The stream of hydrogen and nitrogen is fed to the ammonia synthesis loop, in which the hydrogen and nitrogen are converted to ammonia at high temperature (350-550°C) and high pressure (100-450 bar) [21,22].

Fossil-based ammonia synthesis can be decarbonized by CO_2 capture and storage (CCS), e.g. by storing the CO_2 that is already captured in the process. This removes about 95-98% of the process CO_2 emissions during ammonia synthesis [23]. If fossil fuels are also used for heating in tubular reforming, these CO_2 emissions still require additional CO_2 capture and storage (CCS) steps. It should be mentioned that upstream emissions, such as methane emissions during natural gas extraction also occur, and these can cause a significant CO_2 equivalent emission footprint [14].

Other alternatives for decreasing the carbon intensity of fossil-based ammonia production include carbon capture and utilization (CCU) for methanol synthesis or enhanced oil recovery (EOR), electrified steam methane reforming, methane pyrolysis, and utilization of byproduct hydrogen from ethylene crackers and chlorine plants [14].

1.2.2 Renewable ammonia production

Ammonia can also be produced from renewable resources, such as renewable electricity coupled with water electrolysis for hydrogen production. Furthermore, biomass can be processed to form renewable syngas, a mixture of hydrogen and carbon monoxide. A schematic overview of electrolysis-based ammonia synthesis is shown in **Figure 3**.

Historically, various hydropower-powered electrolysis-based Haber-Bosch plants were operated with capacities up to 400 t-NH_3 d^{-1} and electrolyzer capacities up to 165 MW [24]. Such renewable ammonia plants were operated in various countries, including Egypt, Italy, and Norway [24]. These plants were eventually shut down, or revamped to fossil feedstock due to the emergence of low cost natural gas. The only operational conventional electrolysis-based ammonia plants is located in Peru.

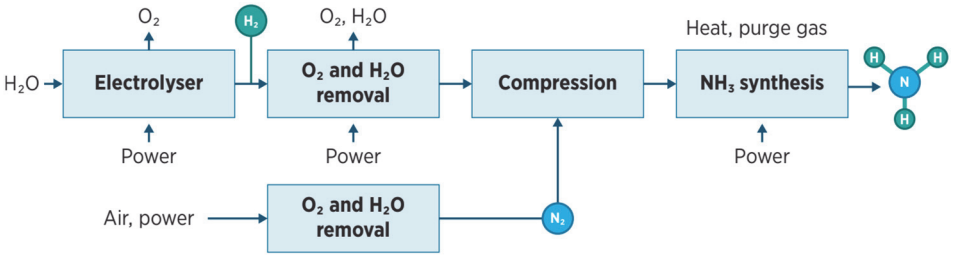

Figure 3: Schematic of electrolysis-based ammonia synthesis. Reproduced from Ref. [14], based on Refs. [25,26].

Recently, ammonia has emerged as a zero carbon fuel and hydrogen carrier, especially with increasing taxation on CO_2 emission [14,15]. Therefore, renewable ammonia has gained traction again. Various large renewable ammonia plants were recently announced, mostly based on onshore wind and solar PV as sources for renewable electricity. The total announced low carbon ammonia capacity is 71 Mt per annum, e.g. roughly a third to half the current ammonia demand [14].

1.3 The ammonia economy

If ammonia is used as a hydrogen carrier, it can be used for both fertilizer and energy applications. In such an *ammonia economy*, energy can be stored in time (i.e., for islanded power systems) and in space (i.e., for transportation form places with abundant, low cost renewable ammonia production to other places) [27–33].

There is significant infrastructure for transportation of ammonia over sea, and ammonia can be used as a marine fuel [15,34,35]. In Japan, an infrastructure is currently set up for the use of imported low carbon fossil-based ammonia and renewable ammonia as a fuel in gas turbines, coal power plants, and fuel cells [36]. Furthermore, ammonia can be decomposed to hydrogen and nitrogen with further purification steps to supply pure hydrogen.

This demand for renewable ammonia goes hand in hand with renewable ammonia production facilities being announced, as discussed in the previous section. Hydrogen utilization for ammonia production in 2050 may be roughly the same as the total current hydrogen usage (**Figure 4**), based on the 1.5°C scenario of IRENA [14]. It is estimated that hydrogen and hydrogen carriers amount to about 15-20% of the energy mix in a decarbonized energy system in Japan and in most countries in Europe [37].

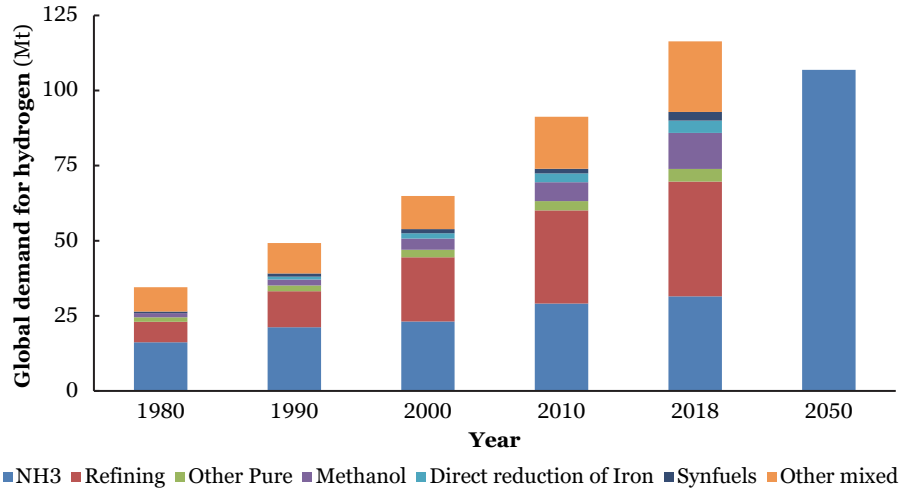

Figure 4: Global demand for hydrogen. Historical hydrogen demand adapted from Ref. [38]. 2050 hydrogen demand for ammonia adapted from Ref. [14], for the 1.5°C scenario.

The four energy-related market for such an *ammonia economy* include (1) ammonia as a transportation fuel, (2) ammonia for stationary electricity generation, (3) ammonia for heat applications, and (4) ammonia as a hydrogen feedstock. An overview of applications of ammonia is shown in **Figure 5**.

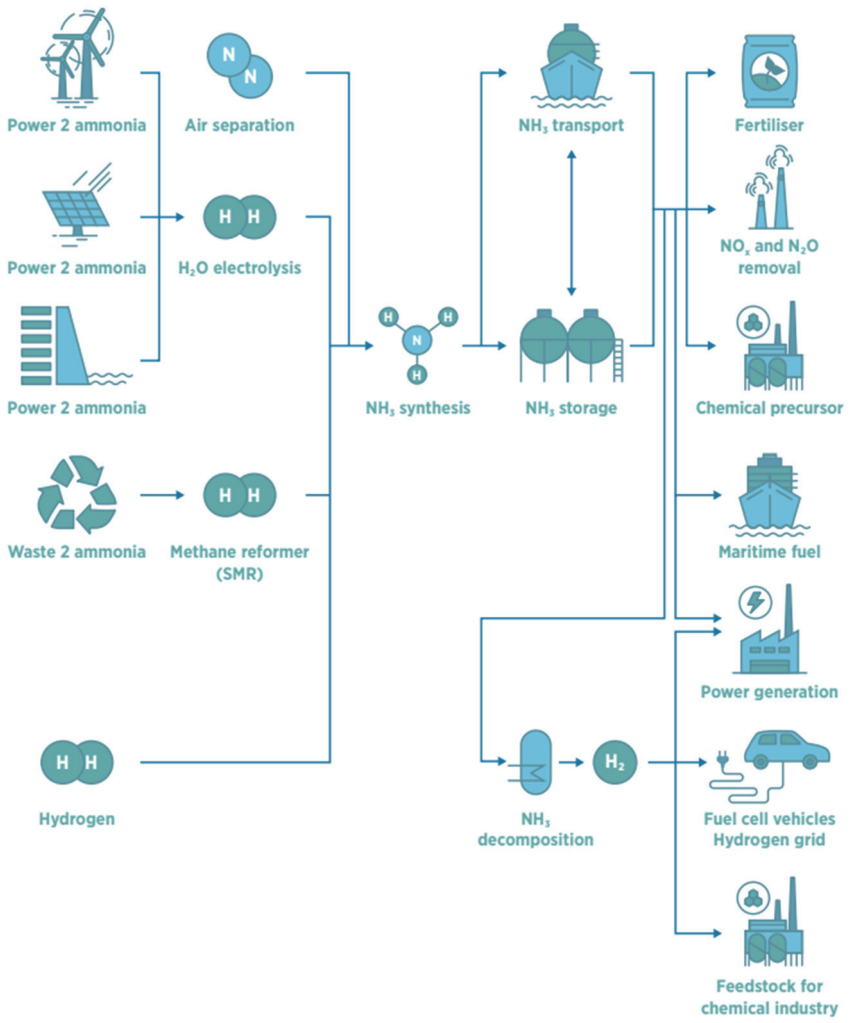

Figure 5: Schematic of the ammonia economy. Adapted from Ref. [14]**, based on and modified from Refs.** [26,39]**.**

1.4 Plasma technology for nitrogen fixation

With the increasing availability of low cost electricity, electrification of chemical processes is currently widely researched. Along with electrochemistry and photochemistry, plasma technology is an emerging option for electrification of the chemical industry [40,41]. Molecules such as carbon dioxide (CO_2), methane (CH_4), and atmospheric nitrogen (N_2) have strong chemical bonds, implying thermal (electro)chemistry and (electronic)catalytic conversion typically require elevated temperatures. In case of plasma-activation, a molecule can be activated by reactive species in the plasma, such as highly energetic electrons [42]. Plasma technologies are further discussed in **Chapter 2**.

Plasma-activation of these molecules may allow for operation under milder conditions, as the molecules are already in an excited state after plasma-activation, potentially leading to a lower remaining activation barrier for the desired reaction. Furthermore, plasma activation of molecules may result in reaction pathways inaccessible under thermal-catalytic, electrochemical, and photochemical conditions [43]. Another potential benefit of plasma technology is the ability to follow load variation of fluctuating power sources, as a plasma can typically be illuminated within seconds or minutes when electricity is available [40,44]. Plasma technology is commercially used to produce ozone (O_3) [45] and acetylene (C_2H_2) [46].

The focus of this research is on plasma-based nitrogen fixation in the form of ammonia (NH_3). Atmospheric nitrogen only dissociates in the gas phase at temperatures above 2175°C [47]. Therefore, a catalyst is typically used to activate nitrogen and decrease the barrier to break the triple N≡N bond (9.79 eV or 945 kJ mol^{-1}). Nitrogen is mainly fixated in the form of ammonia via the catalytic conversion of N_2 and H_2 on iron-based catalysts in the Haber-Bosch process, operating at 350-550°C and 100-450 bar [21,22].

Interestingly, the first industrial nitrogen fixation process was the Birkeland-Eyde process, a plasma-based process, in which N_2 and O_2 are converted to NO_X in a plasma reactor [11,48]. However, the higher energy requirement for the Birkeland-Eyde process as compared to the Haber-Bosch process meant the former was phased out (see **Figure 1**). Plasma-based nitrogen fixation for ammonia synthesis is discussed in more detail in **Chapter 2**.

Some limitations to plasma-based conversions include product selectivity and energy efficiency. The combination of a plasma with a catalyst may aid in the selective conversion of the plasma species toward the desired product. However, all species in the plasma zone can be activated by plasma-generated species such as electrons, plasma radicals, and plasma-excited molecules. This means that not only the reactants in the plasma environment are activated, but also the product. This decreases the energy efficiency for product formation, as well as the product yield.

1.5 Scope and outline

Ammonia synthesis from hydrogen and nitrogen in the presence of a catalyst or sorbent, and a plasma are researched in this thesis. The development of catalytic materials, performance testing, and process design for plasma-catalytic ammonia synthesis are within the scope of this thesis. The questions central to this thesis are as follows:

- Is plasma-catalytic ammonia synthesis a feasible alternative for ammonia synthesis?
- Which plasma-chemical and plasma-catalytic pathways can be used to enhance the ammonia yield in a plasma-reactor?

1.5.1 Background on plasma catalysis

Plasma-catalytic ammonia synthesis is among many different alternatives researched to replace the Haber-Bosch process for small-scale, intermittent operation. Plasma-reactors, plasma-chemistry, and plasma-catalysis are introduced in **Chapter 2**. Furthermore, the current status of plasma-catalytic ammonia synthesis is reviewed, which provides the foundation for the experimental research.

1.5.2 Plasma-catalytic ammonia synthesis

Then, experimental work is presented and analysed to obtain a better understanding of plasma-catalytic ammonia synthesis, and plasma-catalysis more generally. A postulate of Mehta et al. [49] regarding the mechanism of plasma-enhanced catalytic ammonia synthesis with vibrational or electronic N_2 activation is validated with experimental data for Ru-based catalysts at low plasma powers in **Chapter 3**. A mechanism for the observed barrier decrease for plasma-activated N_2 is suggested in **Chapter 4**.

Afterwards, plasma-catalytic ammonia synthesis experiments are performed at higher plasma powers, at which point nitrogen radicals become relevant. In **Chapter 5**, the contribution of plasma chemistry, plasma catalysis with nitrogen radicals, and catalysis with molecular nitrogen is evaluated for Ru-based catalysts. Furthermore, plasma catalysis beyond the thermal equilibrium is discussed. The activity for plasma chemistry and plasma catalysis for various transition metals (Ag, Co, Cu, Pd, Pt, and Ru) is discussed in **Chapter 6**. The similar activity among various transition metals indicates that a mechanism involving N radicals from the plasma and surface-adsorbed H is likely dominant for plasma-catalytic ammonia synthesis at high plasma powers. *In situ* ammonia removal from the plasma phase with a zeolite is discussed in **Chapter 7** as a strategy to improve the ammonia yield.

1.5.3 Evaluation of plasma-catalytic ammonia synthesis

In **Chapter 8**, plasma-catalytic ammonia synthesis is evaluated as an alternative for small-scale ammonia synthesis for energy storage applications. The plasma-catalytic ammonia synthesis process is compared to a scaled-down Haber-Bosch synthesis loop, as well as other emerging technologies for small-scale ammonia synthesis. An outlook and recommendations on the work in this thesis is given in **Chapter 9**.

Chapter 2

Plasma-driven catalytic ammonia synthesis

Summary

Research on plasma-driven ammonia synthesis has recently gained traction in academic literature. In the current Chapter, the literature on plasma-driven ammonia synthesis is summarized. Mechanisms for ammonia synthesis in the presence of a plasma, with and without a catalyst, are distinguished for different plasma conditions. Strategies for catalyst design are discussed, as well as the current understanding regarding the potential plasma-catalyst synergies as function of the plasma conditions and their implications on energy efficiency. Finally, the limitations in currently reported models and experiments are discussed, as an outlook for research opportunities for further unravelling the complexities of plasma-catalytic ammonia synthesis, in order to bridge the gap between the currently reported models and experimental results.

This chapter is partially adapted from:

Rouwenhorst, K. H. R., Engelmann, Y., Van 't Veer, K., Postma, R. S., Bogaerts, A., & Lefferts, L. (2020). Plasma-driven catalysis: green ammonia synthesis with intermittent electricity. Green Chemistry, 22(19), 6258-6287. doi: 10.1039/D0GC02058C

2.1 Introduction

Renewable energy sources, such as wind energy and solar power, increasingly penetrate the electrical power grid, spurring the electrification of the energy landscape [50]. However, these energy sources are fluctuating. Therefore, energy storage is required. For short-term energy storage (up to a few days), a wide range of technologies is available, including batteries and thermo-mechanical storage [51]. In contrast, chemical energy storage is one of the few alternatives for long-term, seasonal energy storage [51,52], the other main option being pumped hydropower [53]. Even though pumped hydropower may be a potential solution for low-cost energy storage in some naturally suited areas [53], the energy density of such systems is low, and pumped hydropower heavily depends on the availability of large natural water formations.

Chemical energy storage in the form of hydrogen is often proposed to solve the intermittency challenge. Hydrogen can be produced from water via electrolysis using renewable electricity, producing oxygen as a by-product. Hydrogen can be combusted to water in a fuel cell or gas turbine, producing electricity again. However, hydrogen is not easily stored over long timespans, considering the severe storage conditions. Therefore, hydrogen carriers are required and ammonia is one of the options [52,54]. Ammonia can be used for stationary energy storage, as well as for fuel applications [33,52,55]. Ammonia is a zero carbon hydrogen carrier, which can be produced from air and water. The current ammonia supply accounts for about 183 Mt per year (2020) [13].

Currently, ammonia (NH_3) is produced mostly as a synthetic fertilizer via thermochemical conversion of hydrogen (H_2) and nitrogen (N_2), which is crucial to produce sufficient food via agriculture to sustain the current world population of almost 8 billion people [3,12]. Hydrogen for this purpose is mostly produced via steam reforming of methane, contributing significantly to global warming caused by emission of CO_2.

Alternative methods to produce ammonia are being researched, both for the purpose of energy storage and/or fertilizer production by using electrical power rather than fossil energy carriers like methane. Plasma catalysis is proposed as one of the options to produce ammonia due to its ability to follow load variation of fluctuating power sources [40,44]. The goal of this Chapter is to introduce the reader to the concepts of plasma chemistry and plasma catalysis, followed by the state of the art of plasma-driven ammonia synthesis.

2.2 Plasma catalysis

Decarbonizing and decentralizing ammonia synthesis requires novel methods for the conversion of nitrogen and hydrogen. Although electrochemical (and to a lesser degree photochemical) ammonia synthesis have received substantial attention in recent years, this remains a scientific challenge. Plasma activation of the stable N_2 molecule is another alternative for electron-driven ammonia synthesis [40,41,43,44,56], inspired by the Birkeland-Eyde process of the early 20th century [4,48]. Plasma-driven conversion has also attracted

recent attention for CO_2 conversion and methane coupling [40,56,57]. In the current section, plasma technology is introduced, with a focus on nitrogen fixation to ammonia. Afterwards, reported activities, mechanisms and prospects for plasma-driven ammonia synthesis are discussed in **section 2.3**, **section 2.4**, and **section 2.5**.

2.2.1 Plasma properties

Plasma can be considered as the fourth state of matter, in which electrons, various types of ions, molecules, as well as their derived radicals and excited species show collective behaviour, which is strongly determined by the influence of electrodynamics due to the charged particles [40,41,58]. This state of matter is typically reached by adding energy to a gas. However, the transition is far more complex than the transitions between solids, liquids and gases.

Plasmas exist in a large variety. The type of plasmas used in plasma catalysis operate near room temperature up to several thousand K, and are typically partially ionized with ionization degrees of 10^{-4} to 10^{-6}. The latter type of plasmas find many industrial applications, e.g. in microelectronics, coating deposition and lighting, as well as emerging applications in green chemistry, pollution control, gas conversion and medical applications [59].

One important parameter identifying a plasma, certainly for applications of plasma catalysis as discussed in this review, is the so-called reduced electric field (E/N), i.e., the electric field strength (E, in V/m) over the total gas number density (N, in m^{-3}). E/N is mostly expressed in Townsend (Td), where 1 Td corresponds to 10^{-21} V m^2. The reduced electric field determines the electron energy distribution function (EEDF), which gives the likelihood of finding an electron with a certain energy in the plasma.

Partially ionized plasmas, generated from a gas breakdown upon application of an electric field, are classified as non-thermal plasmas, because only the electron temperature is elevated far above room temperature. Furthermore, the gas molecules in the plasma can be rotationally, vibrationally or electronically excited, and the degree of excitation can be expressed by rotational, vibrational and electronic excitation temperatures. The electronic excitation temperature is typically comparable to the electron temperature, while the gas (translational) temperature, ion temperature and rotational temperature are also typically equal to each other. The vibrational temperature, however, can be elevated in a plasma above the gas temperature, i.e., when the vibrational levels are overpopulated compared to a Boltzmann distribution at the gas temperature. It is this concept which is often exploited in gas conversion applications to increase process efficiencies and yields [40,60,61].

The various electron impact processes occurring in the plasma, and their corresponding rates, depend on the EEDF and the electron density, which in turn depend on the reduced electric field in the plasma. Next to rotational, vibrational and electronic excitation, ionization and dissociation of the gas molecules can occur as well. The fraction of electron energy lost to those various processes in an H_2:N_2=3:1 gas mixture, as a function of the

reduced electric field (bottom x-axis) and mean electron energy (top x-axis) is shown in **Figure 6**. Based on the electron impact collisions with N_2, three different plasma regimes can be identified:

- Regime I: Below 20 Td, where vibrational excitation of N_2 is dominant.
- Regime II: Between 20 and 200 Td, where electronic excitation of N_2 is most significant.
- Regime III: Above 200 Td, where ionization (mainly from N_2 ground state to N_2^+) and dissociation are the most important N_2 electron impact processes.

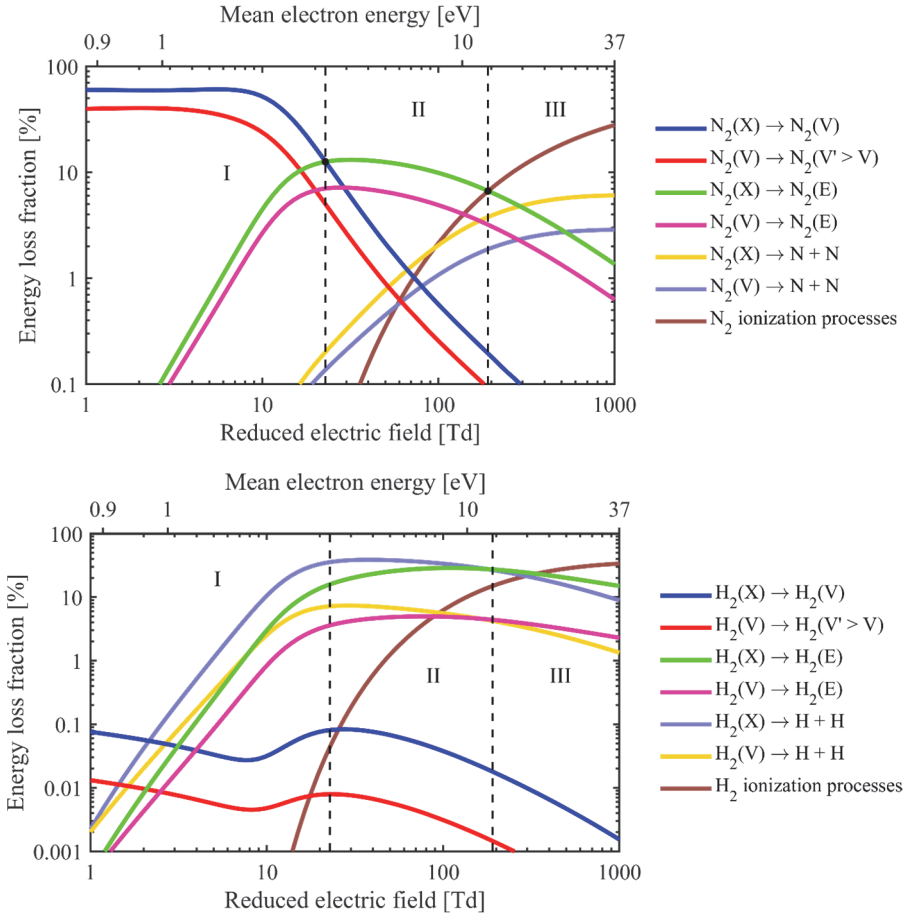

Figure 6: Fraction of electron energy transferred to various important electron impact collisions (i.e. vibrational excitation, electronic excitation, dissociation and ionization) in an H_2:N_2=3:1 mixture at 400 K and a vibrational temperature of 3000 K [49,62], as a function of the reduced electric field (bottom x-axis) and the corresponding mean electron energy (top x-axis), both for N_2 (top) and H_2 (bottom). Note the different y-axis between (top) and (bottom). The notations (X), (V) and (E) denote the ground state, vibrational levels and electronically excited levels of the molecules, respectively.

Note that **Figure 6** specifically applies to the gas mixture H_2:N_2=3:1, and to a fixed gas temperature of 400 K and vibrational temperature of 3000 K; other assumptions lead to somewhat different borders between the different regimes. Thus, **Figure 6** mainly gives an indication of the regimes.

For the sake of information, the same processes are shown in **Figure 6** for H_2. Note that vibrational excitation of H_2 has a contribution less than 0.1 %, in spite of its higher fraction in the gas mixture. On the other hand, electronic excitation and dissociation of H_2 start to be important from much lower E/N values, because the H_2 bond dissociation energy is much lower than for N_2.

2.2.2 Feedstocks

Various feedstocks have been used for plasma-driven ammonia synthesis, but most research focuses on H_2 and N_2 as feedstocks. Furthermore, various authors researched plasma-driven ammonia synthesis from CH_4 and N_2 (e.g., the feedstock for the SMR-based Haber-Bosch process) [63–66], as well as H_2O and N_2 (e.g., the feedstock for the electrolysis-based Haber-Bosch process) [67–72]. The challenge with using CH_4, and even more with using H_2O, is that the ammonia synthesis becomes endergonic. Although such a reaction can be driven by plasma, the energetically favourable reverse reaction is likely to compromise efficiency.

On the other hand, plasma technology may be a pathway to provide the energy required to form ammonia from H_2O and N_2, as the reaction is highly endothermic. Furthermore, H_2O is a sustainable H_2 source. However, a drawback of using H_2O and CH_4 as a hydrogen source is the presence of carbon or oxygen, implying that ammonia is not the only product of the reaction. In the case of CH_4 and N_2 as reactants, C≡N-compounds such as hydrogen cyanide (HCN) are potentially formed, which are extremely poisonous and flammable. For the H_2O and N_2 as feedstock, other reaction products include NO_2^-, NO_3^-, and NH_4^+ in the aqueous phase and H_2O_2, NO_X, O_3 and H_2 in the gas phase [67,68]. The lowest energy consumption reported for NH_3 from H_2O and N_2 is about 5600 GJ t-NH_3^{-1} [67], e.g. far above the theoretical minimum requirement of 18.646 GJ t-NH_3^{-1}. As follows from electrochemical ammonia synthesis, finding a catalyst selective for ammonia synthesis as compared to H_2 production is an unsolved scientific challenge [73].

2.2.3 Plasma reactors

Throughout the years, different kinds of plasmas have been studied for the plasma-catalytic synthesis of ammonia from H_2:N_2 feedstocks. In addition, N_2:H_2O non-catalytic plasma-liquid systems have recently been investigated for ammonia synthesis. The accumulation of approximate number of publications on the various plasma sources through time is shown in **Figure 7**.

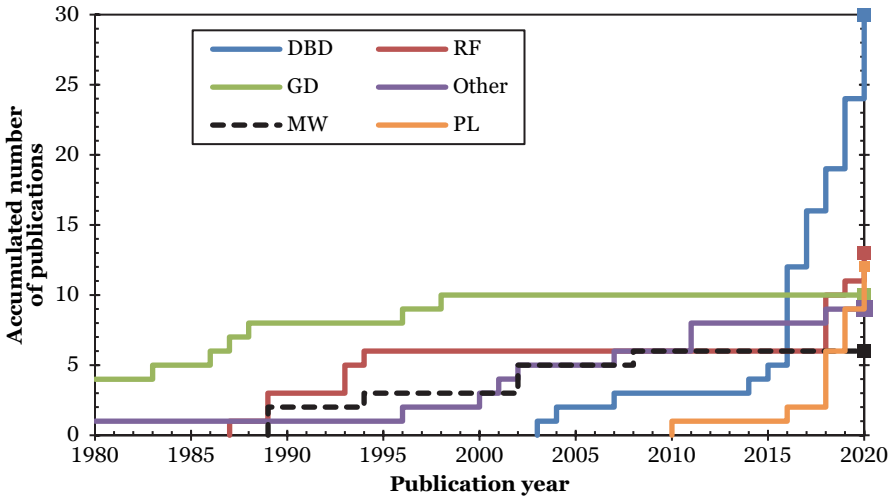

Figure 7: Approximate accumulated number of publications on ammonia formation from H_2:N_2 in the various plasma reactors studied throughout time, as well as from N_2:H_2O non-catalytic plasma-liquid systems. The listed plasma reactors are dielectric barrier discharge (DBD) [49,72,74–101]**, (low pressure) glow discharge (GD)** [102–112]**, microwave plasma (MW)** [113–118]**, (low pressure) radio frequency discharges (RF)** [113–115,119–128]**, miscellaneous plasma reactors and devices (Other)** [129–136]**, and plasma-liquid systems (PL)** [67–70,137–144]**.**

A general consideration for the material choice of the plasma reactor is the corrosive nature of ammonia. Thus, carbon-steel and Cu-containing alloys should not be used. Stainless steel equipment is used for industrial ammonia synthesis, at partial ammonia pressures of up to 75 bar. In case of plasma catalysis, partial ammonia pressures are substantially lower (typically in the order 0.01 bar). Thus, corrosion due to ammonia should not be a critical issue in plasma reactors.

Glow discharges (GDs; in direct current (DC) mode) are the simplest form of self-sustained gas discharges. They are created between two electrodes, i.e. a cathode and anode, to which a constant high potential difference is applied. Electrons are emitted from the cathode and accelerated towards the anode, causing collisions with the gas in the discharge tube. Electron impact excitation creates excited species, which emit photons upon decay to lower levels. This explains the name of these “glow” discharges. Electron impact ionization creates ions and new electrons. The combination of electron emission at the cathode and ionization in the bulk of the gas makes the discharge self-sustained. Such glow discharges are characterised by a well-defined plasma structure and the emission of light, i.e. a glow, at specific locations of the discharge. GDs can be created at low pressure, but also at atmospheric pressure.

Radio-frequency (RF) plasmas, typically operating at low pressure, and can exist in capacitively coupled (CC) or inductively coupled plasma (ICP) mode. CC RF plasmas are in their simplest form also created by applying a potential difference between two electrodes, just like in low pressure GDs. The important difference is that the potential difference is not constant (direct current, DC), but alternating current (AC), with a frequency in the RF range (typically 13.56 MHz). In ICP RF plasmas, an electric current flows through a coil, which can be wound over the plasma reactor or placed on top of it, and it induces an RF electric field in the plasma. The ions only experience a time-averaged electric field, as their characteristic plasma frequency is typically lower than the applied RF frequency, while the light electrons can follow the fluctuating electric field, so they can be more accelerated, giving rise to more electron impact (electronic) excitation, ionization and dissociation of the gas molecules. Vibrational excitation is less important, because of high values of the reduced electric field.

Microwave (MW) discharges are another type of high frequency discharge, typically operating in the GHz regime. In contrast to GDs and CC RF discharges, the plasma reactor is electrode-less, and the power to break down the gas is delivered by the microwaves. Most common is a setup where the microwaves are transferred with waveguides to a quartz discharge tube through which the gas flows, but other MW-based plasma setups are also possible [145,146]. MW discharges can operate from low pressure [145] to atmospheric pressure [146]. Upon increasing the operational pressure, the plasma becomes more thermal.

A dielectric barrier discharge (DBD) consists of two opposing electrodes with at least one electrode covered by a dielectric material (e.g., quartz or alumina). An alternating voltage is applied on the electrodes. Common voltage amplitudes are in the order of a few kV and the frequency is typically in, but not limited to, the kHz range.

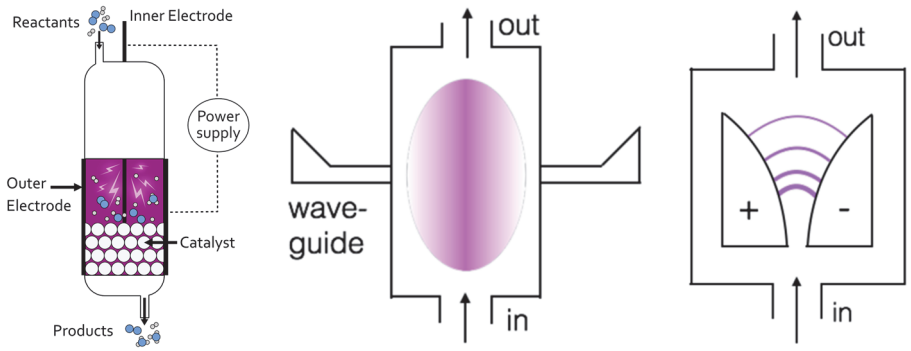

Figure 8: Various plasma reactors used for chemical conversions: dielectric barrier discharge (Left), microwave reactor (Middle), and cylindrical gliding arc (Right). Reproduced from Refs. [40,41]**.**

DBDs for gas conversion applications operate in the filamentary regime with strong, temporally and spatially isolated small discharges throughout the gaseous discharge gap. The complexity of this filamentary behaviour leads to confusing nomenclature in literature. **Section 2.2.4** provides an overview of the most common terms and the types of discharges that are observed in (packed) DBDs. In recent years, most plasma-based ammonia synthesis is performed in DBD reactors (see **Figure 7**), because they operate at atmospheric pressure, they are very flexible and easily allow the integration of catalysts. Schematics for a dielectric barrier discharge reactor, a microwave reactor, and a gliding arc reactor are shown in **Figure 8**.

Besides plasma-catalytic ammonia synthesis, carried out in the above-described gas-phase plasma reactors, ammonia synthesis has recently also been realized in plasma-liquid systems, without using catalysts. This is usually accomplished by plasma jets, as typically used for plasma medicine applications [147]. A plasma jet can operate in argon or helium, but also directly in air or N_2 gas. The plasma is created inside a tube, consisting of (usually) two electrodes, through which the gas flows. Many different designs and geometries are possible, e.g., the powered electrode can be a ring-shape, needle, etc. The counter-electrode can be a ring, but the target to be treated (e.g., liquid in this case) can also act as counter-electrode. Due to the gas flow, the plasma can exit through a nozzle, creating an effluent, or jet. The jet comes into contact with the ambient atmosphere, causing the creation of various reactive oxygen and nitrogen species, or with a more controlled environment, e.g. pure N_2, which is more interesting for ammonia synthesis. Due to the gas flow, the plasma effluent can reach the liquid, located at a distance of several mm from the tip of the plasma device, and the reactive plasma species can be transferred to the liquid phase. The reactive plasma species react with H_2O molecule forming ammonia, but also NO_3^- and NO_2^-, among others, limiting the selectivity of the ammonia synthesis.

2.2.4 Discharge types

As mentioned above, DBDs relevant for plasma catalysis (and gas conversion applications in general) operate in the filamentary regime. The plasma exhibits small discharges, or *micro-discharges*, that do not encompass the complete discharge reactor, and which are often called *filaments,* i.e. thin conducting wires. Sometimes they are also called *streamers*. However, streamer discharges are not specific to occur in DBD systems alone [148,149]. Wang et al. [150] also described a micro-discharge between two packing beads as a *local discharge*, while Kim et al. [151–154] used the term *partial discharges* after Mizuno et al. [155], and Butterworth et al. [156] used the term *point-to-point discharges*.

Surface streamers, *surface discharges* or *surface ionization waves* are terms used for micro-discharges that are observed after a streamer or filament reaches a surface, such as a packing bead. Once the micro-discharge reaches the surface, the discharge continues in a lateral expansion across the surface. This lateral expansion is facilitated by strong electric fields and the ionization processes taking place in the growth direction of the discharge [157,158].

An *afterglow* normally describes the effluent of a plasma reactor. However, the term is sometimes used more broadly to indicate that (plasma) species are no longer exposed to plasma conditions corresponding to micro-discharges. Liu et al. [159] described those two usages as a spatial and temporal definition, respectively.

Homogeneous plasma or *uniform plasma* are terms that have been seen in relation to the filamentary regime of DBDs. This can be confusing because a DBD can operate in either a homogenous or in a filamentary regime. Still, the filamentary plasmas have been described as becoming more uniform, or more homogeneous when a packing is introduced [79]. In addition, such a description has been used when the micro-discharges are still present, but of lower importance [87].

Partial surface discharging, as used by Peeters et al. [160] refers to the fact that not the whole surface area of the electrodes in a DBD reactor has to actively contribute to the discharge. This is due to the charge deposited on the electrode or dielectric surfaces being non-uniform or spatially isolated, due to the overall discharge consisting of small micro-discharges. This influences some electrical characteristics of the DBD [160]. This effect is generally important in packed bed DBDs due to the obstructions in the plasma.

2.2.5 Coupling of plasma and catalyst

Coupling plasma and catalysis is complex. Previously, such mutual influences of the plasma and the catalyst were extensively discussed by Neyts et al. [56,161,162] and Kim et al. [152]. Recent modelling investigations and characterization have provided novel insights [163,164]. This subsection sets the stage for the assessment of plasma-catalytic ammonia synthesis.

Plasma-catalytic reactors are classified as *in-plasma* catalysis reactors or *post-plasma* catalysis reactors [42,152]. In case of in-plasma catalytic reactors, also termed plasma-driven catalytic reactors, the plasma and the catalyst are located in the same position in the reactor [152]. In case of post-plasma catalytic reactors, also termed plasma-assisted catalytic reactors, the plasma generation and the catalyst bed are separated in space [152]. While in-plasma catalysis can be used to activate short-lived plasma-activated species over a catalyst, post-plasma catalysis is only relevant for long-lived species [152]. Thus, plasma catalysis can benefit from the mutual influence of the plasma and the catalyst on one another.

2.2.5.1 Synergy and mutual influence

Plasma catalysis sometimes leads to synergistic effects, in which the result of combining the plasma and the catalyst is larger than the sum of the individual contributions of the plasma and the catalyst [165]. Synergy may be defined in terms of conversion, reaction rate or selectivity. It should be noted that in the case of ammonia synthesis, selectivity is not relevant because there are no by-products for a hydrogen and nitrogen feedstock. However, plasma-catalyst interactions and synergies thereof are not trivial to uncover, as

the underlying principles of plasma catalysis are not fully understood [164,166,167]. Various possible plasma-catalyst interactions have been proposed for ammonia synthesis, as shown in **Figure 9**.

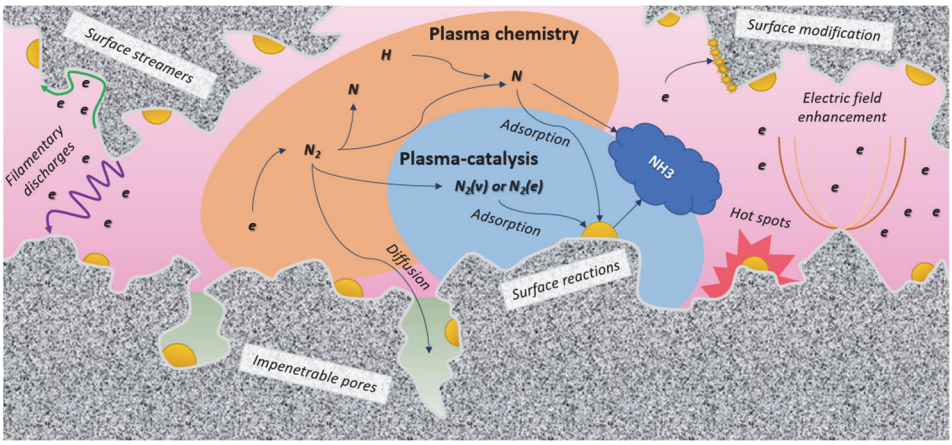

Figure 9: Plasma-catalyst interactions. Inspired by Ref. [161].

A multidisciplinary approach is required to understand the mutual influence of the plasma and the catalyst [152], covering various time-scales and length-scales [42,164,168,169]. So far, most information is obtained by macroscopic performance testing of plasma catalysis reactors. Van Durme et al. [170] were the first to systematically categorize the mutual influence of a plasma and a catalyst, a topic heavily discussed thereafter [56,152,161,162,164,166,167]. Possible mutual influences of a plasma and a catalyst have been reviewed by Kim et al. [152], Neyts et al. [56,161,162] and Whitehead [164,166,167]. The complexity is even more severe, as any change in the catalyst will induce changes in the plasma, which again influence the catalyst. Thus, effects in plasma-catalytic interactions can generally not be isolated [167,171].

The various species present in the plasma environment include electrons, positive and negative ions, photons, radicals, and neutral atoms and molecules in ground state or excited in vibrational or electronic modes [42]. These species may interact with the catalyst in various manners, and catalyst may influence the conversion of N_2 and/or H_2 in the presence of a plasma in three manners, namely (1) by modifying the plasma characteristics, (2) by exploiting the radicals from the plasma environment for reaction pathways other than simple recombination, or (3) via surface reactions of plasma-activated species on the catalyst surface.

The first mechanism, i.e. modifying the plasma characteristics, may influence the plasma chemistry far from the surface, when the catalyst is applied on dielectric packing material. A commonly encountered effect is the electric field enhancement and consequently a decreased plasma onset voltage, as was substantiated by simulations [163,172–174]. The electric field enhancement will also enhance the electron temperature [163,172–174], which

may shift the importance of various electron impact reactions, and thus affect the plasma chemistry. In addition, micro-discharges may form on the surface of the catalytic packing, or even the discharge may entirely move from the gas phase to the catalyst surface, depending on the dielectric constant of the packing beads [150,166].

The second mechanism, i.e. exploiting the plasma radicals for reactions other than recombination, proceeds via facile adsorption on catalyst surfaces [42], without any barrier. In case of noble metals, all further reactions proceeding on the catalyst surface are downhill and the surface has either limited or no activating effect on the hydrogenation reactions. On the other hand, surface reactions can have a strong effect on the dominant reaction pathways and thus on the product distribution. This can even lead to increased conversion when the surface indeed favours reaction pathways to products over recombination reactions, e.g. the latter forming back the reactants. The production of radicals and ions may also open alternative surface reaction pathways [161,175], that are not accessible in thermal catalysis. It should also be noted that radicals and ions in the plasma may react on the surface with other surface species which are formed via dissociative adsorption of non-activated molecules. This mechanism is discussed in more detail in **section 2.4.2**.

The third mechanism, i.e. surface reactions of plasma-activated species, is complex and often not well understood. Dissociative chemisorption can be enhanced via vibrational or electronic excitation of a molecule [41,176], decreasing the apparent activation barrier and increasing the reaction rate in case the dissociative adsorption step is rate limiting in thermal catalysis [94,177]. A recent study also showed that vibrational excitation could enhance Eley-Rideal reactions of molecular species [178]. Such reactions are typically negligible under thermal conditions and it is not fully understood to what extent they contribute to the total conversion under plasma conditions. However, Engelmann et al. [179,180] and Yamijala et al. [181] proposed that Eley-Rideal mechanisms can be dominant plasma-catalytic ammonia synthesis at high plasma powers, which is discussed in **Chapter 6**. These mechanisms and how they impact the total conversion and energy efficiency will be discussed in more detail in **section 2.4.3**.

Besides effects from the presence of reactive plasma species, the surface properties of the catalyst such as the work function and consequently the activity of the surface might be altered due to the presence of plasma, e.g. by the electric fields or surface charging [182–184]. The role of electric fields and surface charging are discussed in **Chapter 4**. Physical modifications of the catalyst surface may also occur due to bombardment with energetic plasma species, causing reduction of the catalyst, coke formation, changes in the physicochemical properties of the catalyst (such as the catalyst work function), and the formation of hot spots. Furthermore, it was reported that surface cracking and peeling of metal nanoparticles can occur in DBD reactors [185]. Similarly, changes in the surface morphology of a metal oxide catalyst after plasma treatment were reported after plasma-illumination in a DBD reactor [186].

A pre-requisite for effective interaction between the plasma and the catalyst is that the plasma-activated species reach the catalytic surface before recombining or decaying to the ground state molecules [166]. Plasma-activated species have a limited lifetime, and thus a limited traveling distance by diffusion, before recombining into neutral molecules, or decaying to the ground state [152]. A direct interaction between the plasma and the catalyst surface is attained when the distance between the plasma and the catalyst surface is smaller than the maximum traveling distance of plasma-activated species [152]. This is especially relevant when the catalyst is porous, as shown in **Figure 9**. Large pores allow the generation of plasma inside the pores, but this is only possible for pores in the (sub-)micron range [163,187–189]. Indeed, a prerequisite is that the pore size must be larger than the Debye length, which is defined by the electron density and temperature in the plasma. In helium, characterized by homogenous plasma, computer simulations revealed that plasma can only be formed in pores with diameters typically above 10 μm [188,190,191]. On the other hand, molecular plasmas typically exhibit streamers, with higher electron density and smaller Debye length. Hence, computer modelling predicts that plasma streamers can propagate in pores of several hundreds of nm diameter, depending on the applied voltage [189,192]. It should be noted that the majority of the pores in a typical support material are smaller than 50 nm. Therefore, only plasma-activated species with a sufficiently long lifetime can penetrate into the pores, while most other species recombine or decay to the ground state before reaching the active catalyst surface within the pores. Thus, the contribution of the external surface area is likely dominant in most cases.

2.2.5.2 Catalyst selection considerations

Depending on the plasma conditions and the chosen catalyst material, different plasma-activated species can determine the catalytic reactions (see **Figure 6**). In order to optimize the plasma-catalyst synergy, it is crucial to couple the right catalyst to the right plasma.

In plasmas with a low degree of dissociation and a high degree of excitation (vibrational or electronic), plasma-activation is used to decrease the operating temperature for processes that are limited by dissociative adsorption. Typically, the optimal active metal is a more noble metal than the optimum for thermal catalysis, which desorbs reaction products easily and thus the operating temperature can be low. Dissociative adsorption of reactants is usually limiting the reaction rate for noble metals. Part of the activation barrier of dissociative adsorption may be overcome through vibrational or electronic excitation of molecules, explaining the plasma-enhanced catalytic activity over a noble metal. The catalyst still has an activating role in this case, as N_2 is not fully dissociated in the plasma environment (see **Chapter 3**). Apart from metallic catalysts, metal nitrides have also been reported for ammonia synthesis [193,194]. Plasma-activation of metals with nitrogen plasmas may yield metal nitride catalysts [195,196].

In plasmas with a higher degree of dissociation, the ideal catalysts will usually be very different from those used in thermal catalysis. Plasma-generated radicals do not need to be dissociated over a surface, as dissociation already occurs in the plasma. Thus, the surface influences recombination reactions, as well as consecutive reactions with H atoms on the catalyst surface. Plasma activation of reactants via formation of radicals often opens pathways that are thermodynamically impossible for ground state reactants; in that case the use of traditional catalysts is likely to be counterproductive as these will catalyse the reverse reaction, back to reactants. Several materials may enhance reaction pathways, such as consecutive reactions with H atoms forming ammonia, instead of recombination of radicals to N_2. Transition metals may be used to hydrogenate the adsorbed NH_x (x=0-2) radicals. For these catalysts, efficient plasma-activation of reactants towards radicals is required [197]. Therefore, the choice of the catalyst is less determined by chemical properties and more by properties influencing the discharge characteristics (e.g. dielectric properties and morphology), thereby influencing the plasma-phase dissociation of activated molecules. A method to modify the plasma by radicals was proposed by Akay et al. [75,92,198], who used a mix of a dielectric material with a supported transition metal catalyst in the plasma reactor. The dielectric material acts as a plasma catalyst promoter (PCP), which modifies the plasma characteristics, whereas the transition metal catalyst performs the catalytic function.

Apart from the choice of the active metal, the choice of the support and promoter composition affect the activity in some cases [94]. As plasmas can only be generated in (sub)-micron pores, oxides with highly porous structures with pore sizes below 1 μm and large internal surface areas are not beneficial for maximum interaction between the active metal catalyst and the plasma (see **Figure 9**) [163]. This is very different form thermal catalysis, requiring an as high as possible active surface area and therefore support materials with high surface area, in order to maximize the productivity per unit of volume of chemical reactors.

2.3 Assessment of plasma-driven ammonia synthesis

This section provides an overview of the most significant developments in plasma-driven ammonia synthesis, with a focus on the coupling between fundamentals from heterogeneous catalysis and plasma catalysis. This forms a framework for plasma-driven ammonia synthesis, and the mechanisms involved. Extensive historical accounts can be found in other reviews [42,58,71,199,200]. The aim of this section is to show how recent insights in mechanisms can aid in the development of the field. The energy efficiency and conversion for various plasma reactor types are compared, describing the state of the art. The discussion on the mechanisms and catalyst selection is coupled with the energy efficiency.

2.3.1 Performance in various types of plasma reactors

Plasma-driven ammonia synthesis was first independently reported by Morren and Perrot in a DBD reactor in 1859 [201], two years after the first report of plasma-driven conversions with a DBD reactor by Werner von Siemens [202]. In the late 19th century, various authors attempted plasma-driven ammonia synthesis, among whom Berthelot [201]. Furthermore, ammonia was first synthesized in a glow discharge by Donkin in 1973 [203]. In general, however, plasma-driven ammonia synthesis was sporadically researched until the 1980s [201,204,205]. Between 1980 and 2000, low pressure glow discharges (LPGDs) received significant attention [102–104,106–115,206–211]. In these publications, the surface (both catalytic and non-catalytic) was often related to the ammonia formation. Ions, more specifically N_2^+ and N_2H^+, were often mentioned to play an important role in the formation of ammonia. Nowadays, atmospheric pressure DBDs are studied most, although some papers also describe low pressure MW and RF discharges [113–115,119–122,125–127].

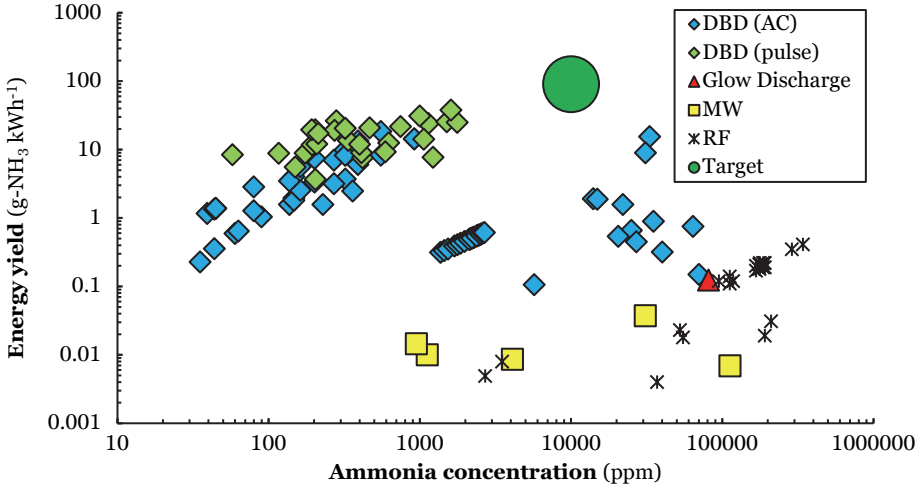

Figure 10: Reported energy yield vs. ammonia concentration. Constructed and extended from [94]. Original references: DBD (AC) [74–76,82,88–90,93,95,97–99,212,213], DBD (pulse) [81,89], Glow Discharge [107], MW [118,214,215] and RF [114,119,122,123,125–127]. In some cases, the reported units have been converted to g-NH_3 kWh^{-1} for the energy yield, and ppm for the ammonia concentration. The reader is referred to the recent review of Carreon [199] for the reported energy efficiency for specific metals.

A summary of quantified plasma-driven conversions to ammonia in various plasma reactors under a wide variety of conditions is shown in **Figure 10**. An energy yield of 100-200 g-NH_3 kWh^{-1} is required to be competitive with alternative technologies for small-scale ammonia synthesis [42,216], as discussed in **Chapter 8**. Furthermore, an ammonia concentration of at least 1.0 mol.% (10,000 ppm) is required to minimize the energy cost of separation and recycling in case of an atmospheric synthesis loop [21], as an ammonia partial pressure of 0.01 bar is required for effective ammonia removal with solid sorbents

[217–220]. Low pressure plasma reactors such as MW and RF plasmas require a near complete conversion at an energy yield of 100-200 g-NH_3 kWh^{-1}, because separation of ammonia is not feasible. The highest energy yield reported so far is 37.9 g-NH_3 kWh^{-1} for a DBD plasma [89], e.g. below the required benchmark of 100-200 g-NH_3 kWh^{-1}. Hereafter, plasma reactors for ammonia synthesis from H_2 and N_2 are discussed.

2.3.1.1 DBD reactors

Most literature is available for plasma-driven ammonia synthesis in a DBD reactor. Already in 1859, Morren and Perrot reported experiments with a DBD reactor [201]. Modern attempts at plasma-driven ammonia synthesis in DBD reactors date from the 1950s, 1960s and beyond [204,205]. Especially since 2000, research on plasma-catalytic ammonia synthesis is mostly performed in DBD reactors [58,199,200]. Various reactor configurations without and with packed bed have been attempted. An overview of the energy yield versus ammonia concentration for various packing materials is shown in **Figure 11**.

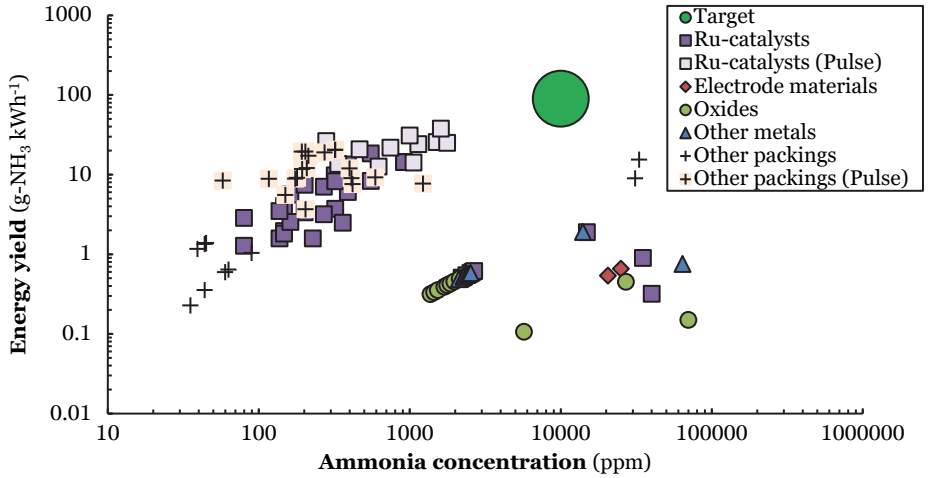

Figure 11: Reported energy yield vs. ammonia concentration for DBD reactors (AC and Pulse). Constructed and extended from Ref. [94]. Original references: DBD (AC) [74–76,82,88–90,93,95,97–99,212,213], DBD (pulse) [81,89].

Electrode materials

Various authors have researched either ammonia synthesis, or ammonia decomposition, with various electrode materials [76,101,107,205,221]. Iwamoto et al. [76] attributed a trend in ammonia synthesis rate for wool-like electrodes to the binding strength of N_{ads} on the metal surface. On the other hand, Yin et al. [107] reported that the ammonia yield increases with increasing electron work function of the electrode material. An increased electron work function implies that the electrons released upon discharging have a higher energy, making dissociation of N_2 in the gas phase more likely.

Oxides

A drawback of a DBD reactor without a packing is the high ratio between plasma volume and surface area for catalytic reactions. Therefore, most authors introduced packing materials, such as oxides [78,84–86,91,97,131,222], dielectric materials [85,90,97,100], and ferro-electrics [98]. Introducing a packing material can lower the discharge power required to ignite the plasma. Furthermore, the presence of a packing material can alter the plasma discharge characteristics [85,100]. Surface functionalization of the oxide can also alter the plasma discharge characteristics [100]. The capacitive and discharge regimes can be modified by the dielectric constant of the material [85].

Ru-based catalysts

The presence of supported metal particles may introduce hydrogenation sites for atomic nitrogen and/or molecular N_2. Ru-catalysts have been studied most among supported metal catalysts [42,49,74,82,83,89,93–96,99,223]. Ru-catalysts are known to have a high activity for ammonia synthesis under mild conditions [224,225]. The rate-limiting step for thermal-catalytic ammonia synthesis over Ru-catalysts is usually the dissociation of N_2 [225]. Ru-catalysts were first used in a membrane-like DBD reactor by Mizushima et al. [95,96]. Afterwards, various authors attempted to disentangle the complexity of reactions in plasma-driven ammonia synthesis in a DBD reactor packed with Ru-catalysts [42,74,82,83,89,93,94,99,223].

In order to distinguish between the rate of homogenous plasma-chemical ammonia synthesis, and the rate of heterogeneous plasma-catalytic ammonia synthesis over the Ru-catalyst, it is important that the rate in a DBD reactor packed with the bare support is low, as discussed in **Chapter 5**. For this reason, various authors reported conversions for the bare support, as well as the supported Ru-catalysts (sometimes with promoters) [74,99,223]. Furthermore, various authors reported that the ammonia synthesis rate depends on the temperature [42,89,94,223]. Catalytic hydrogenation of nitrogen is possible only at sufficient high temperature, allowing for ammonia desorption. Below this onset temperature, plasma-driven ammonia synthesis must be attributed to plasma chemistry rather than catalysis [223].

Various authors introduced alkali promoters [74,89,94,99], which are known to enhance N_2 dissociation by lowering the N_2 dissociation barrier, as well as to enhance ammonia desorption for thermal-catalytic ammonia synthesis [225–229]. The highest reported energy yield for such a system is 37.9 g-NH_3 kWh^{-1} [89], which is overall the highest reported energy yield to date (see **Figure 11**). In case of plasma catalysis with molecular plasma-activated N_2, promoters can enhance the N_2 dissociation rate and thereby the ammonia synthesis rate [94]. However, in case the reaction proceeds via adsorption of NH_X (x=0-2) radicals, the introduction of alkali promoters does not influence the conversion, apart from less desorption limitation of ammonia in the low temperature regime [223].

Other metal catalysts

Next to Ru-based catalysts, other supported metal catalysts were tested for plasma-catalytic ammonia synthesis (and ammonia decomposition) [49,75,79,80,82,92,212,213,215,221,230–235]. In most cases, supported Co, Ni, and Rh catalysts are found to be most active among the tested catalysts [49,79,82,212,213]. Such metals have less ammonia desorption limitations than the classical Fe and Ru catalysts for thermal-catalytic ammonia synthesis. Mehta et al. [49,236] proposed that plasma-activation of N_2 via vibrational excitation leads to a lower barrier for N_2 dissociation, resulting in an enhancement for late-transition metals which are typically rate-limited by N_2 dissociation. On the other hand, Wang et al. [79] proposed that the introduction of metal nanoparticles on γ-Al_2O_3 changes the acid site strength, and thereby the ammonia synthesis rate on γ-Al_2O_3 acid sites. Herrera et al. [80] reported that the introduction of metal nanoparticles on γ-Al_2O_3 has a statistically insignificant difference in macroscopic discharge characteristics in the charge voltage characteristics compared to bare γ-Al_2O_3. Akay et al. [75,92] reported increased ammonia yield on introduction of dielectric materials in a physical mixture with supported Co and Ni catalysts, altering the plasma discharge characteristics.

Other packings

Solid sorbents have also been used for plasma-driven ammonia synthesis [81,88]. The ammonia is removed *in situ*, lowering the ammonia content in the plasma zone, thereby increasing the chance of activating the H_2 and N_2 reactants rather than the ammonia product. Metal halides, such as $MgCl_2$, can absorb ammonia in a solid solution, forming $Mg(NH_3)_xCl_2$ [237]. Peng et al. [81] reported an energy yield of 20.5 g-NH_3 kWh^{-1} in the presence of a $MgCl_2$ sorbent. However, from XRD it was confirmed that Mg_3N_2 was primarily formed, rather than $Mg(NH_3)_xCl_2$. Zeolites are also proposed as a solid sorbent for ammonia [218,238,239]. Shah et al. [88] reported an ammonia concentration of 3.3% at 15.5 g-NH_3 kWh^{-1} energy yield in the presence of zeolite 5A, which is among the highest energy yields reported so far and the only reported energy yield above 10 g-NH_3 kWh^{-1} in combination with an ammonia concentration above 1.0% (see **Figure 11**). Plasma-based ammonia synthesis with *in situ* adsorption on a zeolite is also discussed in **Chapter 7**. A chemical looping system based on MgO and Mg_3N_2 was also proposed by Zen et al. [240,241]. Membrane reactors have also been proposed to either remove the ammonia or to feed the H_2 from the other side of the membrane [95,96,242].

2.3.1.2 Radiofrequency plasma reactors

Reactors operating under radiofrequency (RF) plasma excitation have been researched to a lesser extent, as compared to DBD reactors [199], but have recently gained substantial attention in several research groups [119–121,125–128,243]. In the late 1980s and early 1990s, Uyama et al. and Tanaka et al. used zeolite [114,122] as well as Fe [115,123] and Mo [115] wires as catalyst in the downstream of their low pressure (650 Pa) RF plasma apparatus. Fe catalysts resulted in the highest product yield. They are the only authors to report the

formation of both ammonia and hydrazine [114,115,123] and speculated that the H and NH_x radicals formed in the discharge are the main adsorbates [115].

Recently, Ben Yaala et al. [120,128] placed W and stainless steel catalysts in their low pressure (2 Pa) RF plasma reactor. They reported the thermal decomposition of ammonia at high temperature (above 830 K on W) and the creation of stables nitrides (starting at 650 K on stainless steel), inhibiting ammonia formation [120].

Shah et al. [119,125–127] placed a catalyst bed very close to the plasma electrodes in a low pressure (40 Pa) RF plasma setup. They studied various transition metal-based catalysts [119,126], Ga alloys [119,127] and a Ni-MOF (metal organic framework) [125]. Among the metals, Ni and Sn based catalysts were most active [119]. The Ni-MOF performed better than pure Ni, which was attributed to a higher porosity [125]. Ga alloys, both Ga-In [119,127] and Ga-Pd [119], gave the best results [127]. The ammonia synthesis rate was directly correlated to the H atom radical density [121,127]. Shah et al. [126] also reported on modelling work, from which the mechanism for plasma-catalytic ammonia synthesis in RF reactors was disentangled. Both N_2 and H_2 dissociate in the plasma, after which N adsorbs on the surface. Subsequently, the adsorbed N atoms are hydrogenated by H atoms on the surface or in the gas phase, e.g. the model revealed that both Langmuir-Hinshelwood reactions and Eley-Rideal reactions play a role [126].

2.3.1.3 Microwave plasma reactors

Low pressure (60-600 Pa) plasmas ignited with microwaves (MWs, i.e., GHz frequency range) have received considerably less attention for ammonia synthesis compared to both RF discharges and DBDs [199]. Uyama et al. [113–115,124] studied MW plasmas with catalyst downstream. They found the performance of their MW plasma to be superior to their RF discharge [114,115]. Unlike the RF discharge, there was no significant hydrazine yield. This was attributed to a difference in plasma radicals created in the discharge. The RF discharge caused the adsorption of H and NH_x radicals, while the MW plasma caused the adsorption of N radicals [115]. Kiyooka et al. [130] explored an electron cyclotron resonance plasma, which also operates within a GHz frequency range and at low pressure (600 Pa). They found that N and NH radicals adsorb onto the stainless steel reactor walls and report further hydrogenation on the surface due to H radicals in the plasma (i.e., Eley-Rideal mechanism) until the desorption of ammonia [130].

Siemsen [215] performed experiments and simulations for a MW plasma reactor with downstream Rh catalyst bed. Due to the long distance between MW plasma and catalyst, the excited N_2 molecules do not reach the catalytic surface, and only atomic radicals remain. Simulations revealed that the atoms account for the formed ammonia. Ammonia was not formed without catalyst [215]. Jauberteau et al. [116] report that the adsorption of NH onto the stainless steel reactor walls is the first reaction step towards ammonia, from which either ammonia or adsorbed NH_2 is formed.

To date, only two studies considered ammonia synthesis in atmospheric pressure MW plasmas [118,214], despite the more beneficial process conditions for industrial application. However, the highest energy yields, 0.4 g-NH_3 kWh^{-1} (see **Figure 10**), have been reported for pressures as low as 10-4 bar. In addition, the reported energy yields of MW plasma reactors are orders of magnitude lower than for DBD reactors (see **Figure 10**). The reason may be that the temperatures, even downstream in the afterglow of a MW plasma, are too high for adsorption on a catalyst surface, due to (i) catalytic stability problems, but also (ii) a fundamental limitation, because adsorption always leads to loss in entropy and therefore is exothermic, implying that the equilibrium is unfavourable at very high temperatures.

2.3.1.4 Glow discharges

Various authors have researched glow discharges for ammonia synthesis over the past one and a half centuries [102,103,106–110,203,244–246]. Donkin [203] reported ammonia synthesis in glow discharges as early as 1873, after which Brewer et al. [102,103,245] published more systematic studies with a batch process in 1929 and 1930. Most research has been conducted on low-pressure glow discharges (LPGDs). In 1968 and 1969, Eremin et al. [244,246] considered that the wall may have an effect for ammonia synthesis, and they were the first to deliberately add catalytic materials on the reactor wall. From 1980 onward, various authors investigated a wide range of transition metals, alloys and metal oxides [106–109,247]. Coupling plasma with catalysts is possible in glow discharges, both in a packed bed, and on the walls of the reactor or the electrode.

The mechanism for ammonia synthesis from H_2 and N_2 in glow discharges has been debated over the years. Brewer et al. [102] proposed that ammonia is primarily formed in the plasma phase. On the other hand, Eremin et al. [244,246] and Venugopalan et al. [106,107,109] proposed that ammonia is primarily formed on the reactor wall, which acts as a catalytic surface, as substantiated by experimental data. Venugopalan et al. [106,107,109] and Sugiyama et al. [108] proposed that N atoms are the relevant species for ammonia formation, rather than plasma-activated molecular N_2 species.

2.3.1.5 Arc discharges

Arc reactors such as static arc discharges and gliding arc reactors can also be used for ammonia synthesis, inspired by the commercial Birkeland-Eyde process for NO_X production [11,48]. An advantage of gliding arcs is the scalability [213]. However, research conducted on ammonia synthesis in this type of reactor is limited [129,133,134,248,249]. Brewer et al. [129] first published on the application of low voltage arcs for ammonia synthesis in 1931. A detailed study on ammonia synthesis in an arc plasma was conducted by van Helden et al. [133,134]. Implementing catalysts in arc reactors, for in-plasma catalysis, is not feasible, due to the excessive temperatures. However, post-plasma catalysis is possible, as demonstrated for other reactions, but has not yet been explored for ammonia synthesis in this type of plasma reactors [152].

2.3.1.6 Plasma-liquid systems

Besides plasma-catalytic ammonia synthesis, ammonia has recently also been generated in plasma-liquid systems, albeit without using catalysts. In 2010, Kubota et al. [144] first reported ammonia synthesis in a plasma-liquid system. It is obvious that using H_2O as a feedstock is more energy demanding than H_2 [250]. On the other hand, these very simple plasma setups allow the immediate accumulation and potential storage of ammonia in H_2O, the most benign solvent.

A combined plasma-electrolytic system was proposed for ammonia formation from H, generated from either H_2O molecules or H^+ ions, by Kumari et al. [139], Hawtof et al. [69], Haruyama et al. [137,140–143] and Peng et al. [68,70]. Ammonia was formed by direct interaction of air or N_2 plasma with H_2O, allowing simpler reactors, i.e., no need for counter electrodes in liquids and additional electrolysis. Gorbanev et al. [67] used an atmospheric pressure plasma jet with N_2 containing H_2O vapour, in contact with liquid H_2O. The system offers a selectivity to ammonia of up to 96%, at energy yields up to 0.65 g-NH_3 kWh^{-1} [67]. Experiments without direct plasma-liquid interaction and with isotopically labelled water revealed the major role of H_2O vapour in the feed gas, rather than liquid H_2O, as H-source for the ammonia synthesis [67]. There was some interaction of plasma effluent with the plasma-exposed liquid H_2O, but the latter decreased dramatically when H_2O vapour was introduced in the N_2 feed gas [67].

2.4 Mechanisms for plasma-driven ammonia synthesis

Various mechanisms are conceivable for plasma-driven ammonia synthesis, in the absence and in the presence of a catalyst. A distinction is made between plasma chemistry pathways with N atoms generated in the plasma, either reacting in the plasma phase or over the catalytic surface [77,126], and the catalytic dissociation of excited nitrogen molecules [49,94]. This distinction is made to assess the role of the catalyst. The energy requirement of various pathways is assessed, from which it is suggested that only dissociation over a catalyst (and not beforehand in the plasma phase) has the potential to become sufficiently energy efficient for practical applications. Plasma chemistry mechanisms with experimental validation are discussed. The optimal H_2:N_2 ratio for various mechanisms is discussed from both plasma chemistry and heterogeneous catalysis perspectives.

2.4.1 Plasma phase ammonia synthesis

The plasma phase ammonia synthesis is defined by the conversion taking place in the bulk plasma, away from the surface. In this case, the packing material does not behave as a catalyst (i.e., actively contributing to the conversion process), and merely alters plasma characteristics and flow patterns in the reactor. The ammonia is formed through hydrogenation of nitrogen dissociated by the plasma.

In practice, plasma phase ammonia synthesis is difficult to disentangle from reactions on a surface, as even in the absence of packing material, the reactor walls may play a role in converting plasma-generated species on the wall.

Table 1: Energy requirements for various plasma-activations of N_2 and H_2. Partially adapted from Ref. [58].

	Reaction	N_2/H_2-based kJ mol^{-1} (eV)	NH_3-based MJ kg^{-1}	kWh kg^{-1}	g kWh^{-1}
Dissociation					
N_2 dissociation	$N_2 + e \rightarrow 2N + e$	945 (9.79)	27.7	7.7	129.8
H_2 dissociation	$H_2 + e \rightarrow 2H + e$	436 (4.52)	38.4	10.7	93.7
N_2 & H_2 dissociation			**66.1**	**18.4**	**54.4**
Ionization					
N_2 ionization	$N_2 + e \rightarrow N_2^+ + e$	1505 (15.6)	44.2	12.3	81.5
H_2 ionization	$H_2 + e \rightarrow H_2^+ + e$	1485 (15.4)	130.8	36.3	27.5
N_2 & H_2 ionization			**175.0**	**48.6**	**20.6**
Excitation					
N_2 vibrational excitation	$N_2(X) \rightarrow N_2(v1)$	28.0 (0.29)	0.8	0.2	-
N_2 electronic excitation	$N_2(X) \rightarrow N_2(A3)$	595.1 (6.17)	17.5	4.9	-

Even though ammonia synthesis is exergonic at ambient conditions [227], the reaction does not proceed spontaneously. Both the bonds in molecular hydrogen and molecular nitrogen need to be ruptured for ammonia formation in the gas phase. This can be accomplished by high-energy electrons in the plasma, but at the same time, these high input powers do not only affect the N_2 molecules but can also decompose the produced ammonia. The minimum energy requirement for ammonia formation from plasma chemistry is 66.1 MJ kg-NH_3^{-1} (equivalent to 54.4 g-NH_3 kWh^{-1}), which is due to the energy required for rupturing the N_2 and H_2 bonds by the plasma (27.7 MJ kg-NH_3^{-1} and 38.4 MJ kg-NH_3^{-1}, respectively, see **Table 1**). As discussed in **section 2.3.1**, the energy yield of 54.4 g-NH_3 kWh^{-1} is too low for practical applications. This clearly shows the need for a catalyst. As shown in **Table 1**, only partial activation of N_2 by vibrational or electronic excitation may allow for a sufficiently energy requirement. In this case, both the plasma and the catalyst have a role in the N_2 dissociation reaction (see **section 2.4.3**).

2.4.2 Surface-enhanced plasma-driven ammonia synthesis

In the presence of a surface, ammonia may be produced from molecular N_2 and H_2, or from plasma-generated radicals, depending on the plasma conditions and the catalytic properties of the material at a given temperature and pressure. In the current section, the conversion of plasma-generated radicals to ammonia over a catalyst is discussed, which is coined *surface-enhanced plasma-driven ammonia synthesis* (SEPDAS) [94]. In **section**

2.4.3, the conversion of plasma-activated molecular N_2 to ammonia over a catalyst is discussed, which is coined *plasma-enhanced catalytic ammonia synthesis* (PECAS) [94].

Table 2: Possible surface reactions for surface-enhanced plasma-driven ammonia synthesis (SEPDAS) and plasma-enhanced catalytic ammonia synthesis (PECAS). The * denotes an adsorption site on the catalyst.

	Reaction	Note
Hydrogen adsorption	$H_2 + 2* \rightleftharpoons 2H*$ $H + * \rightleftharpoons H*$	
Nitrogen adsorption	$N_2 + 2* \rightleftharpoons 2N*$ $N + * \rightleftharpoons N*$	Dominant for PECAS Relevant for SEPDAS
NH_X adsorption	$NH + * \rightleftharpoons NH*$ $NH_2 + * \rightleftharpoons NH_2*$	Relevant for SEPDAS
NH_3 desorption	$NH_3* \rightleftharpoons NH_3 + *$	
Surface hydrogenation reactions	$N* + H* \rightleftharpoons NH* + *$ $NH* + H* \rightleftharpoons NH_2* + *$ $NH_2* + H* \rightleftharpoons NH_3* + *$	
Eley-Rideal-reactions	$N* + H \rightleftharpoons NH*$ $NH* + H \rightleftharpoons NH_2*$ $NH_2* + H \rightleftharpoons NH_3*$ $H* + N \rightleftharpoons NH*$ $H* + NH \rightleftharpoons NH_2*$ $H* + NH_2 \rightleftharpoons NH_3*$	Dominant for SEPDAS, see **Chapter 6**

If plasma-generated radicals adsorb on the catalyst surface, they can react to form ammonia. However, N, NH, and NH_2 radicals can also recombine to N_2 and H_2. The rate of ammonia synthesis versus recombination reactions towards H_2 and N_2 depends on the barriers of the relevant surface reactions on the catalyst surfaces. The number of possible surface reactions is much greater than the reactions possible for thermal catalysis, as these also include the reactions of all the different unique species generated in the plasma. The possible surface reactions in case of surface-enhanced plasma-driven ammonia synthesis are listed in **Table 2**.

It should be noted that this scheme presents a case of the second mechanism explained in **section 2.4**, i.e. exploiting the plasma radicals for surface reactions other than recombination. Engelmann et al. [179] developed a microkinetic model for plasma-catalytic ammonia synthesis including plasma-produced N atoms, radical NH_x species and vibrationally excited N_2. From various models it follows that the N_2 dissociative adsorption is no longer rate-limiting for ammonia formation at high plasma powers. The hydrogenation reactions on the surface become rate-limiting for the ammonia formation rate, as substantiated with DFT calculations [49,126,251], and experimental data [126,223]. In

principle, the hydrogenation rate increases with decreasing nitrogen binding strength (i.e., nobler catalysts). However, the N_2 recombination rate is also enhanced for noble catalysts [251]. This is due to a decrease in the barrier for N_2 recombination from 2N* for catalysts with a decreased nitrogen binding energy (E_N) [252]. Thus, the measured activity is the result of competition between hydrogenation on the catalyst to form ammonia and recombination reactions of 2N* to form N_2. However, the density of H atoms in the plasma phase is typically higher than the density of N atoms, which results in a build-up of adsorbed H atoms, promoting the hydrogenation reactions. It should be noted that most transition metals do not have a barrier for H_2 dissociation, resulting in a high coverage of hydrogen for thermal catalysis, unless N_2 is dissociated at sufficient rates [252].

DFT calculations show that Eley-Rideal-type reactions (N*+H→NH* or H*+N→NH*) may also be relevant for surface-enhanced plasma-driven ammonia synthesis [179], due to low enthalpy barriers for these reactions (<30 kJ mol^{-1}) [119]. In thermal catalysis, Eley-Rideal reactions are typically not considered because of entropic reasons. Stable reactant molecules would not only have to overcome the appropriate reaction barrier, they would also need to approach the active site in the right orientation and direction. In the case of plasma-generated N and H atoms, incoming angles are less important, and Engelmann et al. [179], suggested by means of DFT calculations that the reactions are barrierless on all transition metals. Shah et al. [126] combined modelling work and experimental work, from which the authors concluded that the Eley-Rideal-like reaction H+N*→NH* is important for ammonia synthesis over an Fe catalyst in a low pressure RF plasma. The subsequent hydrogenation steps primarily occur over the Fe catalyst via a Langmuir-Hinshelwood mechanism [126], while the contribution of Eley-Rideal-like mechanisms may increase with increasing plasma power and pressure. Ben Yaala et al. [128] performed a series of chemical looping experiments to gain insight in the mechanisms of ammonia synthesis in low pressure RF plasma on a W catalyst. They reported the highest yields for the H_2:N_2=1:1 gas fraction and concluded that the Eley-Rideal reaction H+N*→NH* is a crucial step for the formation of ammonia under these circumstances. It should be noted that W binds nitrogen strongly, which means that the hydrogenation steps are strongly uphill, implying it is not a typical catalyst considered for ammonia synthesis.

Hong et al. [58] also studied the plasma-catalytic ammonia synthesis for different plasma regimes. Their models include significantly more plasma-generated species, but with approximated values that make quantitative evaluation difficult. They concluded that mechanistically the pathways are determined by the abundant amount of H atoms adsorbed to the surface, and they propose that Eley-Rideal reactions are essential in plasma catalysis. They proposed the formation of NH in the plasma, with a subsequent NH+H*→NH_2* reaction, followed by hydrogenation of NH_2* via a Langmuir-Hinshelwood mechanism over the surface.

A DBD typically operates in the filamentary regime, e.g. characterized by micro-discharges, when used for ammonia synthesis. Therefore, Van 't Veer et al. [253] developed a model explicitly considering the role of the micro-discharges and their afterglows, i.e. the weaker plasma in between the micro-discharges, in the ammonia formation mechanisms; see the definitions in **section 2.2.4**. The calculations revealed that, while dissociative adsorption initially determines the major adsorbate, the plasma radicals, and especially the N atoms, actually determine the ammonia formation rate. Thus, electron impact dissociation of N_2 in the plasma, followed by N adsorption, and not N_2 dissociative adsorption at the catalyst surface, was identified as the rate-limiting step for ammonia formation in the DBD plasma at the conditions under study. Eley-Rideal type reactions played an overall important role, especially in the formation of NH*. Further hydrogenation at the catalyst surface yielded ammonia. The afterglows in between the micro-discharges were found to be responsible for the net ammonia production, because during the micro-discharges ammonia is destroyed more (by electron impact dissociation) than it is formed. It should be noted that the mechanism in a DBD highly depends on the plasma and catalyst properties, as **Chapter 3** shows experimentally that the dissociative adsorption of plasma-activated N_2 is dominant in DBD plasmas at low energy input, while dissociation of N_2 in the plasma dominates at high energy input [94,223].

Summarizing, the fraction of N, H, and NH_X radicals depends on the specific energy input (SEI). In turn, the density of these plasma-generated radicals appears to determine whether Langmuir-Hinshelwood mechanisms, or Eley-Rideal-like reactions, or even plasma phase reactions are dominant.

Similar to plasma phase ammonia synthesis, the minimum energy requirement is 66.1 MJ kg-NH_3^{-1} in case of surface reactions with N and H atoms generated in the plasma (equivalent to 54.4 g-NH_3 kWh^{-1}, see **Table 1**). It should be noted that some catalysts are not able to dissociate N_2 at sufficient rates, while H_2 is readily dissociated on many metals. The minimum energy requirement in that case is 27.7 MJ kg-NH_3^{-1} (equivalent to 129.8 g-NH_3 kWh^{-1}, see **Table 1**). This is above the minimum required energy yield of 100 g-NH_3 kWh^{-1}, and potentially interesting for practical applications. It should be noted, however, that both H_2 and N_2 are activated when co-feeding the reactants, so that plasma reactor designs with primarily N_2 activation are required. Strategies for catalyst design for surface-enhanced plasma-driven ammonia synthesis were discussed in **section 2.2.5**.

2.4.3 Plasma-enhanced catalytic ammonia synthesis

Energetically, it is beneficial to prevent full dissociation of the reactants by the plasma (see **Table 1**). Therefore, research has recently focused on enhancing the dissociative N_2 adsorption on catalysts via vibrational or electronic excitation, following the modelling work of Mehta et al. [49]. The authors postulated that dissociative N_2 adsorption is enhanced upon vibrational excitation, while the subsequent hydrogenation steps and ammonia desorption are not affected by plasma activation [49]. The authors predicted that the ammonia synthesis can be enhanced for metals that bind atomic nitrogen weakly on

the catalyst surface (high E_N in **Figure 12**) [49], given that N_2 activation is usually the rate-limiting step for ammonia synthesis. This is based on microkinetic models that incorporate the potential influences of vibrational excitations in N_2, based on density functional theory (DFT) data available in literature (see **Figure 12**). The vibrational energy is often not insufficient for dissociation in plasma phase, due to the large amount of energy needed to break the N_2 triple bond (9.79 eV or 945 kJ mol^{-1}), although vibrationally induced dissociation is reported for some types of plasmas [254,255]. Conversely, the energy barrier for the catalytic dissociation of N_2 on transition metals is considerably lower, e.g. 1.5 eV or or 145 kJ mol^{-1} on Ru(111) [256], and vibrational excitation will have relatively more impact on dissociation on these metals.

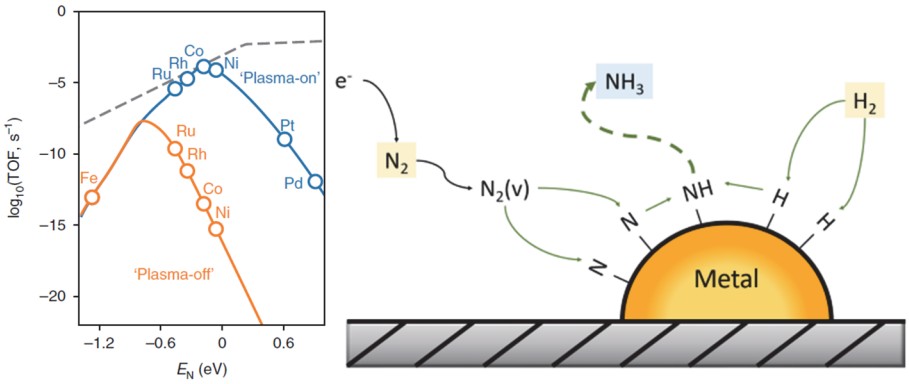

Figure 12: Left: Proposed effect of plasma-induced N_2 activation on the catalytic activity at T=200°C and 1 bar over step sites. The dashed line represents the maximum possible hydrogenation rate. Reproduced from Ref. [49]**. Right: Proposed mechanism for plasma-enhanced catalytic ammonia synthesis via plasma-activated N_2 dissociation. Reproduced from Ref.** [94]**.**

In **Chapter 3**, this claim is substantiated with a kinetic analysis for Ru-based catalysts in a DBD reactor. In case of thermal catalysis (i.e., without a plasma), the apparent activation barrier of ammonia synthesis is about 60-115 kJ mol^{-1}, which can be attributed to the dissociation of N_2 [224,257]. Upon plasma activation, it is found that the apparent activation barrier for ammonia synthesis decreased to about 20-40 kJ mol^{-1}, which was attributed to a lower barrier for N_2 dissociation [94]. It is observed that the ammonia synthesis rate increases upon addition of an alkali promoter, both in thermal catalysis as well as in plasma catalysis [94]. This can be attributed to a decrease in the transition state barrier for N_2 dissociation in the presence of an alkali promoter due to electrostatic attractions [229], confirming that N_2 dissociation is also kinetically relevant in plasma catalysis.

Proving that the catalytic activity enhancement is due to plasma-activated N_2 rather than plasma-generated radicals is difficult and no definitive experimental proof has been provided for transition metals other than Ru so far. In **Chapter 5**, it is found that Ru metal becomes active for ammonia synthesis below the thermal onset temperature, typically

300-400°C [224,225,257–259]. The onset temperature for plasma catalysis is due to the desorption temperature of ammonia from Ru, typically 150-200°C [83,260], e.g. substantially lower than the temperature required for thermal N_2 dissociation at sufficient rates, typically 300-400°C [224,225,257–259]. Given that sufficient radicals are available for adsorption, ammonia can be formed over the metal without the need for N_2 dissociation on the catalyst. In **Chapter 5**, it is found that plasma-activated, molecular N_2 also contributes to the plasma-catalytic conversion at temperatures above 300°C. Furthermore, the plasma-catalytic conversion to ammonia increases with the specific energy input (SEI) [89], which is due to increased plasma-activation of N_2 [49,223].

Another effect observed for plasma-enhanced catalytic ammonia synthesis is ammonia yields beyond the thermodynamic equilibrium limit [223,236]. Mehta et al. [236] developed a model for plasma-enhanced catalytic ammonia synthesis, which estimates the activities for ammonia synthesis and ammonia decomposition. The N_2 activation barrier is the key descriptor, while the hydrogenation steps are lumped in the model. The plasma-activation is assumed to decrease the barrier for N_2 dissociation and therefore increase the rate of N_2 dissociation. The final state of surface-adsorbed N* is assumed to be unaffected by plasma-activation of N_2. Upon varying the N_2 activation barrier, it was shown that plasma-activation can lead to ammonia synthesis beyond the thermal equilibrium. This model was experimentally validated for Ru/MgO and Ru-K/MgO catalysts in **Chapter 6**. Coupling the model of Mehta et al. [236] with experimental data, allows for distinguishing between regimes where plasma-generated radicals are dominant and regimes where plasma-activated molecular N_2 is dominant [223].

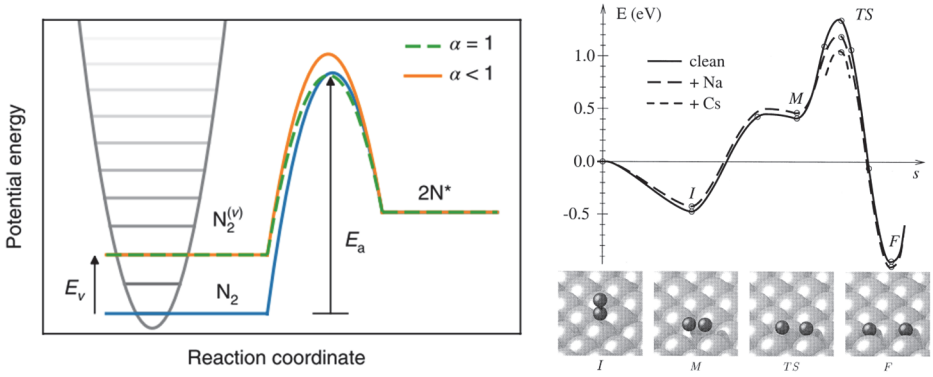

Figure 13: Left: Proposed impact of vibrational excitation on dissociation barrier of N_2. Reproduced from Ref. [49]. Right: Minimum energy path for N_2 dissociation over Ru(0001), without and with alkali promoters. Reproduced from Ref. [229].

As shown in **Figure 13**, Mehta et al. [49] lumped the N_2 dissociation reaction in a single activation barrier to atomic N* on the catalyst surface, which leads to the prediction of enhancing the ammonia synthesis rate for noble catalysts with high N_2 activation barriers (see **Figure 12**). However, N_2 dissociation is more complex in practice with various

intermediates towards 2N* (see **Figure 13**) [229,261,262], as discussed in **Chapter 4**. Furthermore, molecule-surface interactions may lead to energy losses upon adsorption of plasma-activated N_2 [263], thereby limiting the efficiency of plasma activation.

It remains an open question to what degree plasma-activation can lower the N_2 dissociation barrier for metals with a substantial barrier for N_2 dissociation. To account for these effects, Mehta et al. introduced an alpha parameter that represents the efficacy of vibrational excitation to lower the energy barrier. This alpha parameter is obtained from the Fridman-Macheret equation [60]. In reality the efficacy of vibrational excitation also depends on the degree of excitation [264–266] and it is unclear how accurate the Fridman-Macheret approximation is. To the best of our knowledge, more accurate models to describe the vibrational efficacy do not exist yet.

2.5 Plasma-catalytic ammonia synthesis: the complexity ahead

As discussed in the previous section, plasma catalysis could become an alternative for small-scale ammonia synthesis only in two scenarios: (1) N_2 is dissociated by the plasma, while H_2 remains unaffected by the plasma, and (2) N_2 is only partially activated by the plasma. Some general strategies for catalyst design and for effective plasma-catalyst coupling were discussed in **section 2.2.5**. Furthermore, the possible mechanisms leading to plasma-catalytic ammonia synthesis, as well as the complexity of dissociative N_2 adsorption were discussed in **section 2.4**. Hereafter, potential avenues are identified that may be relevant for the development of the field.

It must be stressed that there are several known unknowns, as well as multiple unknown unknowns in plasma catalysis [164,167]. The mutual interactions between the plasma and catalyst imply that a large number of interactions may affect the plasma-driven conversions. Only recently, kinetic models were introduced in an attempt to understand plasma-catalytic ammonia synthesis in terms of the catalytic cycle [49,126,179,236]. These models have provided guidelines and concepts to interpret experimental results, but it remains difficult to link the experimental results to highly simplified models. For instance, plasma-excitations in molecular N_2 are predicted to shift the volcano curve to more noble metals (see **Figure 12**). However, a shift to more noble metals is also expected for NH_X radicals adsorbing and hydrogenating via Langmuir-Hinshelwood reactions, due to an increased hydrogenation rate over more noble metals, as well as less desorption limitations [251]. This implies both options are still open to explain catalytic trends observed in experiments. Secondly, these first models are simplifications in which not all the complexity of plasma-catalysis is incorporated, because all the important contributions to plasma-catalyst interactions are simply not yet fully understood [164,167]. This sometimes results in disagreement between modelling results and trends observed in experiments, as discussed in **section 2.4.3**.

Specifically, the studies by Mehta et al. [49] and Engelmann et al. [179] assume specific plasma conditions that are unaffected by the catalytic reactions. Indeed, while increased TOFs were obtained by Mehta for vibrational excitations and by Engelmann for radical contributions, it is yet to be investigated whether the plasma can sustain a high vibrational temperature and high radical densities while the catalyst consumes these reactive plasma species. This potentially imposes limitations on the ratio of the amount of catalyst to plasma volume.

Thus, it is often difficult to distinguish between the relevant plasma species responsible for the activity enhancement in the presence of a plasma, although a few studies have strong indications for a specific pathway [94,126,223]. Based on a combined experimental and modelling study, Shah et al. [126] proposed that the plasma-catalytic conversion over Fe-catalysts in a low pressure RF reactor is due to dissociation of N_2 by the plasma, with subsequent adsorption and hydrogenation to ammonia over the surface. Based on experiments with various Ru-catalysts, **Chapter 5** shows that the plasma-enhancement over Ru-catalysts in a DBD reactor is due to reactions with NH_X radicals at low temperatures (<300°C), while plasma-activated N_2 with subsequent hydrogenation on the surface may also become increasingly relevant at temperatures where the activity in the absence of plasma is also substantial. Even if the activity enhancement can be proven to be due to plasma-activated N_2 rather than plasma-generated NH_X species, it remains unresolved which plasma-activated N_2 species, e.g. with different levels of vibrational of electronic excitation, is responsible for the activity enhancement over Ru-catalysts observed in various reports [42,89,94]. This is discussed in **Chapter 4**.

Various authors have reported an improvement in the energy efficiency for ammonia formation when using pulsed plasmas rather than AC plasmas [81,89]. For plasma-enhanced catalytic ammonia synthesis, the enhanced efficiency can be understood from the lower overall plasma power, and therefore reduced heat losses [267]. Furthermore, vibrational-translational relaxation is suppressed for pulsed plasmas [268], thereby limiting the gas heating losses. Lastly, the electron energy distribution is different for pulsed plasmas [269].

Jafarzadeh, Bal et al. [182,184,270] recently reported computational studies on enhanced surface binding of CO_2 on various metal cluster surfaces in case of a polarized surface; similar behavior may occur for N_2 binding. Surface polarization may also affect surface reactions in case of ammonia synthesis over metals, but there have not been any studies confirming or ruling out the relevance of such effects. For thermal catalysis and plasma catalysis, electrostatic attraction of alkali metals with N_2 cause an enhancement in N_2 dissociation rates [94,229]. This shows that the electronic characteristics of the catalyst are very relevant for ammonia synthesis.

Furthermore, the effect of periodic discharges and capacitive regimes is not fully understood, both on the catalytic properties of the surface [271,272] and on the plasma characteristics near the catalyst [158,163,273]. For instance, Ardagh et al. [271,272] reported that oscillatory surface binding strengths, induced by for instance electric fields, may enhance

the catalytic activity by orders of magnitude. Furthermore, the waveform and the frequency of the oscillation can determine the catalytic activity [271,272]. As the plasma frequency and waveform is a design parameter which alters both the electron density and electron energy for N_2 activation in the plasma zone, as well as the catalyst surface properties, this potentially adds a new dimension to the complexity of plasma-catalytic systems.

2.6 Outlook

Over the past decades, research on plasma-catalytic ammonia synthesis has transitioned from exploratory and trial-and-error approaches to more fundamental understanding based on experimental and modelling work, as described in detail in this review paper. *Operando* plasma and catalyst diagnostics, such as surface techniques such as XPS and FTIR [120,128], isotopic labelling [274] and spectroscopy [119,275] will aid in further improving our understanding of how plasma and catalyst interact at the molecular level, rather than on the macroscopic level.

Open questions remain, such as which plasma-activated species are dominant for the conversion to ammonia, and under which conditions. For instance, which plasma-activated N_2 species is dominant for plasma-enhanced catalytic ammonia synthesis: electronically excited N_2 or vibrationally excited N_2? Furthermore, to what degree has the complexity of plasma catalysis for plasma-driven ammonia synthesis been uncovered, i.e. what is the role of plasma-generated radicals, and the importance of Langmuir-Hinshelwood versus Eley-Rideal reactions, and which unknown unknowns remain? How does the plasma environment behave very close to a metal nanoparticle on a solid surface? Additional modelling efforts may aid in enhancing the understanding [163].

Secondly, to which degree can our understanding of plasma catalysis aid in developing sufficiently energy-efficient plasma-catalytic ammonia synthesis? Which combination of plasma reactor and catalyst leads to the highest productivity at the lowest energy cost? For now, the highest energy yields are reported for atmospheric pressure DBD reactors (see **Figure 10**). On the other hand, low pressure plasma reactors such as MW and RF reactors lead to a higher degree of vibrational excitation, which may be beneficial for mild N_2 activation before catalytic N_2 dissociation. However, it should be noted that plasma activation is not the only process step for ammonia synthesis from air and water, as H_2 production via electrolysis, N_2 purification and ammonia separation and storage should be considered as well. The most suitable plasma reactor and catalyst are to a high degree linked to the process conditions, such as temperature and pressure for H_2 production, N_2 purification and ammonia separation and storage. This is discussed in **Chapter 8**.

Finally, it is not yet clear whether plasma technology will be the most feasible alternative for decentralized ammonia production in the future. In heterogeneous catalysis, ammonia synthesis has been a guide reaction, due to the perceived simplicity of the reaction and the absence of by-products [22,276]. Thus, plasma-catalytic ammonia synthesis can certainly aid

in improving the understanding of the emerging research field of plasma catalysis. Currently, plasma technology is already used for ozone production and acetylene at large scale [45,46]. Further experimental and modelling research will tell whether plasma catalysis will become a feasible alternative for green ammonia production, and whether plasma-catalytic processes will become industrially viable for other processes, like CO_2 and CH_4 conversions [45].

Chapter 3

Plasma-activated N_2 in plasma-enhanced catalytic ammonia synthesis on Ru-based catalysts: a kinetic analysis

Summary

Plasma-enhanced catalytic ammonia synthesis has been proposed as an alternative pathway for green nitrogen fixation in the case of medium- and small-scale operation. Recently, Mehta et al. [49] postulated that plasma-induced vibrational excitations of N_2 decrease the dissociation barrier, without influencing the subsequent hydrogenation reactions and ammonia desorption at atmospheric conditions. In the current Chapter, this postulation is substantiated with experimental data of unpromoted and promoted, alumina-supported ruthenium-based catalysts. Within the temperature regime for plasma-enhanced catalytic ammonia synthesis on ruthenium-based catalysts (>200°C), synergy is experimentally observed between the catalyst and the plasma by a lowered apparent activation energy. The apparent activation energy for thermal-catalytic ammonia synthesis ranges from 60 kJ mol^{-1} to 115 kJ mol^{-1} depending on the promoters. However, the apparent activation energy for plasma-enhanced catalytic ammonia synthesis ranges from 20 kJ mol^{-1} to 40 kJ mol^{-1}, consistent with the hypothesis that ammonia synthesis is enhanced via plasma-induced vibrational or electronic excitations of N_2. Further support follows from the observation that the effects of promoters and supports on activity are similar for thermal catalysis and plasma-enhanced catalysis. As promoter and support influence the activity via enhancing the N_2 dissociation, it follows that breaking the N≡N bond is still relevant in plasma-enhanced catalytic ammonia synthesis.

This chapter has been published as:

Rouwenhorst, K. H. R., Kim, H.-H., & Lefferts, L. (2019). Vibrationally excited activation of N_2 in plasma-enhanced catalytic ammonia synthesis: a kinetic analysis. ACS Sustainable Chemistry & Engineering, 7(20), 17515-17522. doi: 10.1021/acssuschemeng.9b04997

3.1 Introduction

Ammonia is proposed as a hydrogen carrier in the circular economy [27,32,54]. Various alternatives to the Haber-Bosch process have been proposed for green nitrogen fixation in the form of ammonia, such as electrochemical synthesis, dense metallic membrane reactors, solar thermochemical redox cycles, and plasma-enhanced catalytic synthesis [33,277]. The Haber-Bosch process typically operates in a centralized and continuous manner, usually at least 2000 t-NH_3 d^{-1} [278]. The efficiency of the Haber-Bosch process decreases upon downsizing and upon fluctuating operation [33], which is one of the bottlenecks in matching with renewable energy sources, such as solar and wind [44]. Plasma-enhanced catalytic ammonia synthesis is a potential technology that allows for following load fluctuations in electricity. Non-thermal plasma can be used, in which electrons reach temperatures of a few thousand K, while the heavier radical species remain at a temperature close to the gas temperature [45]. As the nitrogen and hydrogen are activated by electrons and subsequently have a higher energy, higher equilibrium conversions to ammonia can be attained [279].

Even though various authors have researched ammonia synthesis in the presence of a plasma in various types of plasma reactors, i.e. dielectric barrier discharge, microwave, and radiofrequency reactors [40,42,48,56,58,200,280], plasma-enhanced catalysis is poorly understood [80,167].

Recent reviews on plasma-enhanced ammonia synthesis by Bogaerts et al. [40], Hong et al. [58], Li et al. [280], and Peng et al. [200] focused mostly on experimental results of plasma-enhanced ammonia synthesis, rather than the underlying catalytic principles. The recent review of Mehta et al. [41] and **Chapter 2** shed some light on surface processes occurring in plasma-enhanced catalytic ammonia synthesis. Furthermore, the authors discuss how excitation of N_2 can enhance the ammonia synthesis rate on the catalytic surface. Surface processes on catalysts in plasma-enhanced synthesis processes must be understood better for plasma-enhanced catalytic ammonia synthesis to develop further via catalyst material optimization, aiming at energy-efficient plasma-enhanced catalysis [44]. In the current Chapter, plasma-enhanced catalytic ammonia synthesis is investigated using heterogeneous catalysis concepts such as the activation barriers for chemical reactions.

Both conventional iron-based ammonia synthesis catalysts [22,281–283] and ruthenium-based ammonia synthesis catalysts [22,225,281,284] were recently reviewed. The thermal-catalytic reaction mechanism for ammonia synthesis is well understood. Aika et al. [225] found a relation between the electronegativity of both support and promoter and the ammonia synthesis rate on ruthenium-based catalysts for thermal catalysis. The ammonia synthesis rate changes by orders of magnitude among various supports, and ammonia synthesis rate increases with decreasing electronegativity of the support. Further activity enhancement is observed upon addition of alkali or alkaline earth metals as promoters.

Recently, Mehta et al. [49] developed microkinetic models that incorporate the potential influences of vibrational excitations in N_2, based on density functional theory (DFT) results available in literature. Mehta et al. [49] postulated that plasma-induced vibrational excitation of N_2 enhances N_2 dissociation, the rate determining step in thermal-catalytic ammonia synthesis, without influencing the subsequent hydrogenation reactions of NH_x species on the Ru surface and ammonia desorption at atmospheric conditions. The authors claim that the N_2 dissociation can become sufficiently fast, such that the hydrogenation becomes the rate determining step for plasma-enhanced catalysis. However, limited experimental evidence was provided. Ammonia synthesis rates at a single temperature, flow rate and plasma power were reported for Fe/γ-Al_2O_3, Ru/γ-Al_2O_3, Co/γ-Al_2O_3, Ni/γ-Al_2O_3 and Pt/γ-Al_2O_3. However, apparent activation barriers for plasma-enhanced catalytic ammonia synthesis were not evaluated. Therefore, this postulation is evaluated with additional experimental data in the current Chapter. Previously reported data of Kim et al. [89] as well as new data is used for this analysis.

3.2 Results

The experimental set-up and catalyst preparation is described in the supporting information (**section 3.5**) and was reported previously [89]. Various ruthenium-based catalysts were tested for the ammonia synthesis activity (2Ru/γ-Al_2O_3, 10K-2Ru/γ-Al_2O_3, 5Cs-2Ru/γ-Al_2O_3 and 5Mg-2Ru/γ-Al_2O_3). Herein, the numbers represent the wt.% loading of the compounds. The same batch of Ru/γ-Al_2O_3 catalysts is used for all experiments, i.e. for the catalysts without promoter, and the catalysts impregnated with Cs, Mg and K promoters. Thus, the Ru dispersion is the same for all catalysts. Part of the results were previously reported by Kim et al. [89]. The previously reported results and new results are listed in **Table 4** in the supporting information.

3.2.1 Thermal catalysis

The activities for thermal-catalytic ammonia synthesis over 2Ru/γ-Al_2O_3, 10K-2Ru/γ-Al_2O_3, 5Cs-2Ru/γ-Al_2O_3 and 5Mg-2Ru/γ-Al_2O_3 in the temperature window between 200°C and 330°C are shown in Arrhenius plot in **Figure 14**. Herein, the activity for thermal catalysis in μmol h^{-1} g^{-1} is calculated as the ammonia concentration produced, multiplied by the flowrate and divided by the catalyst mass for thermal catalysis. The activity for the unpromoted catalyst is the lowest, which is consistent with previous studies in literature [224,259]. Furthermore, the promotion with Mg appears to be most effective. Due to the limited experimental data available, an apparent activation barrier can only be obtained for 5Mg-2Ru/γ-Al_2O_3, resulting in 104 kJ mol^{-1}. This is in good agreement with typical values in reported in literature, between 100 and 115 kJ mol^{-1} [224,259] (see **Table 3**), for promoted alumina-supported ruthenium-based catalysts.

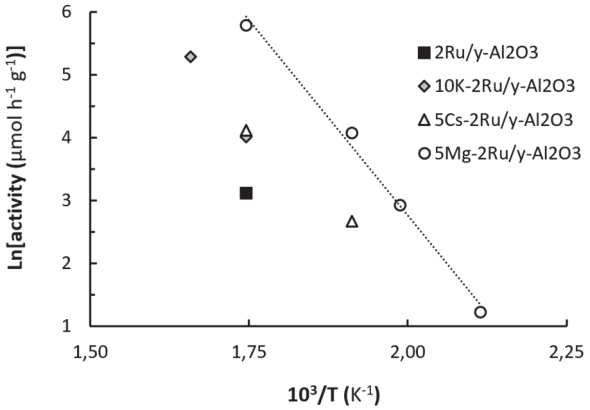

Figure 14: Arrhenius plot of thermal-catalytic ammonia synthesis over various alumina-supported ruthenium-based catalysts. P=1 bar, H_2:N_2=1:4, various flow rates (see Table 4). Black filled squares (■): 2Ru/γ-Al_2O_3; grey filled diamonds (◇): 10K-2Ru/γ-Al_2O_3; white filled triangles (△): 5Cs-2Ru/γ-Al_2O_3; and white filled circles (○): 5Mg-2Ru/γ-Al_2O_3.

3.2.2 Plasma-enhanced catalysis

The activities for plasma enhanced-catalytic ammonia synthesis on 2Ru/γ-Al_2O_3, 10K-2Ru/γ-Al_2O_3, 5Cs-2Ru/γ-Al_2O_3 and 5Mg-2Ru/γ-Al_2O_3 in the temperature window between 200°C and 330°C are shown in an Arrhenius plot in **Figure 15** (left). The ammonia synthesis activity for plasma-enhanced catalysis is higher than for thermal catalysis, as can be seen by comparing **Figure 14** and **Figure 15**. The highest concentration obtained is 0.17 mol.% ammonia for 5Mg-2Ru/γ-Al_2O_3 at 300°C, while a concentration of 0.09 mol.% ammonia was obtained for 10K-2Ru/γ-Al_2O_3 at 330°C. The equilibrium concentration of ammonia at 300°C and 330°C is 0.51 mol.% and 0.31 mol.% at atmospheric pressure and for H_2:N_2=1:4, respectively. The concentration of 0.17 mol.% ammonia at 300°C is 33% of the equilibrium concentration, while the concentration of 0.09 mol.% ammonia at 330°C is 29% of the equilibrium concentration. Thus, the measurements are far below the equilibrium concentration, which is required to minimize the effect of the reverse reaction, e.g. the ammonia decomposition reaction. In principle, a catalyst which is active for the ammonia synthesis reaction is also active for the ammonia decomposition reaction.

When the data for plasma-enhanced catalysis is plotted in an Arrhenius plot in a similar manner as for thermal catalysis (see **Figure 14** and **Figure 15**), no linear correlation is obtained (R^2 0.65-0.93), which is probably caused by variation in the specific energy input (SEI). The SEI is defined as the energy input per amount of volumetric gas flow. Kim et al. [89] reported that the ammonia synthesis rate increases linearly with plasma power at various temperatures, which can be rationalized with the fact that more N_2 molecules can

be activated when increasing the SEI due to the increased electron density. Therefore, a new parameter is proposed to analyze the kinetics of plasma-enhanced catalysis, namely the activity divided by the SEI, allowing for kinetic analysis of experiments with various SEIs. This analysis is only valid when the plasma chemistry contribution is negligible compared to the plasma-enhanced catalysis contribution. To avoid significant heating of the gas by the plasma, the SEI was limited in this study to relatively low values in the range between 83 and 367 J L^{-1}.

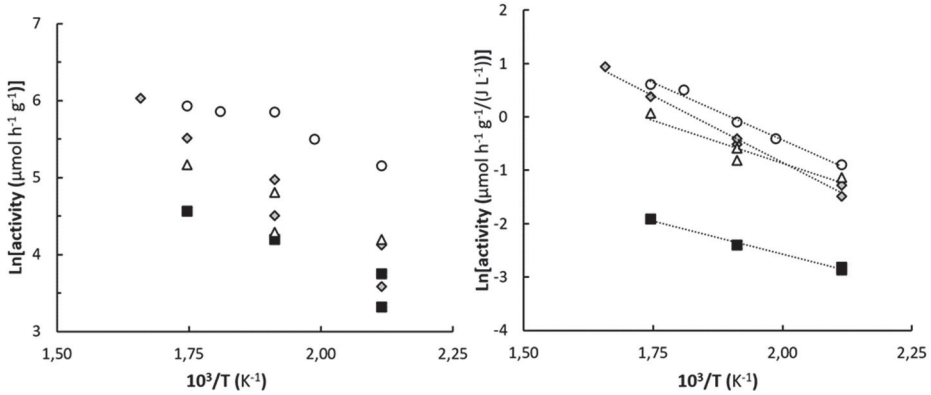

Figure 15: Arrhenius plot of plasma-enhanced catalytic ammonia synthesis over various alumina-supported ruthenium-based catalysts. P=1 bar, H_2:N_2=1:4, various flow rates (see Table 4). Left: Activity defined in same manner as for thermal catalysis (i.e., not divided by the SEI). Right: Activity divided by the SEI. Black filled squares (■): 2Ru/γ-Al_2O_3; grey filled diamonds (◇): 10K-2Ru/γ-Al_2O_3; white filled triangles (△): 5Cs-2Ru/γ-Al_2O_3; and white filled circles (○): 5Mg-2Ru/γ-Al_2O_3.

Figure 15 (right) indeed shows linear correlations in an Arrhenius plot based on activity divided with the SEI, proofing a powerful tool to analyze the kinetics of plasma-enhanced catalysis. This results in apparent activation energies for plasma-enhanced catalytic ammonia synthesis on 2Ru/γ-Al_2O_3, 5Mg-2Ru/γ-Al_2O_3, 10K-2Ru/γ-Al_2O_3 and 5Cs-2Ru/γ-Al_2O_3 (**Figure 15**), resulting in 20 kJ mol^{-1} (R^2=0.99), 36 kJ mol^{-1} (R^2=0.99), 41 kJ mol^{-1} (R^2=0.99) and 27 kJ mol^{-1} (R^2=0.91), respectively. This is significantly lower than the apparent activation energy for thermal-catalytic ammonia synthesis on both unpromoted and promoted ruthenium-based catalysts (typically 60-70 kJ mol^{-1} and 100-115 kJ mol^{-1}, respectively) [257,259].

3.3 Discussion

The apparent activation energies for thermal operation of alumina-supported ruthenium-based catalysts are mostly due to N_2 dissociation, as discussed by Aika et al. [257] and Muhler et al. [224]. It is well established that the rate-determining step for thermal catalysis on conventional ruthenium-based catalysts is the dissociation of nitrogen [228,281,285].

Table 3: Apparent activation energy for thermal-catalytic ammonia synthesis ($E_{a,app-thermal}$), and apparent activation energy for plasma-enhanced catalytic ammonia synthesis ($E_{a,app-plasma}$). * The data obtained in this work.

Catalyst	$E_{a,app-thermal}$ (kJ mol^{-1})	$E_{a,app-plasma}$ (kJ mol^{-1})
2Ru/γ-Al_2O_3	60-70 [224,259]	20*
10K-2Ru/γ-Al_2O_3	100-115 [259]	41*
5Mg-2Ru/γ-Al_2O_3	104*	36*
5Cs-2Ru/γ-Al_2O_3	100-115 [224,259]	27*

The catalytic activity is enhanced by plasma via promoting N_2 dissociation, as is apparent from the differences between thermal catalysis and plasma-enhanced catalysis in terms of both the apparent activation energies as well as the absolute activities (see **Figure 14**, **Figure 15** and **Table 3**). This is in line with the hypothesis that the activity enhancement is due to N_2 excitation in the plasma before adsorption. It cannot be excluded that the hydrogenation reactions on the surface become rate limiting [49], which is also the case for the most active Ru catalysts reported recently [286–288]. However, the strong trends obtained for the plasma-catalytic activity divided by the SEI indicates that plasma-activation of N_2 and the subsequent N_2 dissociation is rate limiting under the current conditions.

3.3.1 Activity trends in plasma-enhanced catalysis

As follows from **Figure 14** and **Figure 15**, the absolute ammonia synthesis activity differs among the catalysts. However, the activity trends among various ruthenium-based catalysts are similar, both for thermal catalysis and plasma-enhanced catalysis. The unpromoted catalyst (2Ru/γ-Al_2O_3) is least active. Among the promoted catalysts, 5Cs-2Ru/γ-Al_2O_3 and 10K-2Ru/γ-Al_2O_3 show similar activity, while 5Mg-2Ru/γ-Al_2O_3 is most active for both thermal catalysis and plasma-enhanced catalysis. This indicates that the reaction mechanisms for thermal catalysis and plasma-enhanced catalysis are similar. As the physical packing structure is the same for the different catalysts, the difference in activity is attributed to a catalytic enhancement of the promoters rather than a plasma modification. Thus, the promoters retain their function for plasma-enhanced catalysis like for thermal catalysis, i.e. electronical promotion of N_2 dissociation [225,281]. The nitrogen adsorption rate is higher for promoted catalysts, as follows from IR spectroscopy [289]. This gives a different sticking probability, which means more of the activated N_2 is adsorbed on promoted catalysts.

As reported by Aika et al. [225], the ammonia synthesis rate on ruthenium-based catalysts is influenced by the electronegativity of both the support and the promoter, where a lower electronegativity leads to a higher ammonia synthesis rate. As shown in **Figure 16**, similar trends are observed for thermal catalysis and for plasma-enhanced catalysis. This again indicates that plasma-enhanced catalysis proceeds via a mechanism similar to thermal catalysis, but with plasma-activation of the reactants.

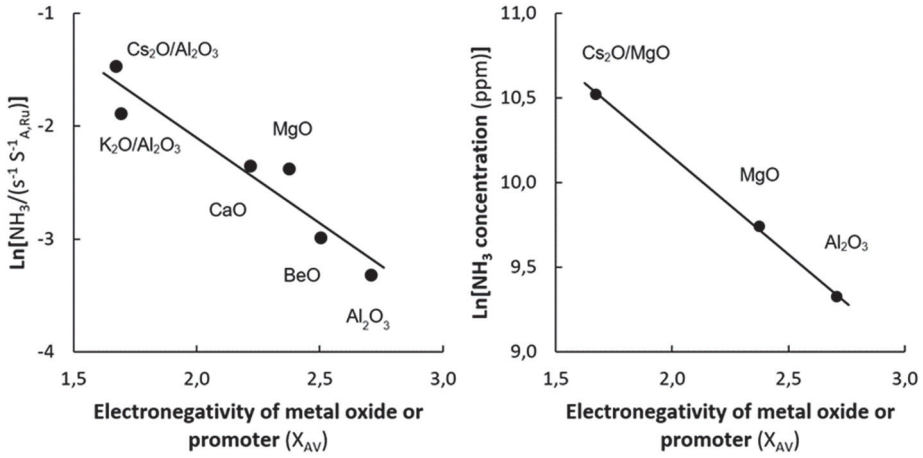

Figure 16: Left: Activity for ammonia synthesis (ammonia synthesis rate expressed as turnover number per active Ru site) as function of electronegativity for thermal-catalytic ammonia synthesis. Experimental data reported in Ref. [290]. Right: Activity for ammonia synthesis (ammonia concentration for the same catalyst mass, temperature and flowrate) as function of electronegativity for plasma-enhanced catalytic ammonia synthesis. Experimental data reported in Ref. [291].

3.3.2 Heating effects and power effects

In principle, heating effects by the DBD plasma influence the experimental reaction rates [292]. Kim et al. [152] and Jidenko et al. [293] reported an increase in temperature with increasing SEI (range 0-400 J L^{-1}) in a DBD reactor. These reactors operate at an ambient surrounding temperature and the temperature increase was reported to be maximum 100°C at a SEI of 400 J L^{-1}. However, when the temperature of the reactor is controlled with an oven, this heating effect of the plasma is expected to be smaller, as the temperature control loop corrects at least partly for the heating effect of the plasma.

Arrhenius-type kinetics show exponential increase in activity with absolute temperature. In supporting information **section 3.5.3**, experimental data with a constant SEI was used to estimate the effect of a temperature offset. From this analysis it follows that the apparent activation energy for plasma-enhanced catalysis hardly increases for a temperature offset of 100°C, remaining substantially lower than for thermal catalysis. From this it follows that the decrease in apparent activation barrier is caused by plasma-activation effect of the reactants.

Kim et al. [89] reported an apparent linear relation between the plasma-enhanced catalytic ammonia synthesis activity and the SEI for a fixed oven temperature for the same reactor configuration as reported in this paper. Using a linear relation between the plasma-enhanced catalytic activity and the SEI appears to be a valid descriptor to analyze the kinetics of plasma-enhanced catalytic ammonia synthesis (**Figure 15**), allowing to

consider experiments performed with different SEIs. The measurements of SEI and activity are experimentally relatively simple, in contrast to measurement of the temperature inside the plasma reactor, requiring complex *in-situ* techniques [152,164].

3.3.3 Plasma-induced excitations in N_2

Mehta et al. [49] postulated that plasma-induced vibrational excitation of N_2 decrease the dissociation barrier, without influencing the subsequent hydrogenation reactions and ammonia desorption. The experimental results in this paper substantiate these claims with the change in apparent activation barrier upon plasma-illumination. Furthermore, for ruthenium-based catalysts, the onset temperature for thermal catalysis (200°C) is the same as the temperature at which the activity for ammonia synthesis in the presence of a plasma is enhanced [42]. This indicates that the desorption step of ammonia is probably not influenced by plasma-induced changes in the electronic structure of the transition metal catalyst.

Electronic excitations and ionic states of N_2 may also be of importance [58]. Based on observed ammonia synthesis rates, it is difficult to discriminate between vibrational excitations and electronic excitations of N_2. Ionic states have very short lifetime at atmospheric pressure, and are probably not relevant in DBD plasma-reactors [167]. Metastable electronically excited N_2 molecules with an energy level of 6.2 eV have a relatively long lifetime in the range 10^{-5}-10^{0} second [294–297], and are predicted to be relevant for the reduced electric fields in DBD plasma-reactors (see **Chapter 2**). However, according to Fridman and Rusanov [298], most of the plasma energy (~97%) is going to vibrational excitation for electrons of 1-3 eV. Thus, vibrational excitations and electronic excitations of N_2 can both be relevant species for excitation of N_2 at atmospheric pressure.

An alternative pathway is the dissociation of N_2 in the plasma with subsequent adsorption of N radicals on Ru. However, this cannot be the dominant mechanism for plasma-enhanced catalytic ammonia synthesis under the current plasma conditions, as it would fail to explain that the trends in activity with electronegativity of the support and promotors are very similar for plasma-enhanced catalysis and thermal catalysis (see **Figure 16**). As these effects are caused by enhancement of N_2 dissociation on the catalyst surface, it follows that the plasma enhances N_2 dissociation on the surface via vibrational excitation, instead of N_2 dissociation in the plasma. Thus, the postulate of Mehta et al. [49] concerning the plasma-induced vibrational excitations of N_2 without influencing subsequent reaction steps is experimentally substantiated, although the role of electronical excitations of N_2 cannot be excluded. The important role of vibrationally excited (and electronically excited) N_2 agrees with the optimum H_2:N_2 ratio in plasma-enhanced catalysis, which shifts to the N_2-rich range as compared to thermal catalysis [89]. N_2-rich conditions provide higher probability for collisions of electrons and N_2 molecules and thus N_2 excitation. H_2 does not require plasma-activation, as it readily dissociates on a Ru surface.

3.3.4 Conditions for plasma-enhanced catalytic ammonia synthesis

Inspired by the discussion so far, various reaction pathways are possible when combining plasma with catalysts. A nomenclature is proposed for those pathways, as there is no general agreement on the definitions of specific plasma-catalyst reaction pathways.

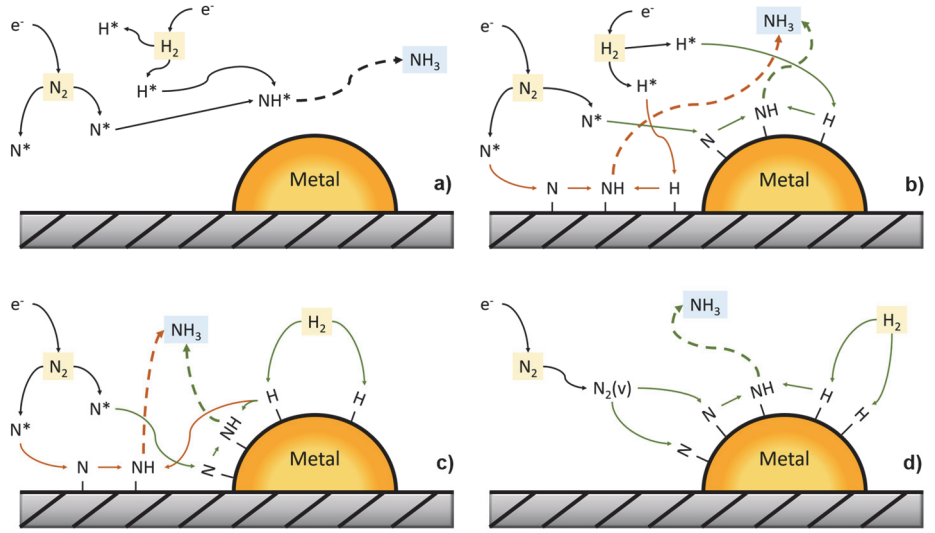

Figure 17: Reaction mechanisms of plasma-phase ammonia synthesis (Top left), surface-enhanced plasma-driven ammonia synthesis (Top right), plasma-enhanced semi-catalytic ammonia synthesis (Bottom left), and plasma-enhanced catalytic ammonia synthesis (Bottom right). Reactions relevant for mechanism are depicted with full arrows, while the subsequent reaction to ammonia is depicted with a dashed arrow. For details, see text.

Ammonia can be synthesized via gas-phase radical chemistry, in which N radicals and H radicals recombine in the plasma-environment to form ammonia. This is coined *plasma-phase ammonia synthesis* (**Figure 17**a). The second pathway is *surface-enhanced plasma-driven ammonia synthesis* (**Figure 17**b), in which N radicals and H radicals adsorb on a surface. The surface has a quenching effect, as the electrons on the surface may interact with the electrophilic radicals [42,58]. Subsequent hydrogenation of NH_x species and ammonia formation may occur over the surface or in the plasma-environment [299]. Both plasma-phase ammonia synthesis and surface-enhanced plasma-driven ammonia synthesis are diffusion limited, non-selective processes. These regimes can be identified based on low apparent activation energies smaller than typically 5 kJ mol^{-1}, due to changes in diffusivity of the reactants and changes in the electronic properties of the electrode with increasing temperature (such as the conductivity and resistivity) [41]. Yin et al. [107] and Iwamoto et al. [76] showed that the electrode properties have an influence on the ammonia synthesis rate. The orders in H_2 and N_2 are both 1, indicating that both N and H radicals are required for the diffusion-limited recombination reaction [58,82]. Both

pathways have a theoretical minimum energy consumption of 18.4 kWh kg-NH_3^{-1}, which is the energy required to break the bonds in both N_2 and H_2 molecules. The lowest energy consumption obtained so far is 48.8 kWh kg-NH_3^{-1}, as reported by Peng et al. [81].

The third pathway is *plasma-enhanced semi-catalytic ammonia synthesis* (**Figure 17**c), in which N radicals adsorb on a surface, while H_2 is dissociated over a catalyst. The term semi-catalytic is used, as the rate limiting step is not catalyzed, i.e. N_2 dissociation. Thus, the catalyst has an activating role for H_2 dissociation, while the catalyst is not able to dissociate N_2 at sufficient rates due to inhibition by adsorbed species (atomic hydrogen or NH_X species). Temperature effects on the ammonia synthesis rate are minor [82] and apparent activation energies lower than 30 kJ mol^{-1} are obtained (see **Chapter 6**). The orders in H_2 and N_2 are 0 and 1, respectively [82]. This is possibly due to full coverage of the transition metal with H-atoms, i.e., the so-called hydrogen inhibition effect as reported for ruthenium-based catalysts at low temperatures [281]. On the other hand, the orders in N_2 are similar in case of plasma-phase ammonia synthesis and in case of surface-enhanced plasma-driven ammonia synthesis. Possibly, the experimental data of Barboun et al. [82] for Ru/γ-Al_2O_3, Co/γ-Al_2O_3 and Ni/γ-Al_2O_3 represents this regime, as for all catalysts the orders in H_2 and N_2 are 0 and 1. However, for thermal-catalytic ammonia synthesis, implying N_2 dissociation on the catalyst surface, the order in H_2 varies widely among transition metal catalysts, ranging from -1.2 to 2.3 for the catalysts in Ref. [300]. Subsequent reactions between hydrogen atoms and nitrogen atoms may occur over the catalyst, as proposed by Mizushima et al. [96]. The theoretical minimum energy consumption is 7.7 kWh kg-NH_3^{-1}, which is required for the rupture of the triple nitrogen bond.

Plasma-phase ammonia synthesis, surface-enhanced plasma-driven ammonia synthesis and plasma-enhanced semi-catalytic ammonia synthesis have a minimum energy consumption which is above the required benchmark for small-scale applications (5-7 kWh kg-NH_3^{-1} [42]). Thus, these pathways cannot provide sufficiently energy efficient ammonia synthesis, even at 100% efficiency to ammonia. However, a lower energy input is feasible if N_2 is only partially activated by the plasma in combination with subsequent dissociation of excited N_2 molecules on a catalyst.

The fourth pathway is *plasma-enhanced catalytic ammonia synthesis* (**Figure 17**d), in which both H_2 and N_2 adsorb dissociatively on the catalyst surface. This is the pathway described by the postulate of Mehta et al. [49]. The nitrogen is vibrationally or electronically excited in the plasma, while the catalyst surface (a transition metal) performs the final rupture of the bond between the two nitrogen atoms as well as dissociation of H_2. Subsequent hydrogenation of NH_x surface species and ammonia desorption occur on a transition metal, unaffected by the plasma [49]. As discussed by Kim et al. [42], the onset temperature for thermal catalysis is the same as the temperature at which the activity for ammonia synthesis in the presence of a plasma is enhanced, indicating that ammonia desorption is probably not influenced by the plasma. This reaction pathway obeys classical thermodynamics, albeit with a change in the equilibrium constant due to the excitation of the reactants by the plasma [279]. A clear Arrhenius-type temperature dependence is

obtained and apparent activation energies are 20-40 kJ mol^{-1} for ruthenium-based catalysts, and are expected to be higher for more noble metals. The orders in H_2 and N_2 also vary depending on the catalyst formulation. In this case, a general theoretical minimum for energy consumption cannot be defined, as the required pre-activation in the plasma to facilitate N_2 dissociation at sufficient rates depends on the transition metal used for plasma-enhanced catalysis. The lowest energy consumption reported so far is 27.8 kWh kg-NH_3^{-1} [89].

In terms of the energy efficiency, plasma-enhanced catalytic ammonia synthesis is the preferred pathway for ammonia synthesis in the presence of a plasma and a catalyst. Pre-requisites for plasma-enhanced catalytic ammonia synthesis are (1) a sufficiently low plasma power such that vibrationally excited and electronically excited N_2 are the dominant plasma-excited species rather than radical species, (2) sufficient number of empty sites for N_2 dissociation, i.e. other surface species do not compete too strongly for the same sites, and (3) operation at temperatures sufficient for desorption of ammonia from the transition metal. Ammonia cannot desorb from the metal surface at temperatures below the onset temperature for thermal catalysis, e.g. about 200°C for ruthenium-based catalysts [301]. For ruthenium-based catalysts, the desorption of ammonia is increasingly inhibited with increasing electronegativity of the support and modifiers [302]. When these pre-requisites are not satisfied, plasma-enhanced catalytic ammonia synthesis over a transition metal is not possible (at measurable rates).

3.4 Conclusion

Ammonia synthesis via plasma-enhanced catalysis at temperatures between 200°C and 330°C has been discussed based on kinetic data. The activation energies deduced from the Arrhenius plot have been compared between thermal catalysis and plasma-enhanced catalysis. Furthermore, apparent activation energies at elevated temperatures (200-330°C) indicate that the ammonia synthesis proceeds via plasma-enhanced catalytic ammonia synthesis on alumina-supported ruthenium-based catalysts instead of plasma-phase ammonia synthesis.

The activity divided by the specific energy input (SEI) was introduced as a new descriptor to analyze the kinetics of plasma-enhanced catalytic ammonia synthesis, allowing considering experiments performed with different SEIs. This indicates that the SEI has a linear influence on the amount of plasma-activated N_2 species, and thereby on the plasma-enhanced catalytic ammonia synthesis activity.

The mechanism of plasma-enhanced catalytic ammonia synthesis involves plasma-induced vibrational excitation or electronic excitation of N_2, with subsequent dissociation on the catalyst surface, without affecting the subsequent hydrogenation steps of NH_x species on the surface as well as ammonia desorption, as previously postulated by Mehta et al.[49]. This postulation was substantiated by the lower apparent activation barriers for plasma-enhanced catalysis for various ruthenium-based catalysts as compared to thermal

catalysis. The observed barriers vary between 20 kJ mol^{-1} and 40 kJ mol^{-1}. The effects of promoters and supports on the activity effects are similar for thermal catalysis and plasma-enhanced catalysis, indicating that the properties of the catalyst to dissociate N_2 are still relevant, also when N_2 is vibrationally or electronically excited.

Four different types of pathways for ammonia synthesis in the presence of a plasma are defined and described, namely (1) plasma-phase ammonia synthesis, (2) surface-enhanced plasma-driven ammonia synthesis, (3) plasma-enhanced semi-catalytic ammonia synthesis, and (4) plasma-enhanced catalytic ammonia synthesis.

3.5 Supporting information

3.5.1 Experimental set-up

The plasma-catalytic reactor is shown in **Figure 18**, consisting of catalyst pellets, quartz tubes, a stainless steel tube, and a power supply. Silver paste, which served as a ground electrode, was painted on the outer surface the quartz tube. The inner diameter of quartz tube (i.e. the dielectric barrier) was 20.5 mm. A stainless steel tube of 13.0 mm diameter was set in the center of the quartz tube. High voltage power supply was consisted of an AC (Trek 20/20B) amplifier and a function generator (Tektronix, AGF310). The plasma-catalytic reactor was located inside an oven. The temperature was measured inside the oven, but outside the plasma reactor.

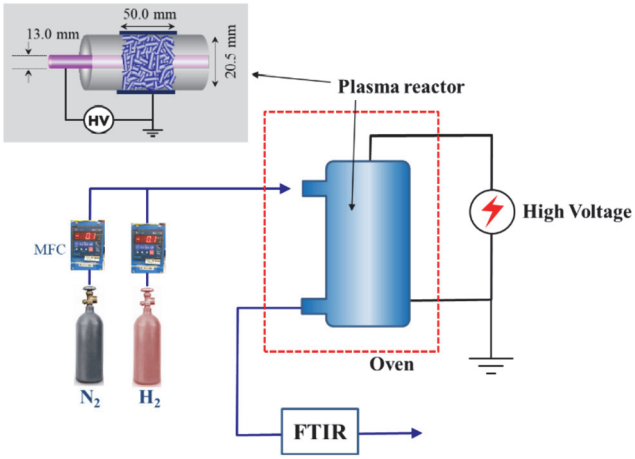

Figure 18: Schematic diagram of the plasma catalysis reactor.

A pellet-shaped Ru/γ-Al_2O_3 catalyst (diameter, 3.2 mm; length, 3.6 mm; surface area, 98.6 $m^2\ g^{-1}$) was used as the reference catalyst in this study. Cesium (Cs), magnesium (Mg), and potassium (K) were loaded as a promoter using a $CsNO_3$, $Mg(NO_3)_2$, and KNO_3 (Wako Chemicals, Ltd.) precursor with an impregnation method, as reported previously [153]. The samples were calcined in air at 500°C for 10 h. The Ru loading amount was 2 wt.%, hereinafter referred to as 2Ru. The promoter loading was 5 wt.% or 10 wt.%, hereinafter

referred to as 5Cs-2Ru, 5Mg-2Ru and 10K-2Ru. The catalyst amount packed in the plasma reactor was approx. 13.5 g. The reactant gas consisted of 80 vol.% N_2 and 20 vol.% H_2. This ratio of N_2:H_2 is different from the stoichiometric ratio (N_2:H_2=1:3), which is normally applied in thermal catalysis. The total flow rate was 4 L min^{-1}. Each gas flow rate was controlled using a mass flow controller (Koflok Co., FCC-3000). Waveforms of the applied voltage and discharge current were monitored using a digital oscilloscope (Tektronix DPO 7054) with a voltage divider (Tektronix P6015) and current probe (Pearson Electronics, Model 2877). The discharge power (P_{dis}) dissipated in the plasma-catalyst reactor was measured by a charge-voltage Lissajous figure software (Insight Co., Ver. 1.72).

The catalysts were characterized using a powder X-ray diffractometer (Rigaku, Model MiniFlex II), employing a Cu-K x-ray source (30 kV, 15 mA) and scan speed of 0.5° min^{-1} for measurements. The ammonia concentration was determined using an on-line Fourier transform infrared (FTIR) spectrometer (Perkin Elmer, SpectrumOne) with a long-pass gas cell and deuterated triglycine sulfate (DTGS) detector. The wavelength used for quantitative analysis of ammonia was 992.5 cm^{-1}. When a plasma parameter (i.e., the voltage or frequency) was changed it took about 10-20 min to reach the steady-state concentration of NH_3 at the reactor outlet. The time profile of NH3 was monitored at 1 min interval with a Timebase software (Perkin Elmer).

The experiments were performed by dr. Hyun-Ha Kim and co-workers at AIST in Japan, as previously reported in Ref. [89].

3.5.2 Experimental data

The experimental data is listed in **Table 4**.

3.5.3 Heating effects and power effects

The temperature in the plasma reactor depends on the SEI and the oven temperature. The change in activity upon increasing the SEI may be due to heating effects [152,162], giving rise to exponential activity changes with increasing temperature, or due to plasma-activation of molecules. Kim et al. found a linear effect of the SEI with the activity [89]. The extreme case of activity changes purely due to temperature effects is discussed here. This is done by comparing the observed activation barriers for data with comparable SEI values.

For the case with purely temperature effects, a correlation between the SEI and the temperature is used. From the reported data of Jidenko et al. [293] and Kim et al. [152] for the linear increase in temperature with SIE, an estimate of potential heating effects is provided in a DBD reactor operating at ambient temperature. These reactors operate at an ambient surrounding temperature and the temperature increase was reported to be maximum 100°C at a SEI of 400 J L^{-1}. However, when the temperature of the oven is controlled for operation at elevated temperatures, the heating effect of the plasma is expected to be smaller, as the temperature control loop will compensate at least partly for

the heating effect of the plasma. Thus, the reported data of Jidenko et al. [293] and Kim et al. [152] serves as an extreme case.

Jidenko et al. [293] measured the gas temperature and electrode surface temperature at flowrates of 0.5-3 L min^{-1} and a power input of 14 W, resulting in 280-1680 J L^{-1} power input. The inlet gas temperature was 20°C. The difference between the gas temperature (determined by the heating of the gas by the oven), and the electrode surface temperature was found to increase by 0.04 °C/(kJ L^{-1}). Thus, the maximum temperature difference between the gas and the surface for the experiments performed with the catalysts is 6-29°C, 6-8°C, 6-9°C, and 8-16°C for the 10K-2Ru/γ-Al_2O_3 , 10K-2Ru/γ-Al_2O_3, 10K-2Ru/γ-Al_2O_3, and 10K-2Ru/γ-Al_2O_3 catalyst, respectively (see **Table 4** for the power inputs).

Table 4: Experimental data for thermal catalysis and plasma-enhanced catalysis. Both previously reported data and new data is presented. The sources for the previously reported data is Ref. [89]. The catalyst weight is 13.5 g. The H_2:N_2 ratio is 1:4.

Catalyst	**Temperature** (°C)	**Flow rate** (L min^{-1})	**Energy input, SEI** (J L^{-1})	**NH_3 concentration** (ppm)	**Ref.**
2Ru/γ-Al_2O_3	200	1	0	0	[89]
	300	1	0	200	[89]
	200	1	483	244	[89]
	200	1	705	376	[89]
	250	1	735	588	[89]
	300	1	650	850	[89]
	300	2	165	233	This study
5Cs-2Ru/γ-Al_2O_3	200	4	0	0	This study
	250	4	0	32	This study
	300	4	0	135	This study
	200	4	206	147	This study
	250	4	163	162	This study
	250	4	217	270	This study
	300	4	164	389	This study
10K-2Ru/γ-Al_2O_3	300	4	0	122	This study
	330	4	0	436	This study
	200	4	158	79.7	This study
	200	4	222	137	This study
	250	4	153	201	This study
	250	4	220	321	This study
	300	4	169	551	This study
	330	4	162	917	This study
5Mg-2Ru/γ-Al_2O_3	200	2	0	15	[89]
	230	2	0	82	[89]
	250	2	0	261	[89]
	300	2	0	1440	[89]
	200	2	420	761	[89]
	230	2	373	1088	[89]
	250	2	386	1641	[89]
	280	2	211	1545	[89]
	300	2	205	1669	This study

It should be noted that Jidenko et al. [293] operated with a power input of 14 W and at 20°C, while the experiments in this work are performed with power inputs of 0.7-12 W and at 200-330°C. Thus, temperature differences between the gas and the surface are insignificant.

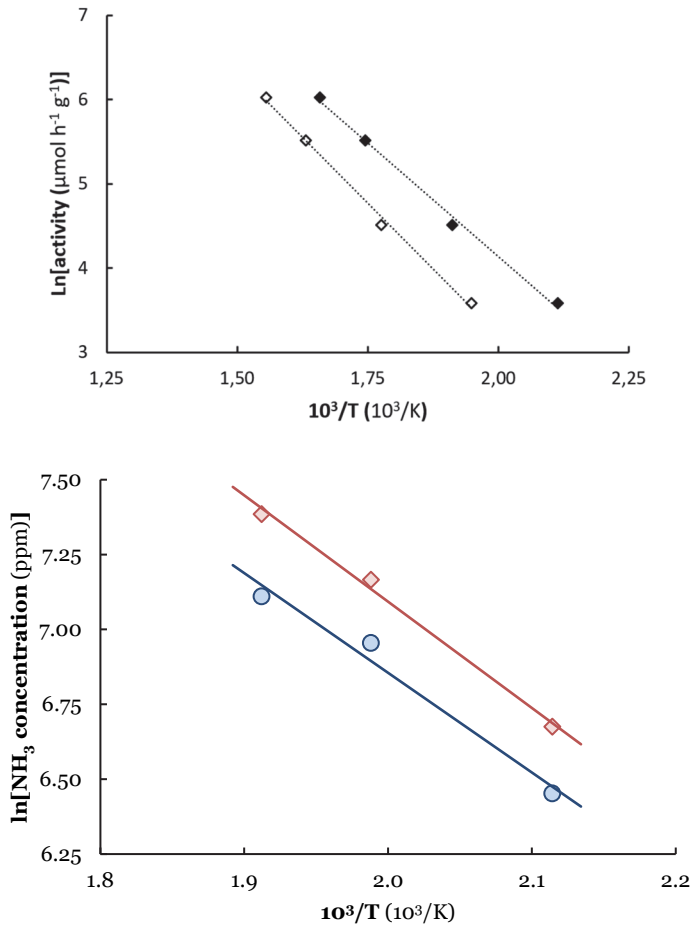

Figure 19: Top: Arrhenius plot of plasma-enhanced catalytic ammonia synthesis on various alumina-supported ruthenium-based catalysts. P=1 bar, H_2:N_2=1:4, 4 L min^{-1} feed rate (see Table 4). Activity defined in same manner as for thermal catalysis (i.e., not divided by the SEI), but a temperature offset is assumed, based on the SEI. Black filled diamonds (◆): 10K-2Ru/γ-Al_2O_3 (original data); and white filled diamonds (◇): 10K-2Ru/γ-Al_2O_3 (40°C offset assumed). Bottom: Arrhenius plot of plasma-enhanced catalytic ammonia synthesis on 5Mg-2Ru/γ-Al_2O_3, based on the data in Table 5. The red diamonds represent the total ammonia concentration, and the blue circles represent the net ammonia concentration from plasma catalysis.

Experimental data for the 10K-2Ru/γ-Al_2O_3 catalyst with a constant SEI (153-169 J L^{-1}) is used. This is done to have a constant plasma-activation of molecules. The temperature is assumed to increase with a rate of 0.25 °C/(J L^{-1}), based on the reported data in literature [152,293]. Thus, a temperature offset of about 40°C is assumed. Using this approach, an Arrhenius plot is obtained (**Figure 19**). It should be noted that the heating effect of the plasma is expected to decrease when the oven temperature increases.

As shown in **Figure 19**, activity data with a constant SEI can be plotted in an Arrhenius plot, yielding trends with a high correlation coefficient (R^2=1.00 for both the original data and the 40°C offset assumed). While for this dataset the apparent activation barrier for plasma-enhanced catalysis is 45 kJ mol^{-1} for the original data, it shifts to 52 kJ mol^{-1} when an offset of 40°C is assumed. Given that the apparent activation barrier for thermal-catalytic ammonia synthesis over potassium-promoted ruthenium-based catalysts is about 100-115 kJ mol^{-1} [259], a heating effect alone cannot explain the increase in activity for plasma-enhanced catalysis. A heating effect of about 260-320°C would be required to obtain an apparent activation barrier of 100-115 kJ mol^{-1}, which is not realistic for SEI values of 153-169 J L^{-1}. The difference in apparent activation energies for plasma-enhanced catalysis and thermal catalysis show that plasma-activation of molecules is an important for plasma-enhanced catalysis.

3.5.4 Activities of the promoted catalysts

First of all a distinction must be made between support effects and promoter effects. Alkaline earth metal oxides such as MgO can be used as support for Ru-based catalysts, which show a higher activity than for example Ru/Al_2O_3 which is thought to be caused by a slight change in Fermi level of the Ru metal caused by a change in electronegativity of the support. This has an effect on the barrier for N_2 dissociation, according to the Brønsted-Evans-Polanyi relation.

Regarding the role of promoters, see the discussion hereafter. Kowalczyk et al. [303] researched Ru catalysts supported on activated carbon with Ba and Cs promoters. Ba is an alkaline earth metal, while Cs is an alkali metal. Kowalczyk et al. [303] suggest that Ba already locates near the Ru at low promoter loadings, resulting in a promoting effect for ammonia synthesis. Above a certain content of Ba, the Ru surface will be covered by Ba, such that the activity actually decreases. On the other hand, an increasing Cs content nearly always leads to a higher activity.

The model for Cs is that it is thought to spread along the activated carbon surface, and thus it is at low promoter content not in strong contact with the Ru metal. At higher Cs content, it is thought that there support surface is 'full' with Cs, and contact with the Ru metal increases.

Aika [225] proposed a similar effect for the Cs promoter on Ru/Al_2O_3 catalysts. Aika proposed that the Cs first spreads on the Al_2O_3 surface. The effectivity of Cs promotion near the the Ru metal increases with Cs loading.

Along these lines, it is possible that the promoter effect of Mg, an alkaline earth metal, of the Ru/Al_2O_3 catalyst in this work is more effective than the promotion of Cs (and K), mainly due to the promoter content. The molar promoter ratio for the various catalysts is as follows:

- **10K-2Ru/γ-Al_2O_3**: 12.9 (mol-K mol-Ru^{-1})
- **5Cs-2Ru/γ-Al_2O_3**: 3.8 (mol-Cs mol-Ru^{-1})
- **5Mg-2Ru/γ-Al_2O_3**: 10.4 (mol-Mg mol-Ru^{-1})

The K/Ru ratio of 12.9 is much higher the Cs/Ru ratio of 3.8, explaining why the activity of the 10K-Ru/γ-Al_2O_3 catalyst is much more active than the 5Cs-Ru/γ-Al_2O_3 catalyst.

For the fresh Ru-Mg/Al_2O_3 sample, no Mg peaks were identified using, see **Figure 8** in Ref. [89]. For the used Ru-Mg/Al_2O_3 sample, a MgO peak was identified using XRD, see **Figure 8** in Ref. [89]. Thus, formation of Ru/MgO during operation cannot be excluded for the Ru-Mg/Al_2O_3 catalyst. Ru/MgO is known to be a more active catalyst for ammonia synthesis as compared to Ru/Al_2O_3.

3.5.5 Effect of SEI

The influence of the gas flow rate was previously discussed in Ref. [89]. **Figure 5**a in Ref. [89] shows that the ammonia formation scales linearly with SEI at 250°C. Thermal catalysis at this temperature is negligible (<150 ppm). Thus, a higher flow rate results in a lower outlet ammonia concentration. This indicates that the ammonia formation rate depends on the rate of formation for plasma-activated species, such as electronically activated N_2.

3.5.6 Reaction rates for plasma-catalytic ammonia synthesis

A simplified rate equation for plasma-catalytic ammonia synthesis is assumed in the main text of this Chapter, where the reaction rate is assumed to be a factor of temperature and plasma power. However, the total rate equation is more complex. Therefore, this section elaborates on all possible contributions from plasma chemistry, thermal catalysis, and plasma catalysis (**Equation 2**).

Equation 2: $$\mathbf{R_{total} = R_{forward,thermal\ catalysis} + R_{forward,plasma\ catalysis} + R_{forward,plasma} + R_{reverse,thermal\ catalysis} + R_{reverse,plasma\ catalysis} + R_{reverse,plasma}}$$

The plasma contribution and is constant with temperature, as found in **Chapter 5** and **Chapter 6**. Thus, it is only a function of the plasma power, and indirectly the SEI. The ammonia formation via plasma phase reaction ($R_{forward,plasma}$) is small in the current Chapter, as the rate of N radical formation is low for SEIs below 1 kJ L^{-1}. As shown in **Figure 9** in Ref. [42], the plasma only ammonia formation rate at 100-150°C yields 132 ppm for 5Mg-2Ru/γ-Al_2O_3 at a flow rate of 2 L min^{-1} and a SEI of ~400 J L^{-1}. The backward plasma phase reaction ($R_{reverse,plasma}$) is assumed to be small up till concentrations of ca.

0.5 mol.% NH_3 (see **Chapter 6**). In principle, the rate of decomposition increases linearly with product concentration (see **Figure 57** in **Chapter 6**). Thus, the contribution of plasma reactions is small when the SEI is below 1 kJ L^{-1}.

The contribution of the forward thermal-catalytic rate ($R_{forward,thermal\ catalysis}$) depends exponentially on the temperature. The reverse thermal-catalytic rate ($R_{reverse,plasma\ catalysis}$) can become relevant when the product concentration is relatively high, and the equilibrium concentration is approached. The contribution of the reverse thermal-catalytic reaction can be suppressed by keeping product concentrations low and far from equilibrium.

The contribution of the forward plasma-catalytic rate ($R_{forward,plasma\ catalysis}$) plasma catalysis depends on both the temperature and plasma power, when the rate-determining step in the reaction is activated. If the rate-determining step in the reaction is not activated, the plasma-catalytic rate is expected to mainly depend on the plasma power. In the current Chapter, the reaction is clearly activated. Evidence for the dependence on both temperature and plasma power can also be found in **Chapter 6**. The temperature effect is similar to thermal catalysis, e.g. an exponential relation with increasing temperature. Furthermore, the concentration of activated N_2 species scales linearly with increasing plasma power (and reduced electric field), as shown in **Figure 55** in **Chapter 6**. This indicates that plasma-catalytic rates at various SEIs can be compared by dividing the formed ammonia via plasma catalysis by the SEI.

The reverse plasma-catalytic rate ($R_{reverse,plasma\ catalysis}$) is assumed to be negligible at low product concentrations, as the relative fraction of activated product will be significantly lower than the relative fraction of activated N_2.

Table 5: Ammonia outlet concentrations from Ref. [42] for 5Mg-2Ru/γ-Al_2O_3 without plasma (plasma off) and with plasma (plasma on), at a flow rate of 2 L min^{-1} and a SEI of ~400 J L^{-1} for plasma on.

Temperature	100°C	150°C	200°C	230°C	250°C
Plasma off	0 ppm	0 ppm	26 ppm	115 ppm	256 ppm
Plasma on	132 ppm	132 ppm	793 ppm	1295 ppm	1612 ppm
Net plasma catalysis	0 ppm	0 ppm	634 ppm	1048 ppm	1225 ppm

The net ammonia formation via plasma catalysis can be estimated by subtracting the thermal catalysis contribution and plasma phase contribution (**Table 5**). The plasma phase contribution is estimated from the low temperature plasma on activity, e.g. where activated processes do not play a role.

The 'plasma on' ammonia concentration and the net plasma-catalytic contribution are shown in **Figure 19**, based on the results from **Table 5**. From **Figure 19** it follows that the apparent activation energy does not change significantly when including or excluding

the plasma phase contribution and thermal-catalytic contribution, due to the relatively small concentrations of ammonia versus the plasma-catalytic contribution. However, at higher plasma powers, or for more active catalysts, these contributions can become more significant.

Chapter 4

On the mechanism for the plasma-activated N_2 dissociation on Ru surfaces

Summary

Plasma-activation of N_2 via vibrational excitations or electronic excitations enhances the dissociative sticking probability on Ru-surfaces with respect to ground-state N_2. In this Chapter, it is proposed that this is primarily due to a weaker nitrogen-nitrogen bond, facilitating direct adsorption of both nitrogen atoms on the metallic surface, a pathway with a high barrier for ground-state N_2 due to the short bond distance of 110 pm. Furthermore, it is shows that the increased sticking probability is not only a heating artefact, as the activation barrier for N_2 dissociation decreases upon plasma-activation. Recent modelling studies show that the binding strengths of surface adsorbates, as well as the barrier for dissociation may change as a result of high electric fields, as well as high degrees of charging metal particles. It is shown that the effect of plasma-induced electric fields is negligible in DBD reactors, and other non-thermal plasma reactors. The effect of alkali promoters on the local electric fields is orders of magnitude larger than the electric field of the plasma. The role of plasma-induced metal surface charging during N_2 dissociation is currently not known for metal clusters on a support.

This chapter has been published as:

Rouwenhorst, K. H. R., & Lefferts, L. (2021). On the mechanism for the plasma-activated N_2 dissociation on Ru surfaces. Journal of Physics D: Applied Physics, 54, 393002. doi: 10.1088/1361-6463/ac1226

4.1 Introduction

Plasma-catalysis is an emerging field for activating strong chemical bonds in molecules such as CO_2, CH_4 and N_2 [40,41,56]. Rather than fully dissociating the molecules in the plasma, mild activation in the plasma via vibrational or electronic excitation, followed by dissociation on a catalyst may allow for a lower activation barrier on the catalyst [43]. For CH_4 it is established that the 1st vibrational level lowers the total activation barrier for dissociation [304], thereby increasing the dissociative sticking probability on Ni(100) surfaces [305]. However, the molecular mechanisms for plasma-catalytic CO_2 and N_2 dissociation are less understood.

Plasmas can be divided in the categories thermal plasmas and non-thermal plasmas [59,60,306,307]. In a thermal plasma, the electrons and the heavier plasma species (molecules, radicals, and ions) are in thermal equilibrium, resulting in temperatures in the order of 10^4 K [307]. In a non-thermal plasma, the electrons are not in equilibrium with the heavier plasma species, resulting in a substantially lower gas temperature as compared to the electron temperature [307]. Non-thermal plasmas can be classified as cold plasmas with a gas temperature typically near room temperature, and warm plasmas with gas temperatures of several 10^3 K [40,307]. The dominating activation channels in cold non-thermal plasmas, e.g. in a dielectric barrier discharge (DBD) reactor [45], are primarily electronic excitations with a minor role for vibrational excitations [40,41]. Warm plasmas combine characteristics of a thermal and non-thermal plasma, with a much higher electron temperature than the gas temperature, while the gas temperature is still typically several 10^3 K [40,307]. The primary activation channel of molecules in such warm plasmas is vibrational excitation [40,41].

Thermal plasmas and warm plasmas typically have such high temperatures, e.g. in the order 10^4 K and 10^3 K [40,307], such that no catalysts exist with sufficient thermal stability. However, various studies have attempted to couple plasma and catalyst in warm plasma reactors [119,126]. Alternatively, the catalyst can be placed after the plasma zone, where temperatures are lower [42,152]. At the other hand, the overall temperature in a cold non-thermal plasma is sufficiently low for plasma-catalyst combination inside the plasma zone [42,56,152].

N_2 is an extremely stable molecule, and breaking the triple N≡N bond is difficult, even in the presence of a catalyst. Typical barriers for thermal-catalytic N_2 dissociation are as high as 60-115 kJ mol^{-1} for Fe and Ru catalysts [224,225,308]. Therefore, N_2 dissociation is usually the rate-determining step for thermal-catalytic NH_3 synthesis [225], and temperatures of 400-500°C are typically required for NH_3 synthesis under industrial conditions [21,22,309].

Plasma-catalytic NH_3 synthesis has been studied widely in recent years [199,200,310], with emphasis on Ru catalysts in DBD reactors [74,82,83,89,94,99,223]. It was reported that plasma-activation of N_2 lowers the N_2 dissociation barrier on Ru catalysts, potentially allowing for operation at lower temperatures [49,94,236]. The barrier for N_2 dissociation decreases from

60-115 kJ mol^{-1} for thermal-catalytic NH_3 synthesis on Ru to 20-40 kJ mol^{-1} for plasma-catalytic NH_3 synthesis on Ru when operating at 0.1-0.4 kJ L^{-1} specific energy input [94], as was discussed in **Chapter 3**. At higher specific energy input, N_2 is increasingly dissociated in the plasma, and adsorption of N radicals will dominate plasma-catalytic NH_3 synthesis [126,179,223], as discussed in **Chapter 5**, **Chapter 6**, and **Chapter 7**.

The goal of this Chapter is to provide an overview of current understanding of plasma-catalytic ammonia synthesis, based on available literature from various disciplines. Therefore, the current understanding of thermal-catalytic N_2 dissociation on Ru catalysts is first discussed [263,311–314]. It is postulated that weakening of the N≡N triple bond by vibrational excitation and electronic excitation in a non-thermal plasma at low SEI leads to an increase in the distance between the nitrogen atoms, thereby facilitating a lower barrier pathway for N_2 dissociation as compared to ground-state N_2. The role of surface heating is also discussed, and it is shown that electric fields in non-thermal plasma are insufficient for enhancing dissociation of N_2 on Ru catalysts. However, the role of plasma-induced charging of metal particles is not well understood at this moment, and this remains an open question in the field of plasma-catalysis.

4.2 Thermal-catalytic N_2 dissociation on Ru catalysts

In the past few decades, theoretical physical chemistry has been used to better understand fundamentals of catalytic reactions [226]. Amongst others, understanding of N_2 dissociation on Ru catalysts is better understood using Ru(0001) as a model system [311,312]. A fundamental understanding of N_2 dissociation may aid in the development of more active catalysts for NH_3 synthesis.

Thermal-catalytic N_2 dissociation is an activated process on most transition metals. In accordance with the Polanyi principle [315,316], metals with a relatively weaker N binding energy have a higher activation barrier for N_2 dissociation [252,317].

From molecular beam experiments it was found that the dissociative sticking probability of N_2 on Ru(0001) increases with incident energy in N_2 [263,313,314], and more specifically vibrational excitation [313]. Various molecular beam experiments for N_2 dissociation on Ru(0001) surfaces are shown in **Figure 20**. In the ground state, the dissociative sticking probability of N_2 is in the order 10^{-6} [313], while the dissociation barrier on Ru(0001) surface is in the order of 100 kJ mol^{-1}. Mild activation of N_2 via vibrational excitation or electronic excitation is expected to increase the sticking probability substantially, as decreasing the nitrogen-nitrogen bond strength or excitation of the N_2 molecule may result in a lower dissociation barrier to be overcome for dissociation on the metal surface [49]. However, even at translational energies as high as 400 kJ mol^{-1} (far above the barrier for N_2 dissociation on Ru(0001)), the dissociative sticking probability is still limited to 10^{-2} and does not approach 1 [263,313]. Apparently, the energy partially dissipates to the surface via another pathway than N_2 dissociation. This limited dissociative sticking is most recently ascribed to translational and rotational motion of N_2 along the surface [311,312].

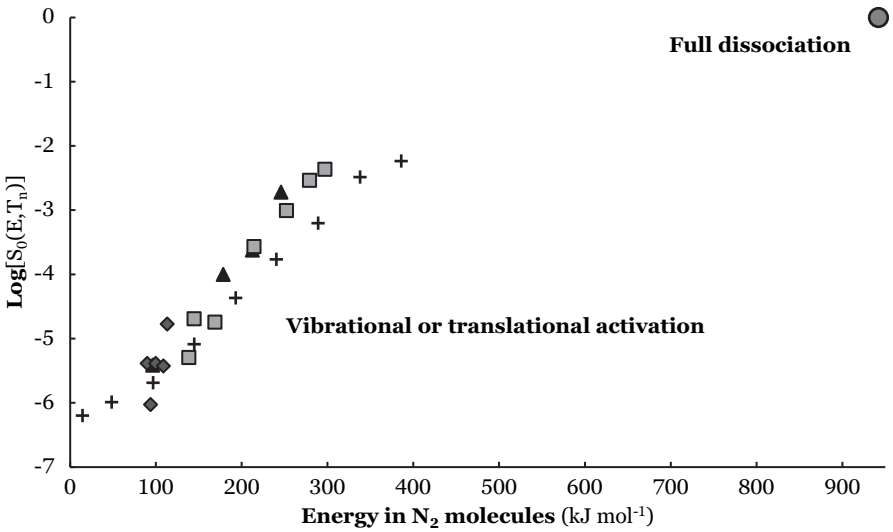

Figure 20: Effect of the N_2 kinetic energy on the dissociative sticking probability from molecular beam experiments. The Figure is constructed based on the Figure 1 in Ref. [263]. Original data from Romm et al. with a nozzle temperature <700 K (crosses), and with a nozzle temperature of 1750 K, probably with more vibrational activation in N_2 (triangles) [313], Egeberg et al. (diamonds) [314], Diekhöner et al. (squares) [263]. The circle represents the sticking probability of N radicals (e.g., fully dissociated N_2).

A high surface coverage affects the N_2 dissociation rate as the number of empty sites decreases, thereby limiting additional adsorption. Furthermore, an increased surface coverage of atoms such as N or S increases the barrier of N_2 dissociation, due to a change in d band density of states (DOS) [229,318,319].

On the other hand, the presence of alkali promoters increases the N_2 dissociation rate on Ru catalysts, as the NH_3 synthesis rate increases upon introducing alkali promoters on Ru catalysts [225,319]. The introduction of alkali promoters has little to no effect on the d band DOS (density of states) [229,318]. Instead, the barrier for N_2 dissociation is decreased by strong electric fields of 0.5-1.0 V $Å^{-1}$ caused by alkali ions via polarization of the nitrogen molecule [229,318,319].

The proposed pathway for thermal-catalytic N_2 dissociation on Ru(0001) is shown in **Figure 21**. Initially, N_2 is physisorbed perpendicularly to the Ru surface (I). Then, N_2 is chemisorbed in a metastable state (M), increasing the nitrogen-nitrogen bond distance from 110 pm to 121 pm [320]. Finally, the nitrogen-nitrogen bond is further weakened in the transition-state (TS), after which complete rupture occurs (F).

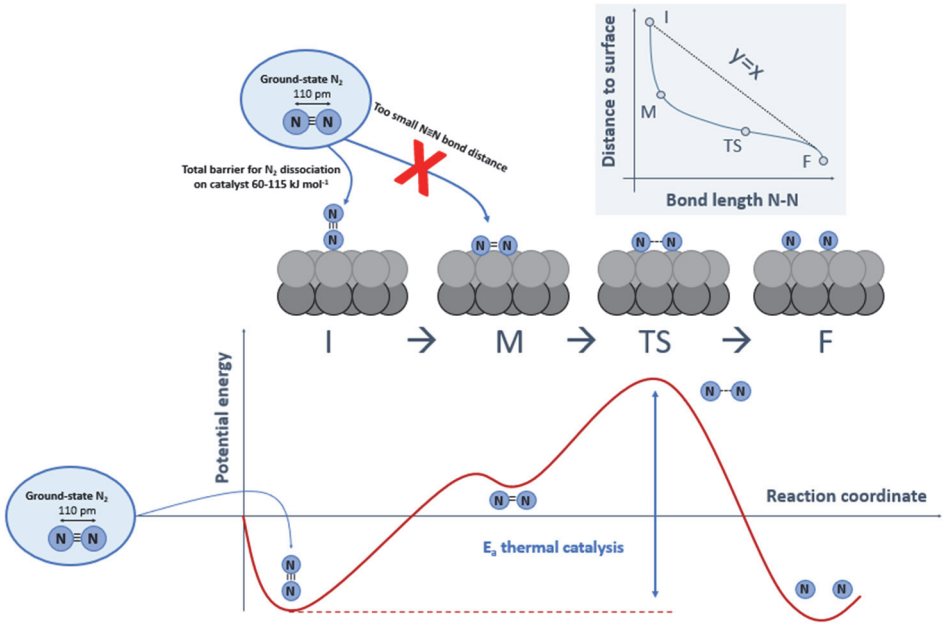

Figure 21: Proposed mechanism for N_2 dissociation on Ru(0001). The bond length b is the bond length between the two nitrogen atoms. The (I) state refers to the physisorbed state in which N_2 is physisorbed perpendicularly to the Ru surface. The (M) state refers to the metastable chemisorbed state, in which the molecular nitrogen-nitrogen bond distance is increased from 110 pm to 121 pm [320]. The (TS) state refers to the transition-state, in which the nitrogen-nitrogen bond is further weakened. The (F) state refers to the total rupture of the N2 molecule to two N atoms. Inspired by Refs. [318,320].

4.3 Plasma-activated N_2 dissociation

The molecular beam experiments in **Figure 20** indicate that the dissociative sticking probability may be increased for N_2 molecules with vibrational excitation and translational excitation in a non-thermal plasma. The question arises whether the increased dissociative sticking probability of N_2 upon plasma-activation is just due to a heating artefact [263], or to a decrease in the barrier for N_2 dissociation [49,94]. Heating effects in non-thermal plasma depend on the type of plasma and may occur very locally caused by plasma-catalyst interaction, possibly enhancing the dissociative adsorption rate of N_2 [162,307].

Recent research has provided support for the hypothesis that the barrier for dissociative adsorption of N_2 on Ru surfaces is decreased for plasma-activated N_2 as compared to ground-state N_2 [49,94]. Mehta et al. [49] postulated that the barrier for N_2 dissociation can be decreased by vibrational excitation, while the subsequent hydrogenation steps of N_{ads} to ammonia were proposed to not change (see **Figure 22**). Supporting experimental evidence is provided in **Chapter 3** for the claim that the barrier for N_2 dissociation is decreased by plasma-activation, based on a kinetic analysis of ammonia synthesis on Ru

catalysts in a DBD reactor. In case of thermal catalysis (i.e., without a plasma), the apparent activation barrier of ammonia synthesis is about 60-115 kJ mol^{-1}, which can be attributed to the dissociation of N_2 [224,257].

Upon plasma activation, the authors found that the apparent activation barrier for ammonia synthesis decreased to about 20-40 kJ mol^{-1}, which was attributed to a lower barrier for N_2 dissociation [94]. This mechanism was found to be relevant for catalysts with, at least some, thermal-catalytic activity combined with relatively low plasma powers (0.1-0.4 kJ L^{-1}). Furthermore, the influence of cations on activity of Ru catalysts has also been described based on the electronegativity of the support and of the alkali promoter for both thermal catalysis and plasma-catalysis in a DBD plasma. In both cases, the activity for N_2 dissociation increases with decreasing electronegativity of the support and the alkali promoter, as is inferred from the higher activity for ammonia synthesis [94].

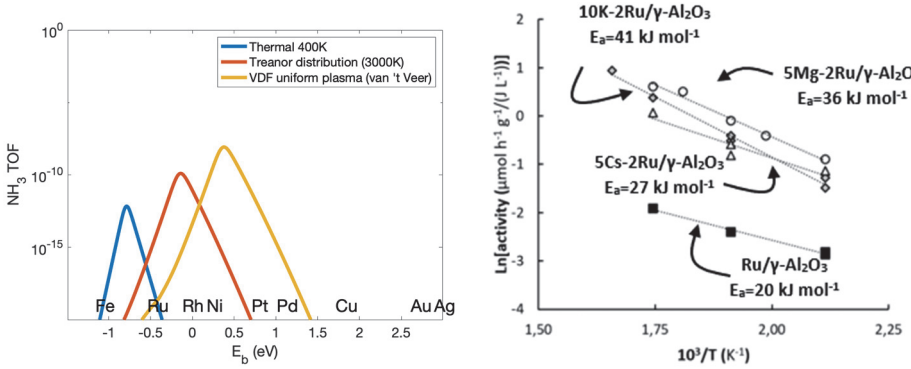

Figure 22: Left: Postulated effect of plasma-induced N2 activation on the catalytic activity at 400 K (thermal catalysis, plasma-activated N_2 with Treanor distribution, and VDF uniform plasma). Reproduced from Ref. [179]. Right: Apparent activation barriers for plasma-catalytic ammonia synthesis on Ru-catalysts at 200-300°C and 1 bar. Reproduced from Ref. [94].

Various authors suggested that the adsorption of N radicals present in the plasma can also be a kinetically relevant pathway for ammonia synthesis in the presence of a plasma and a catalyst [126,179,223], as discussed in **Chapter 5** and **Chapter 6**. This mechanism is dominant in case of relatively high plasma power, when the density of N radicals is substantial, and for catalysts that cannot dissociate N_2, even in case of vibrationally or electronically excited molecular N_2 [58,179,310].

The ratio $\frac{S_N \rho_N}{S_{N_2(ex)} \rho_{N_2(ex)}}$ expresses which of the two pathways is dominant for the adsorption of atomic nitrogen on the surface, activated N_2 or N radicals, where S_N is the sticking probability of N radicals and $S_{N2(ex)}$ is the dissociative sticking probability of plasma-activated N_2, whereas ρ_N and $\rho_{N2(ex)}$ are the densities of N radicals and plasma-activated N_2 in the plasma near the catalyst surface. The term plasma-excited N_2 is used for the

combined vibrationally-excited N_2 molecules and electronically-excited N_2 molecules. From **Figure 20** it follows that the values of S_N and $S_{N2(ex)}$ on Ru(0001) are about 1 and in the order 10^{-2}-10^{-1}, respectively. As N radicals do not have a barrier for adsorption on Ru, the dissociative sticking probability is about 1. Electronically-excited N_2 is assumed to be in the order 10^{-2}-10^{-1}, as this is the sticking probability for translationally-activated N_2 with an energy of 400 kJ mol^{-1} [313], as shown in **Figure 20**. Dominant electronic excitations in N_2 in a DBD reactor have an energy of 600 kJ mol^{-1} ($A^3\Sigma_u$) or 713 kJ mol^{-1} ($B^3\Pi_g$) [321], respectively, so 10^{-2} may be a conservative estimate and 10^{-1} is more likely.

This means the density of plasma-activated N_2 must be more than one or two orders of magnitude higher than that of N radicals for plasma-activated N_2 to be the dominant nitrogen species for plasma-catalytic ammonia synthesis. The densities of activated N_2 and N radicals depend on the plasma characteristics and the power applied [40,41]. Plasma modelling studies provide an estimation of the densities of activated N_2 and N radicals [87,253]. Typical densities for N radicals during the micro discharges in a DBD plasma are in the order 10^{-5} kg m^{-3} [253]. With increasing plasma power, the density of N radicals increases.

Recent modelling work of Van 't Veer et al. [253] shows that densities of above 10^{-3} kg m^{-3} are possible for electronically-excited N_2 molecules during micro-discharges in DBD reactors. In that case, the ratio $\frac{S_N \rho_N}{S_{N_2(ex)} \rho_{N_2(ex)}}$ becomes $\frac{1*10^{-5}}{10^{-1}*10^{-3}} = 0.1$. Alternatively, vibrationally-excited N_2 may dissociate on the Ru surface. For example, the first five vibrational levels for vibrationally-excited N_2 molecules with an excitation level up to about 140 kJ mol^{-1} show densities above 10^{-2} kg m^{-3} during micro-discharges according to Van 't Veer et al. [253]. As shown in **Figure 20**, this results in a dissociative sticking probability in the order $2*10^{-5}$. In that case, the ratio $\frac{S_N \rho_N}{S_{N_2(ex)} \rho_{N_2(ex)}}$ becomes $\frac{1*10^{-5}}{2*10^{-5}*10^{-2}} = 50$, e.g. favouring reactions with N radicals.

Thus, the mechanism with plasma-excited N_2 is plausible in case the plasma power is relatively low, typically below 10^2 J L^{-1} for DBD reactors [94]. For higher plasma powers, typically in the order 10^3-10^4 J L^{-1} for DBD reactors, the reduced electric field increases, which implies a higher fraction of the activated N_2 will be dissociated [40]. It should be noted that the plasma characteristics in a DBD reactor are stochastic (e.g., varying in time and space), and the densities of plasma species vary during the streamer discharges and the afterglow [253,322]. As the catalyst material determines the sticking probability of $S_{N2(ex)}$, this analysis is valid for Ru exclusively.

It should be noted that the ratio $\frac{S_N \rho_N}{S_{N_2(ex)} \rho_{N_2(ex)}}$ is a first approximation to estimate the dominant pathway. The gas temperature, and subsequently the translational energy, the

molar weight and the kinetic diameters of the gas species, among other factors, also influence the collision frequency in the plasma and with the surface. However, the differences in these properties between activated N_2 molecules and N radicals are only minor. Therefore, the ratio $\frac{S_N \rho_N}{S_{N_2(ex)} \rho_{N_2(ex)}}$ allows for a reasonable estimate for the dominant pathway.

It is proposed that the enhancing effect of plasma activation in N_2 dissociation can be understood based on the dissociation mechanism as described in **Figure 21** [318,320]. Plasma-activation by electronic excitation weakens the nitrogen-nitrogen bond, which increases the distance between the nitrogen atoms. In DBD plasmas, plasma-activation via electronic excitations in N_2 is dominant. For example the electronic excitation with an activation energy of 713 kJ mol^{-1} (7.39 eV, the $B^3\Pi_g$ state) results in an interatomic distance of 121 pm [321,323]. For reference, the bond interatomic distance for N_2 in the ground-state ($B^2\Sigma_u^+$) is 110 pm. Alternatively, vibrational excitations in N_2 may result in a similar nitrogen-nitrogen bond weakening [313], potentially with a higher energy efficiency [262]. In case of vibrational excitation, the nitrogen-nitrogen bond varies around an average bond length due to harmonic and anharmonic vibrations. With increasing vibrational excitation, the amplitude increases and the vibration become increasingly anharmonic, resulting in a higher average bond length between the nitrogen atoms.

As discussed in **section 4.2**, the bond-distance varies between the different adsorbed states of N_2 on Ru(0001). Ground-state N_2 first physisorbs perpendicular to the Ru surface (see **Figure 21**), as the interatomic distance for N_2 in the ground state is too small (110 pm) for direct parallel adsorption with both nitrogen atoms interacting with the metal surface, which would be optimal with a nitrogen-nitrogen bond distance of 121 pm [320]. For reference, the nitrogen-nitrogen distance in the physisorbed state perpendicular to the Ru surface is about 112 pm (see **Figure 21**). It is proposed that increased nitrogen-nitrogen bond distance in N_2 due to plasma-activation may open an alternative adsorption pathway. Rather than initial physisorption perpendicular to the Ru surface, it is postulated that plasma-activated N_2 with a bond distance of 121 pm can directly chemisorb on Ru surface sites with both nitrogen atoms in contact with the surface, similar to the M state in thermal catalysis (see **Figure 23**). This allows for a lower total barrier for N_2 dissociation for plasma-activated N_2 as compared to dissociation of N_2 from the ground-state.

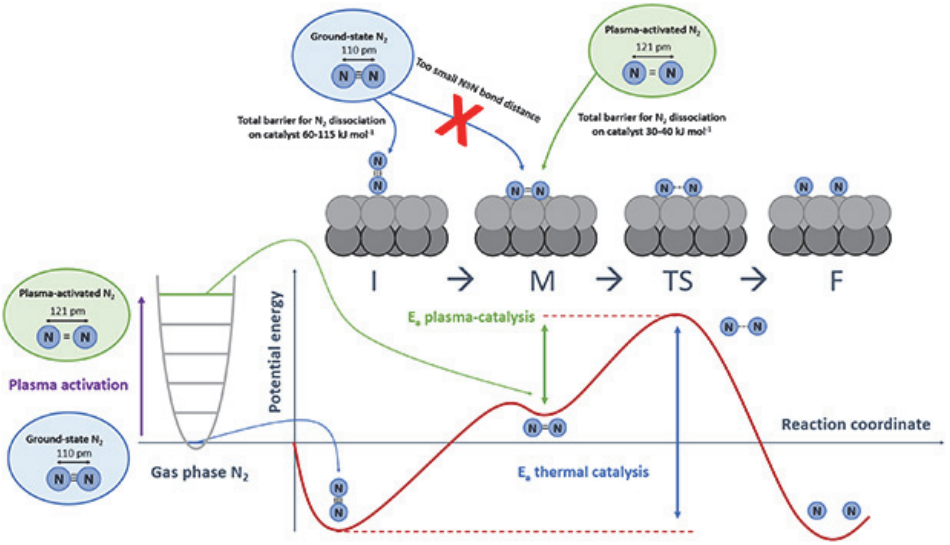

Figure 23: Proposed mechanism for plasma-activated N_2 dissociation on Ru catalysts. The (I) state refers to the physisorbed state in which N_2 is physisorbed perpendicularly to the Ru surface. The (M) state refers to the metastable chemisorbed state, in which the molecular nitrogen-nitrogen bond distance is increased from 110 to 121 pm [320]. The (TS) state refers to the transition-state, in which the nitrogen-nitrogen bond is further weakened. The (F) state refers to the total rupture of the N_2 molecule to two N atoms.

4.4 Effect of the plasma on the catalyst

Upon plasma illumination, there is a mutual influence of the plasma on the catalyst and vice versa [56,161,162,167,170]. Numerous effects have been described to be of potential importance, such as surface heating effects, plasma-induced electric fields, plasma-induced surface polarization, as well as an enhanced adsorption rate of plasma-activated molecules (see **Chapter 2**). Hereafter, the aim is to estimate the potential contributions of these phenomena for plasma-catalytic ammonia synthesis.

4.4.1 The role of surface heating

Plasma-induced heating can be very significant, especially when operating at near-ambient conditions and with high plasma powers [152,167]. Various authors showed that plasma-induced heating increases with increasing plasma power or specific energy input (SEI) [152,292,293]. For catalytic NH_3 synthesis, the effects are twofold: (1) the intrinsic activity for N_2 dissociation and hydrogenation on the catalyst increases with increasing temperature, and (2) product desorption is enhanced with increasing temperature, resulting in more free sites available for adsorption of reactants. In principle, the energy of plasma-activated N_2 that is not used for decreasing the barrier for N_2 dissociation is

dissipated as heat. Furthermore, electrons and radical species such as N, H, and NH_X may adsorb on the surface, further increasing surface heating, as adsorption is exothermic [162]. Radical species such as N, H, and NH_X can also react in the plasma phase itself, resulting in significant heat formation [307].

However, heating effects cannot account for the observed decrease in activation barrier from 60-115 kJ mol^{-1} for thermal-catalytic NH_3 synthesis on Ru to 20-40 kJ mol^{-1} for plasma-catalytic NH_3 synthesis on Ru at 200-330°C and at SEIs of 0.1-0.4 kJ L^{-1} [94], as was discussed in **Chapter 3**. Heating effects may only become significant at substantially higher SEIs [307]. For example, surface heating is found to be at least 125°C for a SEI of 38.4 kJ L^{-1} in **Chapter 6**.

4.4.2 The role of electric fields

Electric fields are present in all types of plasmas including non-thermal plasmas, such as DBDs. The potential role of electric fields has recently gained attention for plasma catalysis in various research groups [182–184,270]. Hereafter, a discussion follows regarding whether plasma-induced electric fields are sufficiently strong to influence catalytic reactions.

As discussed in **section 4.2**, the barrier for N_2 dissociation on Ru catalysts is decreased by alkali promoters, which is attributed to electric fields of 0.5-1.0 V $Å^{-1}$ [229,318]. Shetty et al. [324] recently demonstrated with DFT (density functional theory) calculations that electric fields of ±1.0 V $Å^{-1}$ also lead to a minor increase of 0.1 eV in the binding strength of N_2*. The adsorption of other molecules on surfaces under electric fields has been reported as well. For instance, Susarrey-Arce et al. [325] reported that an electric field as low as 10^{-3} V $Å^{-1}$ changes the mode of adsorption of CO on Pt, i.e. linear adsorption versus bridge bonded CO, without changing the reactivity of CO. Shetty et al. [324] reported an increased CO bond strength on Pt surfaces under electric fields with DFT calculations, albeit the increase was found to be as small as 0.025 eV under an electric field of 1 V $Å^{-1}$. Neyts et al. [182–184,270] performed theoretical studies on the effect of electric fields on the binding strength of CO_2 on various metal surfaces. For strong electric fields of 1.0-1.5 V $Å^{-1}$, the authors reported an increase in CO_2 binding strength on Cu surfaces.

Typical reduced electric fields in DBD reactors operated at atmospheric pressure are in the range of 100 to 1000 Td [40], which translates to electric field strengths between $3*10^{-4}$ and $3*10^{-3}$ V $Å^{-1}$. On the other hand, typical reduced electrical field strengths in low pressure plasma reactors such as radiofrequency (RF) and microwave (MW) reactors are less than 100 Td and gas densities are much lower at lower pressures, resulting in even lower electric field strengths than in DBD reactors. Modelling studies of DBD reactors confirm electric fields strengths of maximum 10^{-3} V $Å^{-1}$ near contact points in packed beds [172,173,188]. Recent imaging studies of the electric field strength near a plasma-surface with iCCD cameras reveal a maximum field strength of about $0.5*10^{-4}$ V $Å^{-1}$ [326]. Thus, plasma-induced electric fields in DBD reactors are much smaller than electric fields that are required to influence the catalytic activity, e.g. by alkali promoters in ammonia synthesis

as discussed above [229,318]. For reference, a reduced electric field of 37200 Td would be required to attain an electric field strength of 1.0 V Å^{-1}, which is not realistic for any type of non-thermal plasma.

Another argument for the negligible role of plasma-induced electric fields is based on experimental results. If electric fields were a dominant factor for plasma-catalytic N_2 dissociation, the role of the alkali promoters would be limited for plasma-catalysis. However, in **Chapter 3** it is found that the role of alkali promoters is equally significant for N_2 dissociation in case of thermal catalysis and plasma catalysis with plasma-activated molecular N_2. In both cases, the activity for ammonia synthesis is about an order of magnitude higher for the alkali promoted catalyst, as compared to the unpromoted catalysts [94]. Concluding, plasma-induced electric fields are too weak to play a significant role in N_2 activation.

4.4.3 The role of charging of metal particles

Hereafter the potential role of charging of metal particles is evaluated for a non-thermal plasma, such as a DBD plasma. Charging of metal particles by excess electrons from the plasma, thereby changing the Fermi level, can influence the N binding energy and consequently the barrier for N_2 dissociation.

Various authors have reported on the role of charging on metal particles in plasmas, especially for CO_2 adsorption. Bal et al. [183] reported in a theoretical study that the binding strength of CO_2, CO, O, and OH increases for single atom catalysts (Ti/Al_2O_3, Ni/Al_2O_3 and Cu/Al_2O_3) in the presence of an excess electron. Furthermore, Bal et al. [184] reported that the binding strength of CO_2 increases on boron nitride (BN) nanosheets in the presence of surface charging. Jafarzadeh et al. [270] reported on nanoclusters of five Ni or Cu atoms on TiO_2. The authors found that the adsorption strength of CO_2 on Ni_5/TiO_2 and Cu_5/TiO_2 increases upon adding negative charge to the surface. Jafarzadeh et al. [182] also reported on the role of excess electrons combined with an electric field for various Cu surfaces. The adsorption energy of CO_2 was found to increase assuming a strong electric field of 1.0-1.5 V Å^{-1} [182], which is however not realistic for any type of non-thermal plasma as discussed above. The combination of a strong electric field of 1.0-1.5 V Å^{-1} and an excess electron further increases the adsorption energy of CO_2 based on theoretical calculations, while an excess electron in absence of an electric field had no significant influence on the binding strength of CO_2 to the Cu facets. Concluding, the effect of charging metal surfaces has been studied by several authors. Effects on adsorption strength have been reported for CO_2 and CO, however, no information is available on any influence on reactivity. Furthermore, no information is available for N_2 adsorption and dissociation. Additional research would be required to assess whether charging of metal particles has any significant effect on N_2 dissociation.

It is currently an open question in the field of plasma-catalysis to what degree metal nanoparticles will be charged by excess electrons. The plasma is locally highly transient,

and the density of electrons varies over time. During the micro discharges, electron density is the highest (typically 10^{21} m^{-3} s^{-1} [253,307]), while the electron density decreases during the afterglow (down to 10^{15} m^{-3} s^{-1} [58,163,307]). The degree of charging of metal nanoparticles depends on the rate of metal surface charging during the micro discharges, and the rate of metal surface discharging during the afterglow. Thus, the degree of metal charging of metal particles varies over time. If there is any significant effect of charging of metal particles, it is expected to occur during the micro discharges. Additional research is required to assess the role of charging metal particles over time.

Concluding, the significance of metal surface charging in plasma-catalysis in general is currently not well understood. Thus, the role and significance of metal surface charging is a known unknown in plasma-catalysis [161,167]. Furthermore, it is unknown whether metal surface charging is sufficient to influence the rate of N_2 dissociation.

4.4.4 Maximizing the plasma-catalyst interaction

Upon coupling a plasma and a catalyst, the plasma is typically exclusively formed with the external surface of the catalyst. Plasmas cannot penetrate pores with a diameter smaller than the (sub-)micron range for atmospheric pressure DBD plasmas [163]. Typical pore diameters of catalysts are smaller than 50 nm [43,310], implying a plasma is not formed inside the pores of the catalyst. Very high onset potentials would be required to generate and sustain plasmas inside such small pores, in accordance with Paschen's law [307].

However, plasma species may still penetrate into the catalyst pores, if the lifetime and diffusion rate is sufficient to reach the metal nanoparticles inside the catalyst pores [152]. The typical diffusion coefficient (D_i) of N_2 molecules is 0.2 cm^2 s^{-1}, while vibrationally activated N_2 species have a lifetime (τ) of about 60 ns [327]. This results in a potential penetration length (L_D) into the pores of about 1.5 μm, as estimated according to $L_D = \sqrt{2D_i\tau}$. Thus, plasma species may penetrate pores to some extent, even though plasma cannot be generated inside pores with a diameter smaller than typically 1 μm.

Therefore, it is desirable to use thin layers of catalyst material in order to maximize the external surface area in structured reactors, such as coated wall reactors [328,329]. In general, macro-porous support materials would be preferred for plasma catalysis, be it that consequently the number of active sites per unit of volume would be small. Furthermore, Paschen's law dictates that the voltage required for breakdown is minimum at about 10 μm, implying a microchannel plasma reactor with a thin catalyst layer would probably be the best way to maximize the plasma-catalyst interaction [152,307], while minimizing the voltage required for breakdown.

4.5 Conclusion

Plasma-activation of N_2 via vibrational excitations or electronic excitations enhances the dissociative sticking probability on Ru-surfaces. This is not an artefact caused by heating, as it is reported that the activation barrier for N_2 dissociation decreases upon plasma-activation.

Plasma-activation of N_2 decreases the nitrogen-nitrogen bond strength, thereby increasing the bond length from 110 pm in the ground-state ($B^2\Sigma_u^+$) to 121 pm by for instance electronic excitation (7.39 eV, the $B^3\Pi_g$ state). It is postulated that the increased bond distance allows for the direct adsorption of both nitrogen atoms in the N_2 molecule on the metallic surface, a pathway prohibited for ground-state N_2 due to the too short bond length of 110 pm.

Recent modelling studies show that for high electric fields or high degrees of charging metal particles, the binding strengths of surface adsorbates may change. It is shown that the role of plasma-induced electric fields is too weak to cause any change in reaction rates in DBD reactors, and other non-thermal plasma reactors. The effect of alkali promoters on the local electric fields is orders of magnitude larger than the electrical field in a DBD reactor. It is not known whether plasma-induced metal surface charging has any effect on N_2 dissociation. Main uncertainties are the extent of surface charging in DBD plasma considering heterogeneity in the plasma and its dynamic behaviour. Additional research would be required to address this.

Chapter 5

Plasma-catalytic ammonia synthesis beyond thermal equilibrium on Ru-based catalysts in non-thermal plasma

Summary

Mehta et al. [236] proposed that plasma-catalytic NH_3 synthesis with plasma-excited N_2 allows for conversions beyond thermal equilibrium. In the current Chapter, it is shown that this is indeed possible with experimental data for Ru-based catalysts, above the temperature where thermal activity for NH_3 synthesis and NH_3 decomposition occurs. This is caused by competition between enhanced adsorption rates and subsequent hydrogenation rates of plasma-excited N_2 and N radical species, and the thermal-catalytic NH_3 decomposition reaction. Below the onset temperature for thermal activity for N_2 dissociation (about 300°C), the plasma-catalytic ammonia synthesis must be attributed to adsorption of N radicals generated in the plasma, with subsequent hydrogenation to NH_3, which can also result in conversions higher than the thermal equilibrium. These findings demonstrate that catalysts with thermal activity are not necessarily optimal for plasma catalysis.

This chapter has been published as:

Rouwenhorst, K. H. R., Burbach, H. G. B., Núñez Paulí, J., Vogel, D. W., Geerdink, B., & Lefferts, L. (2021). Plasma-Catalytic Ammonia Synthesis beyond Thermal Equilibrium on Ru-based Catalysts in Non-thermal Plasma. Catalysis Science and Technology, 11(8), 2834-2843. doi: 10.1039/D0CY02189J

5.1 Introduction

Recently, Mehta et al. [49] postulated that catalytic NH_3 synthesis can be enhanced via vibrational excitation of N_2 molecules in a non-thermal plasma, without affecting subsequent hydrogenation of N containing surface intermediates and desorption of NH_3. Plasma-activation of N_2 is proposed to enhance the nitrogen dissociation rate due to pre-activation of the N_2 molecule, decreasing the apparent barrier for N_2 dissociation, thereby increasing the ammonia synthesis rate [49,330]. This claim was substantiated in **Chapter 3** with a kinetic analysis for Ru-based catalysts in a narrow temperature range (200-330°C) at atmospheric pressure in a dielectric barrier discharge (DBD) reactor with relatively low plasma powers between 83 and 367 J L^{-1}. It was found that the dissociation of N_2 over the catalyst is still the rate-limiting step for ammonia synthesis [94]. This is supported by the similarity between the effects of electronegativity of supports and promotors on activity of Ru-catalysts, for both thermal catalysis and plasma-enhanced catalysis. Lower electronegativity of support and promoter leads to increased activity for NH_3 synthesis due to enhanced N_2 dissociation [94,225]. The barrier for N_2 dissociation was lowered from 60-115 kJ mol^{-1} for thermal catalysis to 20-40 kJ mol^{-1} for plasma-enhanced catalysis over Ru-catalysts [94]. These experiments were performed at low conversion, far away from thermodynamic equilibrium and at relatively low plasma powers.

Several pathways involving species in the plasma and on the catalyst surface may contribute to plasma-catalysis, as discussed in **Chapter 3**. In short, these are radical species generated in the plasma (i.e., N, H, and NH_X), which may react in the plasma phase and/or on the catalyst surface to form NH_3 [179], while also plasma-activated molecular N_2 may dissociate on the catalyst surface [49], with subsequent hydrogenation to form NH_3.

The process conditions (i.e. temperature, pressure, plasma power and properties), as well as the type of catalyst probably determine the dominant pathway. In this Chapter, the dominant pathways for NH_3 synthesis on Ru-based catalysts are determined, in the temperature range between 50°C and 500°C and for a specific energy input (SEI) of the plasma of 11.4-19.2 kJ L^{-1}, e.g. much higher than the plasma powers used in **Chapter 3**. Plasma chemistry dominates at low temperatures (<175°C), as the empty quartz reactor, bare MgO and Ru/MgO all yield the same outlet ammonia concentration. Ru catalyses plasma-driven NH_3 synthesis exclusively at temperatures above 175°C, allowing NH_3 to desorb. Between 175°C and 300°C, ammonia synthesis proceeds mainly via adsorption of N radicals generated in the plasma, which are subsequently hydrogenated to NH_3 on the catalyst. At higher temperatures, the thermodynamic equilibrium of the reactants and the product in the ground state is surpassed, which is attributed to a combination of catalytic ammonia synthesis with both ground state and excited molecular N_2, as well as catalytic hydrogenation of N radicals generated in the plasma, competing with thermal-catalytic ammonia decomposition.

5.2 Results

The experimental procedure can be found in the supporting information (**section 5.6.1**). In the upcoming section, the results of the catalytic tests for MgO, Ru/MgO and Ru-K/MgO with and without plasma are presented. The results of catalyst characterization and plasma characterization with Lissajous plots and UV-Vis spectroscopy can be found in the supporting information (**section 5.6.1**).

5.2.1 Thermal catalysis

The Ru-catalysts were tested for catalytic activity in the absence of a plasma, at atmospheric pressure, a constant H_2:N_2 ratio of 1:1 and a total flowrate of 20 mL min^{-1}, using 130 mg catalyst.

The Ru/MgO catalyst showed little thermal activity for NH_3 synthesis under the conditions used. Ammonia formation never reached the detection limit of the gas analyser, i.e. ~0.07 mol.%, which is equivalent to a catalyst activity of 1440 µmol NH_3 h^{-1} g_{cat}^{-1}. This is in line with results of Aika et al. [331], reporting an NH_3 synthesis rate as low as 60 µmol NH_3 h^{-1} g_{cat}^{-1} on Ru/MgO for H_2:N_2=3:1 at 315°C. Indeed, this is far below the detection limit of the gas analyser used in this work. **Figure 24** presents the result for co-feeding 0.5 or 1.0 mol.% NH_3. Again, no ammonia formation could be detected. However, the Ru/MgO catalyst is active for NH_3 decomposition at 400°C and above, at which temperatures decomposition is thermodynamically possible. The thermodynamic equilibrium is approached at 500°C.

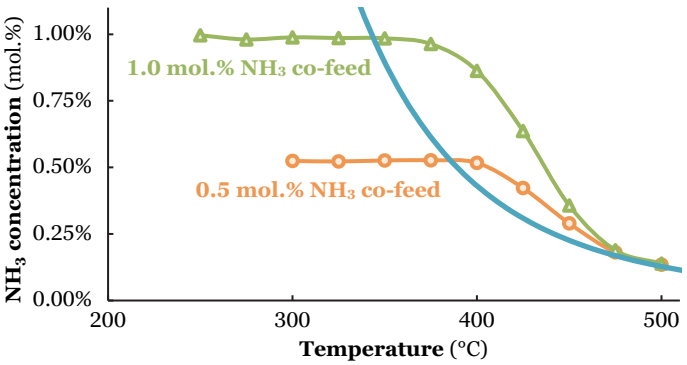

Figure 24: Activity for thermal-catalytic NH_3 decomposition with 0.5 mol.% NH_3 co-feed (orange circles) and 1.0 mol.% NH_3 co-feed (green triangles) on Ru/MgO. Total flowrate 20 mL min^{-1}, H_2:N_2=1:1, catalyst loading 130 mg (250-300 µm).

The potassium-promoted Ru/MgO catalyst (Ru-K/MgO) is more active than the unpromoted Ru/MgO catalyst, for both NH_3 synthesis and NH_3 decomposition (see **Figure 25**), in agreement with literature [224,331]. NH_3 is formed on the Ru-K/MgO catalyst

at about 310°C and above. The NH_3 synthesis rate on Ru-K/MgO is about 1750 µmol NH_3 h^{-1} g_{cat}^{-1} at 315°C, in reasonable agreement with literature values for the NH_3 synthesis rate (560-1060 µmol NH_3 h^{-1} g_{cat}^{-1}) on Ru-K/MgO at the same temperature and a H_2:N_2 ratio of 3:1 [331]. The higher NH_3 synthesis rate reported here can be attributed to the lower H_2:N_2 ratio of 1:1, preventing hydrogen inhibition, which suppresses adsorption of nitrogen [282].

An Arrhenius plot based on the data between 320°C and 355°C results in an apparent activation barrier for NH_3 synthesis of 92 kJ mol^{-1} (see **Figure 36**), in line with literature for NH_3 synthesis on Ru-based catalysts [224,331]. This barrier is attributed to the nitrogen dissociation step, the rate-limiting step for NH_3 synthesis over Ru-based catalysts [225].

Figure 25 also shows that Ru-K/MgO becomes active for NH_3 decomposition at 350°C when co-feeding 1.0 mol.% NH_3, e.g. at significantly lower temperatures than needed for NH_3 decomposition on Ru/MgO (see **Figure 24**). The recombination of N atoms to form N_2 is the rate limiting step for NH_3 decomposition on Ru-based catalysts [332,333]. Summarizing, the potassium-promoted catalyst is significantly more active for both NH_3 synthesis and NH_3 decomposition.

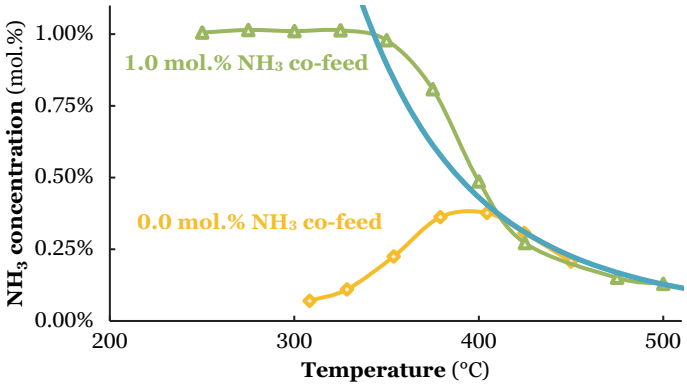

Figure 25: Activity for thermal-catalytic NH_3 synthesis with 0.0 mol.% NH_3 co-feed (yellow diamonds) and NH_3 decomposition with 1.0 mol.% NH_3 co-feed (green triangles) on Ru-K/MgO. Total flowrate 20 mL min^{-1}, H_2:N_2=1:1, catalyst loading 130 mg (250-300 µm).

5.2.2 Plasma catalysis

In case the plasma is illuminated, all reactor packings (MgO, Ru/MgO and Ru-K/MgO) show conversion to NH_3, as shown in **Figure 26**. An empty reactor without a packed bed, but with the spacer and quartz wool, shows an outlet NH_3 concentration of 0.14-0.17 mol.% and independent of temperature, indicating that NH_3 is formed via chemical reactions with in the plasma phase [94]. The presence of a packed bed of MgO particles does

not influence the conversion as compared to the empty reactor, indicating that the MgO surface does not play a significant role in the conversion of plasma-activated species to NH_3. This agrees well with observations in literature [334].

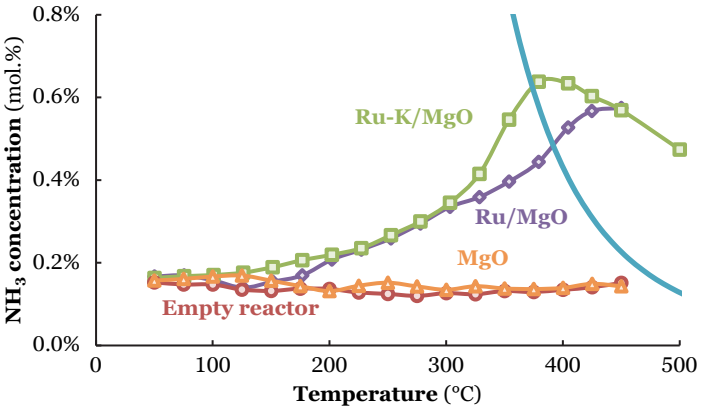

Figure 26: Activity for plasma-catalytic NH_3 synthesis (and decomposition) for empty reactor (only spacer & quartz wool, red circles), MgO (orange triangles), Ru/MgO (purple diamonds), Ru-K/MgO (green squares). Total flowrate 20 mL min^{-1}, H_2:N_2=1:1 (no NH_3 co-feed), catalyst loading 130 mg (250-300 µm), plasma power 3.8 W (SEI=11.4 kJ L^{-1}).

Below 175°C, the conversion obtained with Ru/MgO is similar to the conversion with bare MgO, implying that plasma chemistry is the dominant NH_3 formation mechanism at low temperature, rather than any catalytic contribution on the Ru surface. In fact, ammonia desorption from unpromoted Ru-based catalysts requires at least 180°C [83,260], indicating NH_3 cannot desorb from Ru at sufficient rates at temperatures below 175°C. Above 175°C, the conversion to NH_3 on Ru/MgO increases with increasing temperature. Consequently, the presence of Ru increases the rate of formation of ammonia compared to bare MgO, demonstrating a catalytic effect of Ru. Furthermore, NH_3 formation surpasses the thermodynamic equilibrium at temperatures above 400°C.

Ru-K/MgO has a similar activity profile like Ru/MgO. However, the onset temperature for the catalytic conversion is lower (125°C), which can be attributed to enhancement of NH_3 desorption caused by the potassium promoter [228]. The conversion on Ru-K/MgO and the Ru/MgO is similar up to 300°C. In the temperature window above 300°C, however, the conversion on Ru-K/MgO is higher than on Ru/MgO. This is in line with the onset temperature for thermal-catalytic NH_3 synthesis at 325°C for Ru-K/MgO, as shown in **Figure 25**. Thus, dissociative adsorption of molecular N_2 contributes in this temperature window, in line with claims in literature [89,94]. The highest energy yield obtained for Ru-K/MgO at 390°C is 1.23 g-NH_3 kWh^{-1}, which is far below the target of 150-200 g-NH_3 kWh^{-1} [42].

5.2.3 Plasma catalysis beyond thermal equilibrium

The NH_3 concentration on Ru/MgO goes through a maximum at about 420°C, after which the conversion decreases (see **Figure 26**). Apparently, the Ru/MgO catalyst is active for the thermal NH_3 decomposition reaction above 390°C, in line with **Figure 24**. A similar result is obtained with Ru-K/MgO at temperatures above 370°C, whereas the ammonia concentrations obtained with Ru/MgO and Ru-K/MgO at 450°C and above are the same. The conversion decreases further at higher temperatures. This is in line with theoretical calculations performed by Mehta et al. [236] for catalysts with an intermediate N binding energy, for which conversions beyond the thermal equilibrium are predicted upon plasma-activation of N_2. N_2 dissociation is the rate-determining step for NH_3 synthesis on such catalysts, and plasma-activation enhances the rate of N_2 dissociation towards NH_3 formation.

Figure 27 shows the effect of co-feeding of 0.5 and 1.0 mol.% NH_3 to Ru/MgO and Ru-K/MgO. The results without addition of ammonia in **Figure 26** are repeated in **Figure 27** for easy comparison. The plasma-catalytic conversion on Ru/MgO and Ru-K/MgO is different in the temperature window where thermodynamic equilibrium is not yet achieved, as Ru-K/MgO is more active for NH_3 synthesis. The potassium promoter enhances the ammonia desorption rate due to repulsion between potassium and NH_X [228,335], thereby allowing for a higher reaction rate on Ru-K/MgO. Furthermore, the results in **Figure 27** confirm that Ru-K/MgO is more active for ammonia decomposition than Ru/MgO, as decomposition is observed when increasing tempeature just beyond thermodynamic equilibrium. In case of Ru/MgO, significantly higher temperatures are required before observing significant ammonia decomposition. Above 450°C, both Ru/MgO and Ru-K/MgO approach the same conversion above thermal equilibrium, independent of the co-feed NH_3 concentration. This will be discussed below.

5.2.4 Effect of plasma power

Figure 28 shows that the ammonia concentration on Ru-K/MgO at temperatures above 450°C depends on the plasma power, which was varied between 3.8 W and 6.4 W. Additional experiments at 4.8 W and 6.4 W confirm that the NH_3 concentration obtained at temperatures above 400°C does not depend on co-feeding of ammonia (see **Figure 37** and **Figure 38**), very similar to the result presented in **Figure 27** at 3.8 W power.

5.3 Discussion

The discussion provides an overview of dominant mechanisms for plasma-driven NH_3 synthesis, in the presence and absence of an active catalyst under various process conditions.

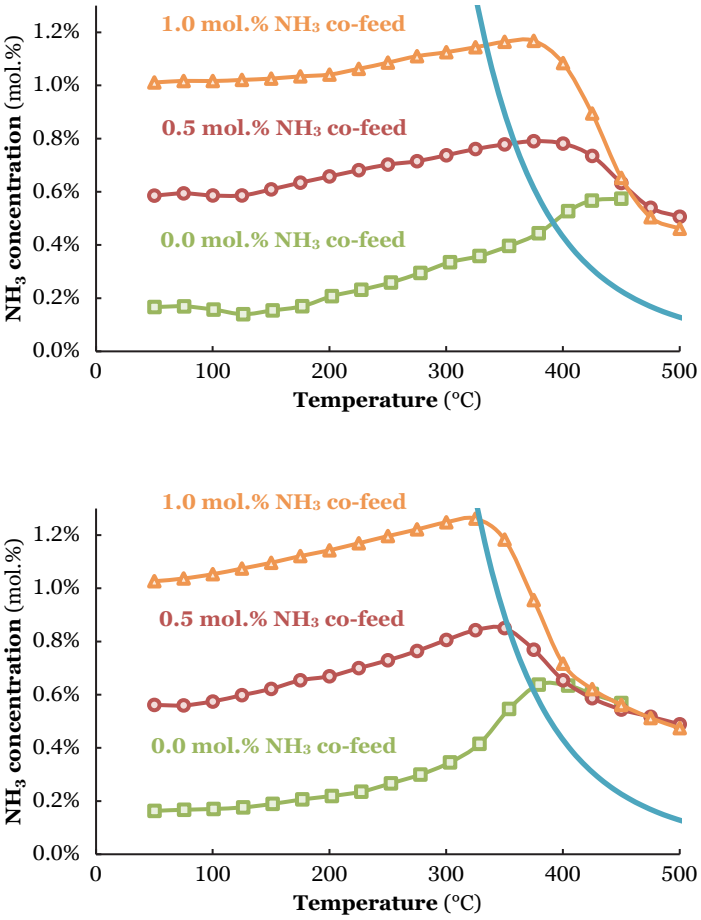

Figure 27: Activity for plasma-catalytic NH_3 synthesis (and NH_3 decomposition) for Ru/MgO (Top) & Ru-K/MgO (Bottom) for various NH_3 co-feed concentrations (0.0 mol.% (green squares), 0.5 mol.% (red circles) and 1.0 mol.% (orange triangles)). Total flowrate 20 mL min^{-1}, H_2:N_2=1:1, catalyst loading 130 mg (250-300 µm), plasma power 3.8 W (SEI=11.4 kJ L^{-1}).

5.3.1 Activity trends for plasma catalysis

Various authors have claimed that the introduction of a transition metal catalyst enhances ammonia synthesis in a non-thermal plasma [74,79,82,83,89,93,96,99]. On the other hand, the reactivity of the support is often not considered in plasma-catalytic systems. However, some authors have reported on the difference in conversion for a supported metal catalyst and the bare support. Peng et al. [74,99] reported on plasma-driven conversion in an empty reactor, with the bare support, as well as with supported metal catalyst (with a promoter)

at near ambient temperature. The plasma-driven conversion decreased in the order Ru-Cs/MgO > Ru/MgO ≈ MgO > empty reactor [99]. Similarly, Wang et al. [79] reported on plasma-conversion on various metal catalysts supported on Al_2O_3 in a DBD reactor, as well as an empty reactor at near-ambient conditions. The plasma-driven conversion decreased in the order Ni/Al_2O_3 ≈ Cu/Al_2O_3 > Fe/Al_2O_3 > bare Al_2O_3 > empty reactor [79]. The plasma-driven conversion in a plasma-reactor packed with Al_2O_3 support increases with increasing temperature with an activity decreasing in the order Co/Al_2O_3 ≈ Ni/Al_2O_3 ≈ Ru/Al_2O_3 > Al_2O_3, as reported by Barboun et al. [82]. Thus, catalytic effects of the transition metal nanoparticles can only be assessed properly when the support reactivity is minimal at the temperatures of operation used for the catalysts. Furthermore, Patil et al. [334] showed that the choice of support material influences the discharge characteristics. Similarly, high metal loadings of 10 wt.% may result in changes in the discharge characteristics [336]. Herrera et al. [80] concluded that the impact of metal nanoparticles on the discharge characteristics is not significant for 5 wt.% metal loadings on Al_2O_3. In the current work, a Ru metal loading of 2 wt.% is used to minimize potential effects of the metal nanoparticles on the discharge characteristics.

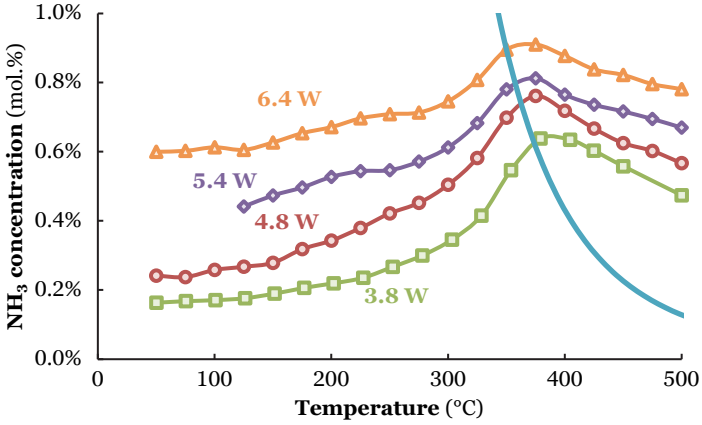

Figure 28: Activity for plasma-catalytic NH_3 synthesis (and NH_3 decomposition) for Ru/MgO for various plasma powers (3.8 W (SEI=11.4 kJ L^{-1}, green squares), 4.8 W (SEI=14.4 kJ L^{-1}, red circles), 5.4 W (SEI=16.3 kJ L^{-1}, purple diamonds) and 6.4 W (SEI=19.2 kJ L^{-1}, orange triangles)). Total flowrate 20 mL min^{-1}, H_2:N_2=1:1 (no NH_3 co-feed), catalyst loading 130 mg (250-300 µm).

As shown in **Figure 26**, the conversion is constant with temperature for the empty reactor (i.e., quartz wool only), as well as for MgO at a SEI of 11.4 kJ L^{-1}. Thus, the MgO support has no significant influence on the plasma-chemical reactions to NH_3, resulting in typically 0.15 mol.% NH_3, as shown in **Figure 26** and **Figure 29**. The fact that NH_3 forms in the plasma phase or on the reactor wall, implies that N, H, and NH_X radials are present in the plasma.

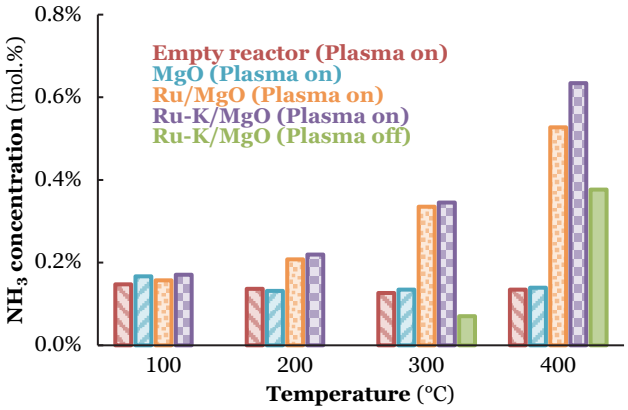

Figure 29: NH_3 outlet concentration for plasma-driven NH_3 synthesis and thermal-catalytic NH_3 synthesis as function of temperature. From left to right: the empty quartz reactor (red striped - plasma on), MgO packing (blue striped - plasma on), Ru/MgO catalyst (orange spotted - plasma on), Ru-K/MgO catalyst (purple checkerboard - plasma on; green single colour - plasma off). Total flowrate 20 mL min^{-1}, H_2:N_2=1:1, no NH_3 co-feed, catalyst loading 130 mg (250-300 µm), plasma power 3.8 W (SEI=11.4 kJ L^{-1}).

NH_3 synthesis is catalysed on the Ru metal in the presence of a plasma when operating above the apparent NH_3 desorption temperature for the Ru/MgO and Ru-K/MgO catalysts, 175°C and 125°C, respectively (see **Figure 26**). The difference in onset temperature is caused by the potassium promoter, which enhances the desorption rate of ammonia [335]. The activity of Ru/MgO and Ru-K/MgO in the presence of a plasma is similar in the temperature window between 200°C and 300°C (see **Figure 26**). Furthermore, the catalysts are not thermally active for NH_3 synthesis in the temperature window below 300°C in absence of plasma, due to kinetic limitations for N_2 dissociation [94,225]. The absence of any effect of potassium on the activity between 200°C and 300°C, suggests that the reaction proceeds dominantly via N radicals rather than mildly excited molecular N_2. The potassium is known to lower the N_2 dissociation barrier, thereby enhancing the N_2 dissociation rate [229], so that N_2 dissociation is apparently not rate determining in plasma catalysis between 200°C and 300°C. This is further supported by density functional theory (DFT) calculations performed by Engelmann et al. [179]. It is suggested that N radicals adsorb on the Ru surface, followed by hydrogenation on the surface and NH_3 desorption (Langmuir-Hinshelwood), in line with the conclusion that N radicals are present in the plasma, as discussed above. However, also Eley-Rideal type of reactions may contribute, e.g. $N+H_{ads} \rightarrow NH_{ads}$, without adsorbing the N radical first, as proposed by Engelmann et al. [179] and Yamijala et al. [181]. Adsorbed N radicals hydrogenate to NH_3 rather than forming N_2 because the hydrogenation reactions are generally faster than recombination to N_2 at temperatures below 300°C [49,319].

Furthermore, H radicals present in the plasma may contribute to fast hydrogenation to ammonia [179]. The dominant reaction pathway, e.g. Langmuir-Hinshelwood or Eley-Rideal mechanism, is discussed in **Chapter 6**.

Ammonia synthesis during plasma-catalysis on Ru-K/MgO is significantly faster than on Ru/MgO in the temperature window between 300°C and 400°C (see **Figure 26** and **Figure 29**), coinciding with the onset temperature for thermal catalysis on Ru-K/MgO (see **Figure 25**). Thus, molecular N_2 can dissociate thermally, implying that dissociation of plasma-activated molecular N_2 is even more facile [94]. The resulting activity is a mixture of a molecular mechanism via N_2 dissociation of both ground-state N_2 and probably plasma-activated N_2, as well as a reaction pathway via N radicals generated in plasma phase, as discussed above. As the concentration of N radicals is typically three to four orders of magnitude lower than plasma-activated molecular N_2 in DBD reactors [58,330], dissociation of ground-state N_2 and plasma-activated N_2 becomes increasingly dominant with increasing temperature.

The contribution of ground state N_2 and plasma-activated N_2 for NH_3 synthesis depends not only on the catalyst activity for N_2 dissociation, but also on the plasma power [94]. In **Chapter 3**, it was demonstrated that dissociation of plasma-activated, molecular N_2 and subsequent hydrogenation is dominant on Ru-catalysts for low plasma powers in the range 0.1-0.4 kJ L^{-1} at 200-300°C [94]. In contrast, the plasma power in the current Chapter is much higher, typically 11-19 kJ L^{-1}, implying substantially higher concentrations of N radicals.

N-recombination to N_2, i.e. the rate limiting step for NH_3 decomposition over Ru-catalysts [332], is fast on Ru-K/MgO at temperatures above 350°C in absence of plasma (see **Figure 25**). Therefore, the thermal-catalytic ammonia concentration is controlled by thermodynamic equilibrium above 350°C. In the presence of a plasma, higher ammonia concentrations are attained than would be expected based on thermodynamic equilibrium (see **Figure 26**, **Figure 27**, and **Figure 28**), which will be discussed hereafter.

5.4 Beyond thermal equilibrium

Plasma-driven conversions surpassing thermodynamic equilibrium is frequently reported for CO_2 splitting [337], dry reforming of methane (DRM) [338] and non-oxidative coupling of methane (NOCM) [339], mostly under conditions where thermal reactions do not contribute at all. The results in **Figure 26**, **Figure 27**, and **Figure 28** show surpassing thermodynamic equilibrium under conditions with significant reaction rates of thermal-catalytic ammonia synthesis as well as thermal-catalytic ammonia decomposition, as schematically presented in **Figure 30**.

The ammonia outlet concentration is the result of the competition between three reactions, i.e. at one hand NH_3 synthesis via molecular reactants N_2, either in the ground state ($r_{f,th}$) or in any excited state, including with radicals ($r_{f,pl}$)) and on the other hand NH_3

decomposition of the ground state NH_3 ($r_{b,th}$) exclusively (see **Equation 3**). Note that no distinction is made between excited nitrogen via vibrational excitation, electronic excitation or dissociation to N radicals for $r_{,pl}$.

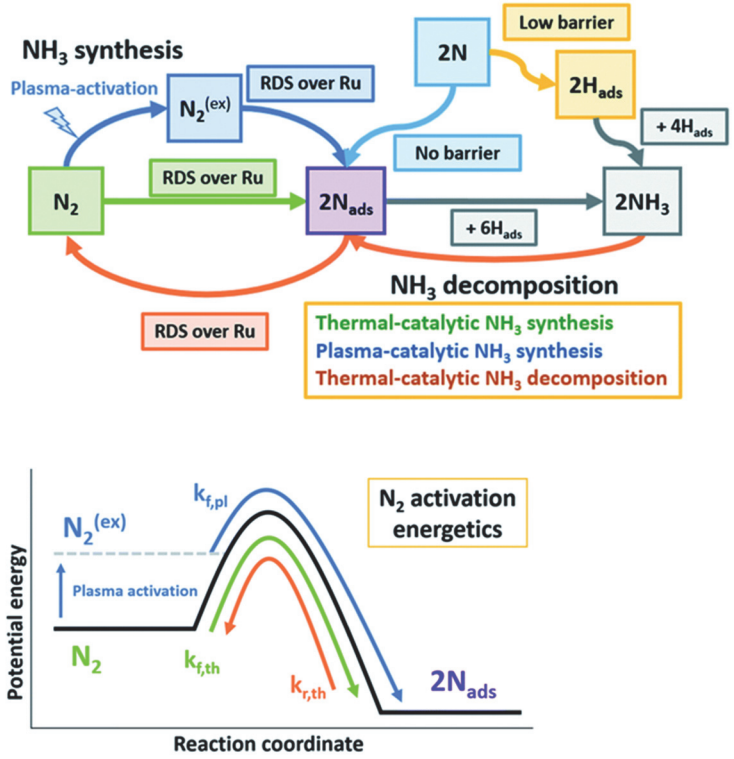

Figure 30: Top: Schematic representation of plasma-catalytic ammonia synthesis above the onset temperature for thermal-catalysis, including reactions with ground state N_2 (thermal catalysis), reactions with plasma-excited N_2 (plasma-enhanced catalysis), and reactions with N radicals (adsorption of N on empty sites and Eley-Rideal reaction with H_{ads}, see Ref. [179]). Bottom: Schematic free energy for thermal-catalytic NH_3 synthesis (green), plasma-catalytic NH_3 synthesis (blue), and thermal-catalytic (& plasma-catalytic) NH_3 decomposition (orange). Based on [236]. See also Equation 3. RDS: Rate determining step.

Irrespective of the inlet concentration of NH_3, the same concentration is attained at a given plasma power above 450°C (see **Figure 27**, **Figure 37**, and **Figure 38**). The increase in ammonia concentration when turning on the plasma thus depends only on the plasma power (see **Figure 28**) and not on the initial ammonia concentration. This indicates that in all cases steady-state is attained. The inlet ammonia concentration smaller than 1.0 mol.% NH_3 has no significant influence on the H_2:N_2 ratio, therefore resulting in the same steady-state NH_3 outlet concentration.

The observation that the ammonia concentration is influenced by the level of pre-activation of N_2 is in agreement with the trends predicted by the model of Mehta et al. [236], explaining the influence of plasma power in terms of lowering activation barriers for N_2 dissociation via pre-activation up till dissociation to N radicals (see the supporting information). In any case, the plasma-driven reaction ($r_{f,pl}$) is apparently faster than thermal ammonia decomposition ($r_{b,th}$), resulting in plasma-catalytic ammonia synthesis beyond equilibrium. This observation also rules out that thermal effects induced by the plasma dominate, because temperature increase would decrease the ammonia concentration, according to the thermodynamic equilibrium.

Equation 3: $\mathbf{R_{NH_3 prod} = r_{f,th} + r_{f,pl} - r_{b,th}}$

It is reasonable to assume that N_2 and/or H_2 are much more activated by the plasma than ammonia, due to the low concentration of NH_3 all experiments (<1.5 mol.%, balance H_2 & N_2 with a ratio of 1:1). For a discussion on the effect of the ammonia concentration, see **Chapter 6**. Furthermore, plasma-activation of NH_3 should not affect the catalytic NH_3 decomposition reaction, as N_2 recombination is the rate-limiting step for NH_3 decomposition on Ru-based catalysts [332]. Therefore, decomposition of plasma-activated ammonia is not included in **Equation 3**. At high ammonia concentrations, however, ammonia may decompose in the micro-discharges [253,274,340].

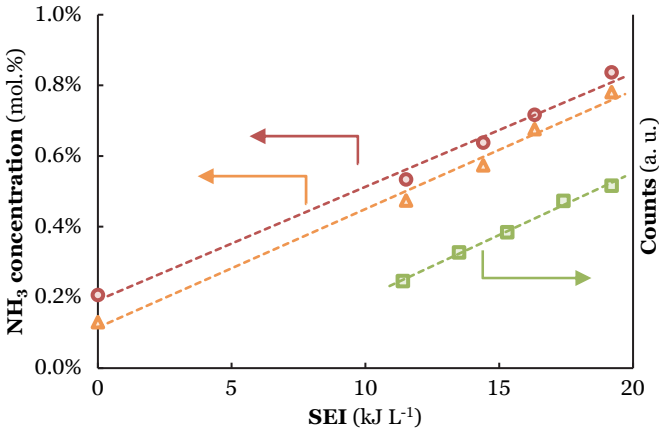

Figure 31: Left axis: NH_3 outlet concentration as function of the SEI at 450°C (red circles) and 500°C (orange triangles) over Ru-K/MgO (based on data from Figure 28). Total flowrate 20 mL min^{-1}, H_2:N_2=1:1 (no NH_3 co-feed), catalyst loading 130 mg (250-300 µm), plasma power 3.8-6.4 W (SEI=11.4-19.2 kJ L^{-1}). Right axis: Intensity of the peak at 337 nm in the UV Vis spectrum (Transition from $N_2(C^3\Pi_u(v=0))$ to $N_2(B^3\Pi_g(v=0))$, green squares), as function of the SEI. The density of NH radicals is also measured at 336.7 nm. However, the density of NH is orders of magnitude lower than that of plasma-activated N_2 [253]. See section 5.6.2.2 for the interpretation of UV-VIS measurements and Figure 35 for the UV-Vis spectra.

Figure 31 shows strong correlations between the NH_3 concentration measured at 450°C with both plasma power and the concentration of excited N_2 molecules in the plasma, as measured with UV Vis spectroscopy (**Figure 35**). The rate of plasma-driven ammonia formation may increase with plasma power, due to two effects. Firstly, with the level of activation of individual N_2 molecules increases, thereby decreasing the activation barrier for dissociation (**Figure 30**). Secondly, increasingly activating N_2 molecules eventually leads to dissociation of highly reactive N radicals. Both effects would lead to increasing reaction rates on the surface.

The observation that catalysts with thermal activity at the operating conditions are not necessarily the optimal choice for plasma catalysis agrees with a theoretical argument formulated in the latest roadmap for plasma catalysis [43]. This notion should have a major impact in the field, as frequently catalysts used in plasma catalysis research are based on the thermal performance of these catalysts. It is now demonstrated that the activity for the reverse reaction is undesirable and different catalysts should be considered when approaching or surpassing thermodynamic equilibrium based on the ground state molecules.

5.5 Conclusion

Plasma-catalytic NH_3 synthesis has been assessed over a wide temperature window (50-500°C). A distinction was made between plasma-chemical and plasma-catalytic effects by performing measurements with an empty quartz reactor, the MgO support and the MgO supported Ru-catalysts. At low temperatures (<175°C), plasma chemistry dominates, resulting in the same ammonia outlet concentration for the empty quartz reactor, the MgO support, and the MgO supported Ru-catalysts. At low temperatures, NH_3 cannot desorb from the Ru surface, thereby inhibiting the plasma-catalytic formation of NH_3 on the Ru surface. It was found that plasma-driven NH_3 synthesis is catalysed by Ru exclusively at temperatures above 175°C, allowing for NH_3 desorption. Furthermore, the potassium promoter has no influence on the plasma-catalytic activity at temperatures with insignificant thermal activity, i.e. typically below 300°C, indicating that adsorption of N radicals on an empty surface site or a reaction of N radicals with H_{ads} via an Eley-Rideal reaction is dominant, with subsequent hydrogenation to NH_3.

At temperatures with significant thermal activity for ammonia synthesis, i.e. above 300°C for Ru-K/MgO, the plasma enhances the catalytic NH_3 synthesis rate, which is due to enhanced dissociative adsorption of plasma-activated N_2. The plasma-catalytic NH_3 synthesis rate is then a combination of the catalytic hydrogenation of N radicals on the Ru surface, and the catalytic NH_3 formation rate from plasma-activated molecular N_2 as well as ground state N_2, i.e. thermal-catalytic NH_3 synthesis.

At elevated temperatures, typically above 400°C, plasma-catalysis results in ammonia concentrations beyond thermodynamic equilibrium. Therefore, plasma-activated molecular N_2 and N radicals contribute to adsorption, increasing the rate of formation of

ammonia, beyond the activity of the catalyst to decompose ammonia. With increasing plasma power, the density of plasma-activated molecular N_2 and N radicals increases, thereby increasing the conversion beyond equilibrium.

5.6 Supporting information

5.6.1 Experimental procedure

Ru/MgO catalysts were tested for the activity for ammonia synthesis in the absence and in the presence of a plasma, as ruthenium-based catalysts are most active for ammonia synthesis under mild conditions [281]. Furthermore, ruthenium-based catalysts have been studied most among transition metals for the plasma-catalytic activity [74,82,83,89,93,94,99]. The MgO support was chosen because of the absence of acid sites, and the high thermal activity for ammonia synthesis [331]. Acid sites on supports such as Al_2O_3 cause ammonia desorption limitations at mild temperatures (<200°C) [79], making the distinction between desorption limitations of an active metal and the support difficult. Furthermore, a potassium alkali promoter is added to enhance the ammonia synthesis [225,228,281]. The potassium promoter enhances the activity for N_2 dissociation and the rate of ammonia desorption [94,225,228].

5.6.1.1 Materials

Ruthenium (III) nitrosyl nitrate ($Ru(NO)(NO_3)_3$, >31.3 wt.% Ru) was purchased from Alfa Aesar. Magnesium oxide (MgO, >97% purity grade, 30 m^2 g^{-1}) and potassium nitrate (KNO_3, 99% purity grade) were purchased from Merck. H_2 and N_2 with a purity grade of 99.999% were purchased from Linde, and water traces were removed using Agilent gas clean purification systems. A gas mixture of 2 vol.% NH_3 in a 98 vol.% N_2 balance gas was purchased from Linde. All materials were used as received. Deionized water was used during catalyst preparation.

5.6.1.2 Catalyst preparation

The $Ru(NO)(NO_3)_3$ precursor was dissolved in water and impregnated on the MgO support using the dry impregnation method. About 1.2 mL^{-1} water was used per gram of MgO. Then, the mixture was dried in an oven at 100°C and atmospheric pressure for 1 h, followed by drying in a vacuum oven at 120°C for 2 h.

The dried catalyst was calcined in 20 mL min^{-1} air flow at 400°C for 2 h in order to oxidize the Ru precursor. Subsequently, the RuO_2 was reduced in a 20 mL min^{-1} H_2 flow at 400°C for 2.5 h. For the Ru-K/MgO catalyst, KNO_3 was dissolved in water and impregnated on the Ru/MgO catalyst, using the dry impregnation method. About 1.2 mL^{-1} water was used per gram of Ru/MgO. Then, the mixture was dried in an oven at 100°C and atmospheric pressure for 1 h, followed by drying in a vacuum oven at 120°C for 2 h. After reduction,

the catalysts were pelletized and crushed. The sieve fraction 250-300 μm was used for the catalytic tests. Last traces of H_2O and nitrates are removed in the reactor at 400°C.

5.6.1.3 Catalyst characterization

The total surface area and pore volume was determined by N_2 chemisorption at -198°C using a Micromeritics Tristar. The samples were outgassed in vacuum at 300°C for 24 h before the analysis. The Ru particle size and metal dispersion were determined by CO chemisorption. The elemental composition was determined by x-ray fluorescence spectroscopy (XRF) using Bruker S8 tiger. The crystalline phases present in the catalyst, as well as the Ru particle sizes were determined with x-ray diffraction (XRD) using a Bruker D2 Phaser diffractometer equipped with a position-sensitive detector over a 2θ range between 10° and 90° using Cu Kα radiation (λ= 1.5418 Å). Particles sizes of Ru are estimated based on the width of the peak at 38° using the Scherrer equation.

K. Altena-Schildkamp is acknowledged for N_2 chemisorption and CO chemisorption measurements. T. M. L. Velthuizen is acknowledged for XRF analysis.

5.6.1.4 Plasma characterization

A PMV 500-4000 power supply was used to illuminate the plasma at 25 kHz. A Picoscope PC Oscilloscope was used to monitor the charge-voltage characteristics. The high voltage electrode was connected to the power supply, and an AC voltage of up to 10 kV peak to peak was applied. A Tektronix P6015A high voltage probe was used to monitor the voltage over the high voltage electrode, while a TT-HV 250 voltage probe was used to measure the voltage over the ground electrode. A capacitor of 8.24 nF was placed in between the ground electrode and the TT-HV 250 voltage probe. An Ocean HDX Spectrometer was used to analyze light emitted by the plasma, just below the catalyst bed, at low temperature.

5.6.1.5 Catalytic tests

A schematic representation of the experimental set-up for the catalytic tests is shown in **Figure 32**. The catalytic tests were carried out in a quartz tubular reactor with an inner diameter of 4 mm and an outer diameter of 6 mm, at atmospheric pressure. A stainless-steel rod of 1 mm diameter is placed inside the reactor as the high voltage electrode. At the outside of the quartz tube, a metal tube is placed as the ground electrode. The temperature was controlled with a thermocouple connected to a heating block, which is placed around the ground electrode. The flowrates of the reactants were controlled with calibrated mass flow controllers (MFCs). Typically, 130 mg of catalyst with particle size 250-300 μm was loaded in the reactor, on top of a layer of quartz wool. A spacer is placed above the catalytic bed to prevent moving of particles due to plasma-illumination and to center the high voltage electrode.

The catalyst was reduced at 400°C in the reactor for 2 h in a gas mixture of 40 mL min^{-1} N_2 and 10 mL min^{-1} H_2. The catalytic tests were performed in a temperature-programmed plasma surface reaction, as previously reported by Parastaev et al. [341]. The heating rate was 2.5 K min^{-1}, which is sufficiently slow such that the temperature ramp approaches a steady-state at a given temperature. The product gases were analyzed using an on-line Pfeiffer Vacuum Thermostar™ gas analysis system, which is a mass spectrometer (MS). The MS signal for NH_3 (17 m/e) was calibrated in the range 0-2 mol.%, resulting in a linear relationship. The signals for H_2 (2 m/e), N_2 (28 m/e) and H_2O (18 m/e) were also monitored semi-quantitatively, as well as a minor NH_3 peak (16 m/e).

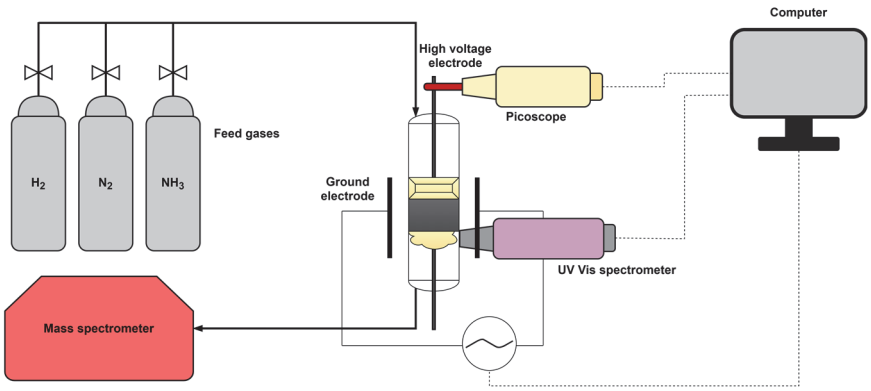

Figure 32: Schematic representation of the experimental set-up. The plasma volume includes the space, the packed bed, and the quartz wool.

5.6.2 Results

5.6.2.1 Catalyst characterization

The catalyst characterization results for MgO, Ru/MgO, and Ru-K/MgO are listed in **Table 6**. The XRD spectrum of Ru/MgO is shown in **Figure 33**. The results are in line with previously reported data [49,224,331].

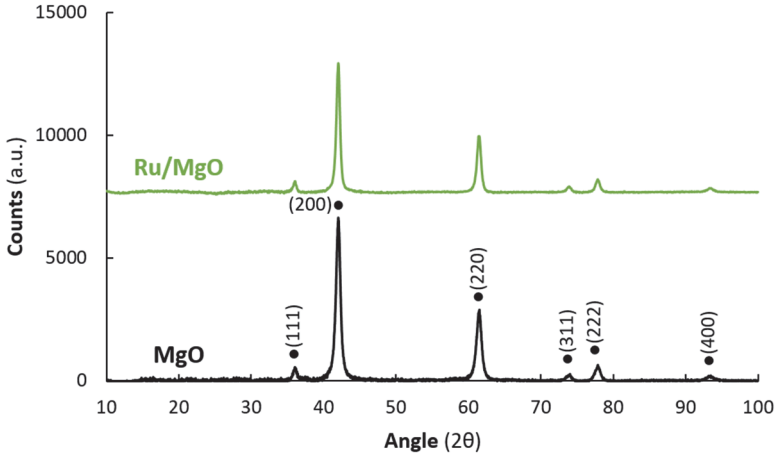

Figure 33: XRD spectrum for MgO and Ru/MgO. The Miller indices indicate the crystalline lattice structures exposed in the MgO.

Table 6: Structural and physical properties of MgO, Ru/MgO, and Ru-K/MgO. [a] Measured with N_2 physisorption. [b] Determined by XRF. [c] Determined by CO chemisorption. [d] Determined by XRD-LB.

Catalyst	S_{BET} ($m^2\ g^{-1}$)[a]	V_{Pore} ($cm^3\ g^{-1}$)[a]	Ru loading (wt.%)[b]	K loading (wt.%)[b]	Ru particle size (nm)[c]	Ru dispersion (%)[c]
MgO	294	0.31	-	-	-	-
Ru/MgO	78	0.21	2.0	-	16[c], 15[d]	9.2
Ru-K/MgO	-	-	1.9	6.1	16[c], 15[d]	9.2

5.6.2.2 Plasma characterization

The voltage and charge were monitored with an oscilloscope, from which the power dissipated can be determined using a Lissajous figure. An example of a Lissajous figure (also termed Q-V plot) is shown in **Figure 34**. In a Q-V plot, the capacitive and discharge behavior of a plasma is monitored. Ideally, a Lissajous figure has the shape of a parallelogram, thereby perfectly separating the capacitive and discharge regime. However, as shown in **Figure 34**, there is an indent in both the positive and negative charge cycle. This can be attributed to a discharge at the contact points at an earlier stage than over the remainder of the surface [80,163]. The choice of the packing had little to no influence on the discharge characteristics, in line with literature data reported by Herrera et al. [80].

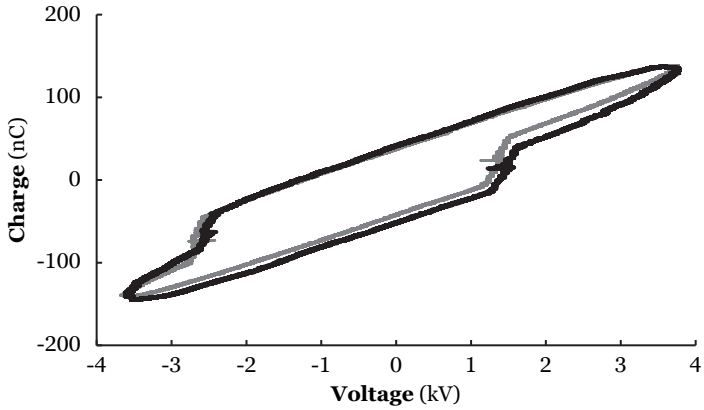

Figure 34: Lissajous figure for MgO (grey) and Ru-K/MgO (black) at 30°C, H_2:N_2=1:1, 20 mL min^{-1}. The total power dissipated is 6.4 W.

An example of an emission spectrum at 6.4 W input power and in pure N_2 is shown in **Figure 35**, in line with literature [49,76]. As follows from the emission spectrum, the most pronounced peaks are found in the regime 290-400 nm, which corresponds to the second positive band from an activated neutral N_2^* molecule ($C^3\Pi_u \rightarrow B^3\Pi_g$) [342]. This implies that photons are emitted upon plasma-activated N_2 falling back from an electronically and/or vibrationally excited state to a lower energy state of N_2.

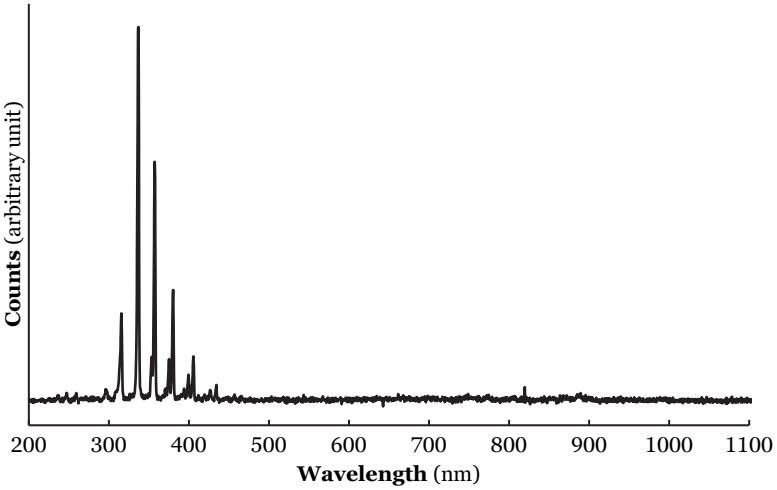

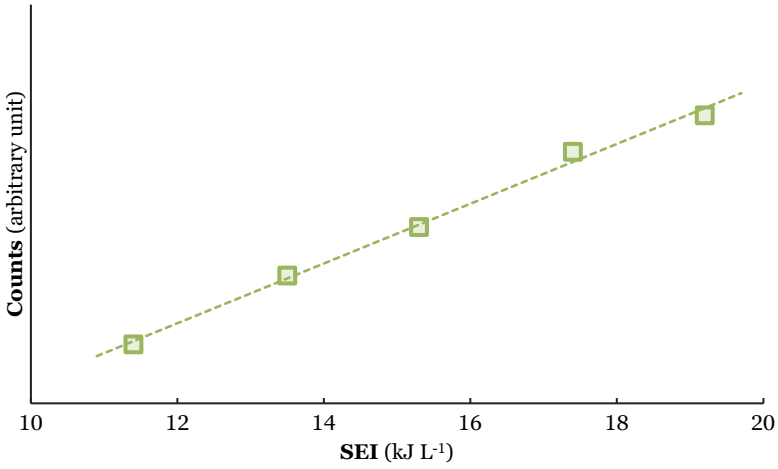

Figure 35: Top: Number of counts for pure N_2, measured in quartz wool just below MgO packing at SEI=19.2 kJ L^{-1}. Flowrate 10 mL min^{-1}. Bottom: Number of counts of UV Vis spectrum at 337 nm (Transition from $N_2(C^3\Pi_u(v=0))$ to $N_2(B^3\Pi_g(v=0))$, green squares), as function of the SEI.

5.6.2.3 Thermal catalysis

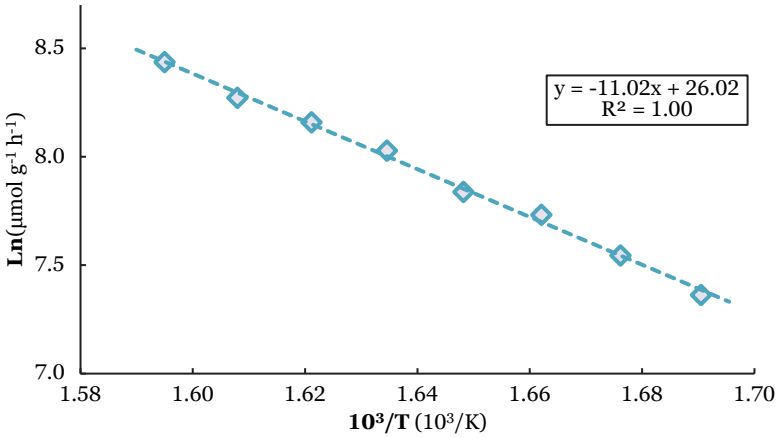

Figure 36: Arrhenius plot for thermal-catalytic NH_3 synthesis on Ru-K/MgO. Total flowrate 20 mL min^{-1}, H_2:N_2=1:1, catalyst loading 130 mg (250-300 µm), 0.0 mol.% NH_3 co-feed. The calculated activation barrier is 92 kJ mol^{-1}.

5.6.2.4 Plasma catalysis beyond thermal equilibrium

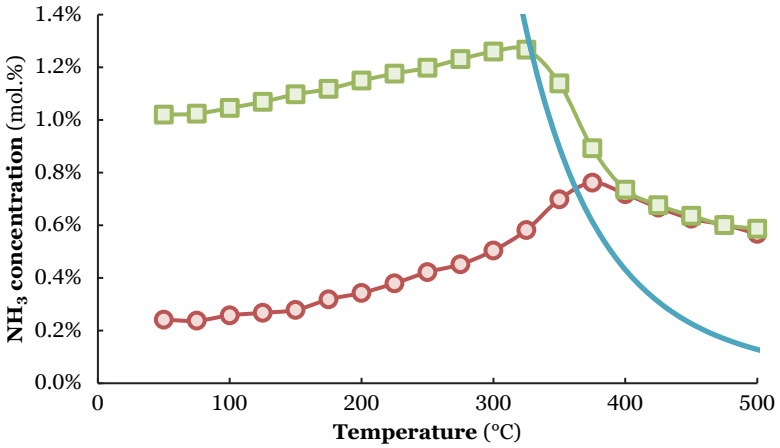

Figure 37: Activity for plasma-catalytic NH_3 synthesis (and NH_3 decomposition) for Ru-K/MgO for various NH_3 co-feed concentrations (0.0 mol.% (red circles) and 1.0 mol.% (green squares)). Total flowrate 20 mL min^{-1}, H_2:N_2=1:1, catalyst loading 130 mg (250-300 µm), plasma power 4.8 W (SEI=14.4 kJ L^{-1}).

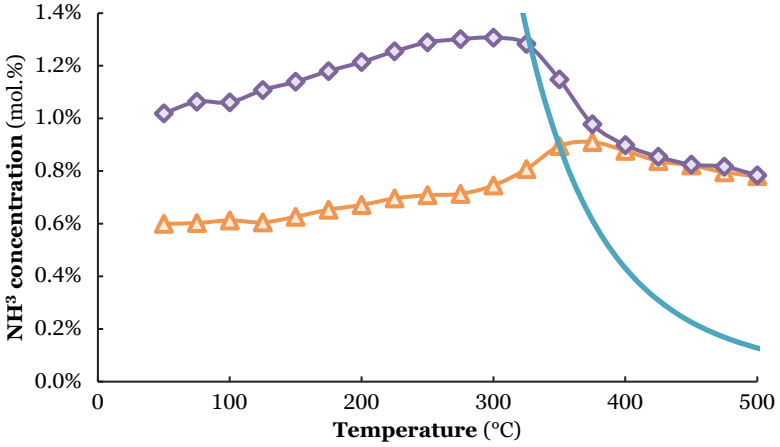

Figure 38: Activity for plasma-catalytic NH_3 synthesis (and NH_3 decomposition) for Ru-K/MgO for various NH_3 co-feed concentrations (0.0 mol.% (orange triangles) and 1.0 mol.% (purple diamonds)). Total flowrate 20 mL min^{-1}, H_2:N_2=1:1, catalyst loading 130 mg (250-300 µm), plasma power 6.4 W (SEI=19.2 kJ L^{-1}).

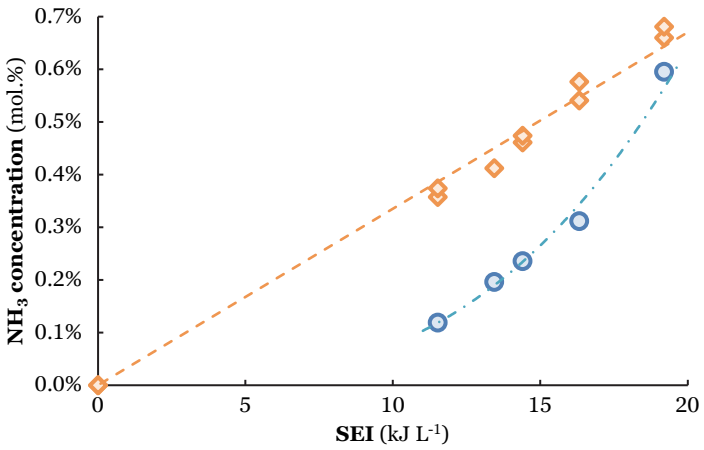

Figure 39: Ammonia outlet concentration as function of the SEI at 50°C (plasma-chemistry only, blue circles) and the difference between the thermal equilibrium and the conversion at 450-500°C (equilibrium conversion, orange diamonds) on Ru-K/MgO.

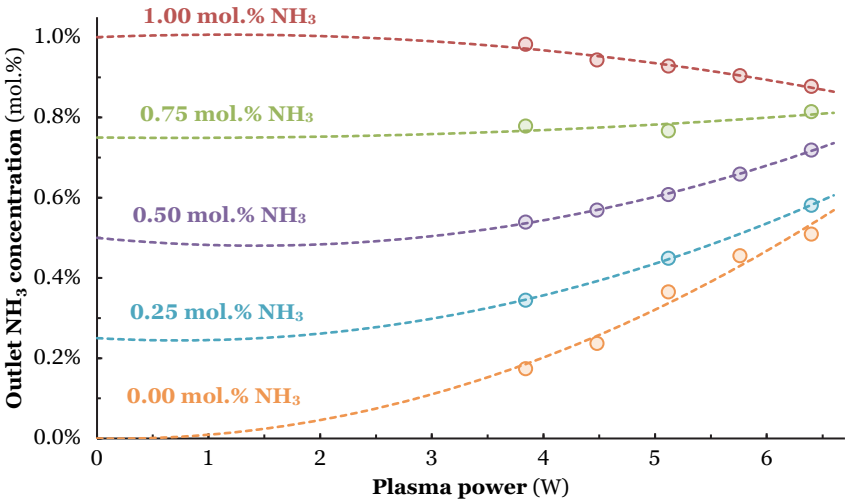

Figure 40: Effect of the plasma power on the activity for plasma-chemical NH_3 synthesis for MgO at ambient conditions, with various NH_3 co-feeding concentrations. Temperature 250°C, total flowrate 20 mL min^{-1}, H_2:N_2=1:1, catalyst loading 150 mg (250-300 µm particles). The plasma power applied under most conditions is 3.8 W.

5.6.3 Discussion

5.6.3.1 Kinetic diameter

- **Ammonia** (ground state): 260 pm
- **Hydrogen** (ground state): 289 pm
- **Nitrogen** (ground state): 364 pm

5.6.3.2 Modelled and experimental plasma-catalytic conversion

The modelling calculations were performed by Ir. Dave Vogel.

In order to model the plasma-catalytic conversion over Ru-based catalysts, the model of Mehta et al. [236] was used without modifications to the source code. The source code was made openly available by Mehta et al. [236]. The authors estimated activities for NH_3 synthesis and NH_3 decomposition, based on a kinetic model. In this model, the N_2 activation barrier is the key descriptor, while the hydrogenation steps are lumped. Plasma-activation is assumed to lower the barrier for N_2 dissociation and therefore increase the rate of N_2 dissociation. However, the final state of adsorbed N_{ads} on the surface is assumed to be the same for dissociated ground-state N_2 and plasma-activated N_2 and only the concentration of N_{ads} is influenced.

Fitting the reactor dimensions

All experiment in our research (both for thermal catalysis and plasma catalysis) were performed at 20 mL min^{-1} with a H_2:N_2 ratio of 1:1, with a catalyst mass of 130 mg and a bed volume of 0.14 cm^3. The CO chemisorption results for Ru/MgO give an area of 0.712 $m^2\ g^{-1}$, resulting in a site density of approximately $6.5*10^{-6}$ mol cm^{-3}.

For using the model for Ru-K/MgO catalyst, a N binding energy of -0.3 eV is assumed, based on the binding energy reported for Ru(0001) at 0.25 ML coverage [343]. Similar coverages were found for microkinetic models of promoted Ru catalysts [344]. The potassium promoter has little to no influence on the N binding energy [226,229], implying E_N=-0.3 eV is used for Ru-K/MgO.

The experimental results for thermal-catalytic ammonia synthesis over Ru-K/MgO (**Figure 36**) are used to fit the model of Mehta et al. This results in an underestimation of the experimental data of four orders of magnitude for a site density of $6.5*10^{-6}$ mol cm^{-3}, i.e. the approximate site density for the used catalyst. An underestimation is more often reported for kinetic models (although not of this magnitude), which is due to the methods used for the generalized gradient approximation in microkinetic models [345]. In order to fit the model to our observations, the site density was increased to $5.0*10^{-2}$ mol cm^{-3} keeping all other physical parameters constant. As shown in **Figure 41**, the trends in the kinetic regime (300-380°C) predicted by the adjusted model agree well with experimental

observations. Thus, the model parameters used for **Figure 41** are also used to predict plasma-catalytic ammonia synthesis.

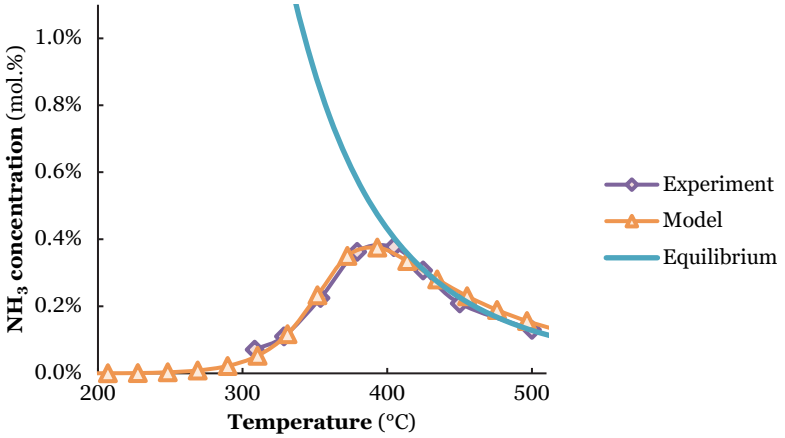

Figure 41: Experimental (purple line) and predicted (orange line) thermal-catalytic NH3 conversion over Ru-K/MgO as function of temperature. Total flowrate 20 mL min^{-1}, H_2:N_2=1:1 (no NH_3 co-feed), catalyst loading 130 mg (250-300 µm). The N binding energy is assumed to be -0.3 eV, based on a Ru(0001) at 0.25 ML coverage [343].

Plasma-activation in N_2

Plasma-activation lowers the barrier for N_2 dissociation [94], as well as the N_2 dissociation probability [262,263]. The plasma-activation is assumed to lower the N_2 dissociation barrier by 0.7 eV. This is based on the difference between the apparent activation barriers calculated for thermal catalysis and plasma-catalysis over promoted Ru-catalysts, which can be attributed to the lower N_2 dissociation barrier [94].

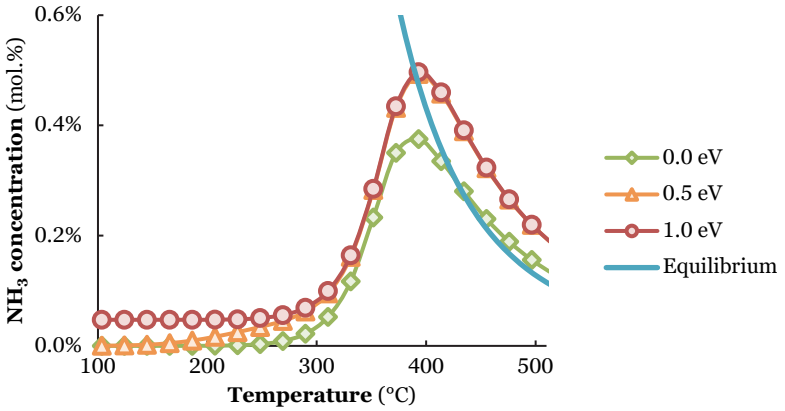

Figure 42: Predicted plasma-catalytic NH_3 conversion over Ru as function of temperature, based on the same reactor configuration as in Figure 41 (i.e., total flowrate 20 mL min^{-1}, H_2:N_2=1:1 (no NH_3 co-feed), catalyst loading 130 mg (250-300 µm)). The N binding energy is assumed to be -0.3 eV based on a Ru(0001) at 0.25 ML coverage [343] and $k_e n_e$ is assumed to be 10^{-3}; the same value was used by Mehta et al. [236]. Various values for a decrease in N_2 dissociation barrier are assumed (0.0 eV, 0.5 eV, and 1.0 eV).

Various values for the lowering of the N_2 dissociation barrier are shown in **Figure 42**. When N_2 is only partially activated in the plasma and the catalyst is required for dissociation (i.e., for low plasma-activations (of <0.5 eV)), the kinetic model of Mehta et al. predicts that there is no NH_3 formation below 200°C due to the negligible rate of N_2 dissociation. Only when the plasma-activation is above the N_2 dissociation barrier on Ru (according to the model 1.0 eV), NH_3 formation is predicted below 200°C. The fact that NH_3 is only formed when the N_2 barrier is completely overcome by the plasma, indicates that NH_3 formation from NH_x radicals or highly activated N_2 is the dominant mechanism for NH_3 synthesis below 200°C, as was experimentally observed below 200°C (see **Figure 26**). It should be noted that the dissociative sticking probability of N_2 on Ru(0001) is far below 100% in reality for a plasma-activation of 1.0 eV [263], which is not incorporated in the model of Mehta et al.

The model of Mehta et al. does not predict a change in conversion at high temperatures on increasing the level of activation from 0.5 eV to 1.0 eV. This is not expected, as an increase of plasma-activated N_2 on the surface should boost the plasma-catalytic ammonia synthesis reaction according to our experimental results (see **Figure 30** and **Figure 31** in the main article). In **Figure 43**, the predicted influence of the N binding energy on the plasma-catalytic conversion to ammonia is shown. The N binding energy is varied to get an estimate of the effect on the conversion beyond thermal equilibrium, as it is probable that the N_2 adsorption rate increases upon increasing plasma-activation of N_2. The N binding energy on Ru is known to decrease with increasing coverage [229,343]. For instance, the N binding energy increases from -0.3 eV at 0.25 monolayer coverage to 0.9 eV at 1.00 monolayer coverage on Ru(0001) [343].

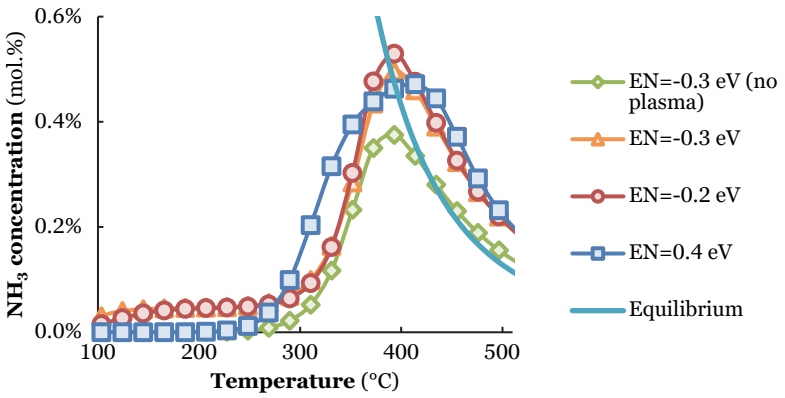

Figure 43: Predicted plasma-catalytic NH_3 conversion over Ru as function of temperature, based on the same reactor configuration as in Figure 40. The N binding energy is varied, while the barrier decrease is assumed to be 0.7 eV, based on experimental results obtained by Rouwenhorst et al. [94] for Ru catalysts. $k_e n_e$ is assumed to be 10^{-3}, similar to values used by Mehta et al. [236]. Various values for site densities are assumed to get similar conversion patterns: $5.0*10^{-2}$ mol cm^{-3} for E_N=-0.3 eV, $1.0*10^{0}$ mol cm^{-3} for E_N=-0.2 eV, and $1.0*10^{4}$ mol cm^{-3} for E_N=0.3 eV.

As shown in **Figure 43**, the model of Mehta et al. [236] predicts a variation in the plasma enhancement below 450°C, depending on the N binding strength. However, the model does not predict a change in conversion above 450°C with the N binding strength. This is not in line with our proposed model (see **Figure 30** and **Figure 31** in the main article) and experiment (see **Figure 27** and **Figure 28** in the main article).

Concluding, the model of Mehta et al. [236] is a first step in understanding the effect of plasma-activation on the effective barrier for N_2 dissociation and the subsequent NH_3 synthesis rate. At low temperatures (**Figure 42**), the model of Mehta et al. provides insight in the role of plasma-activated molecular N_2 and the adsorption of N radicals. However, above 450°C and beyond equilibrium, the model does not predict a variation in conversion to ammonia for different plasma powers, an effect that was experimentally observed (see **Figure 31**).

Chapter 6

Plasma-catalytic ammonia synthesis via Eley-Rideal reactions: a kinetic analysis

Summary

Plasma-catalytic ammonia synthesis is studies as an option to electrify the chemical industry. However, reaction mechanisms for plasma-catalytic ammonia synthesis are not fully understood. Therefore, plasma-catalytic ammonia synthesis is studied for Ru/MgO, Co/MgO, Pt/MgO, Pd/MgO, Cu/MgO, and Ag/MgO. The temperature is varied between room temperature and 500°C, and the plasma power is varied between 3.8 W and 6.4 W (SEI=10-19 kJ L^{-1}). The resulting ammonia production in the presence of a plasma and a catalyst can be distinguished into (1) temperature-independent plasma-based ammonia synthesis, and (2) temperature-dependent plasma-catalytic ammonia synthesis. An experimental kinetic analysis suggests that the Eley-Rideal reaction between N radicals from the plasma with surface-adsorbed H is the rate-determining step for plasma-catalytic ammonia synthesis on Ru/MgO, Co/MgO, Pt/MgO, Pd/MgO, and Cu/MgO, with apparent activation barriers in the range 18-24 kJ mol^{-1}. The plasma-catalytic ammonia synthesis reaction on Ag/MgO is expected to occur via a combination of reactions, e.g. via the same mechanism as the other metals and via direct adsorption of N on the metal surface, followed by hydrogenation on the surface. This results in an apparent activation barrier of 30 kJ mol^{-1} for plasma-catalytic ammonia synthesis on Ag/MgO.

This chapter is in preparation for publication as:

Rouwenhorst, K. H. R., Lefferts, L. (n.d.). Plasma-catalytic ammonia synthesis via Eley-Rideal reactions: a kinetic analysis. In preparation.

6.1 Introduction

Renewable energy sources increasingly penetrate the electricity grid, spurring the electrification of the energy landscape [50]. Plasma-activation of chemical bonds is one of the alternatives considered for electrified chemical processes, next to electrochemical processes [40,41,56]. Plasma-reactions merit from fast response to intermittent electricity, and this potentially allows processes to operate under mild conditions [40–42,56]. The introduction of a catalyst in a plasma-driven process may allow for the selective production of the desired product [56]. However, the fundamentals of the mutual plasma-catalyst influence are not fully understood [43,162].

Plasma-catalytic ammonia synthesis has gained traction as a model system for studying plasma catalysis due to the perceived simplicity of the reaction and the absence of any by-products. Furthermore, ammonia could be used as zero carbon fuel and hydrogen carrier in a hydrogen economy [33,216,346]. Various authors have reviewed plasma-catalytic ammonia synthesis [58,199,200,310,347].

The mechanisms for plasma-catalytic ammonia synthesis are not fully understood [43]. However, various authors have made suggestions regarding possible reaction mechanisms. Mehta et al. [49,236] proposed that plasma-catalytic ammonia synthesis occurs via vibrationally activated N_2. The key assumption is that plasma-activation of N_2 decreases the barrier for N_2 dissociation on the catalyst surface. The subsequent hydrogenation reactions on the catalyst surface are not affected. The activity for ammonia synthesis on different metals varies by orders of magnitude, with a distinctive volcano curve similar to thermal catalysis [49,348]. However, the predicted volcano curve for plasma-catalysis with plasma-activated N_2 shifts towards more noble metals. In **Chapter 3**, it was shown that thermally active Ru-catalysts for NH_3 synthesis can also facilitate plasma-catalytic ammonia synthesis with plasma-activated N_2 [94]. For relatively low specific energy inputs (SEIs) of 0.1-0.4 kJ L^{-1}, molecular plasma-activated N_2 is the dominant species for NH_3 synthesis on Ru-catalysts in the temperature range 200-300°C [94,330].

Chen et al. [349], Engelmann et al. [179], Rouwenhorst et al. [223], Shah et al. [126], and Yamijala et al. [181] proposed that plasma-catalytic ammonia synthesis proceeds via N and NH_X radicals, especially at high plasma powers. The dominant contribution of radical species was demonstrated by various authors for SEIs in the range of 10 to 19 kJ L^{-1} on Ru-catalysts [223], and at 40 kJ L^{-1} on Fe-, Ru-, Co-, and Cu-catalysts [180].

Ammonia synthesis may occur via radical adsorption with subsequent surface reactions, i.e. Langmuir-Hinshelwood reactions. Alternatively, plasma radicals may directly interact with surface-adsorbed species and react to form ammonia via Eley-Rideal reactions. Engelmann et al. [179] performed density functional theory (DFT) calculations, which predicts that adsorption of plasma radicals with subsequent Langmuir-Hinshelwood hydrogenation reactions results in significant difference in activity among different

transition metals for plasma-catalytic ammonia synthesis, varying by orders of magnitude. Eley-Rideal reactions would result in similar activities among transition metals [179].

Thus, various authors have experimentally investigated the plasma-catalytic activity on transition metals in dielectric barrier discharge (DBD) reactors [49,76,79,82,180,336,349,350]. However, the evidence for the dominant reaction mechanisms remains inconclusive. Catalysts with high metal loadings (above 5 wt.%) were used in some studies, making it difficult to distinguish between catalytic enhancement and varying plasma properties due to the presence of metal nanoparticles. Furthermore, most authors kept the temperature constant, not allowing for a kinetic analysis.

In the current work, the activity for plasma-catalytic ammonia synthesis is assessed for various transition metals supported on MgO with low metal loading (2%) in a DBD reactor with SEIs of 10-19 kJ L^{-1}. Additional information on the experimental procedures can be found in **section 6.7.1** and **section 6.7.2**. Plasma chemistry contributions and plasma-catalytic effects are distinguished for Ru/MgO, Co/MgO, Pt/MgO, Pd/MgO, Cu/MgO, and Ag/MgO catalysts. The temperature is varied, allowing for a kinetic analysis. Furthermore, the plasma is kept relatively mild and the NH_3 concentration low (<0.7 mol.%), suppressing the plasma-driven ammonia decomposition rate. Furthermore, kinetic analyses is performed to investigate the rate-determining step(s) for plasma-catalytic ammonia synthesis.

6.2 Results & Discussion

The conversion to ammonia with bare MgO in the presence of plasma is tested to benchmark the conversion to ammonia with the MgO-supported metal catalysts. As shown in **Figure 44**, the conversion on bare MgO is independent of temperature. Clearly, these reactions are not thermally activated. This conversion is attributed in absence of any metal catalyst to radical reactions in the plasma or reactions on the oxide surface, e.g. between N, H, and N_YH_X species [351].

The conversion at room temperature over all catalysts is identical to the conversion over exclusively MgO at room temperature. This indicates that the presence of metal nanoparticles with a relatively low loading (2%) does not significantly influence the plasma chemistry, which is in line with literature for low metal loadings [82,349]. However, the conversion over the catalysts increases with increasing temperature, indicating this is due to an catalytic effect [223].

All catalysts were tested for thermal-catalytic ammonia synthesis, e.g. in absence of plasma. The thermal-catalytic activity of all catalysts is too low to detect any ammonia with the equipment used under the experimental conditions in this study. Therefore, the difference between the ammonia concentration due to plasma chemical reactions, as observed with MgO, and the ammonia concentration observed with supported-metal catalysts is a measure for the rate of plasma-catalytic ammonia formation.

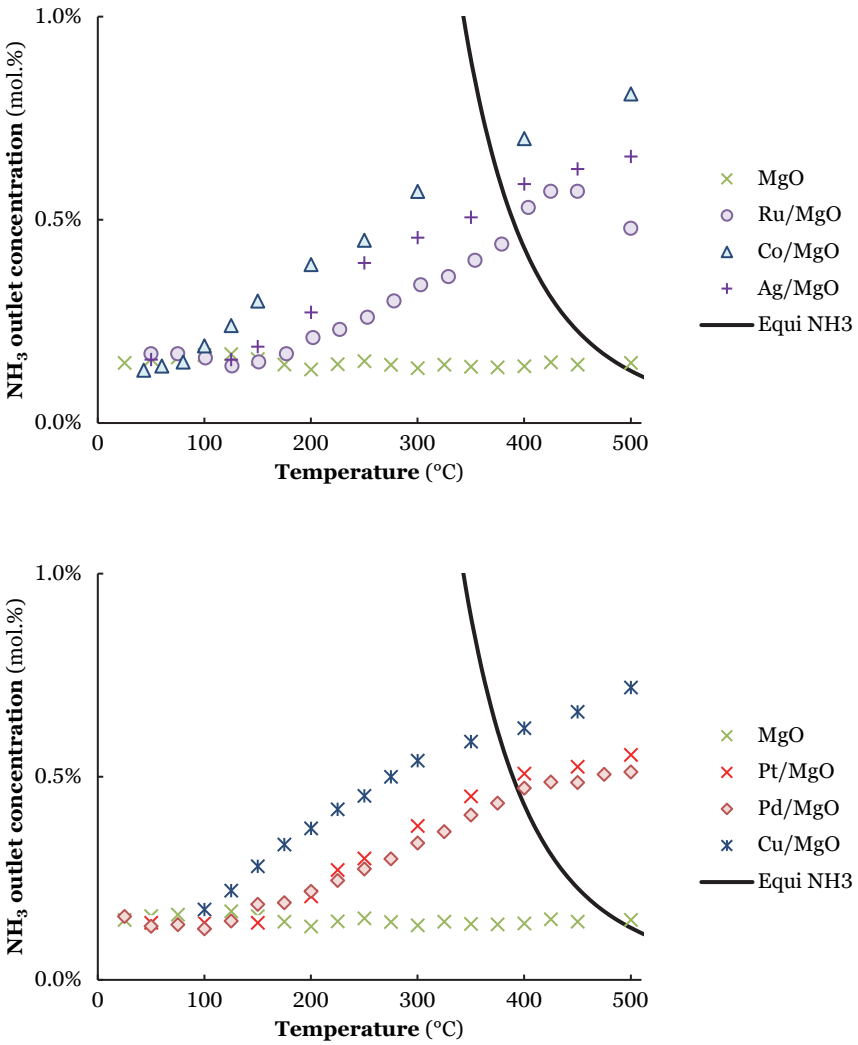

Figure 44: Activity for plasma-chemical NH_3 synthesis and plasma-catalytic NH_3 synthesis (and decomposition) for MgO (green crosses), Ru/MgO (purple circles), Co/MgO (blue triangles), Pt/MgO (red crosses), Pd/MgO (red diamonds), Cu/MgO (blue stars), and Ag/MgO (purple plusses) as function of temperature. Total flowrate 20 mL min^{-1}, atmospheric pressure, H_2:N_2=1:1 (no NH_3 co-feed), catalyst loading 130-150 mg (250-300 µm particles), plasma power 3.8 W (SEI=11.4 kJ L^{-1}).

Ammonia is synthesized beyond thermal equilibrium for all catalysts at temperatures above 400°C (**Figure 44**), in line with results reported in literature [223,236]. Apparently, plasma-catalytic ammonia synthesis is faster than thermal-catalytic ammonia decomposition as well as plasma induced ammonia decomposition. Exclusively Ru/MgO

shows a decrease in ammonia outlet concentration upon increasing the temperature above 400°C (**Figure 44**). Ru/MgO is indeed active for thermal-catalytic ammonia decomposition above 400°C, as observed in ammonia co-feeding experiments in absence of plasma (**Figure 56**), whereas all other catalysts are not significantly active at temperatures up to 500°C. Indeed, Ru is known to be the most active ammonia decomposition catalyst [333,352].

6.2.1 Plasma-catalytic ammonia synthesis activity

The ammonia synthesis rate can be obtained via **Equation 4**, where $r_{M/MgO}$ is the total ammonia synthesis rate in the reactor (μmol-NH_3 min^{-1}), x_{NH3} the outlet NH_3 concentration (mol.%), and F_{gas} the inlet gas flow (20 mL min^{-1}). The correction factor 0.0429 kmol-NH_3 Nm^{-3} accounts for the molar gas density of ammonia.

Equation 4: $r_{\frac{M}{MgO}} \approx 0.0429 * F_{gas} * x_{NH_3} * \rho_{NH_3} * M_{NH_3}$

The normalized plasma-catalytic ammonia synthesis rate ($r_{pc\text{-}norm}$ in μmol m^{-2}_{metal} min^{-1}, **Equation 5**) is obtained by subtracting the rate for plasma-chemical ammonia synthesis on MgO (r_{MgO} in μmol min^{-1}) from the total ammonia synthesis rate in the reactor ($r_{M/MgO}$ in μmol min^{-1}), divided by the quantity of metal adsorption sites (n_{metal} in m^2), as measured with XRD or H_2 chemisorption (see **Table 7**) [49,82,180].

Equation 5: $r_{pc-norm} = \frac{r_{\frac{M}{MgO}} - r_{MgO}}{n}$

As discussed in **section 6.7.3**, the ammonia outlet concentration must be below 0.7 mol.% and plasma powers should be limited to 3.8 W to minimize ammonia decomposition. If these criteria are met, the plasma-catalytic ammonia synthesis rate can be calculated using **Equation 5**. The Arrhenius plots for the different catalysts at ammonia outlet concentrations below 0.5 mol.% and at a plasma power of 3.8 W is shown in **Figure 45**.

The resulting apparent activation barriers for plasma-catalytic ammonia synthesis on the different metals are in the range 18-24 kJ mol^{-1} (see **Figure 45**), except for Ag/MgO showing a higher apparent barrier of 30 kJ mol^{-1}. These barriers are far lower than the activation barrier for Langmuir-Hinshelwood hydrogenation reactions of N, NH, and NH_2 to ammonia, which typically have values of 50-150 kJ mol^{-1}, depending on the metal used, based on DFT (density functional theory) calculations [252,317]. This suggests that the rate-determining step does not occur via a Langmuir-Hinshelwood type surface hydrogenation reaction. The presence of N radicals is supported by the observation that ammonia is also produced in absence of a metal, e.g. with the bare MgO (see **Figure 44**).

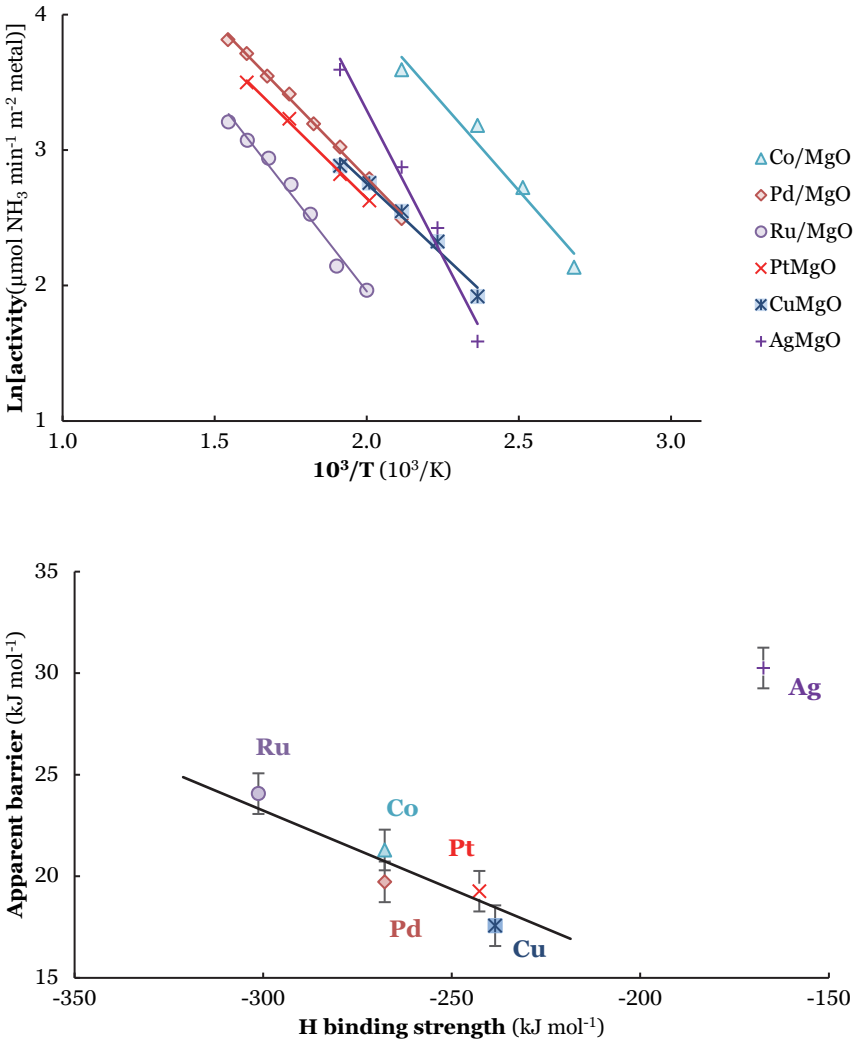

Figure 45: Top: Arrhenius plots for plasma-catalytic NH_3 synthesis on Ru/MgO (purple circles), Co/MgO (blue triangles), Pt/MgO (red crosses), Pd/MgO (red diamonds), Cu/MgO (blue stars) and Ag/MgO (purple plusses). Bottom: Apparent activation barriers for plasma-catalytic ammonia synthesis for various metals versus the H binding energy. Catalysts: Ru/MgO (purple circles), Co/MgO (blue triangles), Pt/MgO (red crosses), Pd/MgO (red diamonds), Cu/MgO (blue stars) and Ag/MgO (purple plusses). The obtained values are valid for an ammonia outlet concentration below 0.5 mol.% NH_3, SEI=11 kJ L^{-1}, flow rate 20 mL min^{-1}, H_2:N_2=1:1.

6.2.2 Effect of plasma power

The plasma-catalytic ammonia synthesis rate was measured for various plasma powers for Ru/MgO, Co/MgO, and Pd/MgO. The plasma-catalytic ammonia synthesis rate for various specific energy inputs (SEIs) at 250°C is shown in **Figure 46**. The plasma-catalytic ammonia synthesis rate increases linearly with SEI for Ru/MgO, Co/MgO, and Pd/MgO. This indicates that an increased concentration of plasma-activated nitrogen and hydrogen species leads to a higher reactivity on the catalyst.

This is consistent with a higher concentration of electronically-activated N_2 species measured with UV-Vis spectroscopy at increasing SEI (see **Figure 46**). Modelling works also show that the rate of N radical formation increases with the reduced electric field, and with increasing electronically-activated N_2 species [310].

Concluding, the increased plasma-catalytic ammonia synthesis rate with increasing SEI is due to a higher concentration of activated nitrogen species.

6.2.3 Effect of H_2:N_2 ratio

The plasma-catalytic ammonia synthesis activity for various H_2:N_2 ratios is shown in **Figure 47**. The metals show the highest activity for N_2-rich plasmas, in line with literature [49,82,180].

UV Vis spectroscopy shows a higher concentration of plasma-activated nitrogen species for a higher N_2 fraction in the feed (see **Figure 54**). Similarly, modelling results also show an increase in N radical formation for N_2 rich plasmas [179]. Thus, a N_2-rich feed results in a higher N formation rate. The higher N formation rate results in a higher probability for reactions between N radicals and a surface adsorbed species, thereby yielding a higher ammonia formation rate [223].

From modelling studies it follows that the density of H radicals is a factor 4-60 higher than the density of N radicals for H_2:N_2 ratios in the range 3:1 up till 1:3 [179,181]. This implies that there are sufficient H atoms available for ammonia formation, suggesting that the N radicals are rate-determining for the plasma-catalytic ammonia synthesis rate.

6.2.4 Proposed reaction mechanisms

All transition metals show an activity within the same order of magnitude, with a turnover frequency of about 10^{-3}-10^{-2} s^{-1} at 250°C (see **Figure 48**). The turnover frequency is estimated from the plasma-catalytic ammonia synthesis rate, divided by the number of active metal sites. The number of active sites is estimated from the total metal surface area exposed, based on the metal nanoparticle size (see **Table 7**) and an assumed site density based on crystallography estimates. Typical site densities are in the order 10^{18}-10^{19} sites per m^2 [353].

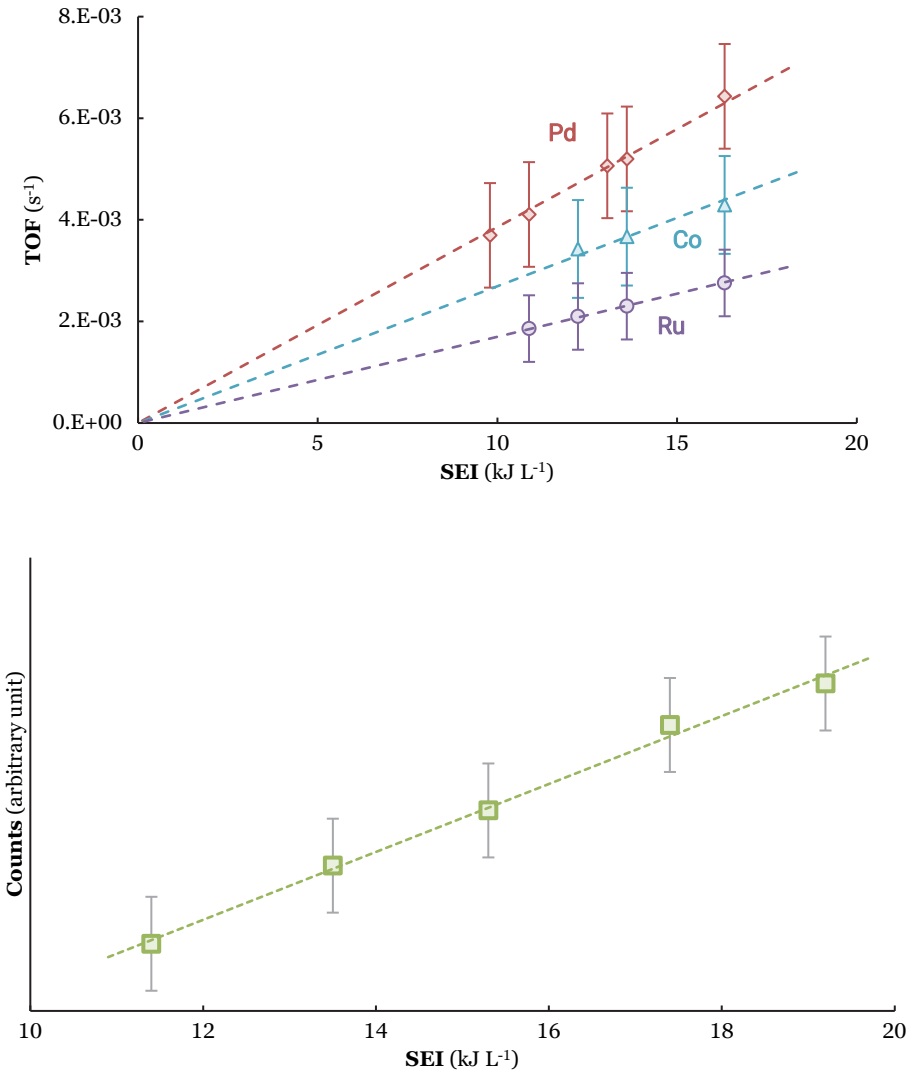

Figure 46: Top: Effect of the specific energy input (SEI) on the activity for plasma-catalytic NH_3 synthesis for Ru/MgO (purple circles), Co/MgO (blue triangles), and Pd/MgO (red diamonds). Temperature 250°C, total flowrate 20 mL min^{-1}, H_2:N_2=1:1, catalyst loading 130-150 mg (250-300 µm particles). Bottom: Number of counts of UV Vis spectrum at 337 nm (Transition from $N_2(C^3\Pi_u(v=0))$ to $N_2(B_3\Pi_g(v=0))$, green squares), as function of the SEI. For additional information, see section 6.7.2.4. For error calculation, see supporting information section 6.7.4.2.

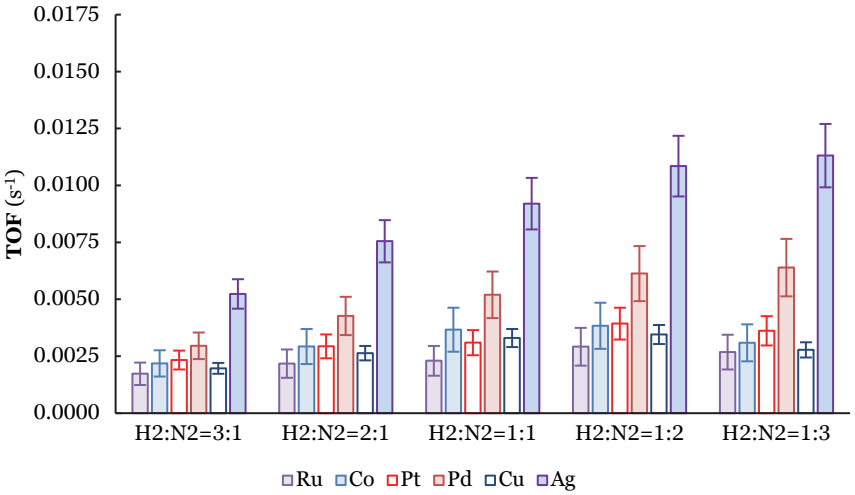

Figure 47: Effect of the H_2:N_2 ratio on the activity for plasma-catalytic NH_3 synthesis for Ru/MgO (purple), Co/MgO (blue), Pt/MgO (red-white), Pd/MgO (red), Cu/MgO (blue-white) and Ag/MgO (blue-purple). Temperature 250°C, total flowrate 20 mL min^{-1}, catalyst loading 130-150 mg (250-300 µm particles), plasma power 3.8 W (SEI=11.4 kJ L^{-1}). For error calculation, see supporting information section 6.7.4.2.

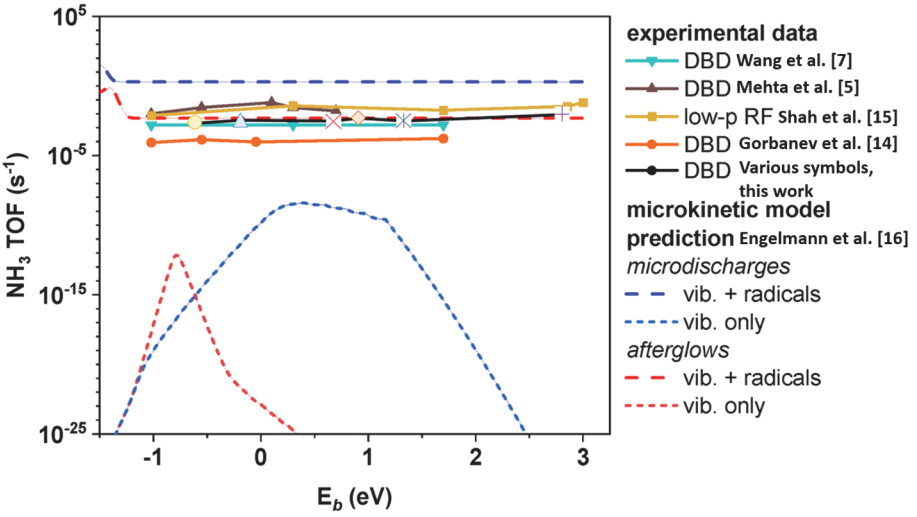

Figure 48: Turnover frequencies (TOFs) calculated in this work (black line, various symbols), compared to literature results. Figure reproduced and modified from Ref. [180]. Black line, various symbols: own data at 250°C, 20 mL min^{-1}, H_2:N_2=1:1, 3,8 W, 130-150 mg catalyst. Blue triangles: Wang et al. [79]. Brown triangles: Mehta et al. [49]. Yellow squares: Shah et al. [119]. Orange circles: Gorbanev et al. [180]. Microkinetic model predictions: Engelmann et al. [179], H_2:N_2=3:1, 400 K.

The similar activity among transition metals is in accordance with previous literature under similar plasma conditions and at similar temperatures [49,180]. The absolute activities for the current work differs from other references, which can be attributed to a difference in temperature, plasma power, plasma type, catalyst loading, pressure, H_2:N_2 loading, flow rate, etc.

The similar activity among metals within the same order of magnitude suggest that N radicals are the dominant reactant nitrogen species for plasma-catalytic ammonia synthesis at relatively high plasma powers (≥1 kJ L^{-1}), as opposed to molecular plasma-activated N_2. The activity of different metals would change by orders of magnitude if molecular plasma-activated N_2 would be dominant, as part of the N_2 dissociation would still occur on the catalyst, e.g. an activated process varying strongly between metals [49,179].

It should be noted that the reported turnover frequencies obtained in this work, e.g. in the order 10^{-3}-10^{-2} s^{-1} are lower than results obtained from microkinetic modelling calculations, which predict activities up to 10^{1} s^{-1} for a uniform plasma, 10^{0} s^{-1} for filamentary discharges, and 10^{-2} s^{-1} for the filamentary afterglow [179]. This discrepancy may be attributed to plasma contact limited to the external surface of the catalyst exposed to the plasma. Most active sites will be located at the internal surface of the catalyst, e.g. not in direct contact with the plasma [43,310]. Thus, the actual plasma-catalytic activity at the external surface is underestimated. A possible solution for future research is to use dense catalyst materials with active metals only exposed at the external catalyst surface, such that the calculated TOF is in line with the exposed external surface.

Ammonia is formed in presence of plasma and bare MgO (see **Figure 44**), e.g. without a catalyst able to break the triple bond of the N_2 molecule. This also suggest ammonia is formed via N radicals. Thus, the increasing activity with increasing plasma power (**Figure 46**) and with increasing nitrogen concentration in the feed (**Figure 47**) can be attributed to an increase in N radicals, reacting to form ammonia. Indirect evidence is provided by UV-Vis spectroscopy (see **section 6.7.2.4** and **section 6.7.2.5**). An increase in plasma power and an increase in nitrogen concentration in the feed results in more plasma-activated N_2, which indirectly implies more N radical formation.

The barriers of 18-24 kJ mol^{-1} for plasma-catalytic ammonia synthesis on Ru, Co, Pt, Pd, and Cu (**Figure 45**) are too low for N_2 dissociation (>50 kJ mol^{-1}), and for NH_X hydrogenation reactions on the metal surface (50-150 kJ mol^{-1}), as follows from density functional theory (DFT) calculations [252,317].

In **Chapter 5**, e.g. with Ru catalysts and similar SEI values between 10 and 19 kJ L^{-1}, it was demonstrated that N radicals are indeed the dominant nitrogen species for plasma-catalytic ammonia synthesis, at temperatures below 300°C, where thermal-catalytic activity for N_2 dissociation is negligible [223]. Thus, ammonia formation via N radicals is a dominant pathway, and N_2 dissociation does not play a significant role.

For all metals, except Ag, the activation barrier decreases with a weaker H-metal binding (**Figure 45**). **Figure 45** shows a strong correlation between the activation barriers and the H binding strength on the different catalysts, suggesting that the rate-determining reaction step involves breaking the H-surface bond. This suggests that the reaction between a N radical from the plasma phase and surface-adsorbed H is rate-limiting for plasma-catalytic ammonia synthesis on Ru, Co, Pt, Pd, and Cu at relatively high plasma powers (≥1 kJ L^{-1}) [330], as schematically represented in **Figure 49**. This is consistent with recent modelling work of Engelmann et al. [179], who assumed plasma properties similar to the current DBD reactor. Subsequent hydrogenation steps to ammonia are expected to be fast, based on microkinetic modelling studies [179,181].

For all metals studied here, except Ag, adsorption of H on the metallic surface is more energetically favourable than recombination to H_2, resulting in high surface coverage of atomic H. The surface coverage of N and NH_x species is negligible for all metals studied here, according to modelling studies [179,354].

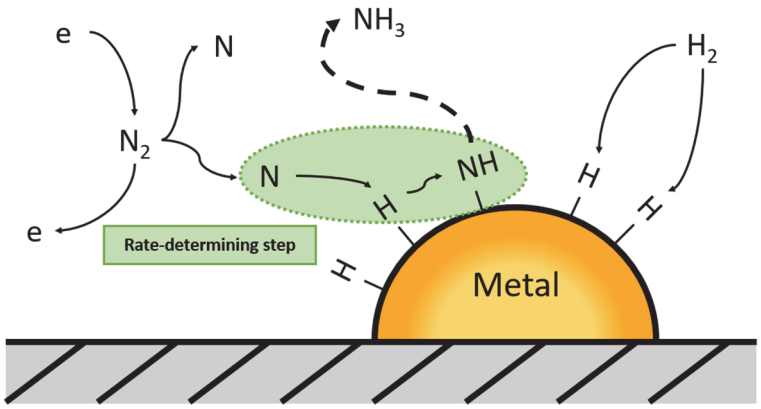

Figure 49: Schematic representation of the proposed rate-determining reaction step for all metals except for Ag, e.g. via the Eley-Rideal Reaction between a N radical from the plasma and surface-adsorbed H.

The exception to the high H surface coverage is Ag, for which recombination to form gaseous H_2 is highly exothermic. Thus, the H surface coverage will be low. This coincides with a higher apparent activation barrier of 30 kJ mol^{-1} as compared to those of the other metals, e.g. 18-24 kJ mol^{-1}.

It is speculated that the activity for plasma-catalytic ammonia synthesis is a mixture of pathways. The first reaction pathway via surface-adsorbed H and a N radical from the plasma may still contribute. However, the higher empty surface fraction may also result in more direct adsorption of N on the surface, with surface hydrogenation to form NH. From DFT calculations for Ag(111), it follows that the reaction $N_{ads}+H_{ads}\rightarrow NH_{ads}+*$ has an activation barrier of 72 kJ mol^{-1} [355]. It is speculated that the measured activity and activation barrier is a combination of these pathways.

6.3 Conclusion

Plasma-catalytic ammonia synthesis was studied for Ru/MgO, Co/MgO, Pt/MgO, Pd/MgO, Cu/MgO, and Ag/MgO. The temperature is varied between room temperature and 500°C, and the plasma power is varied between 3.8 W and 6.4 W. The resulting ammonia production in the presence of a plasma and a catalyst can be distinguished into (1) temperature-independent plasma-based ammonia synthesis, and (2) temperature-dependent plasma-catalytic ammonia synthesis. The kinetic analysis suggests that the reaction between N radicals from the plasma with surface-adsorbed H is the rate-determining step for Ru/MgO, Co/MgO, Pt/MgO, Pd/MgO, and Cu/MgO, with apparent activation barriers in the range 18-24 kJ mol^{-1}. The reaction on Ag/MgO is expected to occur via a combination of reactions, e.g. via the same mechanism as the other metals and via direct adsorption of N on the metal surface, with hydrogenation on the surface. This results in an apparent activation barrier of 30 kJ mol^{-1} for plasma-catalytic ammonia synthesis on Ag/MgO.

6.4 Supporting information

6.4.1 Experimental section

6.4.1.1 Experimental set-up

A schematic representation of the experimental set-up for the catalytic tests is shown in **Figure 50**. The catalytic tests were carried out in a quartz tubular reactor with an inner diameter of 4 mm and an outer diameter of 6 mm, at atmospheric pressure. A stainless-steel rod of 1 mm diameter is placed inside the reactor as the high voltage electrode. At the outside of the quartz tube, a metal tube is placed as the ground electrode. The temperature was controlled with a thermocouple connected to a heating block, which is placed around the ground electrode. The flowrates of the reactants were controlled with calibrated mass flow controllers (MFCs). About 130-150 mg of catalyst with particle size 250-300 μm was loaded in the reactor, on top of a layer of quartz wool. A spacer is placed above the catalytic bed to prevent moving of particles due to plasma-illumination and to center the high voltage electrode.

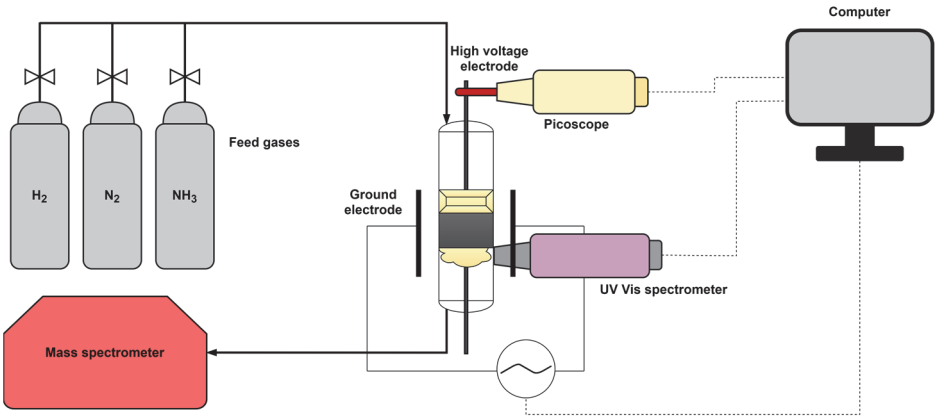

Figure 50: Schematic representation of the experimental set-up. The plasma volume includes the space, the packed bed, and the quartz wool.

The catalyst was reduced at 500°C in the reactor for 2 h in a gas mixture of 40 mL min^{-1} N_2 and 10 mL min^{-1} H_2. The catalytic tests were performed under steady-state conditions. The product gases were analyzed using an on-line Pfeiffer Vacuum Thermostar™ gas analysis system, which is a mass spectrometer (MS). The MS signal for NH_3 (17 m/e) was calibrated in the range 0-2 mol.%, resulting in a linear relationship. The signals for H_2 (2 m/e), N_2 (28 m/e) and H_2O (18 m/e) were also monitored semi-quantitatively, as well as a minor NH_3 peak (16 m/e).

6.4.2 Catalyst preparation & characterization results

Ru/MgO, Co/MgO, Ni/MgO, Pt/MgO, Pd/MgO, Cu/MgO, and Ag/MgO catalysts were tested for the activity for ammonia synthesis in the presence of a plasma. The MgO support was chosen because of the high thermal-catalytic activity for ammonia synthesis on MgO supported Ru catalysts [281].

6.4.2.1 Materials

Cobalt(II) nitrate hexahydrate ($Co(NO_3)_2.6H_2O$, 97.7% min), Palladium(II) nitrate hydrate ($Pd(NO_3)_2.xH_2O$, 99.8% Pd on metal basis), Tetraammineplatinum(II) nitrate ($Pt(NH_3)_4(NO_3)_2$) and Ruthenium(III) nitrosyl nitrate ($Ru(NO)(NO_3)_3$, >31.3 wt.% Ru) were purchased from Alfa Aesar. Copper(II) nitrate trihydrate ($Cu(NO_3)_2.3H_2O$), and Silver nitrate ($AgNO_3$) were purchased from Merck.

Magnesium oxide powder (MgO, >97% purity grade) was purchased from Merck. H_2 and N_2 with a purity grade of 99.999% were purchased from Linde, and water traces were removed using Agilent gas clean purification systems. A gas mixture of 2 vol.% NH_3 in a 98 vol.% N_2 balance gas was purchased from Linde. All materials were used as received. Deionized water was used during catalyst preparation.

6.4.2.2 Catalyst preparation

The metal precursors were dissolved in water and impregnated on the MgO support using the dry impregnation method. About 1.2 mL water was used per gram of MgO. Then, the mixture was dried in an oven at 105°C and atmospheric pressure in air for 1 h, followed by drying in a vacuum oven at 120°C for 2 h.

The dried catalysts were calcined in a calcination oven with 20 mL min^{-1} air flow at 400°C for 2 h (heating rate 10°C min^{-1}) decomposing the metal precursors. Subsequently, the metal oxides were reduced in a 20 mL min^{-1} H_2 flow at 550°C for 2.5 h (heating rate 10°C min^{-1}). After reduction, the catalysts were pelletized using a press and crushed. The sieve fraction 250-300 µm was used for the catalytic tests. Last traces of H_2O were removed in the reactor at 500°C.

6.4.2.3 Catalyst characterization

The total surface area and pore volume was determined by N_2 physisorption at -198°C using a Micromeritics Tristar. The samples were outgassed in vacuum at 300°C for 24 h before the analysis. The metal particle size and metal dispersion were determined by XRD-LB (Line Broadening). When the particle size could not be determined by XRD-LB due to low metal loadings (2 wt.%), and peaks of metal (oxides) overlapping with MgO, H_2 chemisorption was used. The crystalline phases present in the catalysts were determined with X-ray diffraction (XRD) using a Bruker D2 Phaser diffractometer equipped with a position-sensitive detector over a 2θ range between 10° and 90° using Cu Kα radiation (λ= 1.5418 Å). The Scherrer equation was used to calculate the crystallite size of metal nanoparticles (**Equation 6**), where τ is the mean size of crystallites (nm), K is a dimensionless shape factor (0.9), λ is the x-ray wavelength, β is the line broadening at half of the maximum intensity (FWHM in radians), and θ is the Bragg angle.

Equation 6: $\tau = \frac{K\lambda}{\beta \cos(\theta)}$

The elemental composition was determined by x-ray fluorescence spectroscopy (XRF) using a Bruker S8 tiger.

The catalyst characterization results for MgO, Ru/MgO, Co/MgO, Ni/MgO, Pt/MgO, Pd/MgO, Cu/MgO, and Ag/MgO are listed in **Table 7**. The MgO was found to have a total area of 294 m^2 g^{-1} (S_{BET}) and a pore volume of 0.31 cm^3 g^{-1} (V_{Pore}).

It should be noted that the metal surface areas are currently only estimated using one or two techniques. For a fair comparison among metals, multiple techniques should be applied for all metals. Thus, it is recommended for follow-up research to perform additional characterizations to estimate the metal surface areas. The Ru nanoparticle size determined by XRD-LB (15 nm) and CO chemisorption (16 nm) are in agreement.

Table 7: Structural and physical properties of MgO, Ru/MgO, and Co/MgO, Pt/MgO, Pd/MgO, Cu/MgO, and Ag/MgO. * The Ag content could not be determined with XRF, so the Ag content was estimated based on synthesis contents.

Catalyst	**Metal loading** (wt.%)	**Average particle size** (nm)		
	XRF	XRD-LB	CO/H_2 chem.	TEM
Ru/MgO	2.0±0.1	15±1	16±1 (CO)	-
Co/MgO	1.6±0.1	-	5±1 (H_2)	-
Pt/MgO	2.2±0.1	19±1	-	-
Pd/MgO	2.1±0.1	23±1	-	-
Cu/MgO	2.3±0.1	-	-	20±1
Ag/MgO	2.0±0.1*	25±1	-	-

The XRD spectra of MgO, Ru/MgO, Co/MgO, Ni/MgO, Pt/MgO, Pd/MgO, Cu/MgO, and Ag/MgO are listed in **Figure 51**. The Miller indices for the MgO support are also shown in **Figure 51**.

6.4.2.4 Plasma characterization

A PMV 500-4000 power supply was used to illuminate the plasma at 25 kHz. A Picoscope PC Oscilloscope was used to monitor the charge-voltage characteristics. The high voltage electrode was connected to the power supply, and an AC voltage of up to 10 kV peak to peak was applied. A Tektronix P6015A high voltage probe was used to monitor the voltage over the high voltage electrode, while a TT-HV 250 voltage probe was used to measure the voltage over the ground electrode. A capacitor of 8.24 nF was placed in between the ground electrode and the TT-HV 250 voltage probe. An Ocean HDX Spectrometer was used to analyse light emitted by the plasma, just below the catalyst bed, at low temperature.

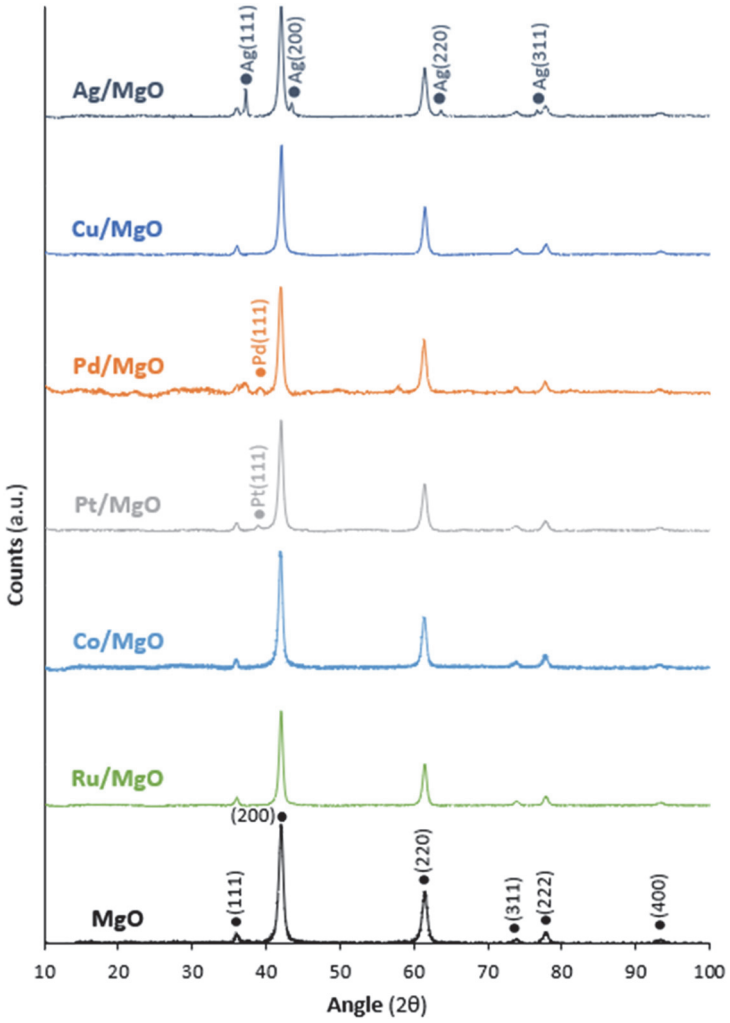

Figure 51: XRD spectra for MgO, Ru/MgO, Co/MgO, Pt/MgO, Pd/MgO, Cu/MgO, and Ag/MgO. The Miller indices indicate the crystalline lattice structures exposed in the MgO.

The voltage and charge were monitored with an oscilloscope, from which the power dissipated can be determined using a Lissajous figure (also termed Q-V plot). An example Lissajous figure for Ru/MgO is shown in **Figure 52**.

In a Q-V plot, the capacitive and discharge behaviour of a plasma is monitored. Ideally, a Lissajous figure has the shape of a parallelogram, thereby perfectly separating the capacitive and discharge regime. However, as shown in **Figure 52**, there is an indent in both the positive and negative charge cycle. This can be attributed to a discharge at the contact points at an earlier stage than over the remainder of the surface [2, 3].

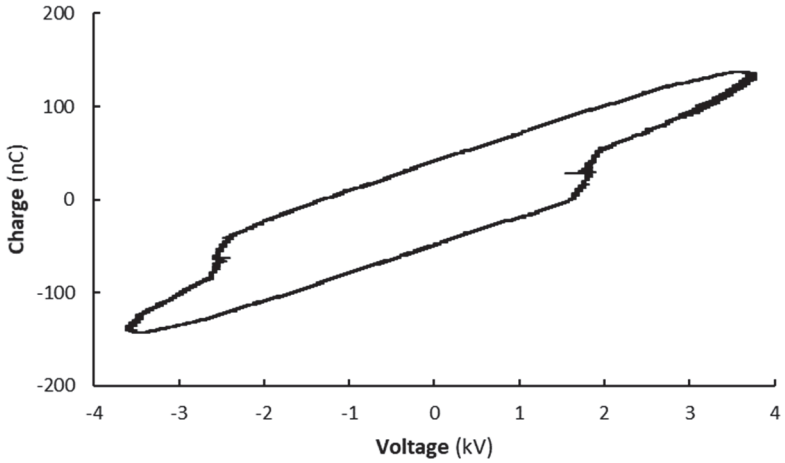

Figure 52: Lissajous figure for Ru/MgO at 30°C, H_2:N_2=1:1, 20 mL min^{-1}. The total power dissipated is 6.4 W.

An example of an emission spectrum at 6.4 W input power and in pure N_2 is shown in **Figure 53**, in line with literature [49,76]. As follows from the emission spectrum, the most pronounced peaks are found in the regime 290-400 nm, which corresponds to the second positive band from an activated neutral N_2^* molecule ($C^3\Pi_u \rightarrow B^3\Pi_g$) [342]. This implies that photons are emitted upon plasma-activated N_2 falling back from an electronically and/or vibrationally excited state to a lower energy state of N_2.

The intensity of the nitrogen signal at 337 nm as function of the plasma power for pure N_2 is shown in **Figure 53**, whereas **Figure 54** shows the influence of the H_2:N_2 ratio. As follows from **Figure 53** and **Figure 54**, the nitrogen activation increases with both an increasing N_2 concentration in the gas phase and with increasing plasma power.

Model calculations discussed in **section 6.7.2.5** and **Figure 55** show that increasing electronically-activation of N_2 also leads to increasing formation of N radials. Thus, **Figure 53** and **Figure 54**, showing increasing UV-Vis signal of electronically-activated N_2, provide indirect evidence for increasing N radical formation.

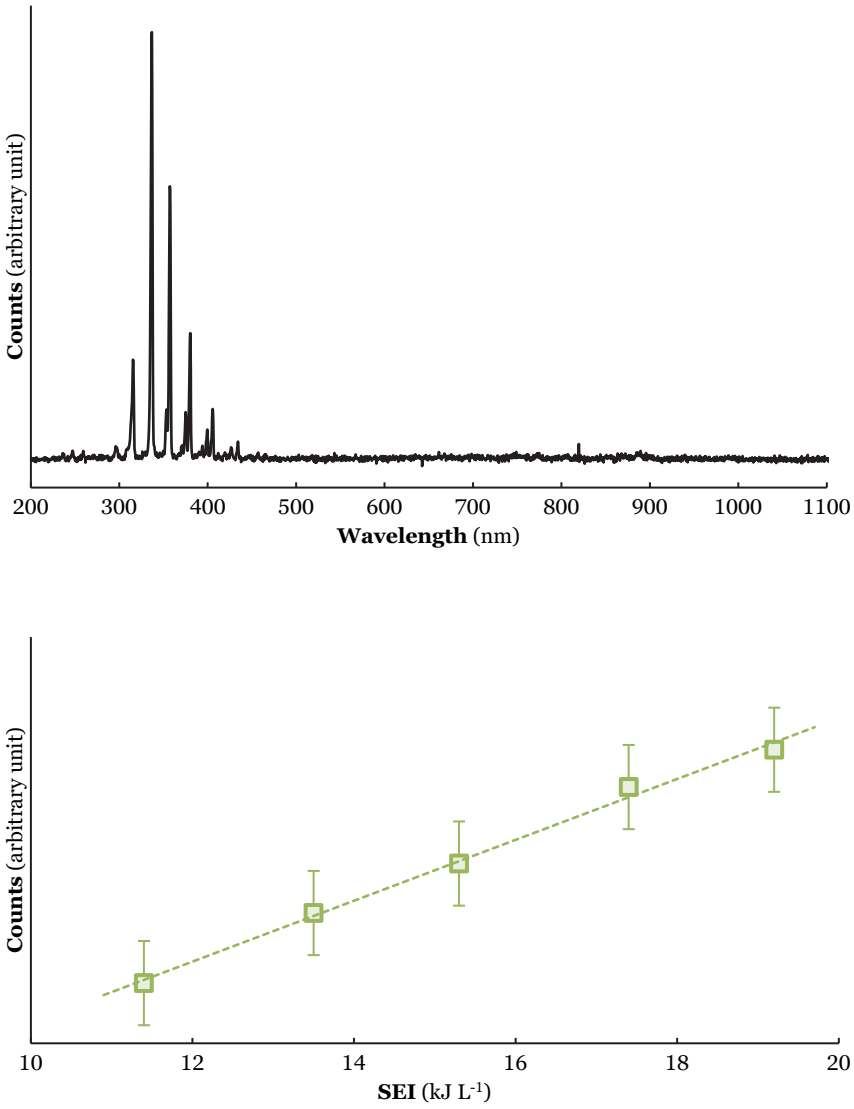

Figure 53: Top: Number of counts for pure N_2, measured in quartz wool just below MgO packing at SEI=19.2 kJ L^{-1}. Flowrate 10 mL min^{-1}. Bottom: Number of counts of UV Vis spectrum at 337 nm (Transition from $N_2(C^3\Pi_u(v=0))$ to $N_2(B^3\Pi_g(v=0))$, green squares), as function of the SEI.

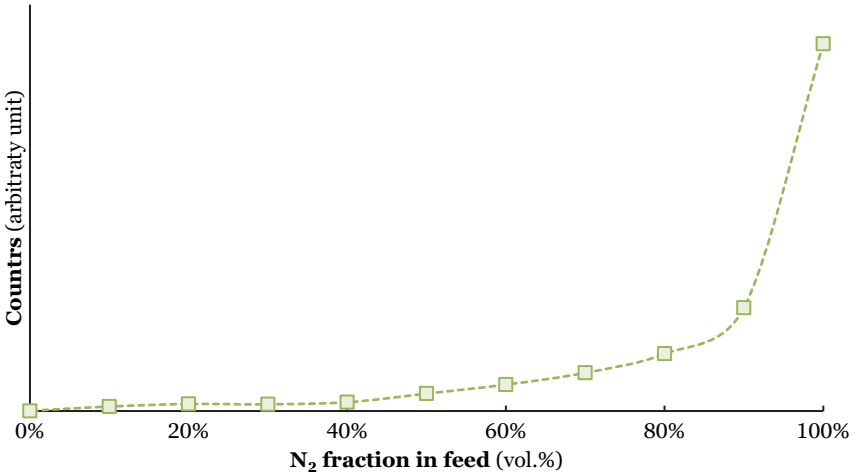

Figure 54: Number of counts for N_2 at 337 nm (Transition from N2($C^3\Pi_u$(v=0)) to $N_2(B^3\Pi_g$(v=0)), green squares), measured in quartz wool just below MgO packing at SEI=19.2 kJ L^{-1}, as function of the nitrogen fraction in the feed. Total flowrate 10 mL min^{-1}.

6.4.2.5 Td value calculation

The reduced electric field can be calculated from the Lissajous plot, and the plasma reactor configuration. As discussed in Ref. [79], the electric field (E) is calculated according to **Equation 7**, where U_b is the breakdown voltage, and $d_{packing\text{-}gap}$ the distance between the high voltage electrode and the ground electrode, corrected for the packing.

Equation 7: $$E = \frac{U_b}{d_{packing-gap}}$$

The corrected gap distance ($d_{packing\text{-}gap}$) is given by **Equation 8**, where d_{gap} is the distance between the high voltage electrode and the ground electrode, and β the gas void fraction.

Equation 8: $$d_{packing-gap} = d_{gap} * \beta$$

The breakdown voltage can be estimated from the Lissajous figures. For example, the Lissajous figure for Ru/MgO at 6.4 W plasma power in **Figure 52** shows a breakdown voltage of U_b=3.74 kV. The diameter of the high voltage electrode (inner electrode) is 1 mm. The ground electrode (outer electrode) is at the outside of the quartz tube, e.g. at 6 mm. Thus, d_{gap}=(6-1)/2=2.5 mm. The quartz tube has no void fraction, so β=0. The catalyst bed is assumed to have a void fraction of β=0.5. This results in an overall void fraction of β=0.21. Thus, the electric field is given by $E = \frac{U_b}{d_{packing-gap}} = \frac{3.74\ kV}{2.5\ mm*0.21} = 70\ kV/cm$. The reduced electric field is calculated using **Equation 9**, where n_0 is the

number of gas species per volume, which is equal to the Loschmidt number at atmospheric pressure and temperature (n_0=2.69*10^{25} m^{-3}). The unit Td is often used for the reduced electrical field, where 1 Td= 10^{-21} V m^2.

Equation 9: $E_n = \frac{E}{n_0}$

Then, the reduced electric field is equal to $E_n = \frac{E}{n_0} = \frac{70\ kV/cm}{2.69*10^{25}\ m^{-3}} = 2.69 * 10^{-19}\ V\ m^2 =$ 260 Td for the experiment at 6.4 W (**Figure 52**). Most experiments were executed at 3.8 W, where E_n=156 Td.

Models are available [40,310] that predict the fraction of N_2 activated to form N radicals, based on the reduced electric field. As shown in **Figure 55**, the majority of N_2 is activated electronically, while N radical formation increases with increasing plasma power.

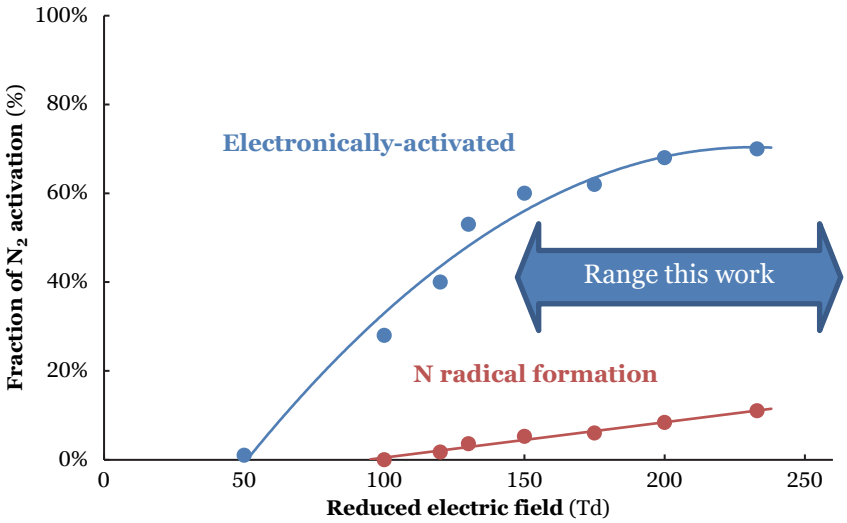

Figure 55: Fraction of plasma-N_2 activations going to electronical excitation of N_2 and N radical formation, based on a pure N_2 gas stream. Data reproduced from ref. [40].

6.4.3 Experimental results

6.4.3.1 Thermal-catalytic NH_3 co-feeding studies

In **Chapter 5**, significant ammonia synthesis activity was not measured for Ru/MgO up till 500°C, whereas Ru-K/MgO showed thermal-catalytic ammonia synthesis activity above 300°C [223]. The other metal catalysts tested also did not show significant ammonia synthesis activity up till 500°C. This is expected, as Ru is the most active metal for N_2 dissociation among the catalysts tested.

Ammonia was co-fed (0.5 mol.% NH_3 and 1.0 mol.% NH_3) in absence of plasma to assess the thermal-catalytic ammonia decomposition activity. Only Ru/MgO showed activity for thermal-catalytic ammonia decomposition, as follows from a decreasing ammonia concentration at temperatures above 400°C (see **Figure 56**). The other catalysts did not show significant activity for ammonia decomposition up till 500°C, as follows from a constant ammonia outlet concentration up till 500°C (not shown here).

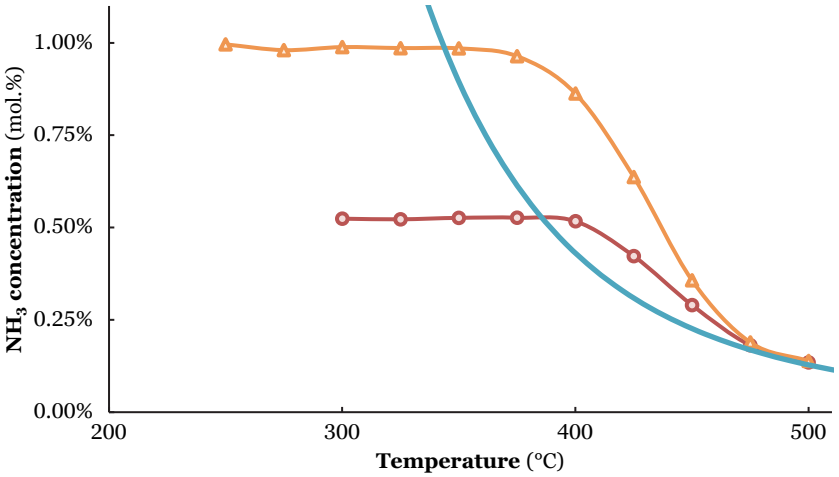

Figure 56: Activity for thermal-catalytic NH3 decomposition with 0.5 mol.% NH_3 co-feed (red circles) and 1.0 mol.% NH_3 co-feed (orange triangles) on Ru/MgO. Total flowrate 20 mL min^{-1}, H_2:N_2=1:1, catalyst loading 130 mg (250-300 µm).

6.4.3.2 Effect of plasma power

Ammonia co-feeding experiments with bare MgO were performed to estimate the contribution of ammonia decomposition in the plasma at various plasma powers. As shown in **Figure 57**, the ammonia formation rate on MgO is faster than the ammonia decomposition rate upon increasing the plasma power when the ammonia concentration is below 0.7 mol.%.

In contrast, ammonia decomposition dominates over ammonia formation at higher ammonia concentrations (above 0.8 mol.%), irrespective of plasma power, as shown in **Figure 57**. The net ammonia formation is calculated from the outlet ammonia concentration minus the ammonia feed concentration. Plasma-induced ammonia decomposition is also reported in literature [253,274,340].

From **Figure 57**, it follows that an increase in ammonia co-feed always increases the ammonia decomposition rate. The rate of ammonia decomposition increases with plasma power, as follows from the more negative slope for 6.4 W, as compared to 5.1 W, and

especially 3.8 W (**Figure 57**). It should be noted that ammonia decomposition will also occur to some extent when ammonia is formed by the plasma, while sufficient plasma power is required to produce measurable quantities of ammonia in the reactor outlet.

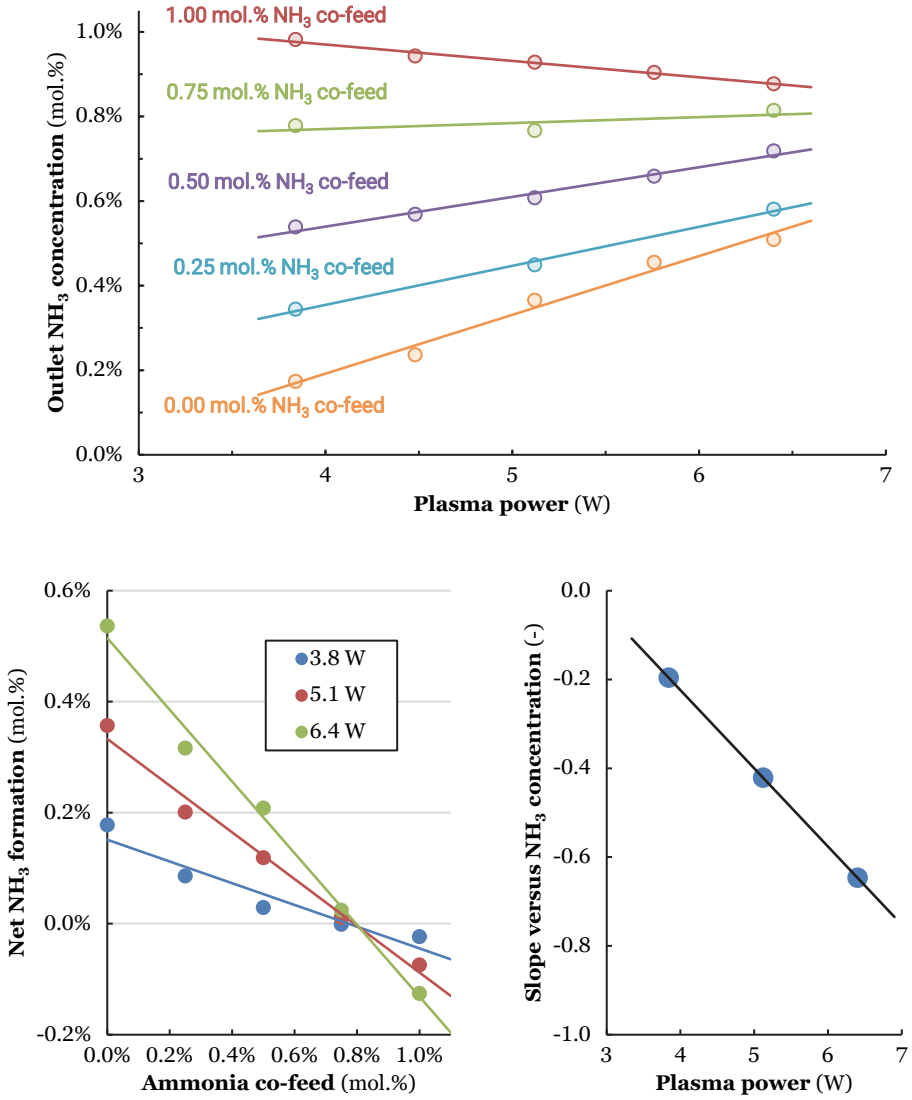

Figure 57: Top: Effect of the plasma power on the rate for plasma-chemical NH_3 synthesis on MgO at ambient conditions, with various NH_3 co-feeding concentrations. Bottom left: Effect of ammonia co-feed on the net rate of formation for plasma-chemical NH_3 synthesis for MgO at ambient conditions, with various plasma powers. Bottom right: Slope of lines in the middle figure versus plasma power. Total flowrate 20 mL min^{-1}, H_2:N_2=1:1, MgO loading 150 mg (250-300 µm particles).

The above analysis implies a compromise in plasma conditions and ammonia outlet concentrations. Only data for the lowest tested plasma power (3.8 W) at NH_3 outlet concentrations below 0.5 mol.% will be used for kinetic analyses, in order to limit the contribution of ammonia decomposition. The relatively low plasma power of 3.8 W is chosen, as it is the minimum plasma power allowing for appreciable NH_3 yields, while having a relatively limited effect of NH_3 concentration on the net NH_3 formation (as compared to the higher plasma powers). The maximum ammonia concentration of 0.5 mol.% is chosen, as the net NH_3 formation approaches zero at higher NH_3 concentrations, indicating a dominant contribution from plasma-induced NH_3 decomposition.

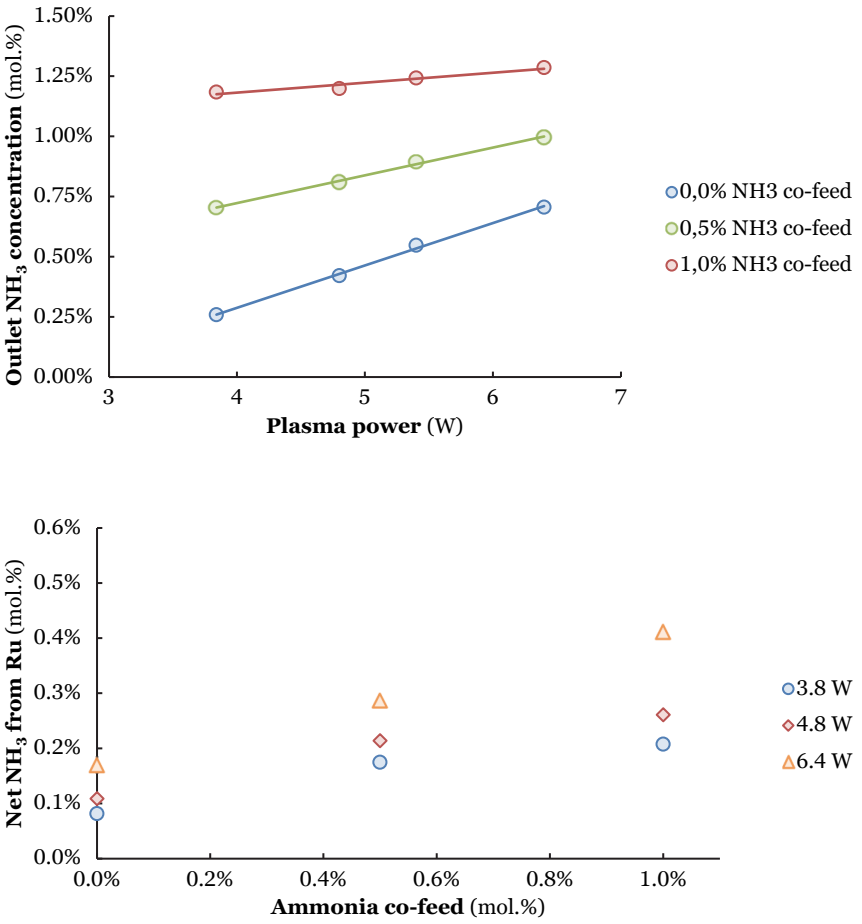

Figure 58: Top: Effect of the plasma power on the activity for plasma-chemical & plasma-catalytic NH_3 synthesis for Ru/MgO, with various NH_3 co-feeding concentrations. Bottom: Net ammonia formation on Ru with various NH_3 co-feeding concentrations and plasma powers. Temperature 250°C, total flowrate 20 mL min^{-1}, H_2:N_2=1:1, Ru/MgO loading 150 mg (250-300 µm particles).

Additional co-feeding studies were performed with Ru/MgO (see **Figure 58**). As opposed to the measurements for MgO (see **Figure 57**), an increase in plasma power results in a higher ammonia outlet concentration, even at ammonia concentrations above 1%. This suggests that the plasma-catalytic ammonia synthesis rate on the Ru surface is higher than the ammonia decomposition rate, yielding a steady-state net ammonia formation rate.

6.4.4 Other

6.4.4.1 Diffusion barriers

In order to check whether the reaction is not limited by N diffusion from the gas phase to the surface, but by the reaction between N and surface-adsorbed H, the barrier for gas diffusion is calculated. According to Ref. [356], the gas diffusion coefficient is proportional to $T^{1.75}$, as given by **Equation 10**, where T_1 and T_2 are two temperatures, R is the gas constant, and $E_{A,app,g}$ is the gas diffusion coefficient.

Equation 10: $\left(\frac{T_1}{T_2}\right)^{1.75} = e^{-\frac{E_{A,app,g}}{R}\left(\frac{1}{T_2}-\frac{1}{T_1}\right)}$

Then, $E_{A,app,g}$ is given by **Equation 11**. At temperatures between 100°C (373 K) and 300°C (573 K), this results in a gas diffusion coefficient of 6.7 kJ mol^{-1}. This is far below the observed barriers of 18-30 kJ mol^{-1}, thus ruling out a diffusion-limited reaction.

Equation 11: $E_{A,app,g} \approx 1.75 R \ln\left(\frac{T_1}{T_2}\right)\left(\frac{1}{T_2}-\frac{1}{T_1}\right)^{-1} = 1.75 * 0.008315\ \text{J mol}^{-1}\text{K}^{-1} * \ln\left(\frac{373\ \text{K}}{573\ \text{K}}\right) * \left(\frac{1}{573\ \text{K}}-\frac{1}{373\ \text{K}}\right)^{-1} = 6.7\ \text{kJ mol}^{-1}$

6.4.4.2 Error bar calculation

The experimental errors for calculating the turnover frequencies (TOFs) are presented hereafter. As an example, the error for the supported metals is calculated at 250°C, 20 mL min^{-1}, H_2:N_2=1:1, and 3.8 W (**Table 8**).

Table 8: Calculated errors for plasma-catalytic ammonia synthesis turnover frequencies (TOFs) at 250°C, 20 mL min^{-1}, H_2:N_2=1:1, and 3.8 W.

Catalyst	NH_3 from plasma-catalysis (mol.%, see **Figure 44**)	Particle size (see **Table 7**)	TOF (*10^{-3} s^{-1})	Upper error (*10^{-3} s^{-1}, %)	Lower error (*10^{-3} s^{-1}, %)
Ru/MgO	0.09±0.02	16±1	2.3	0.69 (30%)	0.62 (27%)
Co/MgO	0.32±0.02	5±1	3.7	1.01 (28%)	0.92 (25%)
Pt/MgO	0.16±0.02	19±1	3.1	0.57 (18%)	0.53 (17%)
Pd/MgO	0.13±0.02	23±1	5.2	1.06 (20%)	0.99 (19%)
Cu/MgO	0.28±0.02	20±1	3.3	0.41 (13%)	0.39 (12%)
Ag/MgO	0.24±0.02	25±1	9.2	1.17 (13%)	1.10 (12%)

The experimental error is estimated, based on the measured ammonia outlet concentration as determined by mass spectrometry. Variation in ammonia outlet concentration between measurements and over time with the mass spectrometer are below

0.02 mol.% NH_3. The error for the nanoparticle size is estimated to be ±1 nm. The surface area then scales with the area of a half sphere, e.g. $2*\pi*(d/2)^2$, where d is the nanoparticle size. The calculated errors are listed in **Table 8**. The errors are in the range 12-30%.

Chapter 7

Improving the energy efficiency of plasma-based ammonia synthesis with *in situ* adsorption

Summary

Plasma-based ammonia synthesis is studied as an option for electrifying the chemical industry. However, the energy efficiency of plasma-based ammonia synthesis is severely limited by ammonia decomposition in the plasma phase. This Chapter shows that the use of zeolite 4A as an adsorbent for *in situ* ammonia removal from the plasma phase suppresses product decomposition, thereby increasing the ammonia yield. It is found that the ammonia yield for plasma-chemical ammonia synthesis with *in situ* ammonia removal is improved by a factor 2 compared to steady-state plasma-chemical ammonia synthesis. Plasma-induced surface heating limits the effective ammonia adsorption capacity of the zeolite, decreasing the adsorption capacity. *In situ* product removal is of interest for plasma chemistry and plasma catalysis in general, as product decomposition in the plasma is a general phenomenon limiting the product yield.

This chapter has been published as:

Rouwenhorst, K. H. R., Mani, S., Lefferts, L. (2022). Improving the energy efficiency of plasma-based ammonia synthesis with in situ adsorption. ACS Sustainable Chemistry & Engineering, 10(6), 1994-2000. doi: 10.1021/acssuschemeng.1c08467

7.1 Introduction

With the emergence of low cost electricity from renewables, electrification of chemical reactions is eminent [50]. Therefore, plasma-catalytic ammonia synthesis has recently gained interest [58,199,200,310]. However, the reaction mechanisms and the relevant process parameters are not fully understood [180,223,236]. The highest reported energy yield for plasma-catalytic ammonia synthesis is 37.9 g-NH_3 kWh^{-1} [89] and most studies report an energy yield below 5 g-NH_3 kWh^{-1} [199,310], e.g. below the benchmark of 150-200 g-NH_3 kWh^{-1} required for commercialization [42,216], see **Chapter 8**.

The low energy yields are in part due to ammonia decomposition by the plasma. Recently, Van 't Veer et al. [253] suggested based on modelling studies that the ammonia formed in the plasma is also decomposed by the plasma during the micro discharges. Further experimental evidence was provided by Navascués et al. [274,340], who demonstrated with isotope labelling studies that ammonia is decomposed in the plasma by electron impact dissociation [340]. Concluding, plasma decomposition of ammonia is significantly limiting the energy yield for ammonia formation in the plasma.

In situ removal of ammonia from the plasma phase might offer a solution for this challenge. Solid acids such as zeolites can be used to remove ammonia from a gas mixture via adsorption [217,218]. The use of zeolites for *in situ* ammonia removal from the plasma phase is proposed in this Chapter, as zeolites are stable solid materials. Zeolite 4A is used as a case study.

Peng et al. [81] showed that $MgCl_2$ can also be used to absorb ammonia during plasma-chemical ammonia synthesis. A drawback of this method is the limited stability of $MgCl_2$, forming MgN_2 during plasma operation. The zeolite used in the current work is more chemically stable against changes in chemical compositions with nitrogen species.

Zeolites were previously researched for plasma-based ammonia synthesis by Gorky et al. [357] and Shah et al. [358]. However, the authors report on steady-state ammonia production rates on zeolite 5A and zeolite beta in the presence of a plasma, rather than the effect of the *in-situ* ammonia adsorption on the zeolite. The authors reported a higher steady-state ammonia production rate for zeolite 5A and zeolite beta as compared to other oxides, such as silica and alumina [357,358]. In the current Chapter, it is observed that the ammonia yield produced with *in situ* ammonia removal from the plasma zone is about two times that of the steady-state experiments. This demonstrates that *in situ* ammonia removal from the plasma zone is able to suppress ammonia decomposition by the plasma, thereby increasing the overall ammonia formation rate.

7.2 Results & Discussion

The experimental procedures can be found in the supporting information (**section 7.5.1**). In the upcoming section, the results and discussion for the *in situ* removal of

ammonia by zeolite 4A are presented. Temperature Programmed Desorption (TPD) results in absence of plasma can be found in **section 7.5.2.3**. The results of the sorbent characterization with BET analysis, XRF, XRD and plasma characterization with Lissajous plots and UV-Vis spectroscopy can be found in **section 7.5.2.2**.

7.2.1 Plasma-based ammonia synthesis with *in situ* adsorption

Plasma-based ammonia synthesis was studied in the presence of a packed bed with zeolite 4A particles with a diameter of 250-300 µm. Ammonia adsorbs on the zeolite until saturation, whereafter the zeolite cannot adsorb additional ammonia and the ammonia concentration in the reactor outlet increases to a steady-state value.

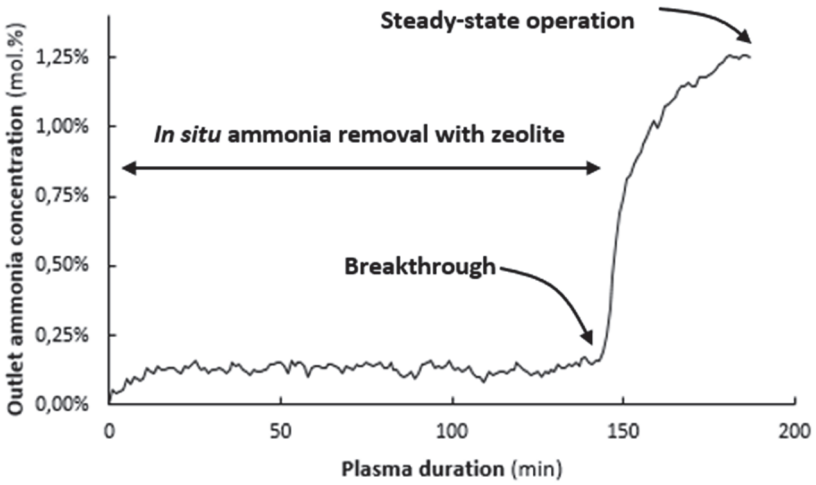

Figure 59: Outlet ammonia concentration as function of the plasma duration. Oven temperature setpoint 25°C, total flow rate 10 mL min^{-1}, H_2:N_2=1:4, plasma power 6.4 W (SEI=38.4 kJ L^{-1}), zeolite loading 600 mg (250-300 µm).

The ammonia concentration in the outlet as function of time is shown in **Figure 59**, for a H_2:N_2 ratio of 1:4 and at a constant flow rate of 10 mL min^{-1} and a constant plasma power of 6.4 W, e.g. a SEI (specific energy input) of 38.4 kJ L^{-1}. The corresponding Lissajous plot is shown in **Figure 66**. It is observed that the ammonia outlet concentration is about 0.1-0.2 mol.% during the first 145 min and increases to about 1.3 mol.% afterwards.

The change in ammonia outlet concentration after 145 min in **Figure 59** is attributed to saturation of the zeolite, resulting in breakthrough of the ammonia in the outlet. To test this hypothesis, the plasma was turned off and the reactor was heated to desorb ammonia from the zeolite (see **Figure 60**). Ammonia was desorbed from the zeolite in absence of the plasma in pure N_2 at 10 mL min^{-1}, and the reactor was heated at a rate of 25°C min^{-1}. A typical result is shown in **Figure 60**. It is observed that ammonia is indeed desorbed from the zeolite. This confirms the *in situ* adsorption of ammonia on the zeolite during the plasma-chemical ammonia synthesis.

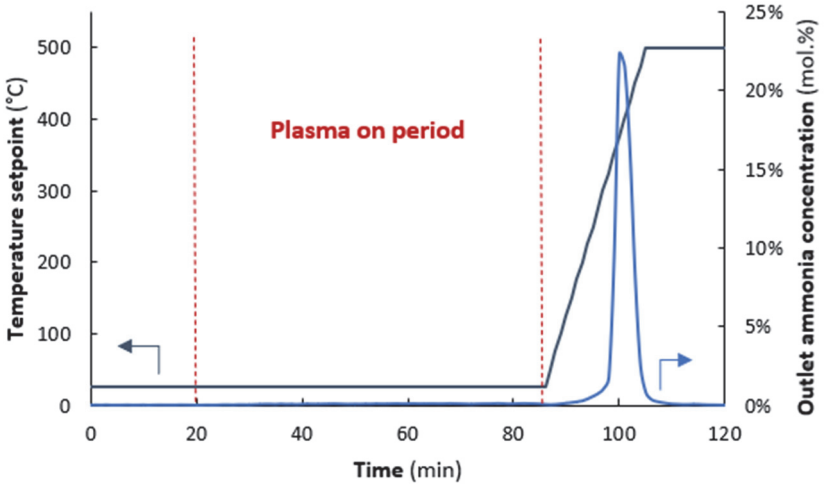

Figure 60: Example experiment for plasma-based ammonia synthesis with in situ adsorption. Reactor temperature (left axis) and outlet ammonia MS signal (right axis) as function of time. Oven temperature setpoint during plasma 25°C. Total flow rate 10 mL min^{-1}, H_2:N_2=1:4, plasma power 6.4 W (SEI=38.4 kJ L^{-1}), zeolite loading 600 mg (250-300 µm). Plasma duration 67 min. Heating rate after plasma-based ammonia synthesis 25°C min^{-1}, 10 mL min^{-1} pure N_2.

Figure 61 shows the amount of ammonia desorbed while varying the plasma duration, at a constant flow of 10 mL min^{-1} and a constant plasma power of 6.4 W. As shown in **Figure 61**, the amount of desorbed ammonia scales linearly with the plasma duration for short plasma durations, independent of the H_2:N_2 ratio. It is observed that most ammonia is initially adsorbed for the H_2:N_2 ratios of 1:1 and 1:2. The amount of adsorbed ammonia stabilizes at about 2.4 mmol-NH_3 g-zeolite^{-1} for all H_2:N_2 ratios. This coincides with the plasma duration required to cause ammonia breakthrough (see **Figure 60**), confirming that the zeolite is saturated with ammonia and the outlet ammonia concentration increases to a steady-state value.

Figure 62 compares the amount of ammonia produced in the first 5 minutes plasma-based ammonia synthesis *with in situ* ammonia removal, i.e. remote from any saturation effects (see **Figure 61**), with the amount of ammonia produced in the same time during steady-state plasma-based ammonia synthesis. The steady-state plasma-based ammonia synthesis yield over 5 min is calculated from the steady-state ammonia outlet concentration, e.g. after zeolite saturation. The amount of ammonia produced by *in situ* removal operation is typically two times the amount of ammonia formed during steady-state operation, indicating a beneficial effect of adsorbing ammonia on zeolite 4A. Furthermore, the ammonia yield is found to be highest for a H_2:N_2 ratio of 1:1 and 1:2, both for steady-state operation and plasma-based ammonia synthesis with *in situ* ammonia removal, in line with observations in literature for steady-state operation at relatively high plasma powers [200].

The highest energy yield for plasma-based ammonia synthesis is about 2.3 g-NH_3 kWh^{-1}, for a H_2:N_2 ratio of 1:2 and a plasma power of 6.4 W. This is about a factor 2 better than the energy yield for steady-state operation, i.e. 1.1 g-NH_3 kWh^{-1}. This improvement is significant, but it should be noted that this is still far below the benchmark of 150-200 g-NH_3 kWh^{-1} required for commercialization of plasma-based ammonia synthesis for small-scale applications (kW range) [42,216].

7.2.2 Plasma-zeolite interactions

The internal pores of the zeolite particles have diameters below <0.1 μm, while the zeolite cages have an even smaller diameter in the sub-nm range. Plasma cannot form inside pores with a diameter below typically 1-10 μm [43,163,187–189], as these pores are smaller than the Debye length, i.e. the minimum distance for electrons to accelerate sufficiently for plasma formation.

Plasma radicals such as N and NH formed outside pores may penetrate into pores up to 1 μm, based on the lifetime of such species and their diffusivity [152]. The resulting penetration depth is typically 1 μm for plasma radicals, much smaller than the radius of the zeolite 4A particles of 125-150 μm, as used in this Chapter.

Thus, adsorbed ammonia is not in contact with the plasma and thereby protected against the plasma. The ammonia concentration in the intraparticle spaces is decreased from typically 1.3% to about 0.15% (see **Figure 59**), diminishing ammonia decomposition by the plasma through for instance electron-impact dissociation, an important pathway for ammonia decomposition in a DBD reactor [340]. Concluding, the higher ammonia production by *in situ* ammonia removal operation as compared to steady-state operation can be attributed to decreased ammonia decomposition in the plasma phase.

7.2.3 Effect of heating

As shown in **Figure 61**, the total ammonia desorbed from the zeolite after plasma-based ammonia synthesis (2.4 mmol-NH_3 g^{-1}) is lower than in the case of ammonia TPD after adsorption of ammonia at ambient temperature and for 2 mol.% NH_3 in N_2 at atmospheric pressure (6.3 mmol-NH_3 g^{-1}). For the thermal ammonia TPD study, two peaks can be identified: the first at 200°C, and the second at 400°C. The peak at 400°C is attributed to strongly bound ammonia through the formation of NH_4^+ on Brønsted acid sites [359]. The peak at 200°C is attributed to physisorbed NH_3 [359]. Exclusively the peak at 400°C is observed after plasma-based ammonia synthesis. This indicates that only strongly bound ammonia on Brønsted acid sites is detected, while physisorbed ammonia is not observed. This suggests that the zeolite is heated, preventing physisorption of ammonia. Plasmas contain highly energetic species, and heat is dissipated by collisions with the surface as well as by recombination of plasma species [42,162].

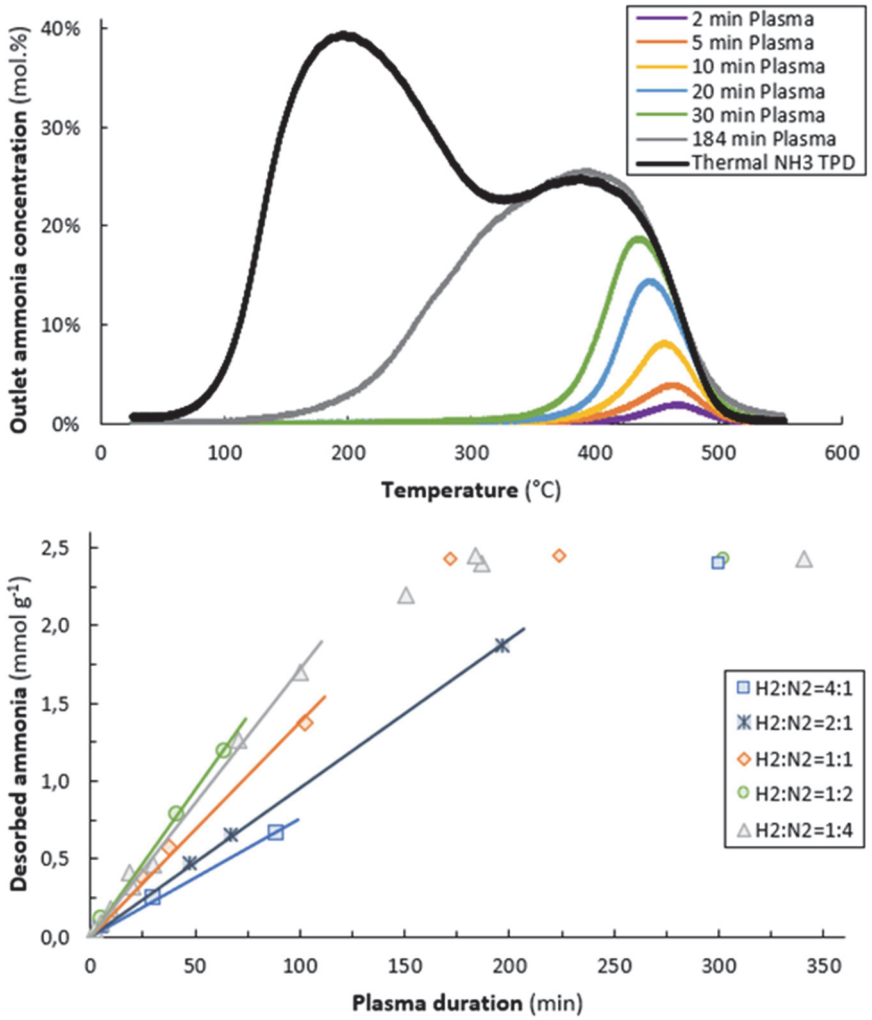

Figure 61: The effect of plasma duration on the amount of ammonia adsorbed on the zeolite. Top: Thermal ammonia TPD signal after ammonia adsorption in absence of plasma (2.0 mol.% NH_3 in N_2, 10 mL min^{-1}), and ammonia TPD signal after plasma-based ammonia synthesis with in situ removal (top, total flow rate 10 mL min^{-1}, H_2:N_2=1:4, plasma power 6.4 W for various plasma durations). Ammonia desorption in absence of plasma in pure N_2 at 10 mL min^{-1}, heating rate of 25°C min^{-1}. Bottom: The effect of plasma duration on the amount of ammonia desorbed for various H_2:N_2 ratios during plasma: 4:1 (blue squares), 2:1 (blue crosses), 1:1 (orange diamonds), 1:2 (green circles), and 1:4 (grey triangles). Oven temperature setpoint 25°C, total flow rate 10 mL min^{-1}, plasma power 6.4 W (SEI=38.4 kJ L^{-1}), zeolite loading 600 mg (250-300 µm). Ammonia desorption in absence of plasma in pure N_2 at 10 mL min^{-1}, heating rate of 25°C min^{-1}.

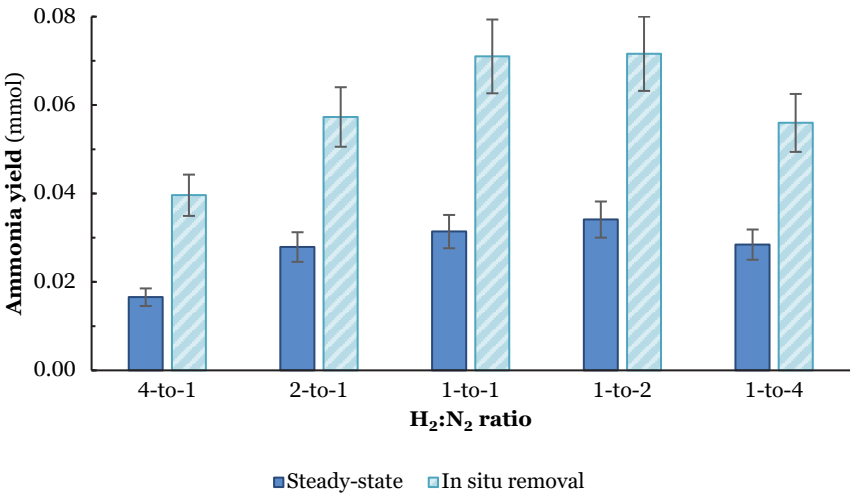

Figure 62: Comparison of cumulative ammonia yield after 5 min plasma for steady-state operation (dark blue) and *in situ* ammonia removal (blue - striped), varying H_2:N_2 ratios. Oven temperature setpoint 25°C, total flow rate 10 mL min^{-1}, plasma power 6.4 W (SEI=38.4 kJ L^{-1}), zeolite loading 600 mg (250-300 µm). Ammonia desorption in absence of plasma in pure N_2 at 10 mL min^{-1}, heating rate of 25°C min^{-1}.

To test the hypothesis of reactor heating, the temperature at the outside of the plasma reactor was measured for various plasma durations using a thermocouple (see **section 7.5.1.4**). The temperature of the oven was regulated at 25°C. As shown in **Figure 63**, the measured temperature at the outside of the reactor increases upon plasma illumination, stabilizing at about 57°C. This confirms that the plasma heats the reactor. It should be noted that the temperature inside the plasma reactor is probably higher than outside the plasma reactor [152,292,293]. As follows from the adsorption isotherm for zeolite 4A (see **Figure 67**), a temperature of about 145°C is required to attain an ammonia capacity of 2.4 mmol-NH_3 g^{-1} for 1.3 mol.% ammonia in the reactor outlet.

7.3 Strategies for *in situ* product removal from plasma-chemical reactors

In this Chapter, the beneficial effect of product removal from the plasma phase for ammonia synthesis is demonstrated. This concept could be more widely applicable for plasma-chemical and plasma-catalytic reactions, as decomposition of products is a general concern in plasma catalysis. In fact, the reverse reaction in the plasma phase was also demonstrated for CO_2 splitting [337], methane coupling [360], and the dry reforming of methane [360]. Hereafter, strategies for product removal from the plasma phase are briefly addressed.

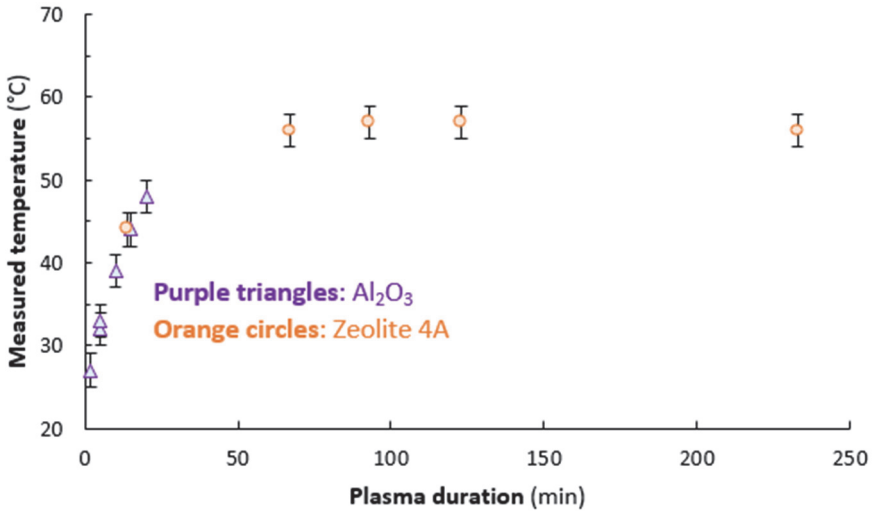

Figure 63: Temperature at the outside of the reactor as function of the plasma duration. Oven temperature setpoint 25°C, total flow rate 10 mL min^{-1}, plasma power 6.4 W (SEI=38.4 kJ L^{-1}), H_2:N_2=1:4, zeolite/alumina loading 600 mg (250-300 µm).

Product absorption in, or adsorption on solid materials is commercially applied in the chemical industry, such as for removal of heavy hydrocarbons from natural gas, as well as for removal of H_2O, CO and CO_2 from gas streams. Furthermore, sorption-enhanced processes have been proposed for CO_2 removal during reforming reactions [361,362] and during the water gas shift reaction [363].

In the current Chapter, the use of zeolites for ammonia removal is demonstrated. Likewise, Peng et al. [81] showed that $MgCl_2$ can be used to absorb ammonia during plasma-chemical ammonia synthesis. A drawback of this is $MgCl_2$ conversion to MgN_2 in the plasma to an important extent, deactivating the sorbent and releasing Cl_2 gas. The zeolite used in the current Chapter is chemically stable, allowing for multiple adsorption-desorption cycles.

A solid material can also be used as a sacrificial material. For example, it is proposed that surplus oxygen from the CO_2 splitting reaction can be removed by oxidation of a metal, thereby preventing the oxidation of CO to CO_2.

Reactor configurations that can be used in a DBD reactor include a fixed bed configuration and a trickle bed configuration. A fluidized bed configuration may be used in for instance a gliding arc reactor, although operating this does not seem trivial.

The product can also be removed from the plasma phase by using a membrane. For example, Hayakawa et al. [364] demonstrated hydrogen production from ammonia decomposition in a plasma reactor with and without a membrane. It was observed that the hydrogen yield was almost doubled upon using a membrane for hydrogen removal from the plasma reactor, apparently limiting the backward reaction, in this case ammonia synthesis.

Lastly, the product can be removed in liquid phase, either by absorption in a liquid medium or by condensation of the product. Product removal by absorption in a liquid medium was recently demonstrated for nitrogen fixation. Gorbanev et al. [365] and Hawtof et al. [69] contacted a nitrogen and steam plasma jet with liquid water, thereby producing ammonia and nitrogen oxides, which were subsequently absorbed in the liquid. Furthermore, Wang et al. [366] produced oxygenates from CO_2 and H_2 in a dielectric barrier discharge (DBD) reactor. Upon cooling the reactor wall with a water jacket, methanol and ethanol were liquefied, thereby limiting product decomposition. This resulted in a higher oxygenate yield as compared to the configuration without water cooling.

7.4 Conclusion

In this Chapter, *in situ* adsorption of ammonia with a zeolite during plasma-chemical ammonia synthesis is demonstrated to increase the ammonia yield as compared to steady-state plasma-based ammonia synthesis. This can be attributed to ammonia adsorption on the zeolite, thereby suppressing ammonia decomposition in the plasma phase. This improves the energy yield for ammonia synthesis by a factor two, e.g. from 1.1 g-NH_3 kWh^{-1} to 2.3 g-NH_3 kWh^{-1}. However, this is still far below the benchmark of 150-200 g-NH_3 kWh^{-1} required for commercialization of plasma-based ammonia synthesis for small-scale applications, see **Chapter 8**. As plasmas cannot penetrate the pores of the zeolite, surface adsorbed ammonia inside the zeolite pores is protected from reactive plasma species. However, plasma-induced heating reduces the sorbent capacity.

In situ product removal from the plasma phase is of interest for plasma conversions in general. Therefore, various strategies for product removal from the plasma phase are proposed, including product liquefaction, membrane separation, and the use of absorbent or adsorbents.

7.5 Supporting information

7.5.1 Experimental procedures

Zeolite 4A was tested for the *in situ* adsorption of ammonia in absence and in the presence of a plasma, as it has a significant capacity for ammonia adsorption, i.e. in the order 1-10 mmol NH_3 per g sorbent [218].

7.5.1.1 Materials and preparation

Zeolite 4A (Na^+ ion exchanged) was obtained from Unilever Research Laboratorium, Vlaardingen. H_2 and N_2 with a purity grade of 99.999% were purchased from Linde, and water traces were removed using Agilent gas clean purification systems. A gas mixture of 2 vol.% NH_3 in a 98 vol.% N_2 balance gas was purchased from Linde. All materials were used as received.

Zeolite 4A was dried in an oven at 100°C and atmospheric pressure for 1 h, followed by drying in a vacuum oven at 120°C for 2 h, removing water. Then, the material was pelletized and crushed. The sieve fraction 250-300 μm was used for the adsorption experiments. Last traces of water were removed in the reactor at 500°C in a 1:1 mixture of N_2 and H_2.

7.5.1.2 Materials characterization

The total surface area and pore volume were determined by N_2 chemisorption at -198°C using a Micromeritics Tristar. The samples were outgassed in vacuum at 300°C for 24 h before the analysis. The experimental composition was determined by x-ray fluorescence spectroscopy (XRF) using Bruker S8 tiger. The crystalline phases present in the catalyst were determined with x-ray diffraction (XRD) using a Bruker D2 Phaser diffractometer equipped with a position-sensitive detector over a 2θ range between 10° and 90° using Cu Kα radiation (λ= 1.5418 Å).

7.5.1.3 Plasma characterization

A PMV 500-4000 power supply was used to illuminate the plasma at 25 kHz. A Picoscope PC Oscilloscope was used to monitor the charge-voltage characteristics. The high voltage electrode was connected to the power supply, and an AC voltage of up to 10 kV peak to peak was applied. A Tektronix P6015A high voltage probe was used to monitor the voltage over the high voltage electrode, while a TT-HV 250 voltage probe was used to measure the voltage over the ground electrode. A capacitor of 8.24 nF was placed in between the ground electrode and the TT-HV 250 voltage probe. An Ocean HDX Spectrometer was used to analyze light emitted by the plasma, just below the catalyst bed, at low temperature.

7.5.1.4 Ammonia synthesis and adsorption experiments

A schematic representation of the experimental set-up for the adsorption experiments is shown in **Figure 64**. The adsorption experiments were carried out in a quartz tubular reactor with an inner diameter of 4 mm and an outer diameter of 6 mm, at atmospheric pressure. A stainless-steel rod of 1 mm diameter is placed inside the reactor as the high voltage electrode. At the outside of the quartz tube of 6 mm outer diameter, a metal tube is placed as the ground electrode. The temperature was controlled with a thermocouple connected to a heating block, which is placed around the ground electrode. The flowrates of the reactants were controlled with calibrated mass flow controllers (MFCs). Typically, 600 mg of adsorbent with particle sizes of 250-300 μm was loaded in the reactor with a bed height of about 4 cm, on top of a layer of quartz wool. A spacer is placed below the quartz wool and above the adsorbent bed to prevent moving of particles due to plasma-illumination and to center the high voltage electrode.

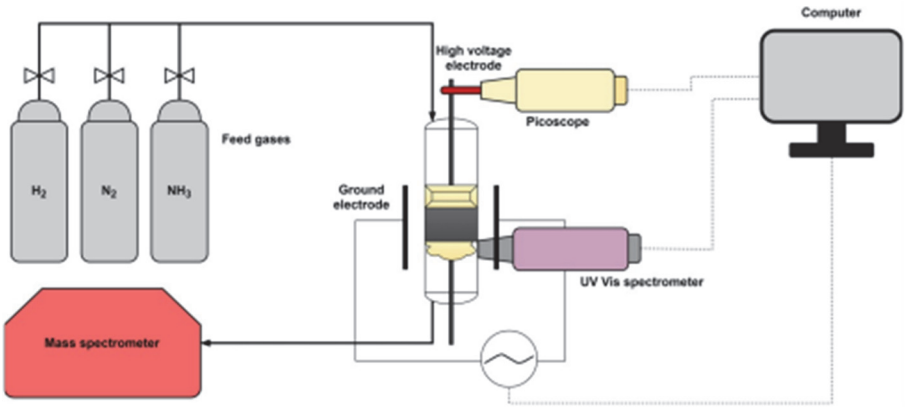

Figure 64: Schematic representation of the experimental set-up. The plasma volume includes the spacers, the packed bed with adsorbents, and the quartz wool.

Residual water was removed from the reactor and adsorbent bed at 500°C for 2 h in a gas mixture of 10 mL min^{-1} N_2 and 10 mL min^{-1} H_2. Afterwards, the reactor was cooled down to room temperature in a gas mixture of 10 mL min^{-1} N_2 and 10 mL min^{-1} H_2. Ammonia adsorption experiments, both in absence and in presence of plasma, were carried out at room temperature, at a total flowrate of 10 mL min^{-1} and with varying H_2 and N_2 ratios. Afterwards, the reactor was heated in absence of plasma with a 10 mL min^{-1} N_2 flow at a heating rate of 25°C min^{-1}.

The product gases were analyzed using an on-line Pfeiffer Vacuum Thermostar™ gas analysis system, which is a mass spectrometer (MS). The MS signal for NH_3 (17 m/e) was calibrated in the range 0-2 mol.%, resulting in a linear relationship. The signals for H_2 (2 m/e), N_2 (28 m/e), and H_2O (18 m/e) were also monitored semi-quantitatively, as well as a minor NH_3 peak (16 m/e).

7.5.2 Results & discussion

7.5.2.1 Material characterization

The material characterization results for zeolite 4A are discussed hereafter. From XRF it followed that the zeolite 4A was composed of mainly Al_2O_3 (31 wt.%), SiO_2 (56 wt.%), and Na_2O (13 wt.%), as expected, with traces of MgO (0.2 wt.%) and K_2O (0.2 wt.%). The BET surface area of zeolite 4A was found to be 341 $m^2\ g^{-1}$, determined by the BET analysis. The pore volume is found to be 0.21 $cm^3\ g^{-1}$ for zeolite 4A, also determined by the BET analysis. The results are in line with previously reported data [367]. The XRD spectra of zeolite 4A is shown in **Figure 65**. The results are in line with previously reported data [368,369].

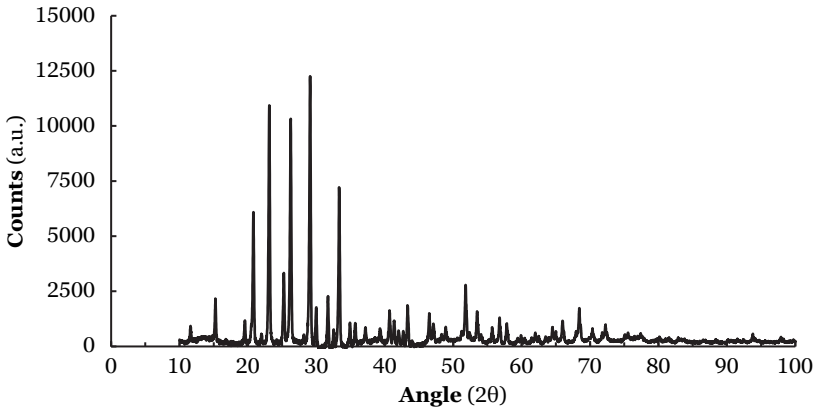

Figure 65: XRD spectrum for zeolite 4A.

7.5.2.2 Plasma characterization

The voltage and charge were monitored with an oscilloscope, from which the power dissipated can be determined using a Lissajous figure. An example of a Lissajous figure (also termed Q-V plot) is shown in **Figure 66**. In a Q-V plot, the capacitive and discharge behavior of a plasma is monitored. Ideally, a Lissajous figure has the shape of a parallelogram, thereby perfectly separating the capacitive and discharge regime. However, there is an indent in both the positive and negative charge cycle, as shown in **Figure 66**. This can be attributed to a discharge at the contact points of particles at an earlier stage than over the remainder of the surface [80,163].

7.5.2.3 Thermal ammonia TPD study with zeolite 4A

Ammonia TPD (temperature programmed desorption) was performed for zeolite 4A after adsorption of ammonia at room temperature in 2 mol.% NH_3 in balance N_2 at 10 mL min^{-1}, instead of ammonia synthesis in a plasma. Subsequently, the gas flow was changed to pure N_2 at 10 mL min^{-1}, and the reactor was heated at a rate of 25°C min^{-1}.

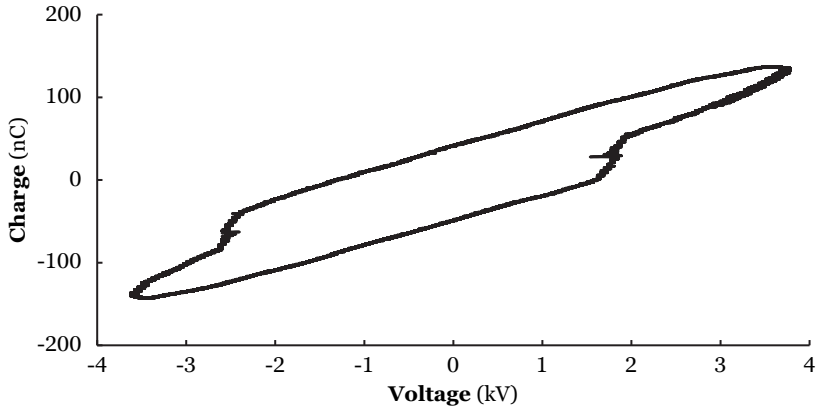

Figure 66: Lissajous figure for zeolite 4A at room temperature, H_2:N_2=1:1, 10 mL min^{-1}. The total power dissipated is 6.4 W.

The resulting NH_3 TPD profile is shown in **Figure 67**. Two peaks can be identified: the first at 200°C, and the second at 400°C. The peak at 400°C is attributed to strongly bound ammonia through electrostatic attraction between Na^+ and the lone electron pair of ammonia [238]. The peak at 200°C is attributed to physisorbed NH_3 [359]. The results are in line with previously reported data [238,359,370,371].

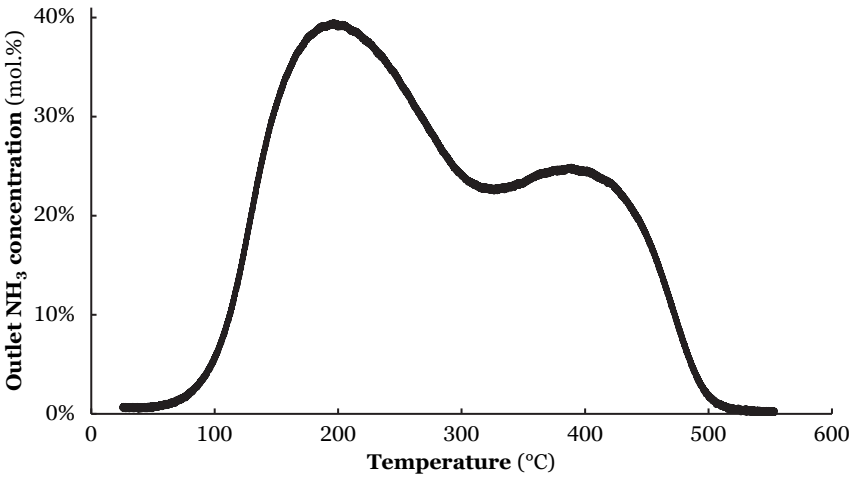

Figure 67: NH_3 TPD profile for zeolite 4A. Zeolite loading 600 mg, 250-300 µm. NH_3 adsorption gas: 2 mol.% NH_3 in N_2 balance at 10 mL min^{-1} at ambient temperature. TPD gas: pure N_2 at 10 mL min^{-1}. Heating rate: 25°C min^{-1}. The obtained ammonia capacity is 6.3 mmol-NH_3 g^{-1}.

The amount of adsorbed NH_3 according the result in **Figure 68** is compared to adsorption isotherms in literature. Helminen et al. [217] reported the amount of ammonia adsorbed for various partial pressures of ammonia. As shown in **Figure 68**, the amount of ammonia adsorbed on zeolite 4A is consistent with the reported isotherm.

7.5.2.4 Ammonia isotherm for heating effect

The observed total ammonia desorbed from the zeolite after plasma-based ammonia synthesis is about 2.4 mmol-NH_3 g^{-1} (see **Figure 61**), e.g. lower than observed for the thermal ammonia TPD at 6.3 mmol-NH_3 g^{-1} (see **Figure 61** or **Figure 67**). In the main manuscript this is attributed to plasma-induced heating.

It is estimated that the temperature inside the reactor using ammonia adsorption data from Helminen et al. [218] for zeolite 4A at 1.3 kPa NH_3 and at 25-120°C. This data is extrapolated, resulting in a decrease with increasing temperature. The observed capacity in our experiments is 2.4 mmol-NH_3 g^{-1} (see **Figure 61**). As shown in **Figure 69**, a temperature of 145°C inside the plasma reactor is required to explain the observed ammonia capacity. This temperature of 145°C is consistent with the lowest ammonia desorption temperature of about 150°C observed for the TPD after plasma illumination (see **Figure 61**).

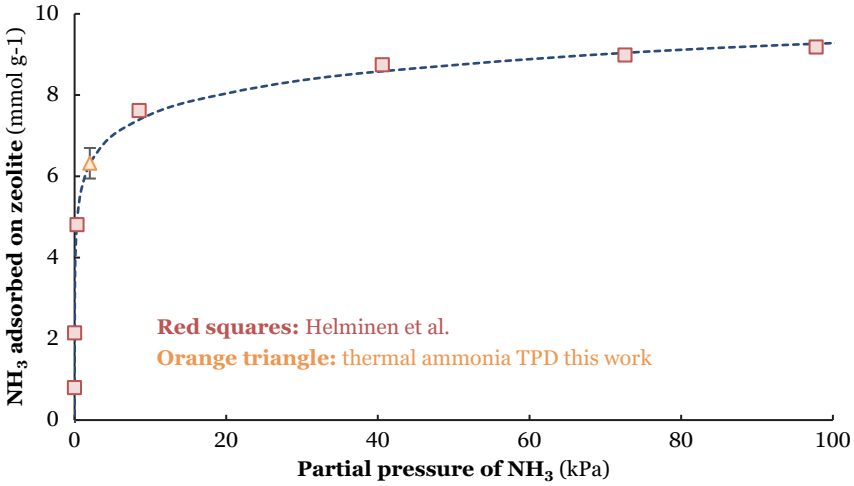

Figure 68: NH_3 adsorption isotherm for zeolite 4A at ambient temperature. Red squares: experimental data of Helminen et al. [217]. Orange triangle: thermal NH_3 TPD in this work. Data normalized per gram zeolite.

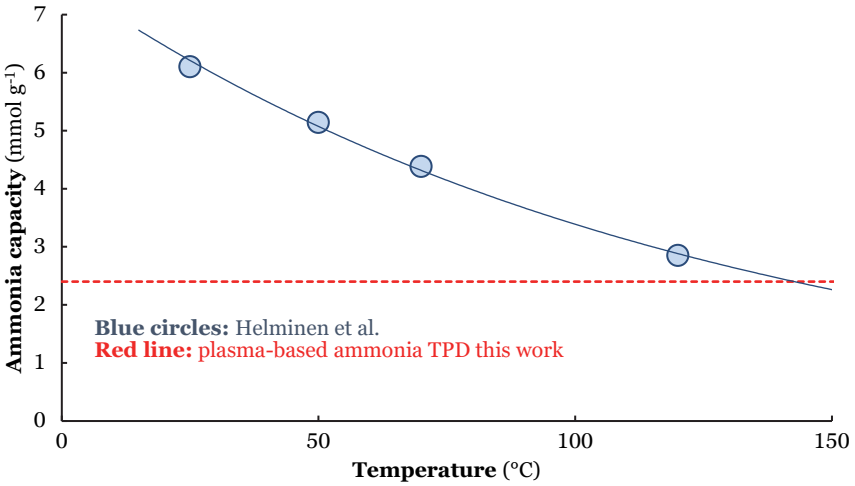

Figure 69: NH_3 adsorption data for zeolite 4A at various temperatures and for 1.3 kPa NH_3. Blue circles: experimental data of Helminen et al. [218]. Red line: NH_3 desorbed after plasma illumination. Data normalized for the zeolite loading in this work (600 mg).

7.5.2.5 Energy cost of zeolite regeneration

The energy cost for zeolite regeneration is assessed hereafter, determining whether it has a significant effect on the energy yield for plasma-chemical ammonia synthesis with *in situ* adsorption.

The heat requirement for desorbing ammonia from the zeolite is given by the sum of the heat required for increasing the temperature of the zeolite and the heat requirement for desorbing ammonia. It is assumed that the temperature is increased from 25°C to 500°C (ΔT=475°C), in accordance with **Figure 60**.

The heat capacity of zeolite 4A at room temperature is about C_p=935 J kg^{-1} K^{-1} [372]. The heat of desorption for ammonia on zeolite 4A is 52.5 kJ mol^{-1} [218]. The ammonia adsorption capacity is p_A=2.4 mmol-NH_3 g^{-1} zeolite, based on the plateau value of the plasma-chemical ammonia synthesis experiments in **Figure 61**.

The contribution of heating the zeolite is then given by $C_P*\Delta T/p_A$=(935/1000)*475/2.4=185 kJ mol^{-1} NH_3 or 10.9 MJ kg^{-1} NH_3. The contribution of the heat of the heat of desorption is 52.5 kJ mol^{-1} NH_3 or 3.1 MJ kg^{-1} NH_3. The sum of the two contributions is about 238 kJ mol^{-1} NH_3 or 13.9 MJ kg^{-1} NH_3.

The highest energy yield obtained for plasma-chemical ammonia synthesis with in situ adsorption is 2.3 g-NH_3 kWh^{-1} or 1565 MJ kg^{-1} NH_3. Concluding, the contribution of the zeolite regeneration is negligible as compared to the energy input of the plasma.

7.5.2.6 Comparison steady-state and *in situ* removal

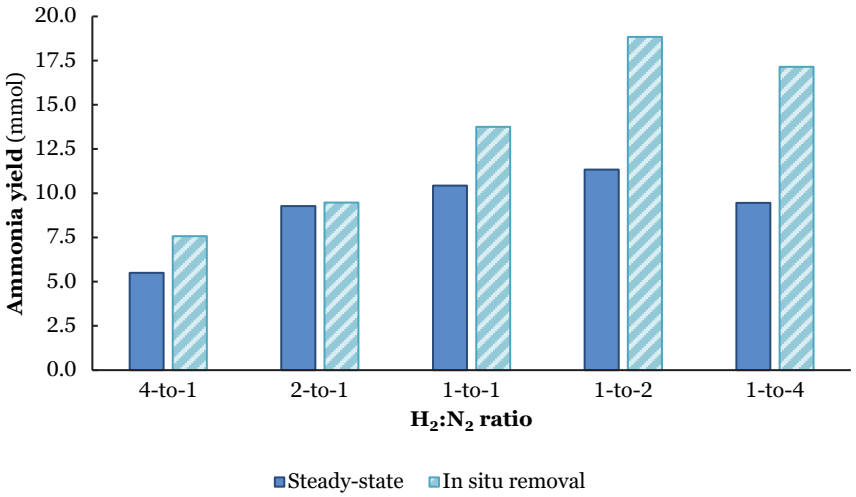

Figure 70: Comparison of cumulative ammonia yield after 75 min plasma for steady-state operation (dark blue) and *in situ* ammonia removal (blue - striped), varying H_2:N_2 ratios. Oven temperature setpoint 25°C, total flow rate 10 mL min^{-1}, plasma power 6.4 W (SEI=38.4 kJ L^{-1}), zeolite loading 600 mg (250-300 µm). Ammonia desorption in absence of plasma in pure N_2 at 10 mL min^{-1}, heating rate of 25°C min^{-1}.

Chapter 8

Feasibility study of plasma-catalytic ammonia synthesis

Summary

Plasma catalysis has recently gained traction as an alternative to ammonia synthesis. Current research is mostly fundamental and little attention has been given to the technical and economic feasibility of a plasma-catalytic ammonia synthesis process. In this Chapter, the feasibility of plasma-catalytic ammonia is assessed for small-scale ammonia synthesis. A brief summary of the state of the art of plasma catalysis is provided as well as a targets and potential avenues for improvement in the conversion to ammonia, ammonia separation and a higher energy efficiency. A best-case scenario is provided for plasma-catalytic ammonia synthesis and this is compared to an electrolysis-based Haber-Bosch process. An ammonia outlet concentration of at least 1.0 mol.% is required after the plasma reactor to limit the recycle size and to allow for efficient product separation. From the analysis, it follows that plasma-catalytic ammonia synthesis cannot compete with the conventional process even in the best-case scenario. Plasma catalysis potentially has a fast response to intermittent renewable electricity. However, low pressure absorbent-enhanced Haber-Bosch processes are also expected to have fast responses to load variations. Low-temperature thermochemical ammonia synthesis is expected to be a more feasible alternative to intermittent decentralized ammonia synthesis than plasma-catalytic ammonia synthesis due to its superior energy efficiency.

This chapter has been partially adapted from:

Rouwenhorst, K. H. R., & Lefferts, L. (2020). Feasibility study of plasma-catalytic ammonia synthesis for energy storage applications. Catalysts, 10(9). doi: 10.3390/catal10090999

8.1 Introduction

Renewable wind energy and solar power increasingly penetrate the electrical power grid, spurring the electrification of the energy landscape [50]. However, as these energy sources are fluctuating, energy storage is required. A wide range of technologies is available for short-term energy storage, including batteries and thermo-mechanical storage, typically up to a few days [51]. Chemical energy storage and pumped hydropower are the main alternatives for seasonal energy storage [51–53]. Even though pumped hydropower is a potential solution for low-cost energy storage in naturally suited areas [53], the energy density of such systems is low, and pumped hydropower heavily depends on the availability of large natural water formations.

Chemical energy storage in the form of hydrogen or hydrogen carriers has been proposed to solve the intermittency challenge. Renewable hydrogen is produced from water via electrolysis using renewable electricity, producing oxygen as a by-product. Hydrogen can be combusted to water in a fuel cell or in a gas turbine, producing electricity again. However, hydrogen is not easily stored on the long-term. Therefore, hydrogen carriers are required and ammonia (NH_3) is one of the options [52,54]. Ammonia is currently mainly produced for fertilizer applications [281,373,374]. However, ammonia may be a hydrogen carrier and zero carbon fuel in the circular economy [27,32,54]. In this case, fluctuating renewables such as solar, tidal and wind power are coupled with chemical plants to produce ammonia.

Currently, ammonia is mainly produced with the Haber-Bosch process, continuously operated at high temperature and pressure, i.e. 350-550°C and 100-450 bar [281,373–375]. The high temperature is required to activate the stable N≡N triple bond on the industrial catalyst, and a high pressure is required to shift the equilibrium to ammonia. Typically, Haber-Bosch plants have high production capacities of up to 3300 t-NH_3 d^{-1}, with a potential increase to 5000-6000 t-NH_3 d^{-1} in the near future [278,376]. This corresponds to a few gigawatt (GW) in the case of an electricity-driven Haber-Bosch plant. Such electrolysis-based Haber-Bosch plants operate at an energy cost of about 26-40 GJ t-NH_3^{-1}, depending on the electrolysis technology used [25]. About 95% of this energy is required for the hydrogen production and the remaining part is required for nitrogen purification and ammonia synthesis. The theoretical minimum energy input for ammonia synthesis from air and water is 21.3 GJ t-NH_3^{-1} [281].

Upon scaling down the Haber-Bosch process, the energy losses increase and the energy consumption for ammonia synthesis increases (see **Figure 71**). Down to the 1-10 megawatt (MW) scale (equivalent to 3-30 t-NH_3 d^{-1}), energy losses are limited and the energy consumption for ammonia synthesis is about 36-40 GJ t-NH_3^{-1} [377]. However, upon further scaling down, energy losses become increasingly severe, and using alternative technologies becomes attractive. Non-conventional technologies typically cannot compete with Haber-Bosch at large-scale, due to the high energy efficiency of Haber-Bosch.

However, alternative technologies operating under milder conditions can be beneficial for small-scale production. This is important for fluctuating operation required in the case of rapid variation in the availability of solar and wind power. Small-scale ammonia synthesis may be relevant for energy storage, specifically for isolated communities.

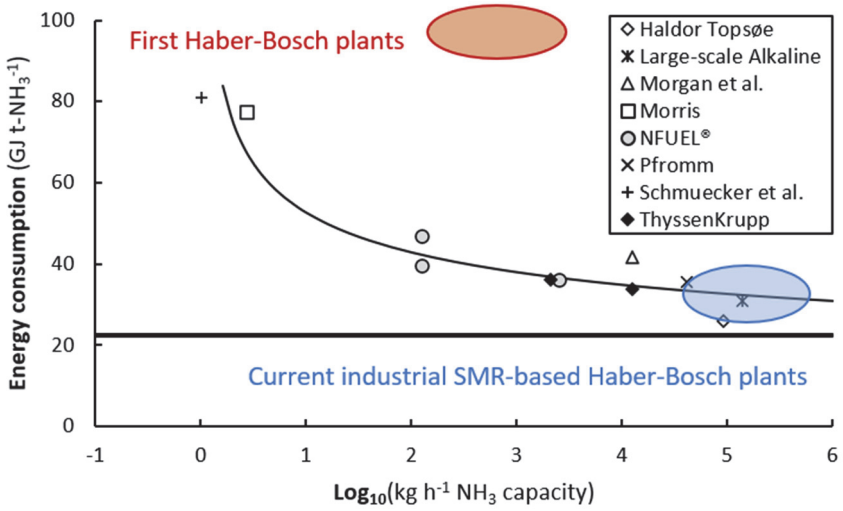

Figure 71: Energy consumption of electrolysis-based Haber-Bosch processes as function of ammonia production capacity. Adapted and modified from Ref. [33]. Original Refs. [378–387]. One megawatt (MW) corresponds to approximately 100 kg-NH_3 h^{-1}.

8.1.1 State of the art of plasma-catalytic ammonia synthesis

Plasma catalysis has recently gained attention for electrification of chemical processes and for energy storage applications [40,41,43,44,310], and for ammonia synthesis in specific [42,58,199]. Plasma is the fourth state of matter, in which electrons, ions, molecules, radicals, and excited species exist in a quasi-neutral state. In case of thermal plasmas, electrons and heavier species have the same temperature. On the other hand, non-thermal plasmas, the electron temperature is significantly higher than that of heavier ions and neutral species. Non-thermal plasmas can be coupled with a catalyst. Excited species generated in the plasma (for instance, vibrationally activated nitrogen, $N_2(v)$) can have an enhanced adsorption rate as compared to ground state molecules. As N_2 dissociation is usually the bottleneck for ammonia synthesis, plasma activation of N_2 may generate a synergistic effect with the catalyst.

Plasma catalysis potentially has a fast response to fluctuating renewable electricity. In the upcoming section, the state of the art of the electrolysis-based Haber-Bosch process and an alternative plasma-catalytic process are discussed. This serves as a starting point for process evaluation of plasma-catalytic ammonia synthesis.

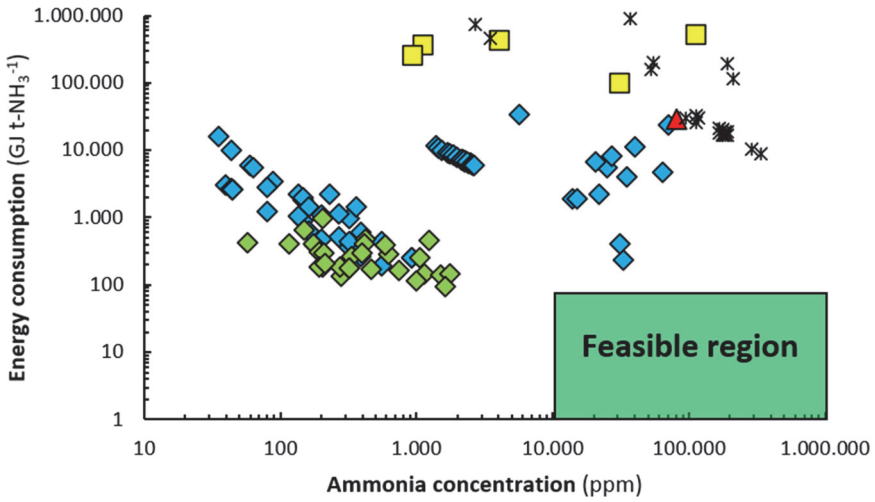

Figure 72: Reported energy yield vs. ammonia concentration at various process conditions. Constructed and extended from [38]. Original references: dielectric barrier discharge (DBD) (alternating current, AC, blue diamonds) [74–76,82,88–90,93,97–99,213,336,388]**, DBD (pulse, green diamonds)** [81,89]**, glow discharge (GD, red triangle)** [107]**, microwave (MW, yellow squares)** [118,123,214,215,389] **and radiofrequency (RF, black stars)** [114,119,122,125–127]**. Note that the feed composition varies among the references, and therefore the ammonia yield. In case of a stoichiometric feed ratio, the ammonia outlet concentration is equal to the yield (at 0.0 mol. % NH_3 inlet). The feasible region is discussed in section 8.1.2.1.**

An overview of reported energy consumptions for ammonia synthesis in various types of plasma reactors is shown in **Figure 72**. Among the plasma reactors, dielectric barrier discharge (DBD) reactors have been studied most extensively since the 2000s [58,199,200], as discussed in **Chapter 2**. Microwave (MW) and radiofrequency (RF) plasmas have been studied in the 1980s-1990s, although recently a few articles have been published on this subject as well [199]. Glow discharges, inspired by the commercial Birkeland-Eyde process for NO_X production in the early 20th century, have been studied in the 1920s-1990s [58,199]. Other technologies, such as arc discharges and plasma jets have only been reported in a few studies, mostly with an exploratory character [71,199]. Various authors have discussed plasma reactors extensively [40,58,162].

8.1.2 Comparison of small-scale Haber-Bosch processes and state of the art plasma catalysis

Figure 73 shows a comparison of reported state-of-the-art data on energy consumption of the electrolysis-based Haber-Bosch process, both at the 10 kW and 10 MW scale, and of plasma-catalytic ammonia synthesis. Electrolysis-based hydrogen production is required for both the Haber-Bosch process and plasma catalysis at an energy consumption of about 31.4 GJ t-NH_3^{-1} [25,309]. Nitrogen is purified via pressure swing adsorption at an energy consumption of about 1.0 GJ t-NH_3 [25]. At the 10 MW scale, the high pressure ammonia

synthesis loop of the Haber-Bosch process has a limited energy loss and consumes about 3.6 GJ t-NH^{-1} [21]. However, at 10 kW, the energy consumption of the high pressure ammonia synthesis loop is as high as 45-50 GJ t-NH_3^{-1} (see **Figure 71** and **Figure 73**). This is mainly due to large heat losses from the synthesis reactor operating at high temperatures.

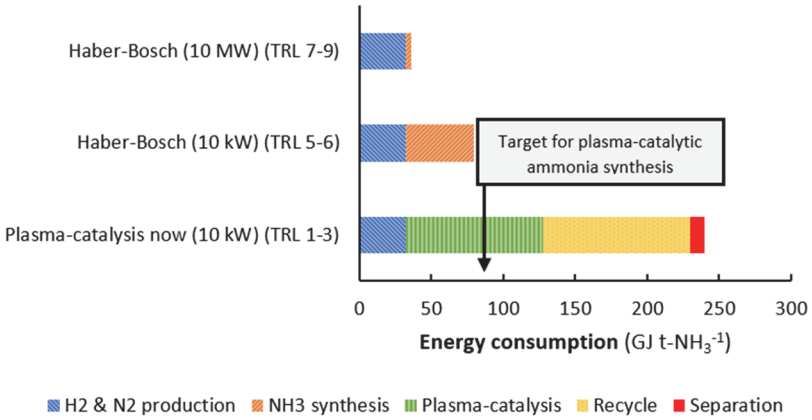

Figure 73: Estimated energy consumption of state-of-the-art, small-scale, electrolysis-based Haber-Bosch, and plasma catalysis. For the Haber-Bosch process, estimates are based on reported energy consumption in Figure 71. For plasma catalysis, the energy consumption for gas recycling and ammonia separation is based on estimates in for low pressure, low conversion systems with solid sorbents as reported in Refs. [21,25]**. The energy consumption for plasma catalysis is based on data from Kim et al.** [89] **for a Ru-MgO/γ-Al_2O_3 catalyst at 0.2% conversion. The energy cost for recycling and separation with solid sorbents is discussed in section 8.3.1. The TRLs (Technology Readiness Levels) apply for the complete system, ranging from TRL=1 to TRL=9, see Ref.** [390]**.**

As shown in **Figure 73**, the state-of-the-art system for a plasma-catalytic ammonia synthesis process has a considerably higher energy consumption than the electrolysis-based Haber-Bosch process, both at the 10 kW scale and at the 10 MW scale. Plasma catalysis allows for operation at milder conditions than conventional catalysis on the industrial iron catalyst. However, plasma catalysis is only beneficial when the energy consumption of a plasma-catalytic ammonia synthesis process is at least equal to the energy consumption of the electrolysis-based Haber-Bosch process at 10 kW (about 80 GJ t-NH_3^{-1}). The best reported value for plasma catalysis is 95 GJ t-NH_3^{-1} at 0.2 mol. % NH_3 [89], while most reported values vary in the range between 10^3 and 10^6 GJ t-NH_3^{-1} at various conversion levels (see **Figure 72**) [199]. Furthermore, the energy consumption of recycling of unconverted N_2 and H_2 for the best reported plasma-catalytic systems is high, due to the low conversion levels (see **Figure 72**). The recycling cost is usually not reported for plasma catalysis (like in **Figure 72**), but is significant in case of low conversions to ammonia, i.e. below 1.0 mol.% NH_3 [21].

8.1.2.1 Targets and strategies for more energy-efficient plasma-catalytic ammonia synthesis

It is estimated that plasma catalysis may be competitive with the Haber-Bosch at a target total energy consumption of 80 GJ t-NH_3^{-1}, based on the comparison with electrolysis-based Haber-Bosch process at 10 kW, equivalent to about 10 kg d-NH_3^{-1} production.

The energy costs of hydrogen production and nitrogen purification is the same for both processes and amount to about 32 GJ t-NH_3^{-1}. Ammonia separation in the Haber-Bosch process is achieved by condensation. However, under mild pressure (<70 bar), condensation is not feasible due to the high vapor pressure of ammonia under ambient conditions (about 7 bar, see **Figure 74**) [21,33]. Therefore, sorbents are currently being developed for ammonia separation and storage, as discussed in **section 8.3.1**. Typically, the energy consumption for ammonia separation with sorbents is about 10 GJ t-NH_3^{-1}, which changes little with ammonia concentration.

This implies that two functionalities primarily determine the feasibility of plasma-catalytic ammonia synthesis, namely (1) plasma catalysis, and (2) separation of NH_3 and recycling of unconverted N_2 and H_2. In principle, the recycle cost is usually not an issue for industrial ammonia synthesis, as the energy cost of recycling is below 1 GJ t-NH_3^{-1} at NH_3 concentrations above 1.0 mol. % in the reactor outlet [21]. However, for the current best-reported data for plasma catalysis, the ammonia concentration is 0.2% (see **Figure 73**), implying recycling costs as high as 100 GJ t-NH_3^{-1}. Clearly, increasing the NH_3 concentration in the outlet of the plasma reactor to above 1.0%, at a reasonable energy cost, is desirable. Another benefit of increasing the conversion level and consequently the ammonia concentration is the reduction in capital investment for recycling, due to the smaller compressor. In the upcoming section, potential improvements for plasma catalysis are discussed. It should be noted, however, that the ammonia decomposition rate increases with increasing ammonia concentration, as discussed in **Chapter 6**.

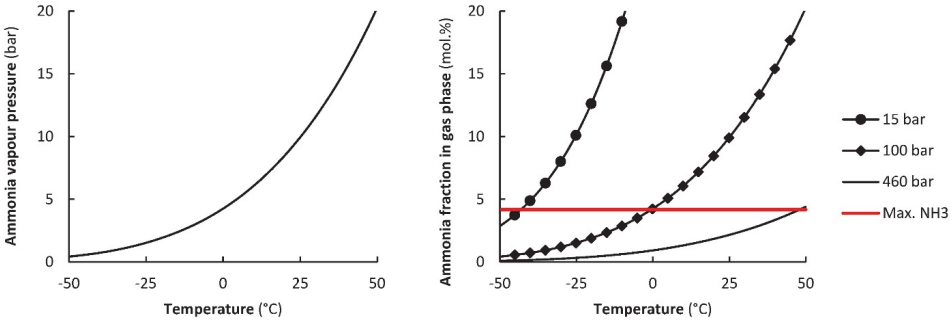

Figure 74: Left: Ammonia vapor pressure as function of temperature. Antoine equation parameters reproduced from Ref. [391]. Right: Ammonia fraction in gas phase as function of the condensation temperature, for various synthesis pressures. The 4.18 mol.% ammonia indication limit is based on the Krupp-Uhde process [375].

8.2 Plasma reactor and catalyst improvements for plasma-catalytic ammonia synthesis

The plasma reactor forms the core of the plasma-catalytic ammonia synthesis process. In this section, the plasma reactor types are evaluated, as well as the necessary coupling with a catalyst.

8.2.1 Plasma reactor type

The first choice to make is the plasma reactor type. While dielectric barrier discharge (DBD) reactors and glow discharge reactors operate at atmospheric pressure (or at elevated pressures [392]), microwave (MW) reactors and radiofrequency (RF) reactors operate at sub-atmospheric pressures. In principle, operating at atmospheric pressure or above is beneficial, as vacuum conditions require expensive equipment and large volumes. Furthermore, separation of ammonia is difficult at low partial pressures.

Metrics to evaluate the plasma reactor type include the energy consumption for ammonia formation (requirement: about 40 GJ t-NH_3^{-1}, see **Figure 73**), as well as the conversion (requirement: ≥ 1.0 mol % NH_3). As shown in **Figure 72**, no data in the literature have attained this so far. It should be noted that the data shown in **Figure 72** vary widely in temperature, pressure, H_2:N_2 ratio, and catalyst choice. However, the apparent general trend is that the energy consumption for ammonia formation is lowest in dielectric barrier discharge reactors. Other reactor types (glow discharges, microwave reactors, and radiofrequency reactors) have an energy consumption of one to four orders of magnitude higher. This may be attributed to the more effective plasma-catalyst coupling for a DBD reactor. Therefore, a dielectric barrier discharge reactor is the preferred plasma reactor type, with the current knowledge.

8.2.1.1 Plasma optimization

Plasma optimization should be focused on maximizing the density of mildly activated molecular nitrogen species (N_2(v) or N_2(e)), rather than radical species, as the mildly activated molecular nitrogen species require less energy input than full dissociation to nitrogen radicals. Mild activation of N_2 to N_2(v) or N_2(e) can primarily be achieved by a relatively low specific energy input (SEI). Upon increasing the SEI, the reduced electric field increases, thereby increasing the fraction of N_2 dissociated in the plasma [40]. Furthermore, N_2-rich feeds are beneficial for activating N_2 rather than H_2 [89].

Various authors have reported an improved energy efficiency upon using pulsed plasmas in a dielectric barrier discharge reactor, rather than a continuous AC plasma [81,89]. For AC plasmas, excited N_2 molecules are readily dissociated due to the continuous presence of activated species. This leads to dissociation and the formation of N radicals, which recombine with other species and form heat. For pulsed plasmas, less of the activated N_2

is dissociated in the plasma due to climbing along the vibrational ladder [267]. Thus, a pulsed plasma dielectric barrier discharge reactor is preferred as the plasma reactor.

Further modifications can be made to the plasma properties, by changing the discharge frequency and the capacitive and discharge regimes. Plasma properties can be modified by the electrode material [76,107], as well as the dielectric constant in the reactor. Performance enhancement may be attained upon the physical mixture of the active catalyst with a dielectric material [75], which can be attributed to a change in electron number density and average energy distribution.

8.2.2 Reaction mechanisms and catalyst optimization

Several mechanisms towards ammonia synthesis in the presence of a plasma are being discussed, as previously discussed in **Chapter 2** and **Chapter 3**. The bond-dissociation energies of N_2 and H_2 are 945 kJ mol^{-1} and 436 kJ mol^{-1} respectively, which translates to 66.1 GJ t-NH_3^{-1} at 100% efficient conversion to ammonia via complete dissociation. This implies that plasma-induced dissociation and subsequent radical reactions can never be sufficiently energy efficient to attain the required 40 GJ t-NH_3^{-1}, as discussed in **section 8.1.2.1**. Thus, a catalyst is required to aid in the dissociation of the molecules. The plasma can activate molecular N_2 via vibrational or electronic excitation, which decreases the barrier for N_2 dissociation on the catalyst, as discussed in **Chapter 3**. Typically, catalysts which are able to dissociate N_2 are also able to dissociate H_2, while some mid-late transition metal catalysts such as Pd and Pt can dissociate H_2, but not N_2.

8.2.2.1 Plasma-catalytic ammonia synthesis with molecular species

Thus, plasma activation of N_2 without complete dissociation is the required pathway for plasma-catalytic ammonia synthesis with a low energy consumption. Mehta et al. [49] proposed that plasma-activated molecular N_2 can enhance the rate of ammonia formation, which was substantiated in **Chapter 3** for Ru-based catalysts at a low plasma power input of 83-367 J L^{-1}. Mehta et al. [49] postulated that the plasma activates the N_2, thereby decreasing the barrier for N_2 dissociation, while subsequent hydrogenation steps are not influenced by the plasma.

Furthermore, Mehta et al. [49] postulated that thermally less active metals can become good catalysts for converting plasma-activated N_2 to ammonia. However, the importance of plasma-activated molecular N_2 (either vibrational or electronic) has been experimentally substantiated exclusively for Ru-based catalysts [94,223]. It remains an open question whether noble metals can become active for N_2 dissociation after vibrational or electronic excitation. On Ru-based catalysts, the apparent barrier for N_2 dissociation over the catalyst decreases by about 40-70 kJ mol^{-1} upon plasma activation [94]. The discussion hereafter focuses on Ru-based catalysts, as a mechanism with excited N_2 has only been proven to be possible for this metal.

The support has a profound effect on the ammonia synthesis activity on Ru-based catalysts [225]. The ammonia synthesis rate can vary by multiple orders of magnitude, depending on the catalyst formulation. For Ru-based catalysts it was found that oxide supports with a low electronegativity show a high ammonia synthesis activity for thermal catalysis [290]. A similar trend was confirmed for plasma-enhanced catalysis (see **Chapter 3**), suggesting that a pathway via excited molecular N_2 is indeed dominant. The introduction of promoters (alkali metals and alkaline earth metals) can further increase the activity [225,229]. The nitrogen dissociation barrier decreases upon the introduction of an alkali metal due to electrostatic interactions [229]. A similar activity improvement upon the introduction of an alkali metal was also reported for Co catalysts [393]. For this mechanism, the temperature should be such that thermal N_2 dissociation on the catalyst and NH_3 desorption from the catalyst are possible. Thus, the temperature for plasma catalysis cannot be much lower than for thermal catalysis.

The lowest reported energy requirement for plasma catalysis so far is for a promoted Ru/Al_2O_3 catalyst [89]. As listed in **Table 9**, trends in thermal catalysis indicate that changes in the catalyst may facilitate a lower energy cost for NH_3 synthesis, given that the right plasma reactor is used. Promoted Ru/MgO catalysts are about 25 times more active than promoted Ru/Al_2O_3 catalysts for thermal catalysis [224]. As similar trends are valid for plasma catalysis at low conversions (see **Chapter 3**), an increased productivity and a lower energy cost may be attained upon using promoted Ru/MgO catalysts. Thus, the energy requirement of 40 GJ t-NH_3^{-1} may be attained using pulsed plasmas combined with a promoted Ru/MgO.

Table 9: Comparison of activity trends over Ru catalysts for thermal catalysis and for plasma catalysis. Thermal catalysis: data of Muhler et al. [224], 385 °C, 1 atm, 40 mL min^{-1}, H_2:N_2 = 3:1, 138 mg catalyst. Plasma catalysis: data of Ruan et al. [291], 180 °C, 60 mL min^{-1}, H_2:N_2 = 3:1, 1.1-3.7 mol % NH_3. Kim et al. [89], 250-300 °C, 1 atm, 1-4 L min^{-1}, H_2:N_2 = 1:4, 17.1 g catalyst, 0.01-0.16 mol % NH_3. Target value for plasma catalysis: 40 GJ t-NH_3^{-1} at 1.0% NH_3 at outlet. "Relative act." refers to the relative ammonia synthesis rate on various catalysts, with Ru/Al_2O_3 as the base-case (1.0).

Catalyst	Thermal Catalysis	Plasma Catalysis			
	Ref. [224] Relative act.	Ref. [291] Relative act.	Ref. [89] Relative act.	Energy Cost (GJ t-$NH_3$$^{-1}$)	
				AC Plasma	Pulsed Plasma
Ru/Al_2O_3	1.0	1.0	1.0	1029-1800	-
Promoted Ru/Al_2O_3	2.5	-	2.8-3.3	313-563	101-141
Ru/MgO	9.2	1.5	-	-	-
Promoted Ru/MgO	62	3.3	-	-	-

8.2.2.2 Best-case scenario for plasma catalysis

As shown in **Figure 73**, the energy costs of the state-of-the-art system for plasma catalysis and recycling are high (about 197 GJ t-NH_3^{-1}). Furthermore, the energy cost for recycling scales with the reciprocal of the single pass conversion. This implies that increasing the conversion by catalyst optimization and plasma optimization inherently decreases the energy cost of the recycle. An ammonia concentration of about 1.0 mol % is required to effectively use the reactor volume for separation, as will be discussed in **section 8.3.1**.

A target of 40 GJ t-NH_3^{-1} at 1.0 mol % ammonia outlet concentration was set for the plasma reactor (see **section 8.1.2.1**). The lowest energy consumption reported so far is for a pulsed plasma DBD reactors with an energy consumption of 95 GJ t-NH_3^{-1} at 0.16 mol % over a Mg-Ru/Al_2O_3 catalyst [89]. Thus, an energy consumption enhancement by a factor 2.4 is required, whereas the conversion should increase by a factor 6.3 to attain feasible operation. Based on trends in thermal catalysis, a rate enhancement is expected by changing the catalyst from promoted Ru/Al_2O_3 to promoted Ru/MgO (see **Table 9**). It should be noted that the plasma activation of NH_3 is an inherent limitation to the energy efficiency at high conversions, as NH_3 is increasingly activated by the plasma with increasing NH_3 concentration.

In order to get an estimate of the best-case scenario (BCS) for plasma-catalytic ammonia synthesis, it is assumed that the barrier decrease for N_2 dissociation equals the energy input for plasma-catalytic NH_3 synthesis. The decrease in the N_2 dissociation barrier on Ru-based catalysts is about 0.7 eV or 70 kJ mol^{-1} [94], which translates to about 4.0 GJ t-NH_3^{-1} or 1.1 kWh kg^{-1}. From **Figure 75**, it follows that an ammonia outlet concentration of 0.35 mol % is required to attain an energy cost of 40 GJ t-NH_3^{-1}. For 1.0 mol % NH_3 concentration at the reactor outlet, the total energy consumption for the plasma reactor (BCS) and the recycling is about 5.0 GJ t-NH_3^{-1} (see **Figure 75**).

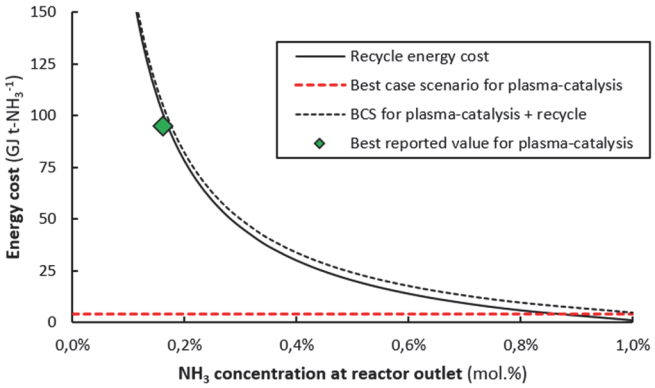

Figure 75: Energy cost of the recycle as a function of the ammonia concentration at the reactor outlet, as well as the best reported value for plasma catalysis, and a best-case scenario for plasma catalysis. The energy cost of recycling is estimated based on values reported by Smith et al. [21]. The best reported value for plasma catalysis is based on data of Kim et al. [89] for pulsed plasmas.

8.3 Ammonia separation and conceptual process design

An evaluation of various process alternatives for ammonia separation in a plasma-catalytic ammonia synthesis process is presented. The cost of such a small-scale process is compared to a small-scale Haber-Bosch synthesis loop. As hydrogen and nitrogen production occur in a similar manner for Haber-Bosch and plasma-catalytic ammonia synthesis, these are not discussed hereafter.

8.3.1 Separation and storage

Ammonia is conventionally separated by condensation. However, this does not allow for efficient and complete separation at low operating pressures, as ammonia has a significant vapor pressure under ambient conditions (7 bar, see **Figure 74**). Therefore, an alternative method for ammonia separation is required for ammonia synthesis under mild pressures [21]. Solid sorbents can be used for this purpose and a wide range of materials has been tested [309].

Among these sorbents, metal halides (e.g., metal chlorides and metal bromides) and zeolites are most promising (see **Table 10**). A benefit of metal halides over zeolites is the higher ammonia density of the storage material. Furthermore, ammonia can be separated at elevated temperatures using metal halides, minimizing the temperature difference between the plasma reactor and the separation step. This saves on the cost of heat integration between the plasma reactor (probably 200-300°C) and the separation step, i.e. 150-250°C for metal halides, as compared to 20-100°C for zeolites. For low conversion systems such as plasma-catalytic ammonia synthesis, the investment cost of the recycle

compressor and heat exchanger generally dominate the investment cost for the synthesis loop [21]. Therefore, metal halides are the preferred option in this case. However, it should be noted that zeolites are of interest if plasma-catalytic ammonia synthesis at room temperature is developed with plasma-activated N_2 as the relevant species. Furthermore, plasma-chemical ammonia synthesis may be combined with *in situ* adsorption on a zeolite to improve the energy yield, as was discussed in **Chapter 7**.

Table 10: Comparison of ammonia separation technologies. Based on Refs. [33,220,239,394,395]. * The energy consumption increases to 20-25 GJ t-NH_3^{-1} at 20 bar [21].

	Condensation	Metal Halides	Zeolites
Separation temperature (°C)	-20 to 30	150-250	20-100
Desorption temperature (°C)	N/A	350-400	200-250
Pressure (bar)	100-450	10-30	10-30
Energy consumption (GJ t-NH_3^{-1})	3-5*	6-11	8
Ammonia at outlet (mol.%)	2-5	0.1-0.3	0.1-0.3
Ammonia capacity (wt.%)	100	5-30	5-15
Ammonia density (kg m^{-3})	680	100-600	30-90
Chemical stability	N/A	Low/Medium	High
Technology readiness level (TRL)	9	4-5	4-5

Ammonia can be stored inside the metal halides. Metal halides absorb ammonia via diffusion of ammonia into the lattice, forming an ammine complex. For instance, ammonia can be absorbed into $CaCl_2$ and $MgCl_2$, forming $Ca(NH_3)_xCl_2$ and $Mg(NH_3)_xCl_2$. Ammonia leakage risks are reduced as compared to liquefied ammonia, as the ammonia vapor pressure in equilibrium with the ammonia loaded metal halides is significantly lower as compared to the vapor pressure of pure ammonia [396]. This decreases safety risks substantially. Thus, ammonia is stored inside metal halides, until ammonia is required for combustion in for instance a fuel cell or engine [33]. A simplified process scheme of a plasma-catalytic ammonia synthesis loop is shown in **Figure 76**. The adsorption-desorption cycle can be achieved by switching between multiple beds or by using moving bed reactors.

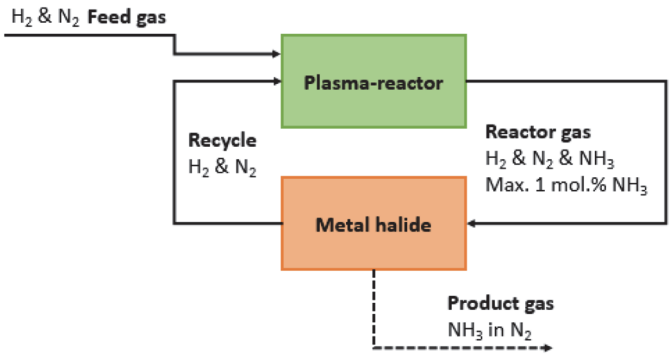

Figure 76: Process scheme of a plasma-catalytic ammonia synthesis loop.

8.3.2 Synergy between the plasma reactor and ammonia storage & storage

As discussed above, synergy may be attained upon matching the operating temperature of the plasma reactor and the ammonia separator. The plasma reactor can operate at temperatures above the onset temperature for plasma-catalysis (typically >150-200°C), where a higher temperature implies a higher ammonia synthesis rate. On the other hand, upon increasing the temperature too much (i.e., above 300°C), the benefits of plasma catalysis over heterogeneous catalysis without a plasma are negligible. Some catalysts show substantial thermal-catalytic activity around 300°C [286,288,397,398], which implies that the use of plasma is not necessary.

Among metal halides, $MgCl_2$ shows suitable absorption-desorption cycles. At an ammonia partial pressure of 10 kPa and at 200°C, two moles of ammonia can be absorbed in $MgCl_2$, forming $Mg(NH_3)_2Cl_2$. Upon increasing the temperature to 300°C, all ammonia can be released again. As ammonia absorption is determined by the kinetic rate of the surface reaction [399], maximizing the available $MgCl_2$ surface area is beneficial. Supporting $MgCl_2$ on an inert oxide can increase the available surface area of $MgCl_2$. Furthermore, nano-pores are formed in the metal halide structure upon ammonia desorption. Possibly, the mechanical stability can be better maintained upon supporting $MgCl_2$ on an inert oxide. Higher ammonia absorption capacities are obtained when loading metal halides on oxide supports [220]. $MgCl_2/SiO_2$ (40 wt.% $MgCl_2$) is the best among the tested materials with an experimental sorbent capacity of about 5 wt.% ammonia at 200°C, whereas the theoretical maximum is 11 wt.% ammonia.

Table 11: Synergy between plasma and ammonia separation and storage. * This includes the energy consumption for plasma-catalytic ammonia synthesis (PC) and the energy consumption for recycling (Rec). The energy consumption for recycling is based on the outlet NH_3 concentration, based on interpolation of estimates in Refs. [21,33]. The state-of-the-art value for plasma catalysis is based on the data of Kim et al. [89], while the best-case scenario is based on an energy input of 0.7 eV due to a decrease in the N_2 dissociation barrier over Ru catalysts (see section 8.2) [94]. The difference between the operating pressure of the plasma reactor and the separation step is to account for the pressure drop over the system.

	State-of-the-Art Plasma Reactor	**BCS Plasma Reactor**	**Separation**
Type	DBD reactor (pulse)	DBD reactor (pulse)	Solid absorbent
Material	Promoted Ru/Al_2O_3 catalyst	More active catalyst	$MgCl_2/SiO_2$
Reaction temperature (°C)	300	200	200
Desorption temperature (°C)	-	-	300
Operating pressure (bar)	1.5	1.5	1.0
Outlet NH_3 concentration (mol. %)	0.16	1.0	0.1
Outlet ammonia pressure (kPa)	1.6	10	0.3
Energy consumption (GJ $t\text{-}NH_3^{-1}$)*	197 (PC:95, Rec:102)	5 (PC:4, Rec:1)	10
Syngas ratio (H_2:N_2)	1:4	1:4	1:4

The operating conditions and the energy consumption for the state-of-the-art plasma reactor and a best-case scenario (BCS) plasma reactor are listed in **Table 11**, as well as the operating conditions for ammonia separation with a $MgCl_2/SiO_2$ sorbent. Due to the similar reaction conditions in the plasma reactor and in the absorption step, heat integration can indeed be minimized. This simplifies the synthesis loop substantially in case of intermittent operation. From **Table 11** it follows that the main improvement required is the energy consumption in the plasma reactor, as was also discussed in **section 8.2.2.2**.

8.3.3 Investment cost comparison

Most of the discussion so far has focused on the energy consumption in the ammonia synthesis loop, as the energy cost is usually the major cost contributor for electricity-driven ammonia synthesis [400]. Given that the energy consumption of small-scale systems is larger, the electricity cost is expected to be a major cost contributor in small-scale systems as well. However, investment costs can become substantial cost factors as well. In this section, an estimate is provided on the capital investment for plasma-catalytic ammonia synthesis as compared to a decentralized Haber-Bosch ammonia synthesis loop. As hydrogen and nitrogen are required for both a small-scale Haber-Bosch process and a plasma-catalytic ammonia synthesis process, the costs for hydrogen production and nitrogen purification are excluded in the analysis.

The capital investment for the ammonia synthesis loop scales with a cost-scaling factor of 0.6 [25], while electrolyzers for hydrogen production scale modularly. Thus, the contribution of the ammonia synthesis loop to the total cost increases upon scale-down. **Figure 77** shows a comparison between the capital investment for the Haber-Bosch ammonia synthesis loop, the state-of-the-art plasma-catalytic ammonia synthesis loop, and a best-case scenario for the plasma-catalytic ammonia synthesis loop. For reference, the capital investment for a low-temperature, absorbent-enhanced Haber-Bosch synthesis loop is also shown. The equipment cost for the plasma generator is estimated to be 0.9 € W^{-1}, based on estimates of van Rooij et al. [401]. The equipment cost of all other components are estimated, based on cost-scaling relations described in Ref. [21].

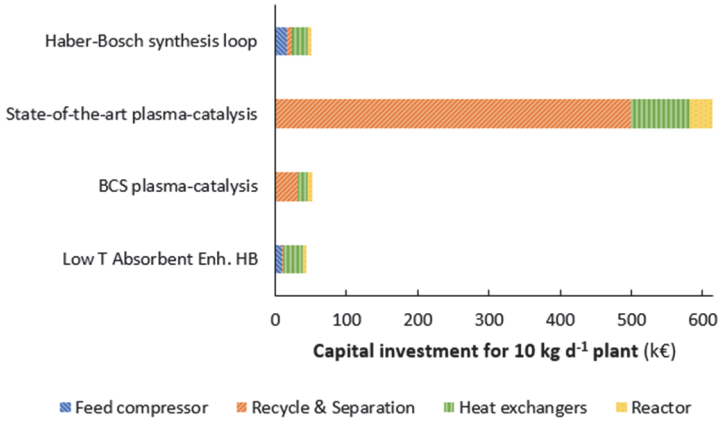

Figure 77: Capital investment for the conventional Haber-Bosch synthesis loop, state-of-the-art plasma catalysis, a best-case scenario for plasma catalysis, and an absorbent-enhanced Haber-Bosch synthesis loop at 10 kg-NH_3 d^{-1} (~10 kW). Estimates for the conventional Haber-Bosch synthesis loop and the absorbent-enhanced Haber-Bosch synthesis loop are based on Ref. [21]. The cost of the plasma reactor is assumed to be the combination of a conventional reactor and a plasma generator source. A cost-scaling factor of 0.6 is used for scale-down of equipment. See also Table 11.

The investment cost of the state-of-the-art plasma-catalytic ammonia synthesis loop is about ten times as high as that of the small-scale Haber-Bosch synthesis loop. The main reason for this is the large recycle, implying a large compressor is required. Furthermore, separation of ammonia is less efficient at low ammonia concentrations, implying large equipment for ammonia absorption. Even for the best-case scenario with minimal heat exchange between the reactor and the sorbent, plasma-catalytic ammonia synthesis is equally expensive like the Haber-Bosch synthesis loop. The high-pressure Haber-Bosch synthesis loop requires a large feed compressor, as well as substantial heat integration between ammonia synthesis at 350-550°C and ammonia separation at near-ambient temperature. On the other hand, the cost of ammonia separation and the recycle compressor are low due to high ammonia partial pressures and relatively high single pass conversions of about 15%. The best-case scenario plasma-catalytic synthesis loop operates at low pressures, thereby eliminating the requirement for a feed compressor. However, the recycle compressor is more expensive, due to low single pass conversions of about 1%. Furthermore, the low ammonia partial pressure also leads to more expensive ammonia separation equipment.

8.4 Plasma-catalytic ammonia synthesis in perspective

All in all, it can be concluded that plasma-catalytic ammonia synthesis does not provide significant investment cost advantages over the Haber-Bosch synthesis loop on a small scale (about 10 kW), even in the best base scenario (see **section 8.3.3**). On the other hand, the energy consumption of the best-case scenario for plasma-catalytic ammonia

synthesis is lower than that of the Haber-Bosch process at 10 kW (see **Figure 78**). At larger scale, the Haber-Bosch process is more energy efficient in any case (see **Figure 78**), implying plasma-catalytic ammonia synthesis is not a viable alternative.

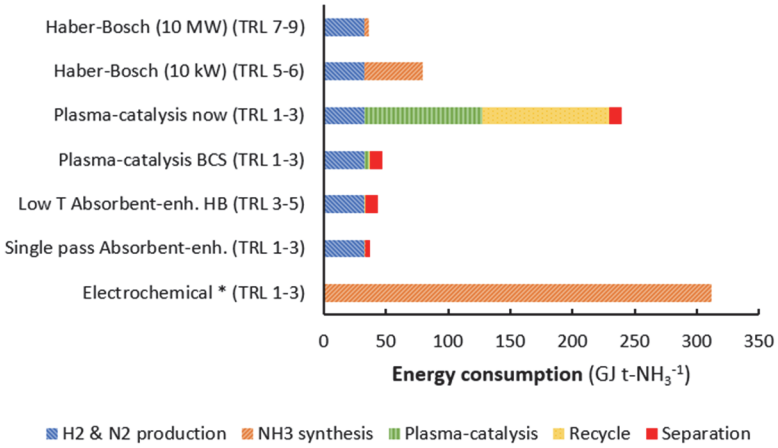

Figure 78: Estimated energy consumption of state-of-the-art small-scale, electrolysis-based Haber-Bosch, plasma catalysis (also best-case scenario), absorbent-enhanced Haber-Bosch, single pass process absorbent-enhanced process, and electrochemical ammonia synthesis. Estimates based on Refs. [21,33,405,406]**. For plasma catalysis, the energy consumption for gas recycling and ammonia separation is based on estimates in for low pressure (1.5 bar), low conversion (0.4 mol.% NH_3) systems with solid sorbents (see also section 8.3.1)** [21,33]**. * For electrochemical ammonia synthesis, only the energy consumption of ammonia production is included and the energy cost of ammonia separation and recycling is not included. TRL stands for technology readiness level. The TRL levels here apply for the complete system. TRL 1 is the basic idea, while TRL 9 is a commercial system. For more details, see Ref.** [390]**.**

In the previous sections, the focus was on improvements of plasma-catalytic ammonia synthesis. However, a wide range of technology is currently being researched as an alternative to the Haber-Bosch process on a small scale. Electrochemical synthesis, photochemical synthesis, homogeneous catalysis, and chemical looping approaches have been reported. The estimated state-of-the-art energy consumption for these technologies is shown in **Figure 78**. An extensive account on these technologies is given by Rouwenhorst et al. [309]. Electrochemical ammonia synthesis is often proposed as an alternative to ammonia synthesis under mild conditions. However, producing significant ammonia concentrations at a low energy cost has proven to be difficult and remains a scientific challenge [73,402,403]. Even if ammonia is produced at a sufficiently low energy cost, the conversion levels and separation of ammonia from the electrolyte become key issues [404]. None of the other technologies can be implemented on a near-term, due to high energy cost and low ammonia yields obtained [309].

Gradual improvements to the Haber-Bosch process have gained considerable research interest as well. The current industrial multiple promoted iron catalyst has been developed over the past century with minor changes in catalyst formulation and optimization of catalyst preparation [10,407]. On the other hand, activated carbon supported Ru catalysts (Ru/AC) have also been implemented in industry to a lesser extent [281]. The implementation of Ru/AC has been limited, due to a higher catalyst cost and a shorter catalyst lifetime than for iron-based catalysts. For the industrial iron-based catalysts and the first generation of Ru-based catalysts (Ru/AC, Ru/Oxide), N_2 dissociation is the rate limiting step, which can be enhanced by the introduction of alkali and alkaline earth promoters [225]. In various cases, ruthenium-based catalysts have been replaced by wüstite-based iron catalysts in ammonia converters, because these catalysts show similar activity [407]. A catalyst that is active at substantially lower temperatures is required to replace iron-based catalysts. Operation at lower temperatures can minimize heat loss to the surroundings during a small-scale operation and thereby decrease the required energy input.

Over the past years, Ru-based catalysts with substantially improved activity have been developed by using new support materials, such as electrides, among others [285–288,393,397,408–413]. The electride used is a $C_{12}A_7{:}e^-$ structure, stable at ambient temperature, consisting of a positively charged framework with the chemical formula $[Ca_{24}Al_{28}O_{64}]^{4+}$ and four extra-framework electrons, accommodated in the cages as counter ions [414]. It has been proposed that the N_2 dissociation rate is enhanced on electride supported Ru-based catalyst, due to a small band gap between the valence band of the electride and the conduction band of the metal [412]. Furthermore, the hydrogen poisoning effect commonly encountered for Ru-based catalysts is thought to be suppressed [411]. For these catalysts, hydrogenation over the catalyst is the rate-limiting step, rather than the N_2 dissociation step [285]. These catalysts show activity at 200-250°C, similar to that of industrial Fe-based catalysts at 350-400°C [397]. These highly active Ru-based catalysts are clearly a competitive alternative to a plasma reactor, as these catalysts are sufficiently active to decrease the reactor temperature similarly to plasma-catalytic ammonia synthesis. Furthermore, plasma catalysis can only be employed at a high energy efficiency (i.e., a low energy consumption), when ammonia conversions are low, as the plasma also activates the product and it is expected that NH_3 concentrations should be limited to about 1.0 mol.% in order to limit plasma activation of the product. This problem is not present for the new generation of Ru-based catalysts, which no longer have the N_2 dissociation as the rate-limiting step. Solid sorbents such as metal halides can also be combined with the new generation of Ru-based catalysts, thereby allowing to decrease the pressure of the ammonia synthesis loop to that of the hydrogen production and nitrogen purification pressure (about 7 bar) [33]. This is coined the absorbent-enhanced Haber-Bosch process.

Even for the best-case scenario (BCS) for plasma catalysis with a 5.8 times improvement in energy consumption for plasma catalysis (see **section 8.2.2.2**), the energy consumption for a plasma-catalytic ammonia synthesis process is higher than for a low

temperature synthesis, absorbent-enhanced Haber-Bosch process (see **Figure 78**). Furthermore, the capital investment for a plasma-catalytic process is expected to be higher than for the absorbent-enhanced Haber-Bosch process, because of the required larger heat exchanger and larger recycle compressor, due to a lower single pass conversion [21]. For reference, the electrolysis-based Haber-Bosch process at 10 MW has a power-to-ammonia efficiency of 52% (LHV), while the best-case scenario for plasma catalysis has a power-to-ammonia efficiency of 39% (LHV). The current energy consumption for plasma-catalytic ammonia synthesis is about 240 GJ t-NH_3^{-1}, leading to a power-to-ammonia efficiency as low as 8% (LHV).

8.5 Outlook

Plasma-catalytic ammonia synthesis does not appear to be a feasible alternative to long-term energy storage in NH_3. In case of N_2 activation for ammonia synthesis, alternative technologies under development for ammonia synthesis appear to be more feasible on the short term and on the long term (see **section 8.4**). Ammonia synthesis from hydrogen and nitrogen is an exothermic reaction [227], implying plasma activation is in principle not desirable.

However, plasma catalysis is an interesting alternative for electrifying in the chemical industry, due to the ability of plasma to activate strong chemical bonds such as CH_4, CO_2 and N_2 [41]. For instance, the bond dissociation energy of the N≡N is 9.79 eV or 945 kJ mol^{-1}, while electrons in DBD reactors typically have energies in the range 2-4 eV. The total barrier for CH_4 activation can be decreased upon vibrational excitation [304], thereby increasing the dissociative sticking probability [305]. Furthermore, plasma-assisted technologies have a fast response to electricity load variations. The plasma may provide very localized heating, thus limiting the heat requirement for the reactor. This can be beneficial for endothermic reactions. Lastly, plasma activation has the potential to provide process intensification. For instance, N_2 activation with a plasma can be of interest for the direct synthesis of NO_X [4,48], thereby eliminating the ammonia synthesis step altogether. As discussed in this Chapter, the product outlet concentration should typically be above 1.0 mol.%, in order to limit the recycle size and to allow for efficient product separation. Alternatively, *in situ* product removal inside the plasma zone can be utilized to enhance the performance of plasma-based chemical processes, as discussed in **Chapter 7**.

Chapter 9

Evaluation and outlook

Summary

The main conclusions from this thesis, as well as recommendations for further research are presented in this Chapter. The main research questions of this thesis are answered. Plasma types are discussed with regard to energy efficiency for ammonia synthesis, as well as other plasma-chemical and plasma-catalytic reactions. Thereafter, reaction mechanisms for plasma-catalytic ammonia synthesis are discussed. Various strategies are outlined to improve the energy yield for ammonia synthesis in plasma reactors. The industrial feasibility of plasma-catalytic ammonia synthesis is also discussed. Lastly, recommendations are been provided for further research directions.

9.1 Introduction

The research discussed in this thesis, supervised by prof. dr. ir. L. Lefferts, and the parallel work of dr. H. Patel and dr. R.K. Sharma at DIFFER, supervised by dr. M.N. Tsampas, evaluate the feasibility of plasma-based nitrogen fixation to form NH_3 and NO_X. At the University of Twente, plasma-enhanced ammonia synthesis was investigated in a dielectric barrier discharge (DBD) reactor, whereas plasma-based nitrogen fixation in a radiofrequency (RF) reactor was investigated at DIFFER. The main conclusions from this thesis, as well as recommendations for further research are presented in this Chapter. The research questions posed at the start of the thesis are answered hereafter:

- Is plasma-catalytic ammonia synthesis a feasible alternative for ammonia synthesis?
- Which plasma-chemical and plasma-catalytic pathways can be used to enhance the ammonia yield in a plasma-reactor?

9.2 Plasma types for ammonia synthesis

One of the goals of this thesis was to evaluate which plasma types is most feasible for plasma-based reactions. As discussed in **Chapter 2**, a literature survey shows that DBD reactors have the lowest energy consumption for plasma-chemical and plasma-catalytic ammonia synthesis (see **Figure 79**). Furthermore, the energy efficiency can be improved by combining the plasma with a suitable catalyst [94,310], or by removing ammonia from the plasma phase via *in situ* adsorption (see **Chapter 7**) [415].

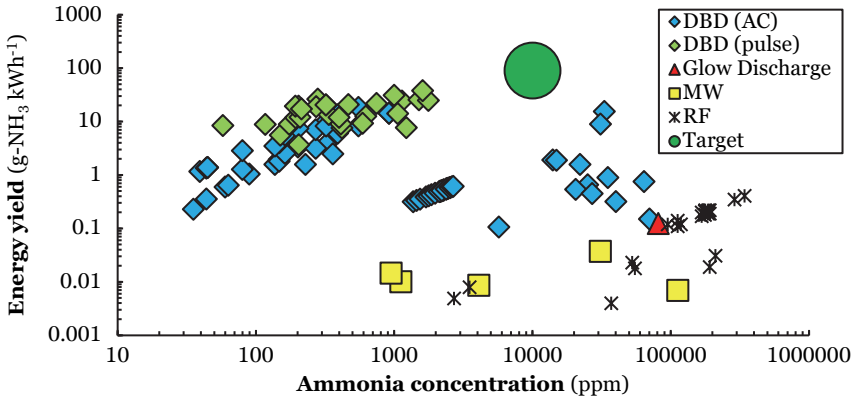

Figure 79: Reported energy yield vs. ammonia concentration. Constructed and extended from [94]. Original references: DBD (AC) [74–76,82,88–90,93,95,97–99,212,213], DBD (pulse) [81,89], Glow Discharge [107], MW [118,214,215] and RF [114,119,122,123,125–127]. In some cases, the reported units have been converted to g-NH_3 kWh^{-1} for the energy yield, and ppm for the ammonia concentration. The reader is referred to the recent review of Carreon [199] for the reported energy efficiency for specific metals.

It should be noted that the preferred plasma-reactor depends on the desired plasma-chemical or plasma-chemical reaction. For example, plasma-based NO_X synthesis historically has the lowest energy consumption in gliding arc reactors and microwave (MW) plasma reactors [11,48]. In warm plasma gliding arc reactors and microwave plasma reactors, there is a high degree of vibrational excitation for N_2 activation [40,41], resulting in a low energy pathway for NO_X synthesis according via the Zeldovich mechanism. Similarly, plasma-based CO_2 conversions show the lowest energy consumption in gliding arc reactors, radiofrequency plasma reactors, and microwave (MW) plasma reactors [61,416]. This is attributed to the lower energy barrier for CO_2 splitting via vibrational excitation than for thermal CO_2 splitting [417].

Electronic excitation and vibrational excitation are the dominant pathway for N_2 activation in non-thermal plasma DBD reactors at mild plasmas (SEI of 0.1-0.4 kJ L^{-1}) [40,41], as discussed in **Chapter 3** and **Chapter 4**. Complete dissociation of N_2 to N radicals via electron impact dissociation becomes relevant at higher plasma powers (5-20 kJ L^{-1}) [223], as discussed in **Chapter 5**, **Chapter 6**, and **Chapter 7**. The lowest reported energy consumption for plasma-catalytic ammonia synthesis is 95 MJ kg-NH_3^{-1} in a DBD reactor packed with Ru-based catalysts [89]. The lowest theoretical energy consumption possible for plasma-catalytic ammonia synthesis is about 2 MJ kg-NH_3^{-1}, based on vibrational activation of N_2 to decrease the N_2 dissociation barrier on Ru-based catalysts (see **Chapter 8**).

As discussed in **Chapter 8**, plasma-based ammonia synthesis is not competitive with other ammonia synthesis technologies, even at the minimum energy consumption of 2 MJ kg-NH_3^{-1} for vibrationally excited N_2. The NH_3 synthesis reaction from H_2 and N_2 is exothermic, implying that all energy input from the plasma is dissipated as heat. Furthermore, utilizing a plasma for nitrogen activation, while operating at (near-) atmospheric pressure results in a low ammonia outlet concentration, typically below 1 mol.%, resulting in a large recycle. This implies a high energy demand for the H_2 and N_2 recycle, and for ammonia removal.

9.3 Reaction mechanisms for plasma-catalytic ammonia synthesis

The experimental Chapters in this thesis provide an overview of the dominant reaction mechanisms for ammonia synthesis in DBD reactors under various reaction conditions. A schematic representation is shown in **Figure 80**.

As discussed in **Chapter 3**, plasma-activation of N_2 leads to a decrease in N_2 dissociation barrier on Ru-based catalysts [94]. Plasma-activation of N_2 via electronic excitation or vibrational excitation leads to a decrease in the nitrogen-nitrogen bond strength [330]. This results in an increased bond distance between the nitrogen atoms, which allows for a lower N_2 dissociation barrier on a Ru-based catalyst, as discussed in **Chapter 4**. Also, the

dissociation probability for nitrogen increases from 10^{-6} for ground-state N_2 to 10^{-2} for highly activated N_2 at 300 kJ mol^{-1} [263]. The dissociated N atoms on the catalyst surface are probably in thermal equilibrium with the surface, and subsequent hydrogenation steps occur via Langmuir-Hinshelwood reactions.

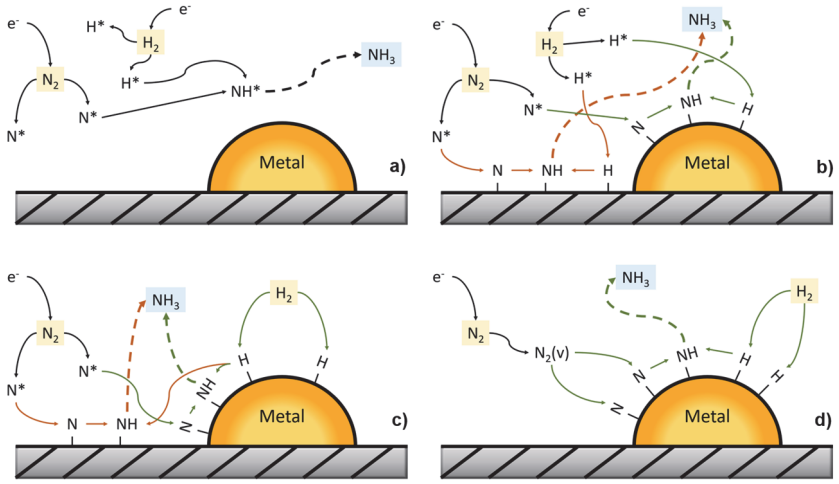

Figure 80: Reaction mechanisms for plasma-catalytic ammonia synthesis at various plasma powers: plasma-phase ammonia synthesis (Top left), surface-enhanced plasma-driven ammonia synthesis (Top right), plasma-enhanced semi-catalytic ammonia synthesis (Bottom left), and plasma-enhanced catalytic ammonia synthesis (Bottom right). Reproduced from Ref. [94]**.**

As discussed in **Chapter 5**, **Chapter 6**, and **Chapter 7**, complete dissociation of N_2 to N radicals via electron impact dissociation can also lead to ammonia formation, albeit at a higher energy consumption. These N radicals can react with other plasma species in the plasma phase to form ammonia [340]. Alternatively, the ammonia may also be decomposed by the plasma via electron impact dissociation [322,340]. Product decomposition can be limited by removing ammonia from the plasma by phase separation, membranes, or sorbents, as discussed in **Chapter 7**.

Furthermore, surface reactions can occur. As discussed in **Chapter 5** and **Chapter 6**, N radicals from the plasma phase can directly react with surface-adsorbed H, with subsequent hydrogenation via Eley-Rideal reactions, rather than Langmuir-Hinshelwood reactions. The high energy of the N radicals reacting from the plasma-phase may cause the formed NH_X species to have a higher energy than surface-adsorbed species in thermal equilibrium [181]. As observed in **Chapter 6**, the choice of transition metal has little effect on the plasma-catalytic ammonia synthesis rate. Langmuir-Hinshelwood reactions of N radicals adsorbing and hydrogenating on the metal surface appears not to be rate-limiting for most transition metals, given the similarity between catalytic activities among transition metals (see **Chapter 6**).

An additional unwanted reaction is the reverse reaction, e.g. ammonia decomposition. For thermal catalysis, a catalyst that catalyses the forward reaction will also catalyse the reverse reaction. Catalysts with thermal-catalytic activity for ammonia decomposition will also decompose ammonia in presence of the plasma, especially beyond thermal equilibrium (see **Chapter 5** and **Chapter 6**). Therefore, the optimum catalyst for thermal-catalytic conversions is typically not the best catalyst for plasma-catalytic conversions, especially when operating beyond thermal equilibrium [43].

9.4 Improving the energy efficiency

Various strategies are outlined to improve the energy yield for ammonia synthesis and NO_X synthesis in plasma reactors, as discussed hereafter.

Firstly, utilizing mild plasmas combined with a suitable catalyst allows for plasma-catalytic ammonia synthesis at a relatively low energy consumption, e.g. reaction mechanisms via plasma-activated N_2 rather than via N radicals.

Mild plasmas may be achieved through innovative plasma reactor designs. According to Paschen's law, the minimum breakdown voltage for atmospheric pressure discharges is found for a gap distance in the order 1-10 μm between the high voltage electrode and ground electrode [307]. Thus, utilizing microreactors with gap distances in the (sub-) micron range can be beneficial to decrease the power required to illuminate the plasma [418]. This results in milder plasma conditions.

Product decomposition is a general concern in plasma-chemical conversions. Ammonia is mainly decomposed during the filamentary microdischarges via electron impact dissociation, while ammonia is formed from N and H radicals during the afterglows [322,340]. Utilizing pulsed plasmas can limit the product decomposition by decreasing the duration of the filamentary discharges. *In situ* product removal from the plasma phase can also limit product decomposition by the plasma, as discussed in **Chapter 7**.

The use of catalytic wall reactors with thin catalyst layers can be beneficial as well, as the plasma typically only has a direct interaction with the catalyst up to 1-10 μm [328]. It should be noted that the gap between the high voltage electrode and ground electrode must be small, as otherwise a high plasma power is required to illuminate the plasma. This would result in a large contribution from the plasma phase, and should be prevented.

Alternatively, dense catalyst support particles can be used, which only have external surface area. The plasma is probably only in direct contact with the external surface of the catalyst.

It may be that the optimum support for a metallic catalyst is not the optimum packing material for a plasma reactor. Therefore, the plasma characteristics may be enhanced by mixing catalyst particles with dielectric materials, which were coined plasma catalyst promoters (PCPs) [75,92,198].

9.5 Industrial feasibility

As discussed in **Chapter 8**, it is highly improbably that plasma technology will be commercialized for ammonia synthesis. This is due to the exothermic nature of ammonia synthesis from H_2 and N_2.. Any addition of electrical energy in the form of plasma is lost as heat, as the energy is not stored in the chemical bond of the ammonia product. Furthermore, thermal-catalytic ammonia synthesis technologies under mild conditions down to 200-300°C, without any plasma activation, are currently under development [419]. Thus, the potential benefits of plasma technology such as a fast ramp-up and ramp-down are not necessarily relevant compared to these novel thermal-catalytic ammonia synthesis technologies, given that plasma-catalytic ammonia synthesis also requires temperatures of at least 200°C (see **Chapter 3**).

Concluding, plasma technology is mostly relevant for highly endothermic reactions such as ozone (O_3) production from O_2 [45], and NO_X synthesis from N_2 and O_2 [48].

9.6 Recommendations

In case of ammonia synthesis, large-scale production is expected to remain based on the high temperature, high pressure Haber-Bosch synthesis loop. However, with increasing penetration of low cost solar and wind energy, the hydrogen feedstock is expected to transition from fossil feedstocks such as natural gas, oil, and coal to renewable electricity and water, utilizing water electrolysis technology. Fluctuations in renewable electricity will be covered by batteries & hydrogen storage buffers, combined with a more flexible Haber-Bosch ammonia synthesis loop [14].

For small scale ammonia synthesis, alternative technologies may become competitive with the high temperature, high pressure Haber-Bosch synthesis loop. Especially sorbent-enhanced ammonia synthesis may become cost competitive with the Haber-Bosch synthesis loop at small scales, as discussed in **Chapter 8**. Sorbent-enhanced ammonia synthesis may find an application for islanded ammonia power systems [33,420,421]. Therefore, it is recommended to increase experimental research efforts for ammonia sorbents, such as metal halides and zeolites, rather than focus on ammonia synthesis catalysts. Furthermore, catalytic ammonia decomposition to hydrogen may become relevant, especially when ammonia becomes the primary hydrogen carrier for intercontinental transport. Mild temperature ammonia decomposition catalysts with a comparable activity to Ru are desirable.

Concluding, plasma-catalytic ammonia synthesis is not expected to be commercialized for industrial operation. However, plasma-catalytic ammonia synthesis is of interest to better understand plasma chemistry and plasma catalysis. Ammonia synthesis is an excellent reaction to study mutual influences of the plasma and the catalyst, due to the absence of byproducts for ammonia synthesis from N_2 and H_2, as well as the extensive literature available for heterogeneously catalysed ammonia synthesis. Thus, it is recommended to

keep using plasma-catalytic ammonia synthesis as a probe reaction to better understand mechanisms in plasma catalysis. As discussed in **Chapter 4**, plasma-induced electric fields do not have a significant effect on plasma-catalytic ammonia synthesis. However, the role of surface charging remains an open question in the field of plasma catalysis.

Product removal from the plasma zone is essential, as the plasma does not only activate reactants, but also the products formed, thereby limiting the energy efficiency. Therefore, it is suggested to apply materials for product removal, such that plasma-induced product decomposition is limited (see **Chapter 7**). Examples of reactor configurations that allow for *in situ* product removal include DBD reactors with a packed bed or a trickle bed, or gliding arc plasmas with a fluidized bed. Alternatively, a water cooled reactor wall can liquefy the formed products, thereby preventing the product decomposition in the plasma zone [366,422]. Effective product removal is probably essential for all plasma-chemical and plasma-catalytic reactions, as plasmas activate both reactants and products.

Concluding, further research on plasma-nitrogen fixation can focus on NO_X synthesis from air, a highly endothermic reaction. This reaction can probably be enhanced via plasma catalysis combined with *in situ* product removal. Further energy efficiency enhancement is expected upon using pulsed plasmas.

Lastly, it is recommended to set requirements for specific plasma-based conversions, based on process plant designs including separation steps after the plasma reactor. For example, is it required to achieve a complete conversion, or can the product be separated from the reactant mixture at lower concentrations? What is the energy consumption of the separation step and the recycle? Lastly, how does plasma technology compare to commercial technologies, as well as to other emerging technologies?

Asking such questions allows for more focused research efforts towards commercialization where plasma technology may be relevant. On the other hand, plasma technology may also be researched out of scientific curiosity, which is the case of plasma-catalytic ammonia synthesis.

References

[1] T.R. Malthus, An Essay on the Principle of Population, 1798.

[2] T. Hager, The Alchemy of Air: A Jewish genius, a doomed tycoon, and the scientific discovery that fed the world but fueled the rise of Hitler, Harmony Books, New York (NY), 2008.

[3] V. Smil, Detonator of the population explosion, Nature. 400 (1999) 415. doi:10.1038/22672.

[4] B.S. Patil, V. Hessel, L.C. Seefeldt, D.R. Dean, B.M. Hoffman, B.J. Cook, L.J. Murray, Nitrogen Fixation, Ullmann's Encycl. Ind. Chem. (2017). doi:10.1002/14356007.a17_471.pub2.

[5] F.A. Ernst, Industrial Chemical Monographs: Fixation of Atmospheric Nitrogen, Chapman & Hall, Ltd., London (UK), 1928.

[6] W. Nernst, Über das Ammoniakgleichgewicht, Zeitschrift Fur Elektrochemie Und Angew. Phys. Chemie. 13 (1907). doi:10.1002/bbpc.19070133205.

[7] A.S. Travis, Nitrogen Capture: The Growth of an International Industry (1900-1940), Springer International Publishing, 2018. doi:10.1007/978-3-319-68963-0.

[8] G. Prieto, F. Schüth, The Yin and Yang in the development of catalytic processes: Catalysis research and reaction engineering, Angew. Chemie - Int. Ed. 54 (2015) 3222–3239. doi:10.1002/anie.201409885.

[9] E. Farber, From Chemistry to Philosophy: The Way of Alwin Mittasch (1869-1953), Chymia. 11 (1966) 157–178. doi:10.2307/27757266.

[10] A. Mittasch, W. Frankenburg, Early Studies of Multicomponent Catalysts, Adv. Catal. 2 (1950) 81–104. doi:10.1016/S0360-0564(08)60375-2.

[11] K.H.R. Rouwenhorst, F. Jardali, A. Bogaerts, L. Lefferts, From the Birkeland-Eyde process towards energy-efficient plasma-based NOX synthesis: A techno-economic analysis, Energy Environ. Sci. 14 (2021) 2520–2534. doi:10.1039/D0EE03763J.

[12] J.W. Erisman, M.A. Sutton, J. Galloway, Z. Klimont, W. Winiwarter, How a century of ammonia synthesis changed the world, Nat. Geosci. 1 (2008) 636–639. doi:10.1038/ngeo325.

[13] O. Hatfield, A review of global ammonia supply, in: NH3 Energy Conf., 2020.

[14] IRENA, Ammonia Energy Association, Innovation Outlook: Renewable Ammonia, Abu Dhabi, 2022. doi:978-92-9260-423-3.

[15] The Royal Society, Ammonia: zero-carbon fertiliser, fuel and energy store, 2020.

[16] D. Fowler, M. Coyle, U. Skiba, M.A. Sutton, J.N. Cape, S. Reis, L.J. Sheppard, A. Jenkins, B. Grizzetti, J.N. Galloway, P. Vitousek, A. Leach, A.F. Bouwman, K. Butterbach-Bahl, F. Dentener, D. Stevenson, M. Amann, M. Voss, The global nitrogen cycle in the Twentyfirst century, Philos. Trans. R. Soc. B Biol. Sci. 368 (2013). doi:10.1098/rstb.2013.0164.

[17] C. Philibert, Direct and indirect electrification of industry and beyond, Oxford Rev. Econ. Policy. 35 (2019) 197–217. doi:10.1093/oxrep/grz006.

[18] J.R. Rostrup-Nielsen, Catalytic Steam Reforming, in: A.J. S., M. Boudart (Eds.), Catal. Sci. Technol., 1st ed., Springer-Verlag, Berlin Heidelberg, 1984: pp. 1–117. doi:10.1007/978-3-642-93247-2_1.

[19] C.H. Bartholomew, R.J. Farrauto, Hydrogen Production and Synthesis Gas Reactions, in: C.H. Bartholomew, R.J. Farrauto (Eds.), Fundam. Ind. Catal. Process. Second Ed., 2nd ed., John Wiley & Sons, Inc., Hoboken (NJ, USA), 2005: pp. 339–486. doi:10.1002/9780471730071.ch6.

[20] M. Appl, Ammonia: Principles and Industrial Practice, 1st ed., Wiley-VCH Verlag GmbH, Weinheim (Germany), 1999. doi:10.1002/9783527613885.

[21] C. Smith, A.K. Hill, L. Torrente-Murciano, Current and future role of Haber–Bosch ammonia in a carbon-free energy landscape, Energy Environ. Sci. 13 (2020) 331–344. doi:10.1039/C9EE02873K.

[22] A. Hellman, K. Honkala, S. Dahl, C.H. Christensen, J.K. Nørskov, Ammonia Synthesis: State of the Bellwether Reaction, in: Compr. Inorg. Chem., 2nd ed., Elsevier Ltd, 2013. doi:10.1016/B978-0-08-097774-4.00725-7.

[23] IRENA, Reaching Zero with Renewables: Capturing Carbon, Abu Dhabi, n.d.

[24] K.H.R. Rouwenhorst, A.S. Travis, L. Lefferts, 1921-2021: A century of renewable ammonia synthesis, (n.d.).

[25] K.H.R. Rouwenhorst, P.M. Krzywda, N.E. Benes, G. Mul, L. Lefferts, Ammonia, 4. Green Ammonia Production, Ullmann's Encycl. Ind. Chem. (2020). doi:10.1002/14356007.w02_w02.

[26] J. Sousa Cardoso, V. Silva, R.C. Rocha, M.C. Hall, M. Costa, D. Eusébio, Ammonia as an energy vector: Current and future prospects for low-carbon fuel applications in internal combustion engines, J. Clean. Prod. 296 (2021). doi:10.1016/j.jclepro.2021.126562.

[27] W.H. Avery, A Role for Ammonia in the Hydrogen Economy, Int. J. Hydrogen Energy. 13 (1988) 761–773. doi:10.1016/0360-3199(88)90037-7.

[28] J.R. Bartels, M.B. Pate, A feasibility study of implementing an Ammonia Economy,

Des Moines (IA), 2008.

[29] F. Schüth, R. Palkovits, R. Schlögl, D.S. Su, Ammonia as a possible element in an energy infrastructure: catalysts for ammonia decomposition, Energy Environ. Sci. 5 (2012) 6278–6289. doi:10.1039/C2EE02865D.

[30] R. Nayak-Luke, R. Bañares-Alcántara, Long-Term Energy Storage: What is the Need and is Ammonia a Solution?, Comput. Aided Chem. Eng. 44 (2018) 1843–1848. doi:10.1016/B978-0-444-64241-7.50302-5.

[31] J. Ikäheimo, J. Kiviluoma, R. Weiss, H. Holttinen, Power-to-ammonia in future North European 100 % renewable power and heat system, Int. J. Hydrogen Energy. 3 (2018). doi:10.1016/j.ijhydene.2018.06.121.

[32] C.H. Christensen, T. Johannessen, R.Z. Sørensen, J.K. Nørskov, Towards an ammonia-mediated hydrogen economy?, Catal. Today. 111 (2006) 140–144. doi:10.1016/j.cattod.2005.10.011.

[33] K.H.R. Rouwenhorst, A.G.J. Van Der Ham, G. Mul, S.R.A. Kersten, Islanded ammonia power systems: Technology review & conceptual process design, Renew. Sustain. Energy Rev. 114 (2019). doi:10.1016/j.rser.2019.109339.

[34] International Transport Forum, Decarbonising Maritime Transport: Pathways to zero-carbon shipping by 2035, 2018.

[35] Alfa Laval, Hafnia, Haldor Topsøe, Vestas, Siemens Gamesa, Ammonfuel – an industrial view of ammonia as a marine fuel, 2020.

[36] S. Muraki, Innovation for Direct Use of Ammonia in the Energy Market, in: Top. Conf. Synth. Renew. Fuels (AIChE Annu. Meet., Orlando (FL), 2019.

[37] M. Kueppers, S. Nicole, P. Pineda, M. Metzger, M. Huber, S. Paulus, H. Joerg, S. Niessen, Decarbonization pathways of worldwide energy systems – Definition and modeling of archetypes, Appl. Energy. 285 (2021). doi:10.1016/j.apenergy.2021.116438.

[38] International Energy Agency, The Future of Hydrogen: Seizing today's opportunities, 2019.

[39] Proton Ventures, Proton Ventures, (2021).

[40] A. Bogaerts, E.C. Neyts, Plasma Technology: An Emerging Technology for Energy Storage, ACS Energy Lett. 3 (2018) 1013–1027. doi:10.1021/acsenergylett.8b00184.

[41] P. Mehta, P. Barboun, D.B. Go, J.C. Hicks, W.F. Schneider, Catalysis Enabled by Plasma Activation of Strong Chemical Bonds: a Review, ACS Energy Lett. 4 (2019) 1115–1133. doi:10.1021/acsenergylett.9b00263.

[42] H.-H. Kim, Y. Teramoto, A. Ogata, H. Takagi, T. Nanba, Plasma Catalysis for

Environmental Treatment and Energy Applications, Plasma Chem. Plasma Process. 36 (2016) 45–72. doi:10.1007/s11090-015-9652-7.

[43] A. Bogaerts, X. Tu, J.C. Whitehead, G. Centi, L. Lefferts, O. Guaitella, F. Azolina-Jury, H.-H. Kim, A.B. Murphy, W.F. Schneider, T. Nozaki, J.C. Hicks, A. Rousseau, F. Thevenet, A. Khacef, M. Carreon, The 2020 Plasma Catalysis Roadmap, J. Phys. D. Appl. Phys. 53 (2020) 1–51. doi:10.1088/1361-6463/ab9048.

[44] R. Brandenburg, A. Bogaerts, W. Bongers, A. Fridman, G. Fridman, B.R. Locke, V. Miller, S. Reuter, M. Schiorlin, T. Verreycken, K.K. Ostrikov, White paper on the future of plasma science in environment, for gas conversion and agriculture, Plasma Process. Polym. (2018) 1–18. doi:10.1002/ppap.201700238.

[45] U. Kogelschatz, Dielectric Barrier Discharge: Their History, Discharge Physic, and Industrial Applications, Plasma Chem. Plasma Process. 23 (2003) 1–46. doi:10.1023/A:1022470901385.

[46] P. Pässler, W. Hefner, K. Buckl, H. Meinass, A. Meiswinkel, H. Wernicke, G. Ebersberg, R. Müller, J. Bässler, H. Behringer, D. Mayer, Acetylene, Ullmann's Encycl. Ind. Chem. (2011) 1–50. doi:10.1002/14356007.a01_097.pub4.

[47] G.E. Moore, H.H. Hansen, Direct observation of the thermal dissociation of molecular nitrogen, J. Chem. Phys. 54 (1971) 441–443. doi:10.1063/1.1674621.

[48] B.S. Patil, Q. Wang, V. Hessel, J. Lang, Plasma N2-fixation: 1900–2014, Catal. Today. 256 (2015) 49–66. doi:10.1016/j.cattod.2015.05.005.

[49] P. Mehta, P. Barboun, F.A. Herrera, J. Kim, P. Rumbach, D.B. Go, J.C. Hicks, W.F. Schneider, Overcoming ammonia synthesis scaling relations with plasma-enabled catalysis, Nat. Catal. 1 (2018) 269–275. doi:10.1038/s41929-018-0045-1.

[50] K.M. Van Geem, V. V. Galvita, G.B. Marin, Making chemicals with electricity, Science (80-.). 364 (2019) 734–735. doi:10.1126/science.aax5179.

[51] E. Simon, Green ammonia, in: REFUEL Kickoff Meet., Denver (CO), 2017.

[52] A. Valera-Medina, H. Xiao, M. Owen-Jones, W.I.F. David, P.J. Bowen, Ammonia for power, Prog. Energy Combust. Sci. 69 (2018) 63–102. doi:10.1016/j.pecs.2018.07.001.

[53] J.D. Hunt, E. Byers, Y. Wada, S. Parkinson, D.P. Van Vuuren, K. Riahi, Global resource potential of seasonal pumped hydropower storage for energy and water storage, Nat. Commun. 11 (2020). doi:10.1038/s41467-020-14555-y.

[54] J. Guo, P. Chen, Catalyst: NH3 as an Energy Carrier, Chem. 3 (2017) 709–712. doi:10.1016/j.chempr.2017.10.004.

[55] S. Giddey, S.P.S. Badwal, C. Munnings, M. Dolan, Ammonia as a Renewable

Energy Transportation Media, ACS Sustain. Chem. Eng. 5 (2017) 10231–10239. doi:10.1021/acssuschemeng.7b02219.

[56] E.C. Neyts, K. Ostrikov, M.K. Sunkara, A. Bogaerts, Plasma Catalysis: Synergistic Effects at the Nanoscale, Chem. Rev. 115 (2015) 13408–13446. doi:10.1021/acs.chemrev.5b00362.

[57] R. Snoeckx, A. Bogaerts, Plasma technology - a novel solution for CO2 conversion?, Chem. Soc. Rev. 46 (2017) 5805–5863. doi:10.1039/c6cs00066e.

[58] J. Hong, S. Prawer, A.B. Murphy, Plasma Catalysis as an Alternative Route for Ammonia Production: Status, Mechanisms, and Prospects for Progress, ACS Sustain. Chem. Eng. 6 (2018) 15–31. doi:10.1021/acssuschemeng.7b02381.

[59] A. Bogaerts, E. Neyts, R. Gijbels, J. Van Der Mullen, Gas discharge plasmas and their applications, Spectrochim. Acta Part B. 57 (2002) 609–658.

[60] A. Fridman, Plasma chemistry, 2008.

[61] R. Snoeckx, A. Bogaerts, Plasma technology – a novel solution for CO2 conversion?, Chem. Soc. Rev. 46 (2017) 5805–5863. doi:10.1039/C6CS00066E.

[62] Y. Uchida, K. Takaki, U.K. Urashima, J.-S. Chang, Atmospheric pressure of nitrogen plasmas in a ferro-electric packed-bed barrier discharge reactor part II: Spectroscopic measurements of excited nitrogen molecule density and its vibrational temperature, IEEE Trans. Dielectr. Electr. Insul. 11 (2004) 491–497. doi:10.1109/TDEI.2004.1306727.

[63] M. Bai, Z. Zhang, M. Bai, X. Bai, H. Gao, Synthesis of Ammonia using CH4/N2 plasmas based on micro-gap discharge under environmentally friendly condition, Plasma Chem. Plasma Process. 28 (2008) 405–414. doi:10.1007/s11090-008-9132-4.

[64] M. Bai, Z. Zhang, M. Bai, X. Bai, H. Gao, Conversion of methane to liquid products, hydrogen, and ammonia with environmentally friendly condition-based microgap discharge, J. Air Waste Manag. Assoc. 58 (2008) 1616–1621. doi:10.3155/1047-3289.58.12.1616.

[65] M. Bai, X. Bai, N. Wang, D. Zhang, K. Zhan, Synthesis of ammonia and liquid fuel by CH4 and N2 plasmas without catalyst at ambient pressure and temperature, in: IEEE Int. Conf. Plasma Sci., Baltimore (United States), 2004: p. 413.

[66] G. Horvath, N.J. Mason, L. Polachova, M. Zahoran, L. Moravsky, S. Matejcik, Packed bed DBD discharge experiments in admixtures of N2 and CH4, Plasma Chem. Plasma Process. 30 (2010) 565–577. doi:10.1007/s11090-010-9241-8.

[67] Y. Gorbanev, E. Vervloessem, A. Nikiforov, A. Bogaerts, Nitrogen fixation with water vapor by non-equilibrium plasma: Towards sustainable ammonia

production, ACS Sustain. Chem. Eng. 8 (2020) 2996–3004. doi:10.1021/acssuschemeng.9b07849.

[68] P. Peng, C. Schiappacasse, N. Zhou, M. Addy, Y. Cheng, Y. Zhang, E. Anderson, D. Chen, Y. Wang, Y. Liu, P. Chen, R. Ruan, Plasma in situ gas-liquid nitrogen fixation using concentrated high-intensity electric field, J. Phys. D. Appl. Phys. 52 (2019). doi:10.1088/1361-6463/ab3ea6.

[69] R. Hawtof, S. Ghosh, E. Guarr, C. Xu, R.M. Sankaran, J.N. Renner, Catalyst-free, highly selective synthesis of ammonia from nitrogen and water by a plasma electrolytic system, Asian J. Chem. 31 (2019) 1–10. doi:10.1126/sciadv.aat5778.

[70] P. Peng, P. Chen, M. Addy, Y. Cheng, Y. Zhang, E. Anderson, N. Zhou, C. Schiappacasse, R. Hatzenbeller, L. Fan, S. Liu, D. Chen, J. Liu, Y. Liu, R. Ruan, In situ plasma-assisted atmospheric nitrogen fixation using water and spray-type jet plasma, Chem. Commun. 54 (2018) 2886–2889. doi:10.1039/c8cc00697k.

[71] P. Peng, C. Schiappacasse, N. Zhou, M. Addy, Y. Cheng, Y. Zhang, K. Ding, Y. Wang, P. Chen, R. Ruan, Sustainable non-thermal plasma-assisted nitrogen fixation - Synergistic catalysis, ChemSusChem. (2019) 1–12. doi:10.1002/cssc.201901211.

[72] D. Xie, Y. Sun, T. Zhu, X. Fan, X. Hong, W. Yang, Ammonia synthesis and by-product formation from H2O, H2 and N2 by dielectric barrier discharge combined with an Ru/Al2O3 catalyst, RSC Adv. 6 (2016) 105338–105346. doi:10.1039/C6RA21351K.

[73] J. Kibsgaard, J.K. Nørskov, I. Chorkendorff, The Difficulty of Proving Electrochemical Ammonia Synthesis, ACS Energy Lett. (2019) 2986–2988. doi:10.1021/acsenergylett.9b02286.

[74] P. Peng, Y. Cheng, R. Hatzenbeller, M. Addy, N. Zhou, C. Schiappacasse, D. Chen, Y. Zhang, E. Anderson, Y. Liu, P. Chen, R. Ruan, Ru-based multifunctional mesoporous catalyst for low-pressure and non-thermal plasma synthesis of ammonia, Int. J. Hydrogen Energy. 42 (2017) 19056–19066. doi:10.1016/j.ijhydene.2017.06.118.

[75] G. Akay, K. Zhang, Process intensification in ammonia synthesis using novel coassembled supported microporous catalysts promoted by nonthermal plasma, Ind. Eng. Chem. Res. 56 (2017) 457–468. doi:10.1021/acs.iecr.6b02053.

[76] M. Iwamoto, M. Akiyama, K. Aihara, T. Deguchi, Ammonia Synthesis on Wool-Like Au, Pt, Pd, Ag, or Cu Electrode Catalysts in Nonthermal Atmospheric-Pressure Plasma of N2 and H2, ACS Catal. (2017) 6924–6929. doi:10.1021/acscatal.7b01624.

[77] J. Hong, S. Pancheshnyi, E. Tam, J.J. Lowke, S. Prawer, A.B. Murphy,

Corrigendum: Kinetic modelling of NH3 production in N2–H2 non-equilibrium atmospheric-pressure plasma catalysis, J. Phys. D. Appl. Phys. 51 (2018). doi:10.1088/1361-6463/aaa988.

[78] Q. Xie, S. Zhuge, X. Song, M. Lu, R. Ruan, Y. Nie, J. Ji, Hydrogenation of plasma-excited nitrogen over an alumina catalyst for ammonia synthesis, Int. J. Hydrogen Energy. 43 (2018) 14885–14891. doi:10.1016/j.ijhydene.2018.06.051.

[79] Y. Wang, M. Craven, X. Yu, J. Ding, P. Bryant, J. Huang, X. Tu, Plasma-Enhanced Catalytic Synthesis of Ammonia over a Ni/Al2O3 Catalyst at Near-Room Temperature: Insights into the Importance of the Catalyst Surface on the Reaction Mechanism, ACS Catal. 9 (2019) 10780–10793. doi:10.1021/acscatal.9b02538.

[80] F. Herrera, G.H. Brown, P. Barboun, N. Turan, P. Mehta, W.. Schneider, J. Hicks, D.B. Go, The impact of transition metal catalysts on macroscopic dielectric barrier discharge (DBD) characteristics in an ammonia synthesis plasma catalysis reactor, J. Phys. D. Appl. Phys. 52 (2019). doi:10.1088/1361-6463/ab0c58.

[81] P. Peng, P. Chen, M. Addy, Y. Cheng, E. Anderson, N. Zhou, C. Schiappacasse, Y. Zhang, D. Chen, R. Hatzenbeller, Y. Liu, Atmospheric Plasma-Assisted Ammonia Synthesis Enhanced via Synergistic Catalytic Absorption, ACS Sustain. Chem. Eng. 7 (2019) 100–104. doi:10.1021/acssuschemeng.8b03887.

[82] P.M. Barboun, P. Mehta, F. Herrera, D.B. Go, W.F. Schneider, J.C. Hicks, Distinguishing Plasma Contributions to Catalyst Performance in Plasma-Assisted Ammonia Synthesis, ACS Sustain. Chem. Eng. 7 (2019) 8621–8630. doi:10.1021/acssuschemeng.9b00406.

[83] Q. Xie, S. Zhuge, X. Song, M. Lu, Non-thermal atmospheric plasma synthesis of ammonia in a DBD reactor packed with various catalysts, J. Phys. D. Appl. Phys. 53 (2019). doi:10.1088/1361-6463/ab57e5.

[84] M. Bai, Z. Zhang, X. Bai, M. Bai, W. Ning, Plasma Synthesis of Ammonia With a Microgap Dielectric Barrier Discharge at Ambient Pressure, IEEE Trans. Plasma Sci. 31 (2003) 1285–1291. doi:10.1109/TPS.2003.818761.

[85] B.S. Patil, A.S.R. Van Kaathoven, F.J.J. Peeters, N. Cherkasov, J. Lang, Q. Wang, V. Hessel, Deciphering the synergy between plasma and catalyst support for ammonia synthesis in a packed dielectric barrier discharge reactor, J. Phys. D. Appl. Phys. 53 (2020) ab6a36. doi:10.1088/1361-6463/ab6a36.

[86] X. Zhu, X. Hu, X. Wu, Y. Cai, H. Zhang, X. Tu, Ammonia synthesis over y-Al2O3 pellets in a packed-bed dielectric barrier discharge reactor, J. Phys. D. Appl. Phys. (2020). doi:10.1088/1361-6463/ab6cd1.

[87] K. van 't Veer, F. Reniers, A. Bogaerts, Zero-dimensional modelling of unpacked and packed bed dielectric barrier discharges: The role of vibrational kinetics in

ammonia synthesis, Plasma Sources Sci. Technol. 29 (2020). doi:10.1088/1361-6595/ab7a8a.

[88] J.R. Shah, F. Gorky, J. Lucero, M.A. Carreon, M.L. Carreon, Ammonia synthesis via atmospheric plasma- catalysis: Zeolite 5A a case of study, Ind. Eng. Chem. Res. 59 (2020) 5167–5176. doi:10.1021/acs.iecr.9b05220.

[89] H.-H. Kim, Y. Teramoto, A. Ogata, H. Takagi, T. Nanba, Atmospheric-pressure nonthermal plasma synthesis of ammonia over ruthenium catalysts, Plasma Process. Polym. 14 (2017) 1–9. doi:10.1002/ppap.201600157.

[90] A. Gómez-Ramírez, A.M. Montoro-Damas, J. Cotrino, R.M. Lambert, A.R. González-Elipe, About the enhancement of chemical yield during the atmospheric plasma synthesis of ammonia in a ferroelectric packed bed reactor, Plasma Process. Polym. 14 (2017) 1–8. doi:10.1002/ppap.201600081.

[91] Y. Nie, X. Song, S. Zhuge, M. Lu, P. Chen, J. Ji, Effect of CaO-modified Al2O3 on the synthesis of ammonia by DBD plasma, Xiandai Huagong/Modern Chem. Ind. 36 (2016) 127–130. doi:10.16606/j.cnki.issn 0253-4320.2016.07.031.

[92] G. Akay, Sustainable Ammonia and Advanced Symbiotic Fertilizer Production Using Catalytic Multi-Reaction-Zone Reactors with Nonthermal Plasma and Simultaneous Reactive Separation, ACS Sustain. Chem. Eng. 5 (2017) 11588–11606. doi:10.1021/acssuschemeng.7b02962.

[93] S. Li, T. van Raak, F. Gallucci, Investigating the operation parameters for ammonia synthesis in dielectric barrier discharge reactors, J. Phys. D. Appl. Phys. 53 (2020). doi:10.1088/1361-6463/ab4b37.

[94] K.H.R. Rouwenhorst, H.-H. Kim, L. Lefferts, Vibrationally excited activation of N2 in plasma-enhanced catalytic ammonia synthesis: a kinetic analysis, ACS Sustain. Chem. Eng. 7 (2019) 17515–17522. doi:10.1021/acssuschemeng.9b04997.

[95] T. Mizushima, K. Matsumoto, J.I. Sugoh, H. Ohkita, N. Kakuta, Tubular membrane-like catalyst for reactor with dielectric-barrier-discharge plasma and its performance in ammonia synthesis, Appl. Catal. A Gen. 265 (2004) 53–59. doi:10.1016/j.apcata.2004.01.002.

[96] T. Mizushima, K. Matsumoto, H. Ohkita, N. Kakuta, Catalytic effects of metal-loaded membrane-like alumina tubes on ammonia synthesis in atmospheric pressure plasma by dielectric barrier discharge, Plasma Chem. Plasma Process. 27 (2007) 1–11. doi:10.1007/s11090-006-9034-2.

[97] J. Hong, S. Prawer, A.B. Murphy, Production of ammonia by heterogeneous catalysis in a packed-bed dielectric-barrier discharge: Influence of argon addition and voltage, IEEE Trans. Plasma Sci. 42 (2014) 2338–2339. doi:10.1109/TPS.2014.2323077.

[98] A. Gómez-Ramírez, J. Cotrino, R.M. Lambert, A.R. González-Elipe, Efficient synthesis of ammonia from N2 and H2 alone in a ferroelectric packed-bed DBD reactor, Plasma Sources Sci. Technol. 24 (2015) 1–7. doi:10.1088/0963-0252/24/6/065011.

[99] P. Peng, Y. Li, Y. Cheng, S. Deng, P. Chen, R. Ruan, Atmospheric Pressure Ammonia Synthesis Using Non-thermal Plasma Assisted Catalysis, Plasma Chem. Plasma Process. 36 (2016) 1201–1210. doi:10.1007/s11090-016-9713-6.

[100] J. Hong, M. Aramesh, O. Shimoni, D.H. Seo, S. Yick, A. Greig, C. Charles, S. Prawer, A.B. Murphy, Plasma Catalytic Synthesis of Ammonia Using Functionalized-Carbon Coatings in an Atmospheric-Pressure Non-equilibrium Discharge, Plasma Chem. Plasma Process. 36 (2016) 917–940. doi:10.1007/s11090-016-9711-8.

[101] K. Aihara, M. Akiyama, T. Deguchi, M. Tanaka, R. Hagiwara, M. Iwamoto, Remarkable catalysis of a wool-like copper electrode for NH3 synthesis from N2 and H2 in non-thermal atmospheric plasma, Chem. Commun. 52 (2016) 13560–13563. doi:10.1039/c6cc06752b.

[102] A.K. Brewer, J.W. WestHaver, The Synthesis of Ammonia in the Glow Discharge, J. Phys. Chem. 33 (1929) 883–895.

[103] A.K. Brewer, J.W. Westhaver, Chemical Action in the Glow Discharge II. Further Investigation on the Synthesis of Ammonia, J. Phys. Chem. 34 (1930) 153–164.

[104] B. Gordiets, C.M. Ferreira, M.J. Pinheiro, A. Ricard, Self-consistent kinetic model of low-pressure N2-H2 flowing discharges: II. Surface processes and densities of N, H, NH3 species, Plasma Sources Sci. Technol. 7 (1998) 379–388. doi:10.1088/0963-0252/7/3/016.

[105] E. Tiede, E. Hey, Über aktiven Stickstoff und Ammoniak-Bildung im Glimmstrom in Abhängingkeit vom Elektroden-Material unter Berücksichtigung katalytischer Probleme, Berichte Der Dtsch. Chem. Gesellschaft (A B Ser. 66 (1933) 85–94.

[106] G.Y. Botchway, M. Venugopalan, Plasma Synthesis of Ammonia in Presence of an Iron Catalyst, Zeitschrift Für Phys. Chemie Neue Folge. 120 (1980) 103–110. doi:10.1524/zpch.1980.120.1.103.

[107] K.S. Yin, M. Venugopalan, Plasma Chemical Synthesis. I. Effect of Electrode Material on the Synthesis of Ammonia, Plasma Chem. Plasma Process. 3 (1983) 343–350. doi:10.1007/BF00564632.

[108] K. Sugiyama, K. Akazawa, M. Oshima, H. Miura, T. Matsuda, O. Nomura, Ammonia synthesis by means of plasma over MgO catalyst, Plasma Chem. Plasma Process. 6 (1986) 179–193. doi:10.1007/BF00571275.

[109] M. Touvelle, J.L.M. Licea, M. Venugopalan, J.L. Mufioz Licea, M. Venugopalan,

Plasma Chemical Synthesis. II. Effect of Wall Surface on the Synthesis of Ammonia, Plasma Chem. Plasma Process. 7 (1987) 101. doi:10.1007/BF01016001.

[110] H. Miura, K. Sugiyama, M. Oshima, S. Kanagawa, T. Matsuda, T. Mitamura, O. Nomura, The Formation of Ammonia in the After-Glow Region of N2 Plasma, Electrochem. Ind. Phys. Chem. 56 (1988) 656–657.

[111] J. Amorim, G. Baravian, G. Sultan, Absolute density measurements of ammonia synthetized in N2–H2 mixture discharges, Appl. Phys. Lett. 68 (1996) 1915–1917. doi:10.1063/1.116293.

[112] B. Gordiets, C.M. Ferreira, M.J. Pinheiro, A. Ricard, Self-consistent kinetic model of low-pressure N2-H2 flowing discharges: I. Volume processes, Plasma Sources Sci. Technol. 7 (1998) 363–378. doi:10.1088/0963-0252/7/3/015.

[113] H. Uyama, O. Matsumoto, Synthesis of Ammonia in High-Frequency Discharges. II. Synthesis of Ammonia in a Microwave Discharge Under Various Conditions, Plasma Chem. Plasma Process. 9 (1989) 421–432. doi:10.1007/BF01083676.

[114] H. Uyama, O. Matsumoto, Synthesis of ammonia in high-frequency discharges, Plasma Chem. Plasma Process. 9 (1989) 13–24. doi:10.1007/BF01015824.

[115] S. Tanaka, H. Uyama, O. Matsumoto, Synergistic effects of catalysts and plasmas on the synthesis of ammonia and hydrazine, Plasma Chem. Plasma Process. 14 (1994) 491–504. doi:10.1007/BF01570208.

[116] J.L. Jauberteau, I. Jauberteau, J. Aubreton, NH3 and NHx<3 radical downstream a microwave discharge sustained in an Ar-N2-H2 gas mixture. Study of surface reactive processes and determination of rate constants, J. Phys. D. Appl. Phys. 35 (2002) 665–674.

[117] T. Fujii, K. Iwase, P.C. Selvin, Mass spectrometric analysis of a N2/H2 microwave discharge plasma, Int. J. Mass Spectrom. 216 (2002) 169–175.

[118] J. Nakajima, H. Sekiguchi, Synthesis of ammonia using microwave discharge at atmospheric pressure, Thin Solid Films. 516 (2008) 4446–4451. doi:10.1016/j.tsf.2007.10.053.

[119] M. Carreon, J. Shah, F. Gorky, P. Psarras, B. Seong, Ammonia yield enhancement by hydrogen sink effect during plasma catalysis, ChemCatChem. 12 (2019) 1200–1211. doi:10.1002/cctc.201901769.

[120] M. Ben Yaala, D. Scherrer, A. Saeedi, L. Moser, K. Soni, R. Steiner, G. De Temmerman, M. Oberkofler, L. Marot, E. Meyer, Plasma-activated catalytic formation of ammonia from N2–H2: influence of temperature and noble gas addition, Nucl. Fusion. 60 (2020). doi:10.1088/1741-4326/ab519c.

[121] M.L. Carreon, D.F. Jaramillo-Cabanzo, I. Chaudhuri, M. Menon, M.K. Sunkara, Synergistic interactions of H2 and N2 with molten gallium in the presence of plasma, J. Vac. Sci. Technol. A Vacuum, Surfaces, Film. 36 (2018) 021303. doi:10.1116/1.5004540.

[122] H. Uyama, T. Uchikura, H. Niijima, O. Matsumoto, Synthesis of Ammonia with RF Discharge. Adsorption of Products on Zeolite, Chem. Lett. 16 (1987) 555–558. doi:10.1246/cl.1987.555.

[123] H. Uyama, T. Nakamura, S. Tanaka, O. Matsumoto, Catalytic effect of iron wires on the syntheses of ammonia and hydrazine in a radio-frequency discharge, Plasma Chem. Plasma Process. 13 (1993) 117–131. doi:10.1007/BF01447174.

[124] H. Uyama, O. Matsumoto, Reaction Scheme of Ammonia Formation in Microwave Discharge from Quenching Reactions of NH Radicals by Hydrogen, Electrochem. Ind. Phys. Chem. 61 (1993) 925–926.

[125] J. Shah, T. Wu, J. Lucero, M.A. Carreon, M.L. Carreon, Nonthermal Plasma Synthesis of Ammonia over Ni-MOF-74, ACS Sustain. Chem. Eng. 7 (2019) 377–383. doi:10.1021/acssuschemeng.8b03705.

[126] J. Shah, W. Wang, A. Bogaerts, M.L. Carreon, Ammonia Synthesis by Radio Frequency Plasma Catalysis: Revealing the Underlying Mechanisms, ACS Appl. Energy Mater. 1 (2018) 4824–4839. doi:10.1021/acsaem.8b00898.

[127] J. Shah, J. Harrison, M. Carreon, Ammonia Plasma-Catalytic Synthesis Using Low Melting Point Alloys, Catalysts. 8 (2018) 437. doi:10.3390/catal8100437.

[128] M. Ben Yaala, A. Saeedi, D.-F. Scherrer, L. Moser, R. Steiner, M. Zutter, M. Oberkofler, G. De Temmerman, L. Marot, E. Meyer, Plasma-assisted catalytic formation of ammonia in N2-H2 plasma on tungsten surface, Phys. Chem. Chem. Phys. 21 (2019) 16623–16633. doi:10.1039/C9CP01139K.

[129] A.K. Brewer, R.R. Miller, The Synthesis of Ammonia in the Low Voltage Arc, J. Am. Chem. Soc. 53 (1931) 2968–2978.

[130] H. Kiyooka, O. Matsumoto, Reaction scheme of ammonia synthesis in the ECR plasmas, Plasma Chem. Plasma Process. 16 (1996) 547–562. doi:10.1007/BF01447008.

[131] M.D. Bai, X.Y. Bai, Z.T. Zhang, B. Mingdong, B. Xiyao, Z. Zhitao, Synthesis of ammonia in a strong electric field discharge at ambient pressure, Plasma Chem. Plasma Process. 20 (2000) 511–520. doi:10.1023/A:1007031906589.

[132] P. Vankan, T. Rutten, S. Mazouffre, D.C. Schram, R. Engeln, Absolute density measurements of ammonia produced via plasma-activated catalysis, Appl. Phys. Lett. 418 (2002) 2000–2003. doi:10.1063/1.1494104.

[133] J.H. Van Helden, W. Wagemans, G. Yagci, R.A.B. Zijlmans, D.C. Schram, R. Engeln, G. Lombardi, G.D. Stancu, J. Röpcke, Detailed study of the plasma-activated catalytic generation of ammonia in N2-H2plasmas, J. Appl. Phys. 101 (2007). doi:10.1063/1.2645828.

[134] J.H. Van Helden, P.J. Van Den Oever, W.M.M. Kessels, M.C.M. Van De Sanden, D.C. Schram, R. Engeln, Production Mechanisms of NH and NH2 Radicals in N2-H2 Plasmas, J. Phys. Chem. A. 3 (2007) 11460–11472.

[135] E. Carrasco, M. Jiménez-Redondo, I. Tanarro, V.J. Herrero, Neutral and ion chemistry in low pressure dc plasmas of H2/N2 mixtures: routes for the efficient production of NH3 and NH4+, Phys. Chem. Chem. Phys. 13 (2011) 19561–19572. doi:10.1039/c1cp22284h.

[136] T. Body, S. Cousens, J. Kirby, C. Corr, A volume-averaged model of nitrogen – hydrogen plasma chemistry to investigate ammonia production in a plasma-surface- interaction device, Plasma Phys. Control. Fusion. 60 (2018) 075011.

[137] T. Sakakura, N. Murakami, Y. Takatsuji, T. Haruyama, Nitrogen Fixation in a Plasma/Liquid Interfacial Reaction and Its Switching between Reduction and Oxidation, J. Phys. Chem. C. 124 (2020) 9401–9408. doi:10.1021/acs.jpcc.0c02392.

[138] W. Gao, J. Guo, P. Wang, Q. Wang, F. Chang, Q. Pei, W. Zhang, L. Liu, P. Chen, Production of ammonia via a chemical looping process based on metal imides as nitrogen carriers, Nat. Energy. 3 (2018) 1067–1075. doi:10.1038/s41560-018-0268-z.

[139] S. Kumari, S. Pishgar, M.E. Schwarting, W.F. Paxton, J.M. Spurgeon, Synergistic plasma-assisted electrochemical reduction of nitrogen to ammonia, Chem. Commun. 54 (2018) 13347–13350. doi:10.1039/c8cc07869f.

[140] T. Haruyama, T. Namise, N. Shimoshimizu, S. Uemura, Y. Takatsuji, M. Hino, R. Yamasaki, T. Kamachi, M. Kohno, Non-catalyzed one-step synthesis of ammonia from atmospheric air and water, Green Chem. 18 (2016) 4536–4541. doi:10.1039/c6gc01560c.

[141] T. Sakakura, S. Uemura, M. Hino, S. Kiyomatsu, Y. Takatsuji, R. Yamasaki, M. Morimoto, T. Haruyama, Excitation of H2O at the plasma/water interface by UV irradiation for the elevation of ammonia production, Green Chem. 20 (2018) 627–633. doi:10.1039/c7gc03007j.

[142] T. Sakakura, N. Murakami, Y. Takatsuji, M. Morimoto, T. Haruyama, Contribution of Discharge Excited Atomic N, N2*, and N2+ to a Plasma/Liquid Interfacial Reaction as Suggested by Quantitative Analysis, ChemPhysChem. 20 (2019) 1467–1474. doi:10.1002/cphc.201900212.

[143] T. Sakakura, Y. Takatsuji, M. Morimoto, T. Haruyama, Nitrogen Fixation through the Plasma/Liquid Interfacial Reaction with Controlled Conditions of Each Phase as the Reaction Locus, Electrochemistry. 88 (2020) 190–194. doi:10.5796/electrochemistry.19-00080.

[144] Y. Kubota, K. Koga, M. Ohno, T. Hara, Synthesis of Ammonia through Direct Chemical Reactions between an Atmospheric Nitrogen Plasma Jet and a Liquid, Plasma Fusion Res. 5 (2010) 042–042. doi:10.1585/pfr.5.042.

[145] H. Conrads, M. Schmidt, Plasma generation and plasma sources, Plasma Sources Sci. Technol. 9 (2000) 441–454. doi:10.1088/0963-0252/9/4/301.

[146] C. Tendero, C. Tixier, P. Tristant, J. Desmaison, P. Leprince, Atmospheric pressure plasmas: A review, Spectrochim. Acta - Part B At. Spectrosc. 61 (2006) 2–30. doi:10.1016/j.sab.2005.10.003.

[147] M. Laroussi, T. Akan, Arc-Free Atmospheric Pressure Cold Plasma Jets: A Review, Plasma Process. Polym. 4 (2007) 777–788. doi:10.1002/ppap.200700066.

[148] U. Ebert, S. Nijdam, C. Li, A. Luque, T. Briels, E. Van Veldhuizen, Review of recent results on streamer discharges and discussion of their relevance for sprites and lightning, J. Geophys. Res. 115 (2010) 1–13. doi:10.1029/2009JA014867.

[149] U. Ebert, C. Montijn, T.M.P. Briels, W. Hundsdorfer, B. Meulenbroek, A. Rocco, E. van Veldhuizen, The multiscale nature of streamers, Plasma Sources Sci. Technol. 15 (2006) S118–S129. doi:10.1088/0963-0252/15/2/S14.

[150] W. Wang, H. Kim, K. Van Laer, A. Bogaerts, Streamer propagation in a packed bed plasma reactor for plasma catalysis applications, Chem. Eng. J. 334 (2018) 2467–2479. doi:10.1016/j.cej.2017.11.139.

[151] H.-H. Kim, A. Ogata, Nonthermal plasma activates catalyst: From current understanding and future prospects, Eur. Phys. J. Appl. Phys. 55 (2011). doi:10.1051/epjap/2011100444.

[152] H.-H. Kim, Y. Teramoto, N. Negishi, A. Ogata, A multidisciplinary approach to understand the interactions of nonthermal plasma and catalyst: A review, Catal. Today. 256 (2015) 13–22. doi:10.1016/j.cattod.2015.04.009.

[153] H.-H. Kim, Y. Teramoto, T. Sano, N. Negishi, A. Ogata, Effects of Si/Al ratio on the interaction of nonthermal plasma and Ag/HY catalysts, Appl. Catal. B Environ. 166–167 (2015) 9–17. doi:10.1016/j.apcatb.2014.11.008.

[154] H.-H. Kim, Y. Teramoto, A. Ogata, Time-resolved imaging of positive pulsed corona-induced surface streamers on TiO2 and γ-Al2O3 supported Ag catalysts, J. Phys. D. Appl. Phys. 49 (2016) 415204. doi:10.1088/0022-3727/49/45/459501.

[155] A. Mizuno, H. Ito, Basic performance of an electrostatically augmented filter consisting of a packed ferroelectric pellet layer, J. Electrostat. 25 (1990) 97–107.

[156] T. Butterworth, R.W.K. Allen, Plasma-catalyst interaction studied in a single pellet DBD reactor: Dielectric constant effect on plasma dynamics, Plasma Sources Sci. Technol. 26 (2017). doi:10.1088/1361-6595/aa6c35.

[157] J. Kruszelnicki, K.W. Engeling, J.E. Foster, Propagation of negative electrical discharges through 2-dimensional packed bed reactors, J. Phys. D. Appl. Phys. 50 (2017) 25203. doi:10.1088/1361-6463/50/2/025203.

[158] K.W. Engeling, J. Kruszelnicki, M.J. Kushner, Time-resolved evolution of micro-discharges, surface ionization waves and plasma propagation in a two-dimensional packed bed reactor, Plasma Sources Sci. Technol. 27 (2018) 085002.

[159] S. Liu, L.R. Winter, J.G. Chen, Review of Plasma-Assisted Catalysis for Selective Generation of Oxygenates from CO2 and CH4, ACS Catal. 10 (2020) 2855–2871. doi:10.1021/acscatal.9b04811.

[160] F.J.J. Peeters, M.C.M. Van de Sanden, The influence of partial surface discharging on the electrical characterization of DBDs, Plasma Sources Sci. Technol. 24 (2015) 015016. doi:10.1088/0963-0252/24/1/015016.

[161] E.C. Neyts, A. Bogaerts, Understanding plasma catalysis through modelling and simulation — a review, J. Phys. D. Appl. Phys. 47 (2014) 1–18. doi:10.1088/0022-3727/47/22/224010.

[162] E.C. Neyts, Plasma-Surface Interactions in Plasma Catalysis, Plasma Chem. Plasma Process. 36 (2016) 185–212. doi:10.1007/s11090-015-9662-5.

[163] A. Bogaerts, Q. Zhang, Y. Zhang, K. Van Laer, W. Wang, Burning questions of plasma catalysis: Answers by modeling, Catal. Today. 337 (2019) 3–14. doi:10.1016/j.cattod.2019.04.077.

[164] J.C. Whitehead, Plasma-catalysis: Is it just a question of scale?, Front. Chem. Sci. Eng. 13 (2019) 264–273. doi:10.1007/s11705-019-1794-3.

[165] J.C. Whitehead, Plasma catalysis: A solution for environmental problems, Pure Appl. Chem. 82 (2010) 1329–1336. doi:10.1351/PAC-CON-10-02-39.

[166] J.C. Whitehead, Plasma-catalysis: Introduction and history, in: X. Tu, T. Nozaki, J.C. Whitehead (Eds.), Plasma Catal. Fundam. Appl., Springer International Publishing AG, 2018: pp. 1–19.

[167] J.C. Whitehead, Plasma-catalysis: The known knowns, the known unknowns and the unknown unknowns, J. Phys. D. Appl. Phys. 49 (2016). doi:10.1088/0022-3727/49/24/243001.

[168] K. Ostrikov, Plasma-nano-interface in perspective: From plasma-for-nano to

nano-plasmas, Plasma Phys. Control. Fusion. 61 (2019). doi:10.1088/1361-6587/aad770.

[169] E.C. Neyts, P. Brault, Molecular Dynamics Simulations for Plasma-Surface Interactions, Plasma Process. Polym. 14 (2017) 1–18. doi:10.1002/ppap.201600145.

[170] J. Van Durme, J. Dewulf, C. Leys, H. Van Langenhove, Combining non-thermal plasma with heterogeneous catalysis in waste gas treatment: A review, Appl. Catal. B Environ. 78 (2008) 324–333. doi:10.1016/j.apcatb.2007.09.035.

[171] B. Wang, X. Xu, W. Xu, N. Wang, H. Xiao, Y. Sun, H. Huang, L. Yu, The Mechanism of Non-thermal Plasma Catalysis on Volatile Organic Compounds Removal, Catal. Surv. from Asia. 22 (2018) 73–94. doi:10.1007/s10563-018-9241-x.

[172] K. Van Laer, A. Bogaerts, Fluid modelling of a packed bed dielectric barrier discharge plasma reactor, Plasma Sources Sci. Technol. 25 (2015). doi:10.1088/0963-0252/25/1/015002.

[173] K. Van Laer, A. Bogaerts, Influence of Gap Size and Dielectric Constant of the Packing Material on the Plasma Behaviour in a Packed Bed DBD Reactor: A Fluid Modelling Study, Plasma Process. Polym. 14 (2017). doi:10.1002/ppap.201600129.

[174] K. Van Laer, A. Bogaerts, How bead size and dielectric constant affect the plasma behaviour in a packed bed plasma reactor: a modelling study, Plasma Sources Sci. Technol. 26 (2017). doi:10.1088/1361-6595/aa7c59.

[175] M. Liu, Y. Yi, L. Wang, H. Guo, A. Bogaerts, Hydrogenation of Carbon Dioxide to Value-Added Chemicals by Heterogeneous Catalysis and Plasma Catalysis, Catalysts. 9 (2019). doi:10.3390/catal9030275.

[176] C.T. Rettner, H. Stein, Effect of vibrational energy on the dissociative chemisorption of N2 on Fe(111), J. Chem. Phys. 87 (1987) 770–771. doi:10.1063/1.453575.

[177] J. Kim, D.B. Go, J.C. Hicks, Synergistic effects of plasma-catalyst interactions for CH4 activation, Phys. Chem. Chem. Phys. 19 (2017) 13010–13021. doi:10.1039/c7cp01322a.

[178] J. Quan, F. Muttaqien, T. Kondo, T. Kozarashi, T. Mogi, T. Imabayashi, Y. Hamamoto, K. Inagaki, I. Hamada, Y. Morikawa, J. Nakamura, Vibration-driven reaction of CO2 on Cu surfaces via Eley–Rideal-type mechanism, Nat. Chem. 11 (2019) 722–729. doi:10.1038/s41557-019-0282-1.

[179] Y. Engelmann, K. van ’t Veer, Y. Gorbanev, E.C. Neyts, W.F. Schneider, A. Bogaerts, Plasma catalysis for ammonia synthesis: Contributions of Eley-Rideal

reactions, ACS Sustain. Chem. Eng. 9 (2021) 13151–13163. doi:10.1021/acssuschemeng.1c02713.

[180] Y. Gorbanev, Y. Engelmann, K. Van 't Veer, E. Vlasov, C. Ndayirinde, Y. Yi, S. Bals, A. Bogaerts, Al2O3-Supported Transition Metals for Plasma-Catalytic NH3 Synthesis in a DBD Plasma: Metal Activity and Insights into Mechanisms, Catalysts. 11 (2021) 1230. doi:10.3390/catal11101230.

[181] S.S.R.K.C. Yamijala, G. Nava, Z.A. Ali, D. Beretta, B.M. Wong, L. Mangolini, Harnessing Plasma Environments for Ammonia Catalysis: Mechanistic Insights from Experiments and Large-Scale Ab Initio Molecular Dynamics, J. Phys. Chem. Lett. 11 (2020) 10469–10475. doi:10.1021/acs.jpclett.0c03021.

[182] A. Jafarzadeh, K.M. Bal, A. Bogaerts, E.C. Neyts, Activation of CO2 on Copper Surfaces: The Synergy between Electric Field, Surface Morphology, and Excess Electrons, J. Phys. Chem. C. 124 (2020) 6747–6755. doi:10.1021/acs.jpcc.0c00778.

[183] K.M. Bal, S. Huygh, A. Bogaerts, E.C. Neyts, Effect of plasma-induced surface charging on catalytic processes: Application to CO2 activation, Plasma Sources Sci. Technol. 27 (2018). doi:10.1088/1361-6595/aaa868.

[184] K.M. Bal, E.C. Neyts, Overcoming Old Scaling Relations and Establishing New Correlations in Catalytic Surface Chemistry: Combined Effect of Charging and Doping, J. Phys. Chem. C. 123 (2019) 6141–6147. doi:10.1021/acs.jpcc.9b01216.

[185] C.J. Lee, D.H. Lee, T. Kim, Modification of catalyst surface from interaction between catalysts and dielectric barrier discharge plasma, J. Nanosci. Nanotechnol. 17 (2017) 2707–2710. doi:10.1166/jnn.2017.13352.

[186] Y. Guo, D. Ye, K. Chen, J. He, W. Chen, Toluene decomposition using a wire-plate dielectric barrier discharge reactor with manganese oxide catalyst in situ, J. Mol. Catal. A Chem. 245 (2006) 93–100. doi:10.1016/j.molcata.2005.09.013.

[187] U. Roland, F. Holzer, F.D. Kopinke, Improved oxidation of air pollutants in a non-thermal plasma, Catal. Today. 73 (2002) 315–323. doi:10.1016/S0920-5861(02)00015-9.

[188] Y.R. Zhang, K. Van Laer, E.C. Neyts, A. Bogaerts, Can plasma be formed in catalyst pores? A modeling investigation, Appl. Catal. B Environ. 185 (2016) 56–67. doi:10.1016/j.apcatb.2015.12.009.

[189] Q.Z. Zhang, A. Bogaerts, Propagation of a plasma streamer in catalyst pores, Plasma Sources Sci. Technol. 27 (2018). doi:10.1088/1361-6595/aab47a.

[190] Y.R. Zhang, E.C. Neyts, A. Bogaerts, Influence of the material dielectric constant on plasma generation inside catalyst pores, J. Phys. Chem. C. 120 (2016) 25923–25934. doi:10.1021/acs.jpcc.6b09038.

[191] Y.R. Zhang, E.C. Neyts, A. Bogaerts, Enhancement of plasma generation in catalyst pores with different shapes, Plasma Sources Sci. Technol. 27 (2018). doi:10.1088/1361-6595/aac0e4.

[192] Q.-Z. Zhang, W.-Z. Wang, A. Bogaerts, Importance of surface charging during plasma streamer propagation in catalyst pores, Plasma Sources Sci. Technol. 27 (2018). doi:10.1088/1361-6595/aaca6d.

[193] R. Kojima, K.-I. Aika, Cobalt molybdenum bimetallic nitride catalysts for ammonia synthesis, Chem. Lett. 29 (2000) 514–515.

[194] C.J.H. Jacobsen, S. Dahl, B.G.S. Clausen, S. Bahn, A. Logadottir, J.K. Nørskov, Catalyst Design by Interpolation in the Periodic Table: Bimetallic Ammonia Synthesis Catalysts, J. Am. Chem. Soc. 123 (2001) 8404–8405. doi:10.1021/ja010963d.

[195] T. Czerwiec, H. Michel, E. Bergmann, Low-pressure, high-density plasma nitriding: mechanisms, technology and results, Surf. Coatings Technol. 108–109 (1998) 182–190. doi:10.1016/S0257-8972(98)00555-6.

[196] J.S.J. Hargreaves, Nitrides as ammonia synthesis catalysts and as potential nitrogen transfer reagents, Appl. Petrochemical Res. 4 (2014) 3–10. doi:10.1007/s13203-014-0049-y.

[197] B. Ashford, X. Tu, Non-thermal plasma technology for the conversion of CO2, Curr. Opin. Green Sustain. Chem. 3 (2017) 45–49. doi:10.1016/j.cogsc.2016.12.001.

[198] E. Chiremba, K. Zhang, C. Kazak, G. Akay, Direct Nonoxidative Conversion of Methane to Hydrogen and Higher Hydrocarbons by Dielectric Barrier Discharge Plasma with Plasma Catalysis Promoters, AIChE J. 63 (2017) 4418–4429. doi:10.1002/aic.15769.

[199] M.L. Carreon, Plasma catalytic ammonia synthesis: state of the art and future directions, J. Phys. D. Appl. Phys. 52 (2019). doi:10.1088/1361-6463/ab3b2c.

[200] P. Peng, P. Chen, C. Schiappacasse, N. Zhou, E. Anderson, D. Chen, J. Liu, Y. Cheng, R. Hatzenbeller, M. Addy, Y. Zhang, Y. Liu, R. Ruan, A review on the non-thermal plasma-assisted ammonia synthesis technologies, J. Clean. Prod. 177 (2018) 597–609. doi:10.1016/j.jclepro.2017.12.229.

[201] M. Alsfeld, E. Wilhelmy, Über die Bildung von Ammoniak aus seinen Elementen durch elektrische Gasentladungen, Ann. Phys. 400 (1931) 89–123. doi:10.1002/andp.1931400010.

[202] W. von Siemens, Ueber die elektrostatische Induction und die Verzögerung des Stroms in Flaschendrähten, Ann. Phys. 178 (1857) 66–122. doi:10.1002/andp.18571780905.

[203] W.F. Donkin, On the direct synthesis of ammonia, London, Edinburgh, Dublin Philos. Mag. J. Sci. 21 (1873) 281–282. doi:10.1098/rspl.1872.0057.

[204] J.C. Devins, M. Burton, Formation of Hydrazine in Electric Discharge Decomposition of Ammonia, J. Am. Chem. Soc. 76 (1954) 2618–2626. doi:10.1021/ja01639a006.

[205] E.N. Eremin, A.N. Maltsev, V.L. Syaduk, Catalytic synthesis of ammonia in a barrier discharge, Russ J. Phys. Ch U.S.S.R. 45 (1971) 635–636.

[206] L. Petitjean, A. Ricard, Emission spectroscopy study of N2-H2 glow discharge for metal surface nitriding, J. Phys. D. Appl. Phys. 17 (1984) 919–929.

[207] J. Loureiro, A. Ricard, Electron and vibrational kinetics in an N2-H2 glow discharge with application to surface processes, J. Phys. D. Appl. Phys. (1993).

[208] J. Amorim, G. Baravian, A. Ricard, Production of N, H, and NH Active Species in N2-H2 dc Flowing Discharges, Plasma Chem. Plasma Process. 15 (1995) 721–731.

[209] P. Bletzinger, B.N. Ganguly, High fractional dissociation efficiency in H2 and H2-N2 gas mixtures in a helical resonator discharge, Chem. Phys. Lett. 247 (1995) 584–588.

[210] R. Nagpal, B.N. Ganguly, P. Bletzinger, A. Garscadden, Power deposition in H and H2-N2 glow discharges, Chem. Phys. Lett. 257 (1996) 386–392.

[211] J. Amorim, G. Baravian, S. Bockel, A. Ricard, G. Sultan, Laser and Emission Spectroscopy in H2 and H2-N2 dc Discharges, J. Phys. III. 6 (1996) 1147–1155.

[212] N.V. Srinath, Plasma catalytic ammonia synthesis at atmospheric pressure in a dielectric barrier discharge reactor, Eindhoven University of Technology, 2017.

[213] B.S. Patil, Plasma (catalyst) - assisted nitrogen fixation: reactor development for nitric oxide and ammonia production, Eindhoven University of Technology, 2017.

[214] X. Bai, S. Tiwari, B. Robinson, C. Killmer, L. Li, J. Hu, Microwave catalytic synthesis of ammonia from methane and nitrogen, Catal. Sci. Technol. 8 (2018) 6302–6305. doi:10.1039/c8cy01355a.

[215] L.G. Siemsen, The synthesis of ammonia from hydrogen and atomic nitrogen on the Rh(110) surface, Iowa State University, 1990.

[216] K.H.R. Rouwenhorst, L. Lefferts, Feasibility study of plasma-catalytic ammonia synthesis for energy storage applications, Catalysts. 10 (2020). doi:10.3390/catal10090999.

[217] J. Helminen, J. Helenius, E. Paatero, I. Turunen, Adsorption Equilibria of Ammonia Gas on Inorganic and Organic Sorbents at 298.15 K, J. Chem. Eng. Data. 46 (2001) 391–399. doi:10.1021/je000273+.

[218] J. Helminen, J. Helenius, E. Paatero, I. Turunen, Comparison of sorbents and isotherm models for NH3-gas separation by adsorption, AIChE J. 46 (2000) 1541–1555. doi:10.1002/aic.690460807.

[219] C.Y. Liu, K. Aika, Ammonia Absorption into Alkaline Earth Metal Halide Mixtures as an Ammonia Storage Material, Ind. Eng. Chem. Res. 43 (2004) 7484–7491. doi:10.1021/ie049874a.

[220] M. Malmali, G. Le, J. Hendrickson, J. Prince, A. McCormick, E. Cussler, Better Absorbents for Ammonia Separation, ACS Sustain. Chem. Eng. 6 (2018) 6536–6546. doi:10.1021/acssuschemeng.7b04684.

[221] M. Akiyama, K. Aihara, T. Sawaguchi, M. Matsukata, M. Iwamoto, Ammonia decomposition to clean hydrogen using non-thermal atmospheric-pressure plasma, Int. J. Hydrogen Energy. 43 (2018) 14493–14497. doi:10.1016/j.ijhydene.2018.06.022.

[222] M. Bai, Z. Zhang, H. Han, Y. Wang, X. Bai, Studies of ammonia synthesis in a strong ionization discharge at ambient pressure, Conf. Rec. - IAS Annu. Meet. (IEEE Ind. Appl. Soc. 2 (2001) 1103–1107. doi:10.1109/IAS.2001.955616.

[223] K.H.R. Rouwenhorst, H.G.B. Burbach, J. Núñez Paulí, D.W. Vogel, B. Geerdink, L. Lefferts, Plasma-Catalytic Ammonia Synthesis beyond Thermal Equilibrium on Ru-based Catalysts in Non-thermal Plasma, Catal. Sci. Technol. 11 (2021) 2834–2843. doi:10.1039/D0CY02189J.

[224] M. Muhler, F. Rosowski, O. Hinrichsen, A. Hornung, G. Ertl, Ruthenium as catalyst for ammonia synthesis, Stud. Surf. Sci. Catal. 101 (1996) 317–326. doi:10.1016/S0167-2991(96)80242-4.

[225] K.-I. Aika, Role of alkali promoter in ammonia synthesis over ruthenium catalysts—Effect on reaction mechanism, Catal. Today. 286 (2017) 14–20. doi:10.1016/j.cattod.2016.08.012.

[226] B. Hammer, J.K. Norskov, Theoretical Surface Science and Catalysis — Calculations and Concepts, Adv. Catal. 45 (2000) 71–129. doi:http://dx.doi.org/10.1016/S0360-0564(02)45013-4.

[227] A. Vojvodic, A.J. Medford, F. Studt, F. Abild-Pedersen, T.S. Khan, T. Bligaard, J.K. Nørskov, Exploring the limits: A low-pressure, low-temperature Haber-Bosch process, Chem. Phys. Lett. 598 (2014) 108–112. doi:10.1016/j.cplett.2014.03.003.

[228] G. Ertl, Mechanisms of Heterogeneous Catalysis, in: React. Solid Surfaces, 1st ed., John Wiley & Sons, Inc., Hoboken (NJ), 2009: pp. 123–139.

[229] J.J. Mortensen, B. Hammer, J.K. Nørskov, Alkali promotion of N2 dissociation over Ru(0001), Phys. Rev. Lett. 80 (1998) 4333–4336.

doi:10.1103/PhysRevLett.80.4333.

[230] Y. Yi, L. Wang, Y. Guo, S. Sun, H. Guo, Plasma-assisted ammonia decomposition over Fe–Ni alloy catalysts for COx-Free hydrogen, AIChE J. 65 (2019) 691–701. doi:10.1002/aic.16479.

[231] L. Wang, Y. Yi, H. Guo, X. Du, B. Zhu, Y. Zhu, Highly Dispersed Co Nanoparticles Prepared by an Improved Method for Plasma-Driven NH3 Decomposition to Produce H2, Catalysts. 9 (2019) 107. doi:10.3390/catal9020107.

[232] S.Q. Sun, Y.H. Yi, L. Wang, J.L. Zhang, H.C. Guo, Preparation and performance of supported bimetallic catalysts for hydrogen production from ammonia decomposition by plasma catalysis, Wuli Huaxue Xuebao/ Acta Phys. - Chim. Sin. 33 (2017) 1123–1129. doi:10.3866/PKU.WHXB201703301.

[233] L. Wang, Y. Yi, Y. Guo, Y. Zhao, J. Zhang, H. Guo, Synergy of DBD plasma and Fe-based catalyst in NH3 decomposition: Plasma enhancing adsorption step, Plasma Process. Polym. 14 (2017). doi:10.1002/ppap.201600111.

[234] L. Wang, Y. Zhao, C. Liu, W. Gong, H. Guo, Plasma driven ammonia decomposition on a Fe-catalyst: Eliminating surface nitrogen poisoning, Chem. Commun. 49 (2013) 3787–3789. doi:10.1039/c3cc41301b.

[235] L. Wang, Y. Yi, Y. Zhao, R. Zhang, J. Zhang, H. Guo, NH3 Decomposition for H2 Generation: Effects of Cheap Metals and Supports on Plasma-Catalyst Synergy, ACS Catal. 5 (2015) 4167–4174. doi:10.1021/acscatal.5b00728.

[236] P. Mehta, P. Barboun, Y. Engelmann, D.B. Go, A. Bogaerts, W.F. Schneider, J.C. Hicks, Plasma-Catalytic Ammonia Synthesis Beyond the Equilibrium Limit, ACS Catal. 10 (2020) 6726–6734. doi:10.1021/acscatal.0c00684.

[237] H.H. Himstedt, M.S. Huberty, A. V. McCormick, L.D. Schmidt, E.L. Cussler, Ammonia synthesis enhanced by magnesium chloride absorption, AIChE J. 61 (2015) 1364–1371. doi:10.1002/aic.14733.

[238] C.Y. Liu, K.-I. Aika, Ammonia Adsorption on Ion Exchanged Y-zeolites as Ammonia Storage Material, J. Japan Pet. Inst. 46 (2003) 301–307. doi:10.1627/jpi.46.301.

[239] C.Y. Liu, K. Aika, Modification of active carbon and zeolite as ammonia separation materials for a new de-NOx process with ammonia on-site synthesis, Res. Chem. Intermed. 28 (2002) 409–417. doi:10.1163/156856702760346824.

[240] S. Zen, T. Abe, Y. Teramoto, Indirect Synthesis System for Ammonia from Nitrogen and Water Using Nonthermal Plasma Under Ambient Conditions, Plasma Chem. Plasma Process. 38 (2018) 347–354. doi:10.1007/s11090-017-9869-8.

[241] S. Zen, T. Abe, Y. Teramoto, Atmospheric Pressure Nonthermal Plasma Synthesis of Magnesium Nitride as a Safe Ammonia Carrier, Plasma Chem. Plasma Process. 39 (2019) 1203–1210. doi:10.1007/s11090-019-10002-z.

[242] Y. Hayakawa, T. Miura, K. Shizuya, S. Wakazono, K. Tokunaga, S. Kambara, Hydrogen production system combined with a catalytic reactor and a plasma membrane reactor from ammonia, Int. J. Hydrogen Energy. 44 (2019) 9987–9993. doi:10.1016/j.ijhydene.2018.12.141.

[243] A.R. Hanna, T.L. Van Surksum, E.R. Fisher, Investigating the impact of catalysts on N2 rotational and vibrational temperatures in low pressure plasmas, J. Phys. D. Appl. Phys. 52 (2019) 345202. doi:10.1088/1361-6463/ab2291.

[244] A.N.C.L.A. Maltsev, E.N. Eremin, Activity of heterogeneous catalysts in the synthesis of ammonia in the glow discharge, Russ. J. Phys. Chem. 9 (1968) 1235–1237.

[245] A.K. Brewer, J.W. Westhaver, Chemical Action in the Glow Discharge. IV, J. Phys. Chem. 34 (1930) 1280–1293. doi:10.1021/j150312a012.

[246] E.N. Eremin, A.N. Maltsev, Behaviour of a catalyst in a glow-discharge plasma, Russ. J. Phys. Chem. 3 (1969) 43.

[247] A. de Castro, F.L. Tabarés, Role of nitrogen inventory and ion enhanced N-H recombination in the ammonia formation on tungsten walls. A DC glow discharge study, Vacuum. 151 (2018) 66–72. doi:10.1016/j.vacuum.2018.02.004.

[248] Y. Zhao, L. Wang, J. Zhang, H. Guo, Enhancing the ammonia to hydrogen (ATH) energy efficiency of alternating current arc discharge, Int. J. Hydrogen Energy. 39 (2014) 7655–7663. doi:10.1016/j.ijhydene.2014.03.128.

[249] Y. Zhao, L. Wang, J.L. Zhang, H.C. Guo, Influence of non-thermal plasma discharge mode and reactor structure on ammonia decomposition to hydrogen, Wuli Huaxue Xuebao/ Acta Phys. - Chim. Sin. 30 (2014) 738–744. doi:10.3866/PKU.WHXB201402141.

[250] J.G. Chen, R.M. Crooks, L.C. Seefeldt, K.L. Bren, R.M. Bullock, M.Y. Darensbourg, P.L. Holland, B. Hoffman, M.J. Janik, A.K. Jones, M.G. Kanatzidis, P. King, K.M. Lancaster, S. V. Lymar, P. Pfromm, W.F. Schneider, R.R. Schrock, Beyond fossil fuel–driven nitrogen transformations, Science (80-.). 360 (2018). doi:10.1126/science.aar6611.

[251] Y. Engelmann, K. van 't Veer, E.C. Neyts, W.F. Schneider, A. Bogaerts, Plasma catalysis for ammonia synthesis: the importance of Eley-Rideal reactions, (n.d.).

[252] S. Wang, V. Petzold, V. Tripkovic, J. Kleis, J.G. Howalt, E. Skúlason, E.M. Fernández, B. Hvolbæk, G. Jones, A. Toftelund, H. Falsig, M. Björketun, F. Studt, F. Abild-Pedersen, J. Rossmeisl, J.K. Nørskov, T. Bligaard, Universal transition

state scaling relations for (de)hydrogenation over transition metals, Phys. Chem. Chem. Phys. 13 (2011) 20760–20765. doi:10.1039/c1cp20547a.

[253] K. Van 't Veer, Y. Engelmann, F. Reniers, A. Bogaerts, Plasma-catalytic ammonia synthesis in a DBD plasma: Role of the micro-discharges and their afterglows, J. Phys. Chem. C. 124 (2020) 22871–22883. doi:10.1021/acs.jpcc.0c05110.

[254] W. Wang, B. Patil, S. Heijkers, V. Hessel, A. Bogaerts, Nitrogen Fixation by Gliding Arc Plasma: Better Insight by Chemical Kinetics Modelling, ChemSusChem. 10 (2017) 2145–2157. doi:10.1002/cssc.201700095.

[255] E. Vervloessem, M. Aghaei, F. Jardali, N. Hafezkhiabani, A. Bogaerts, Plasma-based N2 fixation into NOx: Insights from modeling toward optimum yields and energy costs in a gliding arc plasmatron, ACS Sustain. Chem. Eng. 8 (2020) 9711–9720. doi:10.1021/acssuschemeng.0c01815.

[256] J.S. Hummelshøj, F. Abild-pedersen, F. Studt, T. Bligaard, J.K. Nørskov, CatApp: A web application for surface chemistry and heterogeneous catalysis, Angew. Chemie - Int. Ed. 51 (2012) 272–274. doi:10.1002/anie.201107947.

[257] K.-I. Aika, A. Ohya, A. Ozaki, Y. Inoue, I. Yasumori, Support and promoter effect of ruthenium catalyst: II. Ruthenium/alkaline earth catalyst for activation of dinitrogen, J. Catal. 92 (1985) 305–311. doi:10.1016/0021-9517(85)90265-9.

[258] K. Aika, M. Kumasaka, T. Oma, O. Kato, H. Matsuda, N. Watanabe, K. Yamazaki, A. Ozaki, T. Onishi, Support and promoter effect of ruthenium catalyst. III. Kinetics of ammonia synthesis over various Ru catalysts, Appl. Catal. 28 (1986) 57–68. doi:10.1016/S0166-9834(00)82492-6.

[259] K.-I. Aika, K. Shimazaki, Y. Hattori, A. Ohya, S. Ohshima, K. Shirota, A. Ozaki, Support and promoter effect of ruthenium catalyst. I. Characterization of alkali-promoted ruthenium/alumina catalysts for ammonia synthesis, J. Catal. 92 (1985) 296–304. doi:10.1016/0021-9517(85)90264-7.

[260] R. Pandya, R. Mane, C. V. Rode, Cascade dehydrative amination of glycerol to oxazoline, Catal. Sci. Technol. 8 (2018) 2954–2965. doi:10.1039/c8cy00185e.

[261] S. Dahl, A. Logadottir, R.C. Egeberg, J.H. Larsen, I. Chorkendorff, E. Törnqvist, J.K. Nørskov, Role of Steps in N2 Activation on Ru(0001), Phys. Rev. Lett. 83 (1999) 1814–1817. doi:10.1103/PhysRevLett.83.1814.

[262] M.J. Murphy, J.F. Skelly, A. Hodgson, B. Hammer, Inverted vibrational distributions from N2 recombination at Ru(001): Evidence for a metastable molecular chemisorption well, J. Chem. Phys. 110 (1999) 6954–6962. doi:10.1063/1.478601.

[263] L. Diekhöner, H. Mortensen, A. Baurichter, N2 dissociative adsorption on Ru(0001): The role of energy loss, J. Chem. Phys. 115 (2001) 9028–9035.

doi:10.1063/1.1413746.

[264] L.B.F. Juurlink, R.R. Smith, D.R. Killelea, A.L. Utz, Comparative study of C-H stretch and bend vibrations in methane activation on Ni(100) and Ni(111), Phys. Rev. Lett. 94 (2005). doi:10.1103/PhysRevLett.94.208303.

[265] L.B.F. Juurlink, R.R. Smith, A.L. Utz, The role of rotational excitation in the activated dissociative chemisorption of vibrationally excited methane on Ni(100), Faraday Discuss. 117 (2000) 147–160.

[266] L.B.F. Juurlink, P.R. Mccabe, R.R. Smith, C.L. Dicologero, A.L. Utz, Eigenstate-resolved studies of gas-surface reactivity: CH4(v3) Dissociation on Ni(100), Phys. Rev. Lett. 83 (1999) 868–871. doi:10.1103/PhysRevLett.83.868.

[267] Y. Teramoto, H.-H. Kim, Effect of vibrationally excited N2(v) on atomic nitrogen generation using two consecutive pulse corona discharges under atmospheric pressure N2, J. Phys. D. Appl. Phys. 52 (2019). doi:10.1088/1361-6463/ab3f83.

[268] S. Van Alphen, V. Vermeiren, T. Butterworth, D.C.M. van den Bekerom, G.J. Van Rooij, A. Bogaerts, Power Pulsing to Maximize Vibrational Excitation Efficiency in N2 Microwave Plasma: A Combined Experimental and Computational Study, J. Phys. Chem. C. 124 (2019) 1765–1779. doi:10.1021/acs.jpcc.9b06053.

[269] G. Colonna, A. Laricchiuta, L.D. Pietanza, Time dependent selfconsistent electron energy distribution functions during nano-second repetitive discharges in reacting N2/H2 mixtures, Plasma Phys. Control. Fusion. 62 (2020). doi:10.1088/1361-6587/ab469e.

[270] A. Jafarzadeh, K.M. Bal, A. Bogaerts, E.C. Neyts, CO2 Activation on TiO2-Supported Cu5 and Ni5 Nanoclusters: Effect of Plasma-Induced Surface Charging, J. Phys. Chem. C. 123 (2019) 6516–6525. doi:10.1021/acs.jpcc.8b11816.

[271] M.A. Ardagh, O.A. Abdelrahman, P.J. Dauenhauer, Principles of Dynamic Heterogeneous Catalysis: Surface Resonance and Turnover Frequency Response, ACS Catal. 9 (2019) 6929–6937. doi:10.1021/acscatal.9b01606.

[272] M.A. Ardagh, T. Birol, Q. Zhang, O.A. Abdelrahman, P.J. Dauenhauer, Catalytic resonance theory: SuperVolcanoes, catalytic molecular pumps, and oscillatory steady state, Catal. Sci. Technol. 9 (2019) 5058–5076. doi:10.1039/c9cy01543d.

[273] Z. Mujahid, J. Kruszelnicki, A. Hala, M.J. Kushner, Formation of surface ionization waves in a plasma enhanced packed bed reactor for catalysis applications, Chem. Eng. J. 382 (2020). doi:10.1016/j.cej.2019.123038.

[274] P. Navascués, J.M. Obrero-Pérez, J. Cotrino, A.R. González-Elipe, A. Gómez-Ramírez, Isotope labelling for reaction mechanism analysis in DBD plasma processes, Catalysts. 9 (2019) 1–12. doi:10.3390/catal9010045.

[275] A. Fateev, F. Leipold, Y. Kusano, B. Stenum, E. Tsakadze, H. Bindslev, Plasma Chemistry in an Atmospheric Pressure Ar/NH3 Dielectric Barrier Discharge, Plasma Process. Polym. 2 (2005) 193–200. doi:10.1002/ppap.200400051.

[276] M. Boudart, Ammonia synthesis: The bellwether reaction in heterogeneous catalysis, Top. Catal. 1 (1994) 405–414. doi:10.1007/BF01492292.

[277] N. Cherkasov, A.O. Ibhadon, P. Fitzpatrick, A review of the existing and alternative methods for greener nitrogen fixation, Chem. Eng. Process. Process Intensif. 90 (2015) 24–33. doi:10.1016/j.cep.2015.02.004.

[278] J.R. Brightling, Ammonia and the fertiliser industry: The development of ammonia at Billingham, Johnson Matthey Technol. Rev. 62 (2018) 32–47. doi:10.1595/205651318X696341.

[279] F.Y. Hansen, N.E. Henriksen, G.D. Billing, A. Guldberg, Catalytic synthesis of ammonia using vibrationally excited nitrogen molecules: theoretical calculation of equilibrium and rate constants, Surf. Sci. 264 (1992) 225–234. doi:10.1016/0039-6028(92)90180-E.

[280] S. Li, J.A.M. Jimenez, V. Hessel, F. Gallucci, Recent Progress of Plasma-Assisted Nitrogen Fixation Research: A Review, Processes. 6 (2018). doi:10.3390/pr6120248.

[281] H. Liu, Ammonia Synthesis Catalysts: Innovation and Practice, World Scientific, 2013. doi:10.1142/8199.

[282] H. Liu, Ammonia synthesis catalyst 100 years: Practice, enlightenment and challenge, Cuihua Xuebao/Chinese J. Catal. 35 (2014) 1619–1640. doi:10.1016/S1872-2067(14)60118-2.

[283] H. Liu, W. Han, Wüstite-based catalyst for ammonia synthesis : Structure , property and performance, Catal. Today. 297 (2017) 276–291. doi:10.1016/j.cattod.2017.04.062.

[284] N. Saadatjou, A. Jafari, S. Sahebdelfar, Ruthenium Nanocatalysts for Ammonia Synthesis: A Review, Chem. Eng. Commun. 202 (2015) 420–448. doi:10.1080/00986445.2014.923995.

[285] Y. Kobayashi, M. Kitano, S. Kawamura, T. Yokoyama, H. Hosono, Kinetic evidence: The rate-determining step for ammonia synthesis over electride-supported Ru catalysts is no longer the nitrogen dissociation step, Catal. Sci. Technol. 7 (2017) 47–50. doi:10.1039/c6cy01962e.

[286] M. Kitano, Y. Inoue, Y. Yamazaki, F. Hayashi, S. Kanbara, S. Matsuishi, T. Yokoyama, S.W. Kim, M. Hara, H. Hosono, Ammonia synthesis using a stable electride as an electron donor and reversible hydrogen store, Nat. Chem. 4 (2012) 934–940. doi:10.1038/nchem.1476.

[287] Y. Inoue, M. Kitano, K. Kishida, H. Abe, Y. Niwa, M. Sasase, Y. Fujita, H. Ishikawa, T. Yokoyama, M. Hara, H. Hosono, Efficient and Stable Ammonia Synthesis by Self-Organized Flat Ru Nanoparticles on Calcium Amide, ACS Catal. 6 (2016) 7577–7584. doi:10.1021/acscatal.6b01940.

[288] M. Kitano, S. Kanbara, Y. Inoue, N. Kuganathan, P. V. Sushko, T. Yokoyama, M. Hara, H. Hosono, Electride support boosts nitrogen dissociation over ruthenium catalyst and shifts the bottleneck in ammonia synthesis, Nat. Commun. 6 (2015) 1–9. doi:10.1038/ncomms7731.

[289] K.-I. Aika, J. Kubota, Y. Kadowaki, Y. Niwa, Y. Izumi, Molecular sensing techniques for the characterization and design of new ammonia catalysts, Appl. Surf. Sci. 121–122 (1997) 488–491. doi:10.1016/S0169-4332(97)00343-7.

[290] A. Ozaki, Development of alkali-promoted ruthenium as a novel catalyst for ammonia synthesis, Acc. Chem. Res. 14 (1981) 16–21. doi:10.1021/ar00061a003.

[291] R. Ruan, S. Deng, Z. Le, P. Chen, Non-thermal plasma synthesis of ammonia, WO2009025835A1, 2009.

[292] G. Giammaria, G. van Rooij, L. Lefferts, Plasma Catalysis: Distinguishing between Thermal and Chemical Effects, Catalysts. 9 (2019) 185. doi:10.3390/catal9020185.

[293] N. Jidenko, E. Bourgeois, J.P. Borra, Temperature profiles in filamentary dielectric barrier discharges at atmospheric pressure, J. Phys. D. Appl. Phys. 43 (2010). doi:10.1088/0022-3727/43/29/295203.

[294] M. Simek, V. Babicky, M. Clupek, S. DeBenedictis, G. Dilecce, P. Sunka, Excitation of N2(C 3Πu) and NO(A 2Σ+) states in a pulsed positive corona discharge in N2, N2-O2 and N2-NO mixtures, J. Phys. D. Appl. Phys. 31 (1998) 2591–2602. doi:10.1088/0022-3727/31/19/032.

[295] J. Pinart, M. Smirdec, D. Tessier, J.J. Aaron, M. Goldman, A. Goldman, Quantitative study of the formation of inorganic chemical species following corona discharge. II. Effect of SO 2 traces on the production of HNO 2 and HNO 3 in a humid atmosphere, Atmos. Environ. 31 (1997) 3407–3412. doi:10.1016/S1352-2310(97)00121-0.

[296] J.F. Noxon, Active nitrogen at high pressure, J. Chem. Phys. 36 (1962) 926–940. doi:10.1063/1.1732691.

[297] C.R. Mclarnon, V.K. Mathur, Nitrogen Oxide Decomposition by Barrier Discharge, Ind. Eng. Chem. Res. 39 (2000) 2779–2787. doi:10.1021/ie990754q.

[298] A.A. Fridman, V.D. Rusanov, Theoretical basis of non-equilibrium near atmospheric pressure plasma chemistry, Pure Appl. Chem. 66 (1994) 1267–1278.

doi:10.1351/pac199466061267.

[299] J. Hong, S. Pancheshnyi, E. Tam, J.J. Lowke, S. Prawer, A.B. Murphy, Kinetic modelling of NH3 production in N2-H2 non-equilibrium atmospheric-pressure plasma catalysis, J. Phys. D. Appl. Phys. 50 (2017). doi:10.1088/1361-6463/aa6229.

[300] S. Hagen, R. Barfod, R. Fehrmann, C.J.H. Jacobsen, H.T. Teunissen, I. Chorkendorff, Ammonia synthesis with barium-promoted iron-cobalt alloys supported on carbon, J. Catal. 214 (2003) 327–335. doi:10.1016/S0021-9517(02)00182-3.

[301] C. Leterme, C. Fernández, P. Eloy, E.M. Gaigneaux, P. Ruiz, The inhibitor role of NH3 on its synthesis process at low temperature, over Ru catalytic nanoparticles, Catal. Today. 286 (2017) 85–100. doi:10.1016/j.cattod.2017.01.002.

[302] K. Nagaoka, T. Eboshi, Y. Takeishi, R. Tasaki, K. Honda, K. Imamura, K. Sato, Carbon-free H2 production from ammonia triggered at room temperature with an acidic RuO2/γ-Al2O3 catalyst, Sci. Adv. 3 (2017). doi:10.1126/sciadv.1602747.

[303] Z. Kowalczyk, M. Krukowski, W. Raróg-Pilecka, D. Szmigiel, J. Zielinski, Carbon-based ruthenium catalyst for ammonia synthesis: Role of the barium and caesium promoters and carbon support, Appl. Catal. A Gen. 248 (2003) 67–73. doi:10.1016/S0926-860X(03)00150-9.

[304] R.R. Smith, D.R. Killelea, D.F. DelSesto, A.L. Utz, Preference for Vibrational over Translational Energy in a Gas-Surface Reaction, Science (80-.). 304 (2004) 992–995. doi:10.1126/science.1096309.

[305] P.M. Holmblad, J. Wambach, I. Chorkendorff, Molecular beam study of dissociative sticking of methane on Ni(100), J. Chem. Phys. 102 (1995) 8255–8263. doi:10.1063/1.468955.

[306] K.H.R. Rouwenhorst, F. Jardali, A. Bogaerts, L. Lefferts, Plasma-based NOX synthesis: From the Birkeland-Eyde process towards energy-efficient and cost-effective plasma technology, Energy Environ. Sci. (2021). doi:Under revision.

[307] P.J. Bruggeman, F. Iza, R. Brandenburg, Foundations of atmospheric pressure non-equilibrium plasmas, Plasma Sources Sci. Technol. 26 (2017). doi:10.1088/1361-6595/aa97af.

[308] G. Ertl, Surface Science and Catalysis—Studies on the Mechanism of Ammonia Synthesis: The P. H. Emmett Award Address, Catal. Rev. 21 (1980) 201–223. doi:10.1080/03602458008067533.

[309] K.H.R. Rouwenhorst, P.M. Krzywda, N.E. Benes, G. Mul, L. Lefferts, Ammonia Production Technologies, in: R. Bañares-Alcántara, A. Valera-Medina (Eds.), Techno-Economic Challenges Green Ammon. as Energy Vector, Elsevier Science

Publishing Co Inc, 2020: pp. 41–84. doi:10.1016/B978-0-12-820560-0.00004-7.

[310] K.H.R. Rouwenhorst, Y. Engelmann, K. Van 't Veer, R.S. Postma, A. Bogaerts, L. Lefferts, Plasma-driven catalysis: green ammonia synthesis with intermittent electricity, Green Chem. 22 (2020) 6258–6287. doi:10.1039/D0GC02058C.

[311] C. Díaz, J.K. Vincent, G.P. Krishnamohan, R.A. Olsen, G.J. Kroes, K. Honkala, J.K. Nørskov, Multidimensional effects on dissociation of N2 on Ru(0001), Phys. Rev. Lett. 96 (2006). doi:10.1103/PhysRevLett.96.096102.

[312] C. Díaz, J.K. Vincent, G.P. Krishnamohan, R.A. Olsen, G.J. Kroes, K. Honkala, J.K. Nørskov, Reactive and nonreactive scattering of N2 from Ru(0001): A six-dimensional adiabatic study, J. Chem. Phys. 125 (2006). doi:10.1063/1.2229197.

[313] L. Romm, G. Katz, R. Kosloff, M. Asscher, Dissociative Chemisorption of N2 on Ru(001) Enhanced by Vibrational and Kinetic Energy: Molecular Beam Experiments and Quantum Mechanical Calculations, J. Phys. Chem. B. 101 (1997) 2213–2217. doi:10.1021/jp962599o.

[314] R.C. Egeberg, J.H. Larsen, I. Chorkendorff, Molecular beam study of N2 dissociation on Ru(0001), Phys. Chem. Chem. Phys. 3 (2001) 2007–2011. doi:10.1039/b101177o.

[315] T.R. Munter, T. Bligaard, C.H. Christensen, J.K. Nørskov, BEP relations for N2 dissociation over stepped transition metal and alloy surfaces, Phys. Chem. Chem. Phys. 10 (2008) 5202–5206. doi:10.1039/b720021h.

[316] A. Logadottir, T.H. Rod, J.K. Nørskov, B. Hammer, S. Dahl, C.J.H. Jacobsen, The Brønsted-Evans-Polanyi relation and the volcano plot for ammonia synthesis over transition metal catalysts, J. Catal. 197 (2001) 229–231. doi:10.1006/jcat.2000.3087.

[317] H. Falsig, J. Shen, T.S. Khan, W. Guo, G. Jones, S. Dahl, T. Bligaard, On the structure sensitivity of direct NO decomposition over low-index transition metal facets, Top. Catal. 57 (2014) 80–88. doi:10.1007/s11244-013-0164-5.

[318] J.J. Mortensen, B. Hammer, J.K. Nørskov, A theoretical study of adsorbate-adsorbate interactions on Ru(0001), Surf. Sci. 414 (1998) 315–329. doi:10.1016/S0039-6028(98)00311-2.

[319] Á. Logadóttir, J.K. Nørskov, Ammonia synthesis over a Ru(0001) surface studied by density functional calculations, J. Catal. 220 (2003) 273–279. doi:10.1016/S0021-9517(03)00156-8.

[320] J.J. Mortensen, Y. Morikawa, B. Hammer, J.K. Nørskov, Density Functional Calculations of N2 Adsorption and Dissociation on a Ru(0001) Surface, J. Catal. 169 (1997) 85–92. doi:10.1006/jcat.1997.1661.

[321] H.N. Kucukarpaci, J. Lucas, Simulation of electron swarm parameters in carbon dioxide and nitrogen for high E/N, J. Phys. D. Appl. Phys. 12 (1979). doi:10.1088/0022-3727/12/12/014.

[322] K. van 't Veer, S. van Alphen, A. Remy, Y. Gorbanev, N. De Geyter, R. Snyders, F. Reniers, A. Bogaerts, Spatially and temporally non-uniform plasmas: microdischarges from the perspective of molecules in a packed bed plasma reactor, J. Phys. D. Appl. Phys. 54 (2021). doi:10.1088/1361-6463/abe15b.

[323] A. Lofthus, P.H. Krupenie, The spectrum of molecular nitrogen, J. Phys. Chem. Ref. Data. 6 (1977) 113–307. doi:10.1063/1.555546.

[324] M. Shetty, M.A. Ardagh, Y. Pang, O.A. Abdelrahman, P.J. Dauenhauer, Electric-Field-Assisted Modulation of Surface Thermochemistry, ACS Catal. 10 (2020) 12867–12880. doi:10.1021/acscatal.0c02124.

[325] A. Susarrey-Arce, R.M. Tiggelaar, J.G.E. Gardeniers, A. Van Houselt, L. Lefferts, CO Adsorption on Pt Nanoparticles in Low E-Fields Studied by ATR-IR Spectroscopy in a Microreactor, J. Phys. Chem. C. 119 (2015) 24887–24894. doi:10.1021/acs.jpcc.5b08392.

[326] E. Slikboer, K. Acharya, A. Sobota, E. Garcia-Caurel, O. Guaitella, Revealing Plasma-Surface Interaction at Atmospheric Pressure: Imaging of Electric Field and Temperature inside the Targeted Material, Sci. Rep. 10 (2020). doi:10.1038/s41598-020-59345-0.

[327] A.W. Johnson, R.G. Fowler, Measured lifetimes of rotational and vibrational levels of electronic states of N2, J. Chem. Phys. 53 (1970) 65–72. doi:10.1063/1.1673834.

[328] N. García-Moncada, G. van Rooij, T. Cents, L. Lefferts, Catalyst-assisted DBD plasma for coupling of methane: minimizing carbon-deposits by structured reactors, Catal. Today. 369 (2021) 210–220. doi:10.1016/j.cattod.2020.04.028.

[329] N. García-Moncada, T. Cents, G. van Rooij, L. Lefferts, Minimizing carbon deposition in plasma-induced methane coupling with structured hydrogenation catalysts, J. Energy Chem. 58 (2021) 271–279. doi:10.1016/j.jechem.2020.09.006.

[330] K.H.R. Rouwenhorst, L. Lefferts, On the mechanism for the plasma-activated N2 dissociation on Ru surfaces, J. Phys. D. Appl. Phys. 54 (2021) 393002. doi:10.1088/1361-6463/ac1226.

[331] K. Aika, T. Takano, S. Murata, Preparation and characterization of chlorine-free ruthenium catalysts and the promoter effect in ammonia synthesis. 3. A magnesia-supported ruthenium catalyst, J. Catal. 136 (1992) 126–140. doi:10.1016/0021-9517(92)90112-U.

[332] F. Hayashi, Y. Toda, Y. Kanie, M. Kitano, Y. Inoue, T. Yokoyama, M. Hara, H. Hosono, Ammonia decomposition by ruthenium nanoparticles loaded on inorganic electride C12A7:e–, Chem. Sci. (2013) 3124–3130. doi:10.1039/c3sc50794g.

[333] J.C. Ganley, F.S. Thomas, E.G. Seebauer, R.I. Masel, A Priori Catalytic Activity Correlations: The Difficult Case of Hydrogen Production from Ammonia, Catal. Letters. 96 (2004) 117–122. doi:10.1023/B:CATL.0000030108.50691.d4.

[334] B.S. Patil, A.S.R. van Kaathoven, F. Peeters, N. Cherkasov, Q. Wang, J. Lang, V. Hessel, Deciphering the synergy between plasma and catalyst support for ammonia synthesis in a packed DBD reactor, J. Phys. D. Appl. Phys. 53 (2020) 144003. doi:10.1088/1361-6463/ab6a36.

[335] D.R. Strongin, G.A. Somorjai, The effects of potassium on ammonia synthesis over iron single-crystal surfaces, J. Catal. 109 (1988) 51–60. doi:10.1016/0021-9517(88)90184-4.

[336] B.S. Patil, N. Cherkasov, N.V. Srinath, J. Lang, A.O. Ibhadon, Q. Wang, V. Hessel, The role of heterogeneous catalysts in the plasma-catalytic ammonia synthesis, Catal. Today. 362 (2020) 2–10. doi:10.1016/j.cattod.2020.06.074.

[337] Y. Uytdenhouwen;, K.M. Bal;, E.C. Neyts;, V. Meynen;, P. Cool, A. Bogaerts, How process parameters and packing materials tune chemical equilibrium and kinetics in plasma-based CO2 conversion, Chem. Eng. J. 372 (2019) 1253–1264. doi:10.1016/j.cej.2019.05.008.

[338] J. Kim, M.S. Abbott, D.B. Go, J.C. Hicks, Enhancing C-H Bond Activation of Methane via Temperature-Controlled, Catalyst-Plasma Interactions, ACS Energy Lett. 1 (2016) 94–99. doi:10.1021/acsenergylett.6b00051.

[339] K.C. Szeto, S. Norsic, L. Hardou, E. Le Roux, S. Chakka, J. Thivolle-cazat, A. Baudouin, C. Papaioannou, J.-M. Basset, M. Taoufik, Non-oxidative coupling of methane catalysed by supported tungsten hydride onto alumina and silica–alumina in classical and H2 permeable membrane fixed-bed reactors, Chem. Commun. (2010) 3985–3987. doi:10.1039/c0cc00007h.

[340] P. Navascués, J.M. Obrero-Pérez, J. Cotrino, A.R. González-Elipe, A. Gómez-Ramírez, Unraveling Discharge and Surface Mechanisms in Plasma-Assisted Ammonia Reactions, ACS Sustain. Chem. Eng. 8 (2020) 14855–14866. doi:10.1021/acssuschemeng.0c04461.

[341] A. Parastaev, W.F.L.M. Hoeben, B.E.J.M. van Heesch, N. Kosinov, E.J.M. Hensen, Temperature-programmed plasma surface reaction: An approach to determine plasma-catalytic performance, Appl. Catal. B Environ. 239 (2018) 168–177. doi:10.1016/j.apcatb.2018.08.011.

[342] L.R. Ventura, C.E. Fellows, The N2 second positive (C3Πu → B3Πg) system reviewed: Improved data and analysis, J. Quant. Spectrosc. Radiat. Transf. 239 (2019) 10–15. doi:10.1016/j.jqsrt.2019.106645.

[343] L. Diekhöner, H. Mortensen, A. Baurichter, A.C. Luntz, Coverage dependence of activation barriers: Nitrogen on Ru(0001), J. Vac. Sci. Technol. A Vacuum, Surfaces, Film. 18 (2000). doi:10.1116/1.582376.

[344] S. Dahl, J. Sehested, C.J.H. Jacobsen, E. Törnqvist, I. Chorkendorff, Surface science based microkinetic analysis of ammonia synthesis over ruthenium catalysts, J. Catal. 192 (2000) 391–399. doi:10.1006/jcat.2000.2857.

[345] K. Honkala, A. Hellman, I.N. Remediakis, A. Logadottir, A. Carlsson, S. Dahl, C.H. Christensen, J.K. Nørskov, Ammonia Synthesis from First-Principles Calculations, Science (80-.). 307 (2005) 555–558. doi:10.1126/science.1106435.

[346] L. Ye, R. Nayak-Luke, R. Bañares-Alcántara, E. Tsang, Reaction: "Green" Ammonia Production, Chem. 3 (2017) 712–714. doi:10.1016/j.chempr.2017.10.016.

[347] L.R. Winter, J.G. Chen, N2 Fixation by Plasma-Activated Processes, Joule. (2020) 1–16. doi:10.1016/j.joule.2020.11.009.

[348] S. Dahl, A. Logadottir, C.J.H. Jacobsen, J.K. Norskov, Electronic factors in catalysis: The volcano curve and the effect of promotion in catalytic ammonia synthesis, Appl. Catal. A Gen. 222 (2001) 19–29. doi:10.1016/S0926-860X(01)00826-2.

[349] Z. Chen, B.E. Koel, S. Sundaresan, Plasma-assisted catalysis for ammonia synthesis in a dielectric barrier discharge reactor: key surface reaction steps and potential causes of low energy yield, J. Phys. D. Appl. Phys. 55 (2022) 055202. doi:10.1088/1361-6463/ac2f12.

[350] M. Iwamoto, M. Horikoshi, R. Hashimoto, K. Shimano, T. Sawaguchi, H. Teduka, M. Matsukata, Higher Activity of Ni/γ-Al2O3 over Fe/γ-Al2O3 and Ru/γ-Al2O3 for Catalytic Ammonia Synthesis in Nonthermal Atmospheric-Pressure Plasma of N2 and H2, Catalysts. 10 (2020). doi:10.3390/catal10050590.

[351] H. Zhao, G. Song, Z. Chen, X. Yang, C. Yan, S. Abe, Y. Ju, S. Sundaresan, B.E. Koel, In Situ Identification of NNH and N2H2 by Using Molecular-Beam Mass Spectrometry in Plasma-Assisted Catalysis for NH3 Synthesis, ACS Energy Lett. 7 (2022) 53–58. doi:10.1021/acsenergylett.1c02207.

[352] T.E. Bell, L. Torrente-Murciano, H2 Production via Ammonia Decomposition Using Non-Noble Metal Catalysts: A Review, Top. Catal. 59 (2016) 1438–1457. doi:10.1007/s11244-016-0653-4.

[353] R.W. Maatman, The site density of solid catalyts, J. Catal. 19 (1970) 64–73.

doi:10.1016/0021-9517(70)90297-6.

[354] T. Bligaard, K. Honkala, A. Logadottir, J.K. Nørskov, S. Dahl, C.J.H. Jacobsen, On the compensation effect in heterogeneous catalysis, J. Phys. Chem. B. 107 (2003) 9325–9331. doi:10.1021/jp034447g.

[355] S. Wang, B. Temel, J. Shen, G. Jones, L.C. Grabow, F. Studt, T. Bligaard, F. Abild-Pedersen, C.H. Christensen, J.K. Nørskov, Universal Brønsted-Evans-Polanyi relations for C-C, C-O, C-N, N-O, N-N, and O-O dissociation reactions, Catal. Letters. 141 (2011) 370–373. doi:10.1007/s10562-010-0477-y.

[356] A. Jess, P. Wasserscheid, Chemical Technology: An Integral Textbook, 1st ed., 2013.

[357] F. Gorky, M.A. Carreon, M.L. Carreon, Experimental strategies to increase ammonia yield in plasma catalysis over LTA and BEA zeolites, IOP SciNotes. 1 (2020) 024801. doi:10.1088/2633-1357/aba1f8.

[358] J.R. Shah, F. Gorky, J. Lucero, M.A. Carreon, M.L. Carreon, Ammonia synthesis via atmospheric plasma-catalysis: Zeolite 5A a case of study, Ind. Eng. Chem. Res. 10.1021/ac (2020). doi:10.1021/acs.iecr.9b05220.

[359] M. Takeuchi, T. Tsukamoto, A. Kondo, M. Matsuoka, Investigation of NH3 and NH4+ adsorbed on ZSM-5 zeolites by near and middle infrared spectroscopy, Catal. Sci. Technol. 5 (2015) 4587–4593. doi:10.1039/c5cy00753d.

[360] Y. Uytdenhouwen, K.M. Bal, E.C. Neyts, V. Meynen, P. Cool, A. Bogaerts, On the kinetics and equilibria of plasma-based dry reforming of methane, Chem. Eng. J. 405 (2021). doi:10.1016/j.cej.2020.126630.

[361] M. Shokrollahi Yancheshmeh, H.R. Radfarnia, M.C. Iliuta, High temperature CO2 sorbents and their application for hydrogen production by sorption enhanced steam reforming process, Chem. Eng. J. 283 (2016) 420–444. doi:10.1016/j.cej.2015.06.060.

[362] B. Dou, C. Wang, Y. Song, H. Chen, B. Jiang, M. Yang, Y. Xu, Solid sorbents for in-situ CO2 removal during sorption-enhanced steam reforming process: A review, Renew. Sustain. Energy Rev. 53 (2016) 536–546. doi:10.1016/j.rser.2015.08.068.

[363] E.R. Van Selow, P.D. Cobden, P.A. Verbraeken, J.R. Hufton, R.W. Van Den Brink, Carbon capture by sorption-enhanced water-gas shift reaction process using hydrotalcite-based material, Ind. Eng. Chem. Res. 48 (2009) 4184–4193. doi:10.1021/ie801713a.

[364] Y. Hayakawa, S. Kambara, T. Miura, Hydrogen production from ammonia by the plasma membrane reactor, Int. J. Hydrogen Energy. 45 (2020) 32082–32088. doi:10.1016/j.ijhydene.2020.08.178.

[365] Y. Gorbanev, E. Vervloessem, A. Nikiforov, A. Bogaerts, Nitrogen fixation with water vapor by non- equilibrium plasma: Towards sustainable ammonia production, ACS Sustain. Chem. Eng. (2020). doi:10.1021/acssuschemeng.9b07849.

[366] L. Wang, Y. Yi, H. Guo, X. Tu, Atmospheric Pressure and Room Temperature Synthesis of Methanol through Plasma-Catalytic Hydrogenation of CO2, ACS Catal. 8 (2018) 90–100. doi:10.1021/acscatal.7b02733.

[367] A.R. Sowunmi, C.O. Folayan, F.O. Anafi, O.A. Ajayi, N.O. Omisanya, D.O. Obada, D. Dodoo-Arhin, Dataset on the comparison of synthesized and commercial zeolites for potential solar adsorption refrigerating system, Data Br. 20 (2018) 90–95. doi:10.1016/j.dib.2018.07.040.

[368] Z. Wu, J. Xie, H. Liu, T. Chen, P. Cheng, C. Wang, D. Kong, Preparation, characterization, and performance of 4A zeolite based on opal waste rock for removal of ammonium ion, Adsorpt. Sci. Technol. 36 (2018) 1700–1715. doi:10.1177/0263617418803012.

[369] J.R. Ugal, K.H. Hassan, I.H. Ali, Preparation of type 4A zeolite from Iraqi kaolin: Characterization and properties measurements, J. Assoc. Arab Univ. Basic Appl. Sci. 9 (2010) 2–5. doi:10.1016/j.jaubas.2010.12.002.

[370] J. Li, M. Liu, X. Guo, S. Xu, Y. Wei, Z. Liu, C. Song, Interconnected Hierarchical ZSM-5 with Tunable Acidity Prepared by a Dealumination-Realumination Process: A Superior MTP Catalyst, ACS Appl. Mater. Interfaces. 9 (2017) 26096–26106. doi:10.1021/acsami.7b07806.

[371] Y. Li, R. Liu, Q. Guo, H. Bian, A. Lan, X. Li, P. Han, T. Dou, Efficient synthesis of high silica SSZ-13 zeolite via a steam-assisted crystallization process, J. Porous Mater. 26 (2019) 1879–1888. doi:10.1007/s10934-019-00784-0.

[372] L. Qiu, V. Murashov, M.A. White, Zeolite 4A: Heat capacity and thermodynamic properties, Solid State Sci. 2 (2000) 841–846. doi:10.1016/S1293-2558(00)01102-X.

[373] A. Nielsen, Ammonia: Catalysis and Manufacture, 1st ed., Springer-Verlag, Berlin Heidelberg, 1995.

[374] J.M. Jennings, Catalytic Ammonia Synthesis: Fundamentals and Practice, 1st ed., Plenum Press, New York, 1991.

[375] M. Appl, Ammonia, 2. Production Processes, Ullmann's Encycl. Ind. Chem. (2012) 295–338. doi:10.1002/14356007.o02_o11.

[376] European Fertilizer Manufacturers' Association, Production of Ammonia, Brussels (Belgium), 2000.

[377] Proton Ventures B.V., Sustainable ammonia for food and power, Nitrogen+Syngas. (2018) 1–10.

[378] H. Vrijenhoef, Dutch initiatives to store sustainable energy in the form of ammonia, in: NH3 Fuel Conf., Minneapolis (MN), 2017.

[379] M. Reese, C. Marquart, M. Malmali, K. Wagner, E. Buchanan, A. McCormick, E.L. Cussler, Performance of a Small-Scale Haber Process, Ind. Eng. Chem. Res. 55 (2016) 3742–3750. doi:10.1021/acs.iecr.5b04909.

[380] T. Brown, Ammonia technology portfolio: optimize for energy efficiency and carbon efficiency, (2018).

[381] E.R. Morgan, J.F. Manwell, J.G. McGowan, Sustainable Ammonia Production from U.S. Offshore Wind Farms: A Techno-Economic Review, ACS Sustain. Chem. Eng. 5 (2017) 9554–9567. doi:10.1021/acssuschemeng.7b02070.

[382] P.H. Pfromm, Towards sustainable agriculture: Fossil-free ammonia, J. Renew. Sustain. Energy. 9 (2017). doi:10.1063/1.4985090.

[383] M. Will, Realisation of Large-Scale Green Ammonia Plants, in: NH3 Fuel Conf., Pittsburgh (PA), 2018.

[384] M. Will, L. Lüke, Realisation of large-scale Green Ammonia plants, in: NH3 Event, Rotterdam (the Netherlands), 2018.

[385] J.P. Vrijenhoef, Opportunities for small scale ammonia production, in: Int. Fertil. Soc., London (UK), 2017: pp. 1–16.

[386] J. Schmuecker, D. Toyne, Making demonstration amounts of renewable ammonia and using it to fuel a farm tractor, in: NH3 Event, Rotterdam (the Netherlands), 2019.

[387] J.B. Hansen, P. Han, The SOC4NH3 Project in Denmark, in: NH3 Event, Rotterdam (the Netherlands), 2019.

[388] T. Mizushima, K. Matsumoto, J.I. Sugoh, H. Ohkita, N. Kakuta, Tubular membrane-like catalyst for reactor with dielectric-barrier- discharge plasma and its performance in ammonia synthesis, Appl. Catal. A Gen. 265 (2004) 53–59. doi:10.1016/j.apcata.2004.01.002.

[389] C. Wildfire, V. Abdelsayed, D. Shekhawat, M.J. Spencer, Ambient pressure synthesis of ammonia using a microwave reactor, Catal. Commun. 115 (2018) 64–67. doi:10.1016/j.catcom.2018.07.010.

[390] G.A. Buchner, K.J. Stepputat, A.W. Zimmermann, R. Schomäcker, Specifying Technology Readiness Levels for the Chemical Industry, Ind. Eng. Chem. Res. 58 (2019) 6957–6969. doi:10.1021/acs.iecr.8b05693.

[391] D.R. Stull, Vapor Pressure of Pure Substances. Organic and Inorganic

Compounds, Ind. Eng. Chem. 39 (1947) 517–540. doi:10.1021/ie50448a022.

[392] B. Eliasson, U. Kogelschatz, B. Xue, L. Zhou, Hydrogenation of Carbon Dioxide to Methanol with a Discharge-Activated Catalyst, Ind. Eng. Chem. Res. 5885 (1998) 3350–3357. doi:10.1021/ie9709401.

[393] Y. Inoue, M. Kitano, M. Tokunari, T. Taniguchi, K. Ooya, H. Abe, Y. Niwa, M. Sasase, M. Hara, H. Hosono, Direct Activation of Cobalt Catalyst by 12CaO·7Al2O3 Electride for Ammonia Synthesis, ACS Catal. (2019) acscatal.8b03650. doi:10.1021/acscatal.8b03650.

[394] C.Y. Liu, K. Aika, Effect of the Cl/Br Molar Ratio of a CaCl2-CaBr2 Mixture Used as an Ammonia Storage Material, Ind. Eng. Chem. Res. 43 (2004) 6994–7000. doi:10.1021/ie049873i.

[395] J.D. Beach, J.D. Kintner, A.W. Welch, Removal of gaseous NH3 from an NH3 reactor product stream (Patent), 20180339911, 2018.

[396] T. Zhang, H. Miyaoka, H. Miyaoka, T. Ichikawa, Y. Kojima, Review on Ammonia Absorption Materials: Metal Hydrides, Halides, and Borohydrides, ACS Appl. Energy Mater. 1 (2018) 232–242. doi:10.1021/acsaem.7b00111.

[397] M. Kitano, Y. Inoue, M. Sasase, K. Kishida, Y. Kobayashi, K. Nishiyama, T. Tada, S. Kawamura, T. Yokoyama, M. Hara, H. Hosono, Self-organized Ruthenium-Barium Core-Shell Nanoparticles on a Mesoporous Calcium Amide Matrix for Efficient Low-Temperature Ammonia Synthesis, Angew. Chemie - Int. Ed. 57 (2018) 2648–2652. doi:10.1002/ange.201712398.

[398] R. Shi, X. Zhang, G.I.N. Waterhouse, Y. Zhao, T. Zhang, The Journey toward Low Temperature, Low Pressure Catalytic Nitrogen Fixation, Adv. Energy Mater. 10 (2020). doi:10.1002/aenm.202000659.

[399] C. Smith, M. Malmali, C.Y. Liu, A. V. McCormick, E.L. Cussler, Rates of Ammonia Absorption and Release in Calcium Chloride, ACS Sustain. Chem. Eng. 6 (2018) 11827–11835. doi:10.1021/acssuschemeng.8b02108.

[400] J. Armijo, C. Philibert, Flexible production of green hydrogen and ammonia from variable solar and wind energy: Case study of Chile and Argentina, Int. J. Hydrogen Energy. 45 (2020) 1541–1558. doi:10.1016/j.ijhydene.2019.11.028.

[401] G.J. van Rooij, H.N. Akse, W.A. Bongers, M.C.M. van de Sanden, Plasma for electrification of chemical industry: A case study on CO2 reduction, Plasma Phys. Control. Fusion. 60 (2018). doi:10.1088/1361-6587/aa8f7d.

[402] A.R. Singh, B.A. Rohr, M.J. Statt, J.A. Schwalbe, M. Cargnello, J.K. Nørskov, Strategies Toward Selective Electrochemical Ammonia Synthesis, ACS Catal. 9 (2019) 8316–8324. doi:10.1021/acscatal.9b02245.

[403] S.Z. Andersen, V. Čolić, S. Yang, J.A. Schwalbe, A.C. Nielander, J.M. McEnaney, K. Enemark-Rasmussen, J.G. Baker, A.R. Singh, B.A. Rohr, M.J. Statt, S.J. Blair, S. Mezzavilla, J. Kibsgaard, P.C.K. Vesborg, M. Cargnello, S.F. Bent, T.F. Jaramillo, I.E.L. Stephens, J.K. Nørskov, I. Chorkendorff, A rigorous electrochemical ammonia synthesis protocol with quantitative isotope measurements, Nature. 570 (2019) 504–508. doi:10.1038/s41586-019-1260-x.

[404] L. Hollevoet, M. De Ras, M. Roeffaers, J. Hofkens, J.A. Martens, Energy-Efficient Ammonia Production from Air and Water Using Electrocatalysts with Limited Faradaic Efficiency, ACS Energy Lett. 5 (2020) 1124–1127. doi:10.1021/acsenergylett.0c00455.

[405] J.M. McEnaney, A.R. Singh, J.A. Schwalbe, J. Kibsgaard, J.C. Lin, M. Cargnello, F. Jaramillo, J.K. Nørskov, Ammonia synthesis from N2 and H2O using a lithium cycling electrification strategy at atmospheric pressure, Energy Environ. Sci. 10 (2017) 1621–1630. doi:10.1039/C7EE01126A.

[406] F. Jiao, B. Xu, Electrochemical Ammonia Synthesis and Ammonia Fuel Cells, Adv. Mater. (2018) 1–5. doi:10.1002/adma.201805173.

[407] H. Liu, W. Han, C. Huo, Y. Cen, Development and application of wüstite-based ammonia synthesis catalysts, Catal. Today. (2019) 1–18. doi:10.1016/j.cattod.2019.10.031.

[408] J. Wu, J. Li, Y. Gong, M. Kitano, T. Inoshita, H. Hosono, Intermetallic Electride Catalyst as a Platform for Ammonia Synthesis Communications Angewandte, Angew. Chemie - Int. Ed. 58 (2019) 825–829. doi:10.1002/anie.201812131.

[409] W. Gao, P. Wang, J. Guo, F. Chang, T. He, Q. Wang, G. Wu, P. Chen, Barium Hydride-Mediated Nitrogen Transfer and Hydrogenation for Ammonia Synthesis: A Case Study of Cobalt, ACS Catal. 7 (2017) 3654–3661. doi:10.1021/acscatal.7b00284.

[410] M. Hattori, S. Iijima, T. Nakao, H. Hosono, M. Hara, Solid solution for catalytic ammonia synthesis from nitrogen and hydrogen gases at 50 °C, Nat. Commun. 11 (2020). doi:10.1038/s41467-020-15868-8.

[411] J. Kammert, J. Moon, Y. Cheng, L.L. Daemen, S. Irle, V. Fung, J. Liu, K. Page, X. Ma, V. Phaneuf, J. Tong, A.J. Ramirez-Cuesta, Z. Wu, Nature of Reactive Hydrogen for Ammonia Synthesis over a Ru/C12A7 Electride Catalyst, J. Am. Chem. Soc. 142 (2020) 7655–7667. doi:10.1021/jacs.0c02345.

[412] M. Hara, M. Kitano, H. Hosono, Ru-Loaded C12A7:e- Electride as a Catalyst for Ammonia Synthesis, ACS Catal. 7 (2017) 2313–2324. doi:10.1021/acscatal.6b03357.

[413] Y. Gong, J. Wu, M. Kitano, J. Wang, T. Ye, J. Li, Y. Kobayashi, K. Kishida, H. Abe,

Y. Niwa, H. Yang, T. Tada, H. Hosono, Ternary intermetallic LaCoSi as a catalyst for N 2 activation, Nat. Catal. 1 (2018) 178–185. doi:10.1038/s41929-017-0022-0.

[414] S. Matsuishi, Y. Toda, M. Miyakawa, K. Hayashi, T. Kamiya, M. Hirano, I. Tanaka, H. Hosono, High-density electron anions in a nanoporous single crystal: [Ca24Al28O64]4+ (4e-), Science (80-.). 301 (2003) 626–629. doi:10.1126/science.1083842.

[415] K.H.R. Rouwenhorst, S. Mani, L. Lefferts, Improving the energy yield of plasma-based ammonia synthesis with in situ adsorption, ACS Sustain. Chem. Eng. 10 (2022) 1994–2000. doi:10.1021/acssuschemeng.1c08467.

[416] G. Chen, R. Snyders, N. Britun, CO2conversion using catalyst-free and catalyst-assisted plasma-processes: Recent progress and understanding, J. CO2 Util. 49 (2021) 101557. doi:10.1016/j.jcou.2021.101557.

[417] A. Bogaerts, T. Kozák, K. Van Laer, R. Snoeckx, Plasma-based conversion of CO2: Current status and future challenges, Faraday Discuss. 183 (2015) 217–232. doi:10.1039/c5fd00053j.

[418] J.H. Lozano-Parada, W.B. Zimmerman, The role of kinetics in the design of plasma microreactors, Chem. Eng. Sci. 65 (2010) 4925–4930. doi:10.1016/j.ces.2010.03.056.

[419] K.H.R. Rouwenhorst, A.G.J. Van der Ham, L. Lefferts, Beyond Haber-Bosch: The renaissance of the Claude process, Int. J. Hydrogen Energy. 46 (2021) 21566–21579. doi:10.1016/j.ijhydene.2021.04.014.

[420] V.N. Sagel, K.H.R. Rouwenhorst, J.A. Faria, Green Ammonia Enables Sustainable Energy Production in Small Island Developing States: A Case Study on the Island of Curaçao, Renew. Sustain. Energy Rev. 161 (2022). doi:10.1016/j.rser.2022.112381.

[421] V.N. Sagel, K.H.R. Rouwenhorst, J.A. Faria, Renewable Electricity Generation in Small Island Developing States: The Effect of Importing Ammonia, Energies. 15 (2022) 3374. doi:10.3390/en15093374.

[422] L. Wang, Y. Yi, C. Wu, H. Guo, X. Tu, One-Step Reforming of CO2 and CH4 into High-Value Liquid Chemicals and Fuels at Room Temperature by Plasma-Driven Catalysis, Angew. Chemie - Int. Ed. 56 (2017) 13679–13683. doi:10.1002/anie.201707131.

[423] A.J. Boero, K. Kardux, M. Kovaleva, D.A. Salas, J. Mooijer, S. Mashruk, M. Townsend, K. Rouwenhorst, A. Valera-Medina, A.D. Ramirez, Life cycle assessment of future energy carriers: The environmental impact of ammonia-based electricity, Energies. 14 (2021) 6721. doi:10.3390/en14206721.

[424] R.M. Nayak-Luke, C. Forbes, Z. Cesaro, R. Bañares-Alcántara, K.H.R. Rouwenhorst, Techno-Economic Aspects of Production, Storage and Distribution of Ammonia, in: R. Bañares-Alcántara, A. Valera-Medina (Eds.), Techno-Economic Challenges Green Ammon. as Energy Vector, Elsevier Science Publishing Co Inc, 2020: pp. 191–208. doi:10.1016/B978-0-12-820560-0.00008-4.

[425] K.H.R. Rouwenhorst, O. Elishav, B. Mosevitzky Lis, G.S. Grader, C. Mounaïm-Rousselle, A. Roldan, A. Valera-Medina, Future Trends, in: R. Bañares-Alcántara, A. Valera-Medina (Eds.), Techno-Economic Challenges Green Ammon. as Energy Vector, Elsevier Science Publishing Co Inc, 2020: pp. 303–319. doi:10.1016/B978-0-12-820560-0.00013-8.

[426] K.H.R. Rouwenhorst, G.J. van Rooij, L. Lefferts, Plasma-assisted conversion of CO2, in: T.R. Reina, J.A. Odriozola, H. Arellano-Garcia (Eds.), Eng. Solut. CO2 Convers. A Glob. Chall., Wiley-VCH Verlag GmbH, 2022: pp. 429–462. doi:10.1002/9783527346523.ch18.

[427] K.H.R. Rouwenhorst, T. Brown, Techno-economic considerations for ammonia production, storage and transportation, in: K.-I. Aika, H. Kobayashi (Eds.), CO2 Free Ammon. as an Energy Carr., Springer Nature, 2022. doi:10.1007/978-981-19-4767-4.

Summary

This PhD thesis presents an investigation into plasma-catalytic ammonia synthesis in a dielectric barrier discharge (DBD) plasma reactor. Ammonia (NH_3) can be synthesized from hydrogen gas (H_2) and nitrogen gas (N_2). Ammonia has current applications as intermediate for the fertilizer industry and the chemical industry. About 45% of the current pure hydrogen demand in industry is used for ammonia production. Future applications of ammonia include its use as zero-carbon fuel and as hydrogen carrier. Thus, ammonia may play a significant role in a decarbonized energy landscape, as discussed in **Chapter 1**.

Currently, ammonia is produced via the Haber-Bosch process. In this process, hydrogen and nitrogen gas are compressed to 100-450 bar. Thereafter, the feed gas is combined with a recycle stream and the mixture is heated to 400-500°C. The gas mixture is then converted to ammonia over an iron-based catalyst with multiple promoters, until equilibrium conversion is achieved. The typical single pass conversion of hydrogen and nitrogen in this process is 15-20%. After the reactor, the gas mixture is cooled down to room temperature (or below) to liquefy the produced ammonia. The gas mixture is then recycled together with the feed gas.

The Haber-Bosch process has its limitations for renewable ammonia synthesis. Firstly, renewable electricity sources such as solar and wind are fluctuating, while the Haber-Bosch process typically relies on a continuous production. Secondly, the iron-based catalyst is only active for ammonia synthesis at elevated temperatures of around 400-500°C. This is due to the strong triple nitrogen-nitrogen bond for atmospheric nitrogen, which needs to be broken on the catalyst in order to synthesize ammonia.

This PhD thesis investigates whether pre-activation by a non-thermal plasma can loosen the nitrogen-nitrogen bond before reacting on the catalyst, thereby allowing for operation under milder conditions. A non-thermal plasma can be operated in a dielectric barrier discharge (DBD) plasma reactor at near-ambient temperatures. Highly energetic electrons are formed through electric fields and collisions with molecules, such as molecular nitrogen. The bulk of the gas will remain at near-ambient temperatures. Low temperature operation of the plasma reactor implies that the equilibrium shifts towards ammonia formation, implying the process can be operated at ambient pressure. Another benefit of the plasma reactor is that it is fed with electricity, and the mild operating conditions imply that the reactor can be easily started up and shut down. An overview of previous research on plasma-catalytic ammonia synthesis, as well as a current understanding of reaction mechanisms involved can be found in **Chapter 2**.

The bulk of this PhD thesis focuses on mechanistic understanding of reactions relevant for plasma-catalytic ammonia synthesis at various plasma intensities. First, plasma-catalytic ammonia synthesis at relatively mild plasma intensities is discussed, e.g. at specific energy

inputs below 1 kilojoule per liter. In previous research, it was postulated that the activation barrier for nitrogen dissociation on the catalyst could be reduced by pre-activating the nitrogen molecules in a plasma. This could possibly result in a higher ammonia production on the catalyst. In **Chapter 3**, this is demonstrated with experimental data for ruthenium-based catalysts that vibrational or electronic activation of nitrogen molecules in the plasma increases the ammonia production rate via a lower activation barrier for nitrogen dissociation. In **Chapter 4**, a mechanism is suggested for the reduced activation barrier for nitrogen dissociation on ruthenium-based catalysts.

Plasma-catalytic ammonia synthesis at higher plasma intensities are discussed thereafter, e.g. at specific energy inputs in the order of 10 kilojoules per liter. Under these conditions, part of the nitrogen molecules is activated by the electrons in the plasma to such an extent that the molecules are broken in the plasma to form nitrogen radicals. These nitrogen radicals are highly reactive, and open new reaction pathways for plasma-catalytic ammonia synthesis.

In **Chapter 5**, the contributions of plasma chemistry, plasma catalysis, and thermal catalysis are evaluated for ruthenium-based catalysts. It is found that plasma chemistry reactions increase with increasing plasma power due to the formation of nitrogen and hydrogen radicals in the plasma. Also, ammonia can be formed via nitrogen radicals reacting with the ruthenium surface, resulting in plasma-catalytic ammonia synthesis. This becomes relevant at temperatures where ammonia can desorb from the ruthenium surface and when surface hydrogenation becomes sufficiently fast. Thermal-catalytic ammonia synthesis becomes relevant under the same conditions like without plasma, e.g. above 300°C. Plasma-catalytic ammonia synthesis reactions are typically faster than the thermal-catalytic ammonia decomposition reaction, resulting in ammonia synthesis beyond thermal equilibrium above 450°C.

Reaction mechanisms with nitrogen radicals are further investigated in **Chapter 6**. Various transition metals are tested for their activity, namely cobalt, copper, palladium, platinum, ruthenium, and silver. All catalysts are found to have a similar activity for plasma-catalytic ammonia synthesis. This is different from traditional thermal-catalytic ammonia synthesis, where the activity among transition metal catalysts varies by orders of magnitude. It is found that a dominant reaction step for plasma-catalytic ammonia synthesis is the Eley-Rideal reaction between a nitrogen radical from the plasma and a surface-adsorbed hydrogen atom on the catalyst surface.

One of the limitations of plasma conversions is that not only the reactants are activated by the plasma, but also the products. This limits the energy efficiency of plasma-catalytic ammonia synthesis. A zeolite 4A adsorbent was introduced to the plasma reactor. Ammonia can be removed *in situ* from the plasma zone via adsorption on the zeolite. Ammonia is located inside the pores of the adsorbent, where the plasma cannot penetrate to decompose the ammonia. As discussed in **Chapter 7**, the introduction of the adsorbent improves the energy yield for plasma-based ammonia synthesis by a factor two.

The techno-economic feasibility of plasma-catalytic ammonia synthesis is discussed in **Chapter 8**. The process is compared to a Haber-Bosch ammonia synthesis process, and emerging technologies for small-scale ammonia synthesis. It is found that plasma-catalytic ammonia synthesis is not economically feasible, even for the optimal plasma activation van stikstof. The reason for this is the exothermic nature of the ammonia synthesis reaction from hydrogen and nitrogen, implying that any plasma activation of molecules ends up as a heat loss. In **Chapter 9**, it is concluded that research on plasma conversions should focus on endothermic reactions, such as nitrogen oxide synthesis from air. Alternatively, ammonia synthesis at mild operating conditions may be achieved through more active catalysts and solid sorbents for ammonia separation.

Samenvatting

Deze PhD thesis beschrijft een onderzoek naar plasma-katalytische ammoniak synthese in een dielectric barrier discharge (DBD) plasma reactor. Ammoniak (NH_3) kan geproduceerd worden vanuit waterstof gas (H_2) en stikstof gas (N_2). Ammoniak wordt momenteel gebruikt als tussenproduct voor de kunstmest industrie en de chemische industrie. Ongeveer 45% van de pure waterstof productie wordt momenteel gebruikt voor ammoniak productie. Toekomstige toepassingen voor ammoniak zijn het gebruik als koolstofloze brandstof en als waterstof drager. Dus, ammoniak kan een significante rol spelen in een koolstofloos energie landschap, zoals wordt besproken in **Hoofdstuk 1**.

Momenteel wordt ammoniak geproduceerd via het Haber-Bosch proces. In dit proces worden waterstof en stikstof gas gecomprimeerd tot 100-450 bar. Daarna wordt dit voedingsgas gecombineerd met een recyclestroom en deze mix wordt verwarmd naar 400-500°C. De gas mix wordt dan omgezet naar ammoniak met behulp van een ijzer-gebaseerde katalysator die verschillende promotoren bevat, totdat de evenwichtsomzetting is bereikt. De typische enkele stap conversie van waterstof en stikstof in dit proces is 15-20%. Na de reactor wordt de gas mix afgekoeld naar kamertemperatuur (of daaronder) om de geproduceerde ammoniak vloeibaar te maken. De gas mix wordt daarna gerecycled samen met het voedingsgas.

Het Haber-Bosch proces heeft limiteringen voor hernieuwbare ammoniak productie. Ten eerste fluctueren hernieuwbare elektriciteitsbronnen zoals zon en wind, terwijl het Haber-Bosch proces normaliter continu opereert. Ten tweede is de ijzer-gebaseerde katalysator enkel actief voor ammoniak productie op hoge temperaturen rond 400-500°C. Dit komt door de sterke driedubbele stikstof-stikstof binding van atmosferische stikstof, elke gebroken moest worden op de katalysator om ammoniak te kunnen produceren.

Deze PhD thesis onderzoekt of pre-activatie door niet-thermische plasma de stikstof-stikstof binding kan verzwakken voordat het reageert op de katalysator, waardoor het proces onder mildere condities kan opereren. Een niet-thermische plasma kan geopereerd worden in een dielectric barrier discharge (DBD) plasma reactor op temperaturen nabij kamertemperatuur. Hoogenergetische elektronen worden gevormd via elektrische velden en via botsingen met moleculen, zoals moleculair stikstof. Het grootste deel van het gas blijft op een temperatuur nabij kamertemperatuur. Het opereren van de plasma reactor op lage temperatuur betekent dat het evenwicht verschuift naar ammoniak formatie, waardoor het proces geopereerd kan worden op mildere drukken. Een ander voordeel van de plasma reactor is dat het gevoed wordt met elektriciteit, en de milde operationele condities betekenen dat de reactor gemakkelijk kan worden opgestart en gestopt. Een overzicht van eerder onderzoek omtrent plasma-katalytische ammoniak synthese, evenals de huidige kennis van relevante reactie mechanismes zijn beschreven in **Hoofdstuk 2**.

Het grootste deel van deze PhD thesis focust op het mechanistische begrip van reacties relevant voor plasma-katalytische ammoniak productie bij verschillende plasma intensiteiten. Ten eerste wordt plasma-katalytische ammoniak productie onder relatief milde plasma intensiteiten beschreven, met een specifieke energie toevoer onder 1 kilojoule per liter. In eerder onderzoek werd gepostuleerd dat de activatie barrière voor stikstof dissociatie op de katalysator verlaagd kan worden door pre-activatie van stikstof moleculen in een plasma. Dit zou mogelijk kunnen resulteren in een hogere ammoniak productie op de katalysator. In **Hoofdstuk 3** wordt gedemonstreerd met experimentele data voor ruthenium-gebaseerde katalysatoren dat vibrationele of elektronische activatie van stikstof moleculen in het plasma inderdaad de ammoniak productiesnelheid verhogen via een verlaagde activatie barrière voor stikstof dissociatie. In **Hoofdstuk 4** wordt een mechanisme voorgesteld voor de verlaagde activatie barrière voor stikstof dissociatie op ruthenium-gebaseerde katalysatoren.

Plasma-katalytische ammoniak synthese onder hogere plasma intensiteiten wordt hierna beschreven, met een specifieke energie toevoer rond 10 kilojoules per liter. Onder deze condities wordt een deel van de stikstof moleculen dusdanig geactiveerd door de elektronen in het plasma, dat de moleculen gebroken worden in het plasma om stikstof radicalen te vormen. Deze stikstof radicalen zijn erg reactief, en dit opent nieuwe reactiepaden voor plasma-katalytische ammoniak synthese.

In **Hoofdstuk 5** worden de contributies van plasma chemie, plasma katalyse, en thermische katalyse geëvalueerd voor ruthenium-gebaseerde katalysatoren. Het blijkt dat plasma chemie reacties versnellen met toenemende plasma sterkte vanwege de formatie van stikstof en waterstof radicalen in het plasma. Tevens kan ammoniak worden gevormd via stikstof radicalen die reageren met het ruthenium oppervlak, hetgeen resulteert in plasma-katalytische ammoniak synthese. Dit wordt relevant op temperaturen waarbij ammoniak kan desorberen van het ruthenium oppervlak en wanneer oppervlakte hydrogenering snel genoeg wordt. Thermisch-katalytische ammoniak synthese wordt relevant onder dezelfde condities als zonder plasma, dus boven 300°C. Plasma-katalytische ammoniak synthese reacties zijn typisch sneller dan de thermisch-katalytische ammoniak decompositie reactie, hetgeen resulteert in ammoniak synthese voorbij thermisch evenwicht boven 450°C.

Reactiemechanismes met stikstof radicalen worden verder onderzocht in **Hoofdstuk 6**. Verschillende transitiemetalen zijn getest voor de activiteit, namelijk kobalt, koper, palladium, platina, ruthenium, en zilver. Alle katalysatoren hebben een vergelijkbare activiteit voor plasma-katalytische ammoniak synthese. Dit verschilt van traditionele thermisch-katalytische ammoniak synthese, waarbij de activiteit tussen verschillende transitie metaal katalysatoren met enkele orders van grootte verschilt. De dominante reactie stap voor plasma-katalytische ammoniak synthese is de Eley-Rideal reactie tussen een stikstof radicaal vanuit het plasma en een oppervlak-geadsorbeerd waterstof atoom op het katalysator oppervlak.

Een limitatie van plasma conversies is dat niet alleen de reactanten worden geactiveerd door het plasma, maar ook de producten. Dit limiteert de energie efficiëntie van plasma-katalytische ammoniak synthese. Een zeoliet 4A sorptiemiddel is geïntroduceerd in de plasma reactor. Ammoniak kan *in situ* verwijderd worden uit de plasma zone via adsorptie op het zeoliet. Ammoniak bevindt zich in de poriën van het sorptiemiddel, waar het plasma niet kan penetreren om de ammoniak af te breken. Zoals wordt besproken in **Hoofdstuk 7** verbetert de introductie van een sorptiemiddel de energieopbrengst van plasma-gebaseerde ammoniak synthese met een factor twee.

De techno-economische haalbaarheid van plasma-katalytische ammoniak synthese wordt besproken in **Hoofdstuk 8**. Het proces wordt vergeleken met een Haber-Bosch ammoniak synthese proces, en opkomende technologieën voor kleine schaal ammoniak synthese. Het blijkt dat plasma-katalytische ammoniak synthese niet economisch haalbaar is, zelfs niet voor de optimale plasma activatie van stikstof. De reden hiervoor is de exotherme aard van de ammoniak synthese reactie vanuit waterstof en stikstof, hetgeen betekent dat elke plasma activatie van moleculen resulteert in een warmte verlies. In **Hoofdstuk 9** wordt geconcludeerd dat onderzoek naar plasma conversies zich zou moeten focussen op endotherme reacties, zoals stikstof oxide productie vanuit lucht. Verder kan ammoniak synthese onder milde condities gerealiseerd worden doormiddel van actievere katalysatoren en vaste sorptiemiddelen voor ammoniak scheiding.

Acknowledgements

My PhD started off with a nice surprise. Louis van der Ham, the daily supervisor during my MSc thesis put in the effort to nominate me for a KHMW award. When I went for a conference in Pittsburgh, and had booked an AirBnB in a sketchy neighborhood, I was like: well tomorrow I have to present my work outside university for the first time, help! But then, I opened my laptop and I got an e-mail from the KHMW, congratulating me on winning the 1st place in the category gas industry. Obviously, this helped me a lot to get through my presentation the next day. Thank you so much, Louis, for putting in the effort to go the extra mile for me, and for always being there as a person for me. Throughout my PhD, I have enjoyed the coffee talks we had every now and then, as well as the PPD supervision opportunity you gave me. We even published another paper together!

This NH3 Fuel Conference in Pittsburgh made me part of the ammonia energy community. From then on I would do some odd jobs for the Ammonia Energy Association, such as drafting some summaries of what had occurred during the conferences in the years to follow, as well as writing some articles for their website. Last year, this resulted in an opportunity to co-write a report on renewable ammonia. Furthermore, Trevor Brown invited me to join the employee ranks of the Ammonia Energy Association. Trevor, I am very grateful for the confidence, and the opportunities you have given me at such a young age! To some extent, this goes for all people within the ammonia energy community, who have invited me to co-write book chapters, and papers.

At these conferences I also met people from my other current employer, Proton Ventures. The speeches from Hans and Jacco during the ammonia energy conference have been an inspiration for me to continue working in the field of ammonia energy. Now I am part of a great team of engineers, and a special shoutout goes out to Stefano, Cheng, Gerard, Nitish, and Ioanna, who have been my most direct colleagues in the innovation department. From time to time it may not have been easy to have someone around who works two jobs, and tries to finish a PhD, but you have never put pressure on me during this time. I appreciate this, but above all I appreciate the joy we had together to kick-start the ammonia economy!

But now let me go back to my research topic during my PhD. During my MSc thesis, it all started off with googling “ammonia PhD” around March 2018. I wanted to continue work on ammonia and I liked catalysis. And there it was: a PhD available on the topic of “plasma-catalytic ammonia synthesis” at the University of Twente, great! So, I applied, and I was accepted to join CPM as a PhD student from September 2018 onward.

Looking back on the four years of my PhD, I would like to thank Leon Lefferts for the fruitful discussions and his critical attitude towards science. From time to time we had our disagreement, especially on style. Leon likes to keep it to the experiments and everything that we “can know”, and I like to philosophize away. However, I believe that I needed someone like Leon as a supervisor, e.g. someone who would keep me thinking linearly and

not dream away in a web of vaguely connected interesting research areas. So, thank you for that and hopefully we can continue the research we started with some follow-ups in the area of NO_X synthesis.

In this line, I would also like to acknowledge Rolf Postma, who actually performed the groundwork for the grant that led to my PhD position. Rolf was the other Dutchie in the group among PhD students and PostDocs and we liked to discuss all kinds of topics, such as politics, science, etc., especially over a bottle of beer during the Friday afternoon. I am very happy that Rolf is now also active in the field of ammonia energy and we will keep crossing paths from time to time.

The Friday afternoon drinks at CPM, especially during the early years of my PhD, were quite extravagant. Oftentimes, these drinks would last till late, such that we partied till deep into the night in the city center of Enschede. An especially memorable moment was the drunk cycling to the city involving me and Maria falling of a bike, while still being at the University. We decided to walk thereafter. Also, I still remember the moment that Shahab was on the floor with some Disney attributes during Sinterklaas, after we drank quite some strong alcohol together. Also memorable were the football matches we watched together, as well as the Karaoke nights with for example Pengyu, Nuria, Giuseppe, Shilpa, Tushar, and Pengcheng.

My office mate Guido taught me the first steps into the realm of plasma catalysis. Also, Guido learned me some “useful” Italian words for party purposes. And generally, it is great to have someone around who has the attitude to enjoy life, and not just blindly focus on work.

Obviously, PhD research executed around the year 2020 cannot be discussed without acknowledging the COVID-19 pandemic. In early March 2020, I was in Curacao together with Jimmy Faria, Guido Mul, and Leon Lefferts for the RESILIENT Island Workshop on power-to-ammonia-to-power. During the final day of the conference, it was announced that the airspace would be shut down, which obviously caused some stress for all of us. We sat in a car with less than 1.5 meters apart and we made it safely home. However, a few days later I would turn 25 and we would all be in complete lockdown. Even when we were allowed to be partially back in the office, we had to keep our distance for safety reasons and masks were mandatory (outside the lab).

Luckily I had housemates, Alexander and Dave, which made life a lot nicer. We had our own little research group at home which we dubbed the “Breemars Institute of Technology”. We also did crazy things, like shaving our hair off (well Alexander at least, Dave was too vain to join us); we just wanted to see how that would look like and feel, and the lockdown would take a while anyway, enough time to regrow the hair.

I would also like to acknowledge our Friday night sessions, where we would have plenty of fun, and do Researchgate battles. We would all grab our laptops and work on some PhD stuff or other matters, but never the stuff we did not feel like working on. Of course, this

included bad music, mainly obscure Dutch music. Alexander and Dave: thank you for all of that!

Let me now get back to the CPM research group. Next to Leon, two assistant professors (now one is associate professor) were part of the group. I know Jimmy and Aayan as two hardworking academics with a bright future ahead. Jimmy is a true family man, which showed during our trip to Curacao when he missed his daughters and wife, which is something I strongly admire. After all, we are humans, not robots in the academic rat race. Always feel free to contact me regarding anything like ammonia.

Throughout my PhD I had the privilege to supervise many good students, and some truly excellent students. I like to thank all of them for their efforts and also for sticking with me till the end, and for listening to my dreamy ideas for research from time to time. I hope above all you all had fun during your research. For example, I remember some nice pub quizzes, and eating pancakes together the COVID-19 pandemic. So, Alex, Daan, Hugo, Judit, Martijn, Raymond, Robby, Ruben, Samuel, Sybe, and Victor: thank you for choosing with me as your supervisor. I would also like to especially acknowledge co-PhD students Kevin and Yannick from Antwerp, who were collaborating with me on a review paper on plasma-catalytic ammonia synthesis, together with Annemie. It is always great to have colleagues at other universities who are so open in their communication. Not everyone realizes this, but we are in science together!

Drinking coffee is very important during the PhD research. Especially during the final year of my PhD it was painfully obvious that I drink a lot of coffee. A new system was recently implemented with a count of coffees per day, which made it very clear how much coffee I drink per day.

I enjoyed drinking coffee with the fellow CPM members, such as our secretaries Anne and Dorothy, and previous technician Tom. Also, I would go to other groups to drink some extra coffee. For example, I would often drink coffee with Nicole. This was very nice, as it allowed for going outside of the CPM bubble, so thank you for the realistic view on PhD research, Nicole.

However, the person I probably spent most time with drinking coffee is Bert, our technician and group manager of CPM. From time to time, he would give his sober advise on how to do research, and what is possible and what not. Bert was a bit like a second supervisor to me, but one with the practical experience rather than the academic experience. Oftentimes we would also just drink coffee to discuss life, which was as enjoyable. Bert, thank you for all those hours and let's continue to drink a beer on the Friday afternoon!

I also want to especially acknowledge Karin and Ties, who have been very helpful throughout my PhD with characterizations. Furthermore, it was good to always have a crew of "tukkers" at the coffee table. I especially enjoyed the discussions about the personal life, which is at least as important as being good colleagues work-wise.

Although I did not fully manage to the final months of my PhD research, I strived to not gain any PhD kilograms. So, sport is another thing to do during PhD. This is why I joined PhotoKai and AC Membranes as goalkeeper for the futsal competitions. Thank you for the fanatic, but happy times in the sports hall.

Also, one could see me walk around on campus during the lunch break together with Jord and Harm, previous CPM students currently pursuing their PhD within and outside CPM. They also offered me wit some fun and sober realizations of PhD life, which was always mixed with some good jokes, so thank you for that!

During the last year of my PhD I got new room mates, namely fellow PhD candidate Fernando Bernal and PostDoc Xinming Xing. We had some nice discussions about research, and I hope my taste for music did not disturb you too much!

Now that my time had nearly come to an end at CPM, I wanted to make sure someone would carry the torch. When Lola recently mentioned she had a short stint with plasma-catalysis in Manchester, I saw my chance! She now carries on the plasma catalysis work, which hopefully helps her securing a permanent academic position. During my final year, several new PhD candidates (Rem, Janek, and Martim) joined our group. I hope I did not come across as a PhD granddad. I wish you all the best with your PhD projects!

The biggest support throughout my entire life has been my family, and in more recent years the female additions to the family. I like to thank my parents Tonnie and Caroline for always being there for me. I realize I caused my parents quite some grey hairs while growing up. I used to be quite a lazy student up till recently. I also like to thank them so much for keeping the stress away in multiple aspects, while learning me how to balance study and work from a reasonable youth. I also want to acknowledge my brother for always being there, and for all the places we went to together.

Later on Jeffrey added Michelle to the family, who has been like an older sister to me, sometimes muttering to me, but always with the greatest intention. Over the past year, my girlfriend Sietske has been my greatest support, and continues to be so.

In conclusion, I like to thank all who have positively contributed to where I am now, including my friends from Haaksbergen and University, which has been quite a rollercoaster with a lot of peaks in recent years!

List of Publications

Per August 2022

Journal articles

1. **Rouwenhorst, K. H. R.**, Van Der Ham, A. G. J., Mul, G., & Kersten, S. R. A. (2019). Islanded ammonia power systems: Technology review & conceptual process design. *Renewable and Sustainable Energy Reviews*, 114. doi: 10.1016/j.rser.2019.109339 Ref. [33]

2. **Rouwenhorst, K. H. R.**, Kim, H.-H., & Lefferts, L. (2019). Vibrationally excited activation of N_2 in plasma-enhanced catalytic ammonia synthesis: a kinetic analysis. *ACS Sustainable Chemistry & Engineering*, 7(20), 17515-17522. doi: 10.1021/acssuschemeng.9b04997 Ref. [94]

3. **Rouwenhorst, K. H. R.**, & Lefferts, L. (2020). Feasibility study of plasma-catalytic ammonia synthesis for energy storage applications. *Catalysts*, *10*(9). doi: 10.3390/catal10090999 Ref. [216]

4. **Rouwenhorst, K. H. R.**, Engelmann, Y., Van 't Veer, K., Postma, R. S., Bogaerts, A., & Lefferts, L. (2020). Plasma-driven catalysis: green ammonia synthesis with intermittent electricity. *Green Chemistry*, 22(19), 6258-6287. doi: 10.1039/D0GC02058C Ref. [310]

5. **Rouwenhorst, K. H. R.**, Burbach, H. G. B., Núñez Paulí, J., Vogel, D. W., Geerdink, B., & Lefferts, L. (2021). Plasma-Catalytic Ammonia Synthesis beyond Thermal Equilibrium on Ru-based Catalysts in Non-thermal Plasma. *Catalysis Science and Technology*, 11(8), 2834-2843. doi: 10.1039/D0CY02189J Ref. [223]

6. **Rouwenhorst, K. H. R.**, Jardali, F., Bogaerts, A., & Lefferts, L. (2021). Plasma-driven nitrogen fixation: From the Birkeland-Eyde process towards energy-efficient plasma technology. *Energy & Environmental Science*, 14(5), 2520-2534. doi: 10.1039/D0EE03763J Ref. [11]

7. **Rouwenhorst, K. H. R.**, Van der Ham, A. G. J., & Lefferts, L. (2021). Beyond Haber-Bosch: The renaissance of the Claude process. *International Journal of Hydrogen Energy*, 46(41), 21566-21579. doi: 10.1016/j.ijhydene.2021.04.014 Ref. [419]

8. **Rouwenhorst, K. H. R.**, & Lefferts, L. (2021). On the mechanism for the plasma-activated N_2 dissociation on Ru surfaces. *Journal of Physics D: Applied Physics*, 54, 393002. doi: 10.1088/1361-6463/ac1226 Ref. [330]

9. Boero, A. J., Kardux, K., Kovaleva, M., Salas, D. A., Mooijer, J., Mashruk, S., Townsend, M., **Rouwenhorst, K. H. R.**, Valera-Medina, A., & Ramirez, A. D. (2021). Life cycle assessment of future energy carriers: The environmental impact of ammonia-based electricity. *Energies*, 14(20), 6721. doi: 10.3390/en14206721 Ref. [423]

10. **Rouwenhorst, K. H. R.**, Mani, S., & Lefferts, L. (2022). Improving the energy efficiency of plasma-based ammonia synthesis with *in situ* adsorption. *ACS Sustainable Chemistry & Engineering*, 10(6), 1994-2000. doi: 10.1021/acssuschemeng.1c08467 Ref. [415]

11. Sagel, V. N., **Rouwenhorst, K. H. R.**, & Faria, J. A. (2022). Green Ammonia Enables Sustainable Energy Production in Small Island Developing States: A Case Study on the Island of Curaçao. *Renewable and Sustainable Energy Reviews*, 161. doi: 10.1016/j.rser.2022.112381 Ref. [420]

12. **Rouwenhorst, K. H. R.**, Travis, A. S., & Lefferts, L. (2022). 1921-2021: A century of renewable ammonia synthesis. *Sustainable Chemistry*, 3(2), 149-171. doi: 10.3390/suschem3020011 Ref. [24]

13. Sagel, V. N., **Rouwenhorst, K. H. R.**, & Faria, J. A. (2022). Renewable electricity generation in small island developing states: the effect of importing ammonia. *Energies*, 15(9), 3374. doi: 10.3390/en15093374 Ref. [421]

14. **Rouwenhorst, K. H. R.**, & Lefferts, L. (n.d.). Plasma-catalytic ammonia synthesis via Eley-Rideal reactions: a kinetic analysis. In preparation.

15. David, W.I.F. et al. (incl. **Rouwenhorst, K. H. R.**) (n.d.). 2022 roadmap on ammonia as a carbon-free fuel. *Journal of Physics: Energy*. In preparation.

Reports

1. IRENA, & Ammonia Energy Association (Lead author: **Rouwenhorst, K. H. R.**) (2022). Innovation Outlook: Renewable Ammonia. Abu Dhabi (United Arab Emirates). ISBN: 978-92-9260-423-3 Ref. [14]

Book chapters

1. **Rouwenhorst, K. H. R.**, Krzywda, P. M., Benes, N. E., Mul, G., & Lefferts, L. (2020). Ammonia Production Technologies. In R. Bañares-Alcántara, & A. Valera-Medina (Eds.), *Techno-Economic Challenges of Green Ammonia as Energy Vector* (pp. 41-84). Elsevier Science Publishing Co Inc. doi: 10.1016/B978-0-12-820560-0.00004-7 Ref. [309]

2. Nayak-Luke, R. M., Forbes, C., Cesaro, Z., Bañares-Alcántara, R., & **Rouwenhorst, K. H. R.** (2020). Techno-Economic Aspects of Production, Storage and Distribution

of Ammonia. In R. Bañares-Alcántara, & A. Valera-Medina (Eds.), *Techno-Economic Challenges of Green Ammonia as Energy Vector* (pp. 191-208). Elsevier Science Publishing Co Inc. doi: 10.1016/B978-0-12-820560-0.00008-4 Ref. [424]

3. **Rouwenhorst, K. H. R.,** Elishav, O., Mosevitzky Lis, B., Grader, G. S., Mounaïm-Rousselle, C., Roldan, A., & Valera-Medina, A. (2020). Future Trends. In R. Bañares-Alcántara, & A. Valera-Medina (Eds.), *Techno-Economic Challenges of Green Ammonia as Energy Vector* (pp. 303-320). Elsevier Science Publishing Co Inc. doi: 10.1016/B978-0-12-820560-0.00013-8 Ref. [425]

4. **Rouwenhorst, K. H. R.**, van Rooij, G. J., & Lefferts, L. (2021). Plasma-assisted conversion of CO_2. In T. R. Reina, J. A. Odriozola, & H. Arellano-Garcia (Eds.), *Engineering Solutions for CO2 conversion: A global Challenge* (pp. 429-462). Wiley-VCH Verlag GmbH. doi: 10.1002/9783527346523.ch18 Ref. [426]

5. **Rouwenhorst, K. H. R.**, & Brown, T. (2022). Techno-economic considerations for ammonia production, storage and transportation. In K-I. Aika, K. Eguchi & H. Kobayashi (Eds.), *CO_2 free Ammonia as a Fuel: Production, Combustion, and Power Generation*. Springer Nature. doi: 10.1007/978-981-19-4767-4 Ref. [427]

Encyclopedia articles

1. **Rouwenhorst, K. H. R.**, Krzywda, P.M., Benes, N. E., Mul, G., & Lefferts, L. (2020). Ammonia, 4. Green Ammonia Production. In *Ullmann's Encyclopedia of Industrial Chemistry*. doi: 10.1002/14356007.w02_w02 Ref. [25]

Patents

1. Liang, C., **Rouwenhorst, K. H. R.**, De Cillis, S., & Fagioli, G. (2022). Hybrid ammonia decomposition system. *Filed*.

Oral presentations

1. **Rouwenhorst, K. H. R.**, Van der Ham, A. G. J., Mul, G., & Kersten, S. R. A. (2018). Power-to-Ammonia-to-Power (P2A2P) for Local Electricity Storage in 2025. *NH3 Fuel Conference*. Pittsburgh (PA).

2. **Rouwenhorst, K. H. R.**, Van der Ham, A. G. J., Mul, G., & Kersten, S. R. A. (2019). Power-to-Ammonia-to-Power (P2A2P) for Local Electricity Storage in 2025. *KVGN Nieuwjaar meeting*. Den Haag (The Netherlands). (Invited)

3. **Rouwenhorst, K. H. R.**, Krzywda, P. M., Van der Ham, A. G. J., Kersten, S. R. A., Mul, G., & Lefferts, L. (2019). Scale-down strategies and state of the art of technologies for power-to-ammonia. *NH3 Event*. Rotterdam (The Netherlands).

4. **Rouwenhorst, K. H. R.**, & Lefferts, L. (2019). Plasma-enhanced catalytic ammonia synthesis. *Workshop Twente-Eindhoven-Antwerpen-Amsterdam on Plasma Catalysis*. Eindhoven (The Netherlands).

5. **Rouwenhorst, K. H. R.** (2019). Power-to-ammonia-to-power (P2A2P) for electricity storage. *MESA+ Day*. Enschede (The Netherlands). (Invited)

6. **Rouwenhorst, K. H. R.**, & Lefferts, L. (2019). Plasma-enhanced catalytic ammonia synthesis as a technology for decentralized power-to-ammonia applications. *AIChE Annual Meeting*. Orlando (FL).

7. **Rouwenhorst, K. H. R.** (2020). Islanded power-to-ammonia-to-power (P2A2P) for electricity storage for the Caribbean islands. *RESILIENT-Island Workshop*. Willemstad (Curaçao). (Invited)

8. **Rouwenhorst, K. H. R.** (2020). Understanding the mechanisms in plasma-catalytic ammonia synthesis. *Plasma Forum organized by KIT*. Online.

9. **Rouwenhorst, K. H. R.** (2021). Reaction mechanisms and process considerations for plasma-nitrogen fixation. *IPP ITED Seminar.* Munich (Germany), Online. (Invited)

10. **Rouwenhorst, K. H. R.** (2021). The role of ammonia in the hydrogen economy. *Shell internal R&D seminar.* Amsterdam (The Netherlands), Online. (Invited)

11. **Rouwenhorst, K. H. R.** (2021). Ammonia, the 'Oil of Renewables'?. *CAMPFIRE Symposium 2021*. Stralsund (Germany). (Invited on behalf of Proton Ventures)

12. **Rouwenhorst, K. H. R.**, & L. Lefferts (2021). Reaction mechanisms and process considerations for plasma-nitrogen fixation. *Solvay Workshop on "Plasma Technology and Other Green Methods for Nitrogen Fixation"*. Brussels (Belgium). (Invited)

13. **Rouwenhorst, K. H. R.** (2021). Nuclear-based ammonia production. *Nuclear Hydrogen Initiative workshop*. Online. (invited on behalf of the Ammonia Energy Association)

14. **Rouwenhorst, K. H. R.** (2022). Nuclear-based ammonia production. *NRC's 2022 Virtual Regulatory Information Conference*. Online. (Invited on behalf of the Ammonia Energy Association)

15. **Rouwenhorst, K. H. R.** (2022). The role of ammonia in the hydrogen economy. *Intensive Hydrogen Course. Energy Delta Institute.* Online. (Invited on behalf of the Ammonia Energy Association)

16. **Rouwenhorst, K. H. R.** (2022). Update from the Ammonia Energy Association (Low carbon ammonia plants). *Nitrogen + Syngas*. Berlin (Germany). (Invited on behalf of the Ammonia Energy Association)

17. **Rouwenhorst, K. H. R.**, & Lefferts, L. (2022). Reaction mechanisms and process considerations for plasma-catalytic ammonia synthesis. *NCCC XIII*. Noordwijkerhout (The Netherlands).

18. **Rouwenhorst, K. H. R.** (2022). Green ammonia: a carbon-free future for fertilizers. *The 14th Stamicarbon Symposium*. Utrecht (The Netherlands). (Invited on behalf of the Ammonia Energy Association)

19. Gielen, D., & **Rouwenhorst, K. H. R.** (2022). The Role of Renewable Ammonia in the Energy Transition. *IRENA*. Online. (Invited on behalf of the Ammonia Energy Association)

20. **Rouwenhorst, K. H. R.** (2022). Making and breaking renewable ammonia with current and future technology. *NH3 Event*. Rotterdam (The Netherlands). (Invited on behalf of Proton Ventures)

21. **Rouwenhorst, K. H. R.**, & Lefferts, L. (2022). Reaction mechanisms and process considerations for plasma-catalytic ammonia synthesis. *5th International Symposium on Plasmas for Catalysis and Energy Materials (ISPCEM)*. Liverpool (United Kingdom).

22. **Rouwenhorst, K. H. R.** (2022). Ammonia as energy carrier. *Jiao Tong University Summer school*. Online. (Invited on behalf of the Ammonia Energy Association)

23. Castellanos, G., & **Rouwenhorst, K. H. R.** (2022). IRENA Insights: Innovation Outlook - Renewable Ammonia. *IRENA*. Online. (Invited on behalf of the Ammonia Energy Association)

24. **Rouwenhorst, K. H. R.** (2022). Innovation Outlook: Renewable Ammonia. *Cummins workshop on Ammonia*. Online. (Invited on behalf of the Ammonia Energy Association)

Poster presentations

1. **Rouwenhorst, K. H. R.**, & Lefferts, L. (2019). Plasma-enhanced ammonia synthesis: Reaction mechanisms involved at various process conditions. *NCCC*. Noordwijkerhout (The Netherlands).

2. **Rouwenhorst, K. H. R.**, Kim, H-H., & Lefferts, L. (2019). Plasma-enhanced ammonia synthesis: from plasma-phase ammonia synthesis towards plasma-enhanced catalytic ammonia synthesis. *ISPC*. Naples (Italy).

3. **Rouwenhorst, K. H. R.**, & Lefferts, L. (2019). Plasma-catalytic ammonia synthesis for decentralized power-to-ammonia applications: a kinetic analysis for Ru-based catalysts. *EuropaCat*. Aachen (Germany).

4. **Rouwenhorst, K. H. R.**, Kim, H-H., & Lefferts, L. (2020). Plasma-enhanced ammonia synthesis: from plasma-phase ammonia synthesis towards plasma-enhanced catalytic ammonia synthesis. *NCCC*. Noordwijkerhout (The Netherlands).

Other contributions

1. Supervision of various BSc and MSc students, February 2019-September 2022.
2. Supervision of various groups for the MSc course Process Plant Design on the topic of "*Integrated CO_2 capture and methanol synthesis*", February 2021-July 2021.
3. Table guest at *NH_3 Event*, June 2nd 2021, Rotterdam, The Netherlands.
4. Session chair at *"Ammonia Energy Conference 2021"*, November 7th-9th 2021, Boston, United States. Organization workshop on *"nuclear-based ammonia production"*. (On behalf of the Ammonia Energy Association).
5. Host at various webinars on *"Low carbon ammonia projects"*, starting in April 2022 (ongoing). (On behalf of the Ammonia Energy Association).
6. Part of the Scientific Committee of the "*1st Symposium on Ammonia Energy"*, September 1st-2nd 2022, Cardiff, United Kingdom. Session co-chair on "*Novel Ammonia Production Methods*".
7. Guest Editor of Virtual Special Issue on "*Sustainable integrated ammonia, nitric acid and nitrogen based fertilizer production with CO_2 sequestration by processed intensified catalytic plasma processes"* in *ACS Sustainable Chemistry & Engineering* (IF=9.224 in 2021), September 2022.
8. Part of the Editorial Team of the *Journal of Ammonia Energy*, an open access journal by Cardiff University Press.
9. Part of the Founding Team of the ISPT Platform "G*reen ammonia*" (on behalf of the Ammonia Energy Association), launched in September 2022.